Modélisation et simulation numérique de la propagation d'ondes électromagnétiques dans les câbles coaxiaux.

Akram Beni Hamad

INSTITUT POLYTECHNIQUE DE PARIS

NNT : 2022IPPAE013

Thèse de doctorat

Modélisation et simulation numérique de la propagation d'ondes électromagnétiques dans les câbles coaxiaux

Thèse de doctorat de l'Institut Polytechnique de Paris
préparée à l'Ecole Nationale Supérieure de Techniques Avancées

École doctorale n°574 Mathematiques Hadamard (EDMH)
Spécialité de doctorat : mathématiques appliquées

Thèse présentée et soutenue à Palaiseau, France, le 30/09/2022, par

Akram Beni Hamad

Composition du Jury :

Patrick Ciarlet Professeur, ENSTA Paris, France.	Président
Julien Diaz Directeur de recherche, INRIA Bordeaux, France.	Rapporteur
Francesca Rapetti Maître de conférences, Université Nice, France.	Rapporteuse
Juliette Chabassier Chargée de recherche, INRIA Bordeaux, France.	Examinatrice
Claire Scheid Maître de conférences, Université Nice, France.	Examinatrice
Patrick Joly Directeur de recherche, INRIA Saclay, France.	Directeur de thèse
Sébastien Imperiale Chargé de recherche, INRIA Saclay, France.	Co-directeur de thèse
Moez Khenissi Full professor, Université de Sousse, Tunisie.	Co-directeur de thèse

Je dédie cette thèse à mes chers parents.

« Tous les mots du monde ne sauraient exprimer l'immense amour que je vous porte, ni la profonde gratitude que je ressens pour tous les efforts et les sacrifices que vous n'avez cessé de faire pour mon éducation et mon bien-être. »

Remerciements

Tout d'abord, je tiens à remercier mon directeur de thèse Patrick Joly. J'ai beaucoup appris avec lui sur le plan scientifique et humain. Il m'a guidé avec beaucoup d'attention dans la réalisation de cette thèse. Je le remercie pour les discussions fructueuses et les conseils judicieux ainsi que pour l'aide appropriée à la rédaction de ce manuscrit.

Je remercie également Sébastien Imperiale pour son aide, ses conseils, ses nouvelles idées, sa disponibilité pour répondre à mes questions, et son encadrement lors de l'élaboration de ce travail.

Mes remerciements vont également à Moez Khinissi. Merci pour la confiance, pour vos conseils, et surtout, pour avoir été là pour moi dans tous les moments difficiles.

Je tiens à remercier Julien Diaz et Francesca Rapetti, qui m'ont fait l'honneur d'accepter de rapporter cette thèse et qui ont relu attentivement ce manuscrit. Je vous remercie pour tous vos commentaires constructifs. Un grand merci aux autres membres du jury. En particulier je remercie Patrick Ciarlet pour avoir accepté d'en être le président. Merci également à Juliette Chabassier et Claire Scheid pour leur intérêt et leur attention à mon travail.

Mes remerciements vont également à Geoffrey Beck pour l'excellente collaboration que nous avons eu. Merci Geoffrey pour tous tes conseils et les discussions que nous avons eues. J'espère que nous continuerons à travailler ensemble.

Merci à tous les membres de l'équipe POEMS de m'avoir chaleureusement accueilli dans ce laboratoire où règnent convivialité et bonne humeur. Je tiens à remercier particulièrement Anne-Sophy et Eliane pour leur grande humanité. Elles m'ont aidé à trouver une année de financement pour avancer et finir ma thèse en France. Je remercie aussi Nicolas et Éric pour l'écoute et la disponibilité et pour la discussion que nous avons faite pour l'implémentation d'un code Galerkin Discontinu. Je remercie chaleureusement Corinne pour ses conseils, son travail et son aide dans les tâches administratives difficiles.

Je remercie du fond de mon cœur tous les membres du laboratoire LAMMDA pour leur soutien et leurs précieux conseils. J'y apprécie l'ambiance sympathique qui règne entre les collègues.

Évidemptment, je remercie tous les doctorants, post-doctorants, stagiaires passés et présents. Je remercie particulièrement le génie Mahran qui était toujours disponible pour m'aider mathématiquement et humainement. Je remercie Radhia et Basma pour les bons moments et les discussions amusantes dans notre groupe $\mathcal{R}\&\mathcal{F}$. Je remercie également Mohamed et Houssem : Je suis fier de vous appeler mes amis et peu importe ce qui se passe dans la vie, je peux toujours compter sur vous deux.

Enfin, je tiens à remercier mes parents Noureddine et Kira, mes frères Amir et Amjed, et mes sœurs Mouna, Maha et la petite Aïda, qui ont toujours été là pour me soutenir et m'encourager.

Table des matières

Chapitre 1

Introduction et motivation

La simulation numérique, notamment en régime transitoire, de la propagations d'ondes électromagnétiques dans des réseaux de câbles électriques co-axiaux est un enjeu très important dans des nombreuses applications scientifiques et industrielles, que cela concerne les réseaux de communication, l'alimentation électrique de capteurs piézo-électriques ou le contrôle du réseau ferroviaire de la SNCF. En effet, l'un des enjeux est le contrôle non destructif de ces câbles. Le contrôle non destructif des défauts [6, 1, 11] s'appuie souvent sur la modélisation et les simulations prospectives des grandeurs électriques se propageant dans des réseau électriques.

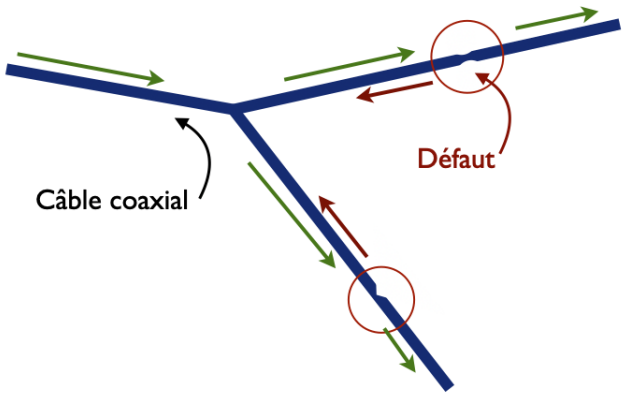

FIGURE 1.1 – Réseau électrique.

Un câble coaxial a une structure de type cylindrique et est constitué d'un matériau diélectrique qui entoure un fil intérieur métallique (dont la présence est nécessaire pour permettre la propagation des ondes le long du câble aux fréquences d'intérêt) et est entouré d'une gaine extérieure. Le modèle mathématique de base pour la propagation des ondes dans un tel câble est fourni par les équations de Maxwell 3D, la difficulté principale provenant de la géométrie du domaine de calcul, un câble a des dimensions transverses très petites devant sa dimension longitudinale, et dans le caractère inhomogène des matériaux qui le composent. Effectuer des simulations numériques réalistes représente aussi un challenge scientifique : les échelles très différentes mises en jeu sont telles que, même si les phénomènes que l'on souhaite simuler relèvent des équations de Maxwell 3D, passer par la simulation numérique 3D s'avère très coûteux en temps de calcul.

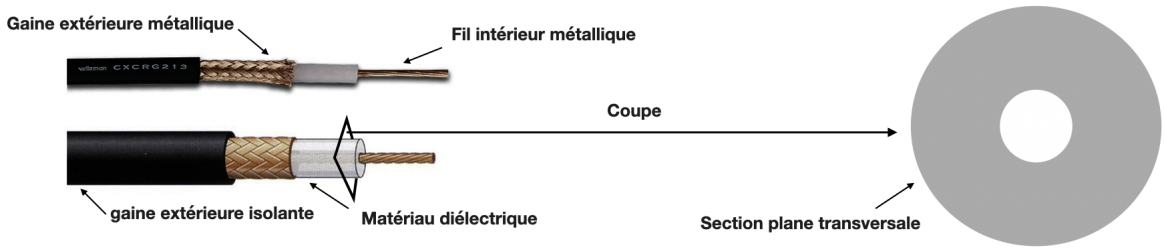

FIGURE 1.2 – Câble coaxial (Modification d'une figure obtenue sur le Web [1]).

C'est pourquoi il est naturel de chercher à proposer des modèles mono-dimensionnels approchés en cherchant à exploiter le fait que les dimensions transverses d'un câble sont très petites devant la dimension longitudinale. Les modèles sous-jacents principalement utilisés sont basés sur la représentation des câbles coaxiaux par un modèle 1D appelé modèle du télégraphiste qui traite de la propagation de la tension et du courant le long d'un quadripôle RLCG infinitésimal (voir figure 1.3) (voir [44] pour le cas cylindrique). Cette approche est utilisée depuis bien longtemps en génie électrique, mais elle n'est vraiment bien maîtrisée et comprise que dans des situations idéales ou académiques, comme par exemple le cas d'un câble homogène parfaitement cylindrique en régime harmonique, situation dans laquelle la décomposition de la solution en modes de propagation permet de justifier complètement le modèle 1D.

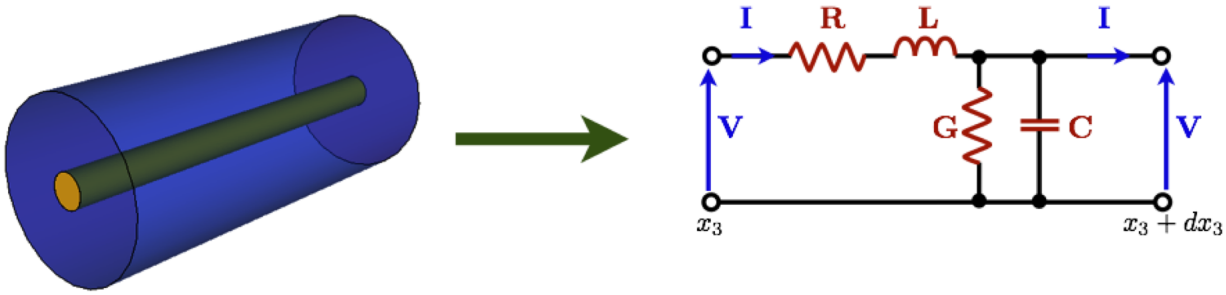

FIGURE 1.3 – Un câble coaxial comme succession de quadripôles RLCG infinitésimaux ((figure reprise de [10]).

Pour les applications réalistes, toutefois, il est nécessaire de savoir prendre des situations beaucoup plus complexes, incluant le caractère hautement hétérogène de la structure interne des câbles électriques (ce qui peut résulter suivant les cas de leur fabrication même ou de phénomènes d'usure) ainsi que des imperfections de géométrie (dues notamment à des endommagements), des jonctions de câbles sans parler des phénomènes de pertes par effet de peau liées au caractère imparfaitement conducteur des gaines par exemple.

Dans ces cas, la simple approche modale se révèle bien impuissante pour proposer des modèles approchés réalistes, ce qui se comprend assez bien : il faut à la fois aboutir à un modèle suffisamment simple (c'est à dire mono-dimensionnel) pour se prêter à une simulation numérique efficace tout en étant suffisamment riche pour garder en mémoire la structure 3D complexes des câbles et en restituer leurs effets utiles pour les applications visées.

1. https://www.lextronic.fr/cable-coaxial-noir-50-ohms-91-mm-64308.html

Pour répondre à ces enjeux, au cours des dix dernières années une théorie de modèles de câbles simplifiés de "type 1D" a été développée au sein de l'équipe POEMS à partir d'une analyse asymptotique rigoureuse des équations de Maxwell 3D, le petit paramètre de l'analyse étant la dimension transverse des câbles. Cela a débuté au cours de la thèse de Sébastien Imperiale [35] dans le cadre de l'approximation de capteurs piézo-électriques en collaboration avec le CEA List. Ces travaux initiaux ont débouché notamment sur deux articles, [33] et [34], où sont établis des modèles limites appelés "modèles de télégraphistes généralisés" et ce dans une configuration très générale (câble hétérogène de section variable avec présence possible de pertes). Ensuite, dans sa thèse [10] effectuée dans le cadre du projet ANR SODDA (sur le contrôle non destructif de réseaux de câbles, projet porté par le CEA List), Geoffrey Beck a étendu cette théorie au cas d'un câble multi-conducteurs [12] (le câble contient plusieurs fils métalliques), puis à des modèles simplifiés d'ordres supérieurs, à la prise en compte de l'effet de peau [13] et enfin à la jonction de plusieurs câbles.

Ces modèles ont été justifiés d'un point de vue mathématique mais la phase véritablement opérationnelle du travail, notamment tout ce qui concerne les applications numériques, n'a pas été abordée.

C'est dans le cadre et dans le contexte décrit plus haut que se situe cette thèse avec, au départ, un triple objectif :

1. Proposer, analyser et implémenter des méthodes numériques efficaces pour la résolution des problèmes approchés.
2. Quantifier les erreurs induites par des modèles approchés, et par conséquent en cerner les limites de validité, par le biais de la comparaison entre simulations numériques 1D et 3D.

De façon cachée, ce second objectif en sous-tend un troisième puisque, comme on l'a dit précédemment, se contenter de codes existants pour la résolution des équations de Maxwell 3D est difficile. C'est pourquoi, afin d'atteindre l'objectif 2, il fallait au préalable :

3. Concevoir des méthodes numériques pour la résolution des équations de Maxwell 3D dédiées à la prise en compte de la structure particulière des câbles électriques, en particulier l'existence de deux très petites dimensions transverses.

Cet objectif qui a bien sûr un intérêt en soi indépendamment des modèles asymptotiques a de fait constitué l'enjeu principal de cette thèse.

Les difficultés d'une approche numérique 3D

Afin de mettre en évidence les difficultés liées au troisième objectif évoqués, entrons un peu dans les détails relatifs à la discrétisation des équations de Maxwell dans un câble mince.

Un câble coaxial droit de longueur L (voir la figure 1.2) est, comme déjà dit plus haut, constitué d'un matériau diélectrique qui entoure un fil intérieur métallique (dont la présence est nécessaire pour permettre la propagation des ondes le long du câble aux fréquences d'intérêt) et est entouré d'une gaine extérieure. En première approximation, les structures interne et externe sont toutes deux constituées de matériaux parfaitement conducteurs, de sorte que le champ électromagnétique est confiné dans la partie diélectrique (pour les questions relatives aux fils internes et externes non parfaitement conducteurs, le lecteur peut se référer à [13]). Cette partie diélectrique peut être définie comme une succession

longitudinale de sections planes transversales 2D avec un trou.

Dans les applications industrielles, les câbles sont fins, mathématiquement nous considérerons que sa dimension transversale est proportionnelle à un petit paramètre $\delta \ll 1$. En utilisant une analyse asymptotique des équations de Maxwell 3D avec $\delta \to 0$, plusieurs modèles simplifiés 1D ont été rigoureusement présentés dans la thèse de Geoffrey Beck [10]. Si certains de ces modèles ont été justifiés d'un point de vue mathématique par des estimations d'erreurs lorsque le câble a une géométrie cylindrique, il n'existe pas, à notre connaissance, de comparaison numérique quantitative entre le modèle 1D et la théorie de Maxwell 3D. Pour ce faire, il faut effectuer des simulations 3D avec des équations de Maxwell 3D. Il s'agit d'un défi de calcul, d'autant plus que le câble est fin, et l'objectif de cette thèse est d'aborder précisément ces questions. Pour mieux cerner les difficultés à traiter, il convient de mentionner qu'un problème de simulation typique contient naturellement trois longueurs :

— le diamètre du câble δ,

— la longueur d'onde moyenne le long du câble λ,

— la longueur caractéristique de la propagation L.

En raison de la structure allongée du domaine de propagation Ω, il est naturel d'utiliser des mailles allongées avec une taille de pas h dans la direction longitudinale x_3 et une taille de pas h_T dans les directions transversales. Ces paramètres sont contraints par les caractéristiques des problèmes comme suit

— $h_T \ll \delta$, pour bien traiter la structure interne du câble et bien représenter les variations du champ électromagnétique à l'intérieur de chaque section transversale,

— $h \ll \lambda$, pour représenter avec précision les variations de la solution dans la direction longitudinale.

En pratique, comme $\delta \ll L$, nous aurons $h_T \ll h$ ce qui conduit à un nombre énorme de degrés de liberté.

Lorsque la discrétisation temporelle, avec un pas de temps Δt, est impliquée, on est confronté à un choix :

(i) Soit on utilise une discrétisation temporelle totalement explicite, auquel cas, pour des raisons de stabilité (conditions CFL), Δt est contraint par le petit pas spatial h_T, c'est-à-dire $\Delta t \leq c^{-1} h_T$ où c est une constante qui a la dimension d'une vitesse. Cela impose clairement des pas de temps très petits.

(ii) Soit on utilise une discrétisation temporelle totalement implicite et inconditionnellement stable. Dans ce cas, il n'y a plus de contrainte sur Δt pour des raisons de stabilité mais le problème est qu'un grand système linéaire doit être résolu à chaque itération temporelle.

En résumé, chacune des deux solutions ci-dessus entraînerait des coûts de calcul prohibitifs (si ce n'est des calculs hors de portée) : soit le nombre de pas de temps est beaucoup trop grand, cas (i), soit le coût de chaque itération temporelle est beaucoup trop élevé, cas (ii). C'est pourquoi notre objectif de trouver un compromis entre les solutions (i) et (ii) dans lequel

(a) Δt serait limitée par le pas d'espace longitudinal h seulement, comme pour un problème de propagation 1D discrétisé avec un schéma explicite

(b) Le coût de chaque itération temporelle resterait raisonnable.

Cet objectif sera atteint par une approche hybride de discrétisation temporelle qui serait implicite dans les directions transversales, assurant (a), mais explicite dans la direction longitudinale, assurant (b).

Contributions et plan de la thèse

Ce qui suit est un résumé des principales contributions présentées dans ce travail. Cette thèse comporte cinq chapitres :

Chapitre 2 : Méthode numérique pour les câbles cylindriques

Dans ce chapitre, nous proposons une méthode numérique efficace pour la résolution des équations de Maxwell 3D dédiée à la prise en compte de la structure particulière des câbles électriques, en particulier l'existence de deux très petites dimensions transverses. L'idée consiste à utiliser un maillage prismatique anisotrope, avec un pas du maillage transverse h_T et un pas de maillage longitudinale h, tout en se basant sur un schéma hybride implicite-explicite.

Pour mettre en oeuvre cette méthode, la première étape consiste à faire une discrétisation longitudinale du câble, puis une discrétisation transverse de chaque section, enfin une discrétisation en temps. Notre approche est de distinguer le rôle des variables spatiales transverses $\mathbf{x}_T$ et celui de la variable longitudinale x_3 et d'exploiter le découplage entre la composante transverse $\mathbf{E}_T$ du champ électrique et sa composante longitudinale E_3. Le champ $\mathbf{E}_T$ est alors approché par des éléments de Nedelec dans chaque section S_j et par des éléments affines par morceaux selon la direction longitudinale. Par contre le champ E_3 est approché avec des éléments $\mathbb{P}_1$ sur chaque section $S_{j+\frac{1}{2}}$ et par des éléments $\mathbb{P}_0$ discontinus par morceaux selon la direction longitudinale.

Nous montrons que le schéma est inconditionnellement stable par rapport au pas de l'espace transverse h_T et conditionnellement stable par rapport au pas de l'espace longitudinal. Donc le schéma est stable sous la condition CFL : $\Delta t \leq c^{-1}\ h$.

La méthode présentée a été implémenté dans le logiciel Xlife++ [2](développé au département UMA de l'ENSTA).

Chapitre 3 : Modèle limite 1D et comparaison 3D / 1D

Dans ce chapitre, nous présentons un modèle limite 1D appelé le modèle télégraphiste, qui résulte d'une analyse asymptotique appliqué aux équations de Maxwell 3D en considérant que δ est un paramètre qui devient infiniment petit. Afin de rendre ce document "self-contained", nous avons choisi de rappeler brièvement la méthode pour obtenir, au moins formellement, ce modèle (plus de détails sont donnés en Annexe A). Ce modèle 1D obtenu prend en compte les propriétés physiques et géométriques des câbles à l'intérieur duquels la propagation de champ électromagnétique a lieu. Ce modèle limite s'écrit comme suit

$$\begin{cases} C(x_3)\ \partial_t \mathbf{V} + G^{\infty}(x_3)\,\mathbf{V} + \displaystyle\int_0^t K_e(x_3, t-s)\,\mathbf{V}(x_3, s)\,ds + \partial_3 \mathbf{I} = 0, \\ L(x_3)\ \partial_t \mathbf{I} + \partial_3 \mathbf{V} = 0, \end{cases} \tag{1.1}$$

2. https://uma.ensta-paris.fr/soft/XLiFE++/

où les inconnues sont le potentiel électrique $\mathbf{V}$ et le courant électrique $\mathbf{I}$. Les coefficients "effectifs" ou "homogénéisés" sont : C (la capacité) , L (l'inductance), G^∞ et K_e sont calculés via la résolution numérique des problèmes elliptiques posés dans les sections droites du câble. Ce calcul numérique peut être remplacé dans certaines situations par un calcul analytique. Nous présenterons cette approche dans l'annexe A.

Nous présentons ensuite une méthode numérique pour l'approximation de (1.1), la difficulté principale résidant dans la prise en compte des terme non locaux en temps (convolutions) de façon garantie stable. Pour se faire nous nous sommes inspirés de l'approche développée dans un cadre général dans [4] et d'une façon plus adaptée à notre configuration [35].

Enfin nous faisons des comparaisons entre calculs 1D et 3D qui nous permettent de valider (et cerner les limites de validité) le modèle asymptotique.

Les résultats de deux chapitres 2 et 3 ont fait l'objet d'une publication [2] dans le journal "Computational Methods in Applied Mathematics".

Chapitre 4 : Modèle limite 1D d'ordre 2 et comparaison 3D / 1D

Nous reprenons la structure du chapitre 3 en rappelant dans un premier temps la construction du modèle d'ordre 2, en nous limitant toutefois au cas d'un câble purement cylindrique à section hétérogène sans pertes. Ce modèle limite a pour principal intérêt de rendre compte des principaux effets dispersifs dus à l'hétérogénéité des câbles. Ce modèle prend la forme suivante :

$$\left\{\begin{array}{lcl} C_\delta(\partial_3)\,\partial_t V^{\delta,2} + \partial_3\, I^{\delta,2} & = & 0, \\ L_\delta(x_3,\partial_3)\,\partial_t I^{\delta,2} + \partial_3\, V^{\delta,2} & = & 0, \end{array}\right. \tag{1.2}$$

à comparer au modèle lorsque $K_e = 0$. Cette fois, $C_\delta(x_3,\partial_3)$ et $L_\delta(\partial_3)$ sont des opérateurs de capacité et inductance, opérateurs elliptiques d'ordre 2 en la variable x_3 :

$$\left\{\begin{array}{l} C_\delta(x_3,\partial_3) := C(x_3) - \delta^2\,\partial_3\Big(\gamma_C(x_3)\,\partial_3\Big), \\ L_\delta(x_3,\partial_3) := L(x_3) - \delta^2\,\partial_3\Big(\gamma_L(x_3)\,\partial_3\Big), \end{array}\right. \tag{1.3}$$

où les nouveaux coefficients $L_g, C_g, \gamma_C, \gamma_L$ font intervenir de nouveaux problèmes elliptiques 2D dans les sections transverses du câble.

Faute de temps, et pour simplifier la présentation de nos résultats nous allons focaliser notre attention sur le cas où les coefficients ne dépendent pas de la variable x_3.

Nous présentons ensuite une méthode numérique pour la discrétisation de ce modèle et terminons par des comparaisons entre calculs 1D et 3D qui illustrent l'intérêt du modèle d'ordre supérieur.

Ce chapitre est le fruit d'une collaboration avec Geoffrey Beck et fera l'objet d'une publication.

Chapitre 5 : Méthode numérique pour les câbles non cylindriques

Dans un câble non cylindrique le découplage - naturel dans le cas cylindrique - entre $\mathbf{E}_T$ et E_3 disparaît à cause des variations en x_3 de la section transverse. Dans ce but, afin de préserver autant que faire se peut les avantages de la méthode du cas cylindrique, nous proposons une approche basée sur les ingrédients suivants :

— utilisation d'un technique de mapping "section par section" entre le câble non cylindrique et un câble cylindrique de référence,

— utilisation d'une transformation de Piola anisotrope pour définir les nouvelles inconnues dans le domaine de référence.

L'avantage est que le nouveau problème est posé dans un domaine cylindrique. L'inconvénient est que le nouveau problème à résoudre comporte de nouveaux termes qui dépendent de la géométrie du câble (et disparaissent dans le cas cylindrique) et ne se prêtent plus bien à l'approximation par éléments finis proposée au chapitre 2.

Pour contourner cette difficulté, nous proposons une approche hybride éléments finis/Galerkin discontinue, la partie Galerkin discontinue servant à traiter les nouveaux termes. La méthode résultante se révèle coïncider avec la méthode du chapitre 2 dans le cas d'un câble cylindrique et se révèle posséder des propriétés de complexité (coût calcul) et stabilité similaires à celles du cas cylindrique.

Ce chapitre fera l'objet d'une publication.

Chapitre 6 : Couches PML pour les câbles

Pour traiter des câbles infinis ou très longs il est évidemment souhaitable de pouvoir borner artificiellement le domaine de calcul. Une des méthodes désormais très populaire est la méthode des couches absorbantes parfaitement adaptées ou PML (Perfectly Matched Layers).

Pour le problème 3D, si la construction de telles couches via la méthode de "complex scaling" usuelle ne pose pas de problème de principe, l'utilisation pratique de ces PML dans la configuration des câbles se heurte de fait à deux difficultés :

— la possibilité d'utiliser des couches PML avec les méthodes numériques proposées dans la thèse,

— la stabilité de ces modèles PML, laquelle n'est pas a priori garantie par la théorie.

Nous avons partiellement réussi et partiellement échoué dans le traitement de ces difficultés mais il nous a paru utile de faire état de nos efforts et résultats sur ces questions.

— Pour la prise en compte numérique des PML dans notre code de calcul, nous nous sommes inspirés des travaux de Baffet, Grote, Kachanovska et Imperiale [7] pour le cas de l'équation des ondes. La principale difficulté est d'aboutir à une formulation variationnelle compatible avec les éléments finis présentés au chapitre 2, ce qui repose sur l'introduction astucieuse d'inconnues auxiliaires.

— Faute de temps, la question de la stabilité n'a pu être abordée qu'au travers de simulations numériques. Si les PML se révèlent stables dans le cas d'un câble homogène, ce n'est plus le cas dès que la vitesse de propagation des ondes électromagnétiques varie dans la section du câble. Nos expériences numériques nous amènent à penser que cette instabilité est due au modèle continu et non à sa discrétisation.

Dans l'état actuel des choses, la question de la stabilité des PML, et encore plus la construction de PML stables, est largement ouverte et nécessite une analyse beaucoup plus approfondie.

Cependant, il est important de mentionner que l'utilisation de cette méthode s'est révélée efficace dans le cas des modèles approchés 1D, ce que nous allons illustré à la fin de ce chapitre.

Chapter 2

An efficient numerical method for electromagnetic wave propagation in a cylindrical co-axial cables

Contents

2.1 Introduction

In this chapter, we propose a new efficient numerical method to solve the 3D Maxwell equations in an elongated cylindrical coaxial cable. The originality of our approach comes from the fact that we use an anisotropic prismatic mesh, with a transverse mesh h_T and a longitudinal mesh h, which is consistent with the cable geometry, while relying on a hybrid implicit-explicit scheme. Furthermore, by studying the complexity and the stability properties of the proposed scheme, we show that it is unconditionally stable with respect to the transverse step-size and conditionally stable with respect to the longitudinal one.

This chapter is organized as follows :

After setting the problem (Section 2.2, we rewrite, in Section 2.3, Maxwell's equations in a specific form whose interest is to distinguish the transverse and longitudinal components of the electric field and make appear specific decoupling. Section 2.4 is dedicated to the semi-discretization in space. We first treat the discretization with respect to the longitudinal variable (Section 2.4.1) then with respect to the transverse variable (Section 2.4.2). It turns out that the proposed discretization can be re-interpreted via prismatic edge's element [15, 20] on prisms (Section 2.4.3). In Section 2.4 we describe the semi-discrete scheme in an algebraic form. The section 2.5 concerns the time discretization. In Section 2.5.1, we propose a hybrid implicit-explicit scheme, whose complexity and stability properties are analyzed in Sections 2.5.2 and 2.6. At the end of this chapter, in section 2.7, we present numerical results that confirm the efficiency of our approach.

2.2 Position of the problem

We consider a cylindrical cable for which the cross section is independent of x_3 (Figure 2.1) and we assume, for simplicity of the exposition, that the length L is infinite so that

$$\Omega = S \times \mathbb{R}, \quad (\text{ i.e. } S(x_3) = S \text{ (independent of } x_3), \quad \partial S = \Gamma_e \cup \Gamma_i. \tag{2.1}$$

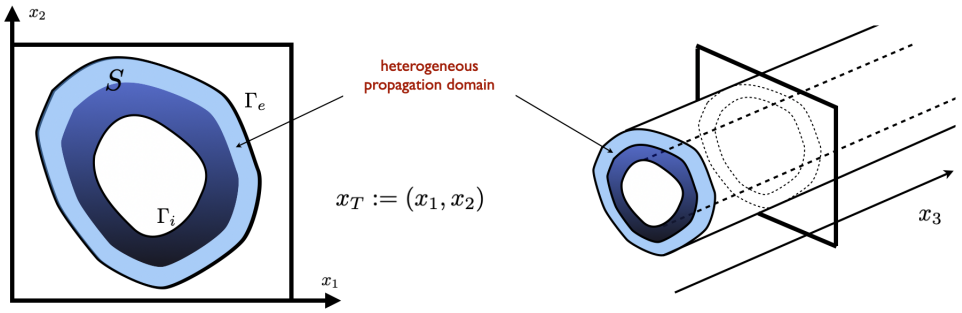

FIGURE 2.1 – Left : slice of the domain $S(x_3) = S$, right :the geometry of the domain Ω.

The dielectric material is characterized by the electrical permittivity ε and the magnetic permeability μ which are both functions of the space variable $\mathbf{x} \in \Omega$ and satisfy the usual assumptions

$$0 < \mu_- \leq \mu(\mathbf{x}) \leq \mu_+, \quad 0 < \varepsilon_- \leq \varepsilon(\mathbf{x}) \leq \varepsilon_+, \qquad \text{a.e. } \mathbf{x} = (x_1, x_2, x_3) \in \Omega.$$

We shall also consider the possibility that the cable can be, at least locally, conducting, which is modelled through the conductivity σ,

$$0 \leq \sigma(\mathbf{x}) \leq \sigma_+, \qquad \text{a.e. } \mathbf{x} = (x_1, x_2, x_3) \in \Omega. \tag{2.2}$$

Note that the translational invariance in x_3 concerns only the geometry of the domain Ω, not the coefficients ε , σ and μ. The propagation of waves in the cable Ω, through the

unknowns $\mathbf{E}(\mathbf{x},\mathbf{t})$ (the electric field) and $\mathbf{H}(\mathbf{x},\mathbf{t})$ (the magnetic field) is governed by 3D Maxwell's equations completed with perfectly conducting boundary conditions on $\partial\Omega$,

$$\begin{cases} \varepsilon\,\partial_t\mathbf{E} + \sigma\,\mathbf{E} - \boldsymbol{\nabla}\times\mathbf{H} = \mathbf{0}, & \text{in } \Omega\times\mathbb{R}^+. \\ \mu\,\partial_t\mathbf{H} + \boldsymbol{\nabla}\times\mathbf{E} = \mathbf{0}, & \text{in } \Omega\times\mathbb{R}^+, \\ \mathbf{E}\times\mathbf{n} = 0, & \text{on } \partial\Omega\times\mathbb{R}^+, \end{cases} \tag{2.3}$$

where t is the time, $\boldsymbol{\nabla}\times$ the 3D curl operator and $\mathbf{n}$ stands for the unit outward normal. The model is completed with initial conditions (for simplicity again we suppose the absence of source terms, without any loss of generality)

$$\mathbf{E}(\cdot,0) = \mathbf{E}_0, \quad \mathbf{H}(\cdot,0) = \mathbf{H}_0. \tag{2.4}$$

Our method will be developed for the second order electric field formulation of the problem, obtained after elimination of the magnetic field,

$$\left| \begin{array}{ll} \varepsilon\,\partial_t^2\mathbf{E} + \sigma\,\partial_t\mathbf{E} + \boldsymbol{\nabla}\times\,\mu^{-1}\,\boldsymbol{\nabla}\times\mathbf{E} = \mathbf{0}, & \text{in } \Omega\times\mathbb{R}^+, \\ \mathbf{E}\times\mathbf{n} = \mathbf{0}, & \text{on } \partial\Omega\times\mathbb{R}^+, \\ \mathbf{E}(\cdot,0) = \mathbf{E}_0, \quad \partial_t\mathbf{E}(\cdot,0) = \varepsilon^{-1}\left(\boldsymbol{\nabla}\times\mathbf{H}_0 - \sigma\,\mathbf{E}_0\right) & \text{in } \Omega. \end{array} \right. \tag{2.5}$$

Our approach is based on a particular rewriting of that well separating the roles of the longitudinal and transverse space variables (resp, longitudinal and transverse electric fields).

For simplicity, without any loss of generality, we shall present our method in the case $\sigma = 0$.

2.3 An adequate reformulation of the continuous problem

We introduce the longitudinal and transverse space variables $\mathbf{x} = (\mathbf{x}_T, x_3)$, $\quad \mathbf{x}_T = (x_1, x_2)$ and decompose the electric field into transverse ($\mathbf{E}_T$) and longitudinal (E_3) components,

$$\mathbf{E} = \begin{pmatrix} \mathbf{E}_T \\ E_3 \end{pmatrix} \qquad \text{with} \quad \mathbf{E}_T = \begin{pmatrix} E_1 \\ E_2 \end{pmatrix}.$$

To rewrite (2.5), we shall use the following transverse curl and gradient operators (note that the index T refers to transverse derivatives),

$$\mathrm{rot}_T\mathbf{E}_T = \partial_1 E_2 - \partial_2 E_1, \quad \mathbf{rot}_T\, E_3 = \begin{pmatrix} \partial_2 E_3 \\ -\partial_1 E_3 \end{pmatrix}, \quad \nabla_T\, E_3 = \begin{pmatrix} \partial_1 E_3 \\ \partial_2 E_3 \end{pmatrix}. \tag{2.6}$$

The first one is a scalar rotational operator whereas the second is a vectorial rotational operator that can be seen as a "rotated" gradient

$$\mathbf{rot}_T\, E_3 = -\mathbf{e}_3\times\nabla_T E_3, \quad \text{with} \quad \mathbf{e}_3\times E_T = \begin{pmatrix} -E_2 \\ E_1 \end{pmatrix} \quad \text{and} \quad \mathbf{e}_3 = (0,0,1)^t.$$

Warning to the reader : In what follows, and for the sake of simplicity, we shall often identify in the same notation the 2D transverse field $\mathbf{E}_T = (E_1, E_2)$ and the 3D vector field $\mathbf{E}_T = (E_1, E_2, 0)$, without mentioning it. This in particular gives a sense to $\mathbf{e}_3 \times \mathbf{E}_T$ that we identify with $(-E_2, E_1)$.

These rotational operators are related to the 3D curl operator via

$$\boldsymbol{\nabla} \times \mathbf{E} = \begin{pmatrix} \mathbf{rot}_T E_3 + \mathbf{e}_3 \times \partial_3 \mathbf{E}_T \\ \\ \mathrm{rot}_T \mathbf{E}_T \end{pmatrix}.$$

Thus, the Maxwell's equations (2.5) can be rewritten (this is a straightforward computation) as

$$\left| \begin{array}{l} \varepsilon\, \partial_t^2 \mathbf{E}_T - \partial_3\Big(\mu^{-1} \partial_3 \mathbf{E}_T\Big) + \mathbf{rot}_T\Big(\mu^{-1} \mathrm{rot}_T \mathbf{E}_T\Big) + \partial_3\Big(\mu^{-1} \nabla_T E_3\Big) = 0, \\ \varepsilon\, \partial_t^2 E_3 + \mathrm{rot}_T\Big(\mu^{-1} \mathbf{rot}_T E_3\Big) + \mathrm{div}_T\Big(\mu^{-1} \partial_3 \mathbf{E}_T\Big) = 0. \end{array} \right. \tag{2.7}$$

2.4 A hybrid discretization method in space

We shall use a Galerkin approach based of the weak (variational) formulation of (2.7). In order to give the weak formulation of this problem, we introduce the functional spaces

$$\left| \begin{array}{l} H(\mathbf{rot}; \Omega) := \Big\{ \Big(\mathbf{E}_T, E_3\Big) \in L^2(\Omega)^2 \times L^2(\Omega) \,/\, \mathbf{rot}_T E_3 \,+\, \mathbf{e}_3 \times \partial_3 \mathbf{E}_T \in L^2(\Omega)^2, \mathrm{rot}_T \mathbf{E}_T \in L^2(\Omega) \Big\}, \\ V := H_0(\mathbf{rot}; \Omega) = \Big\{ \mathbf{E} \in H(\mathbf{rot}; \Omega) \,/\, \mathbf{E} \times \mathbf{n} = 0 \text{ on } \partial\Omega \Big\}. \end{array} \right.$$

We aim at finding $\Big(\mathbf{E}_T, E_3\Big) \in V$ such that for any test function $\Big(\widetilde{\mathbf{E}}_T, \widetilde{E}_3\Big) \in V$, we have

$$\left| \begin{array}{l} \dfrac{d^2}{dt^2}\, \mathbf{m}\Big(\mathbf{E}_T, \widetilde{\mathbf{E}}_T\Big) + \mathbf{k}_3\Big(\mathbf{E}_T, \widetilde{\mathbf{E}}_T\Big) + \mathbf{k}_T\Big(\mathbf{E}_T, \widetilde{\mathbf{E}}_T\Big) - c_{3T}\Big(E_3, \widetilde{\mathbf{E}}_T\Big) = 0, \\ \dfrac{d^2}{dt^2}\, m\Big(E_3, \widetilde{E}_3\Big) + k_T\Big(E_3, \widetilde{E}_3\Big) - c_{3T}\Big(\widetilde{E}_3, \mathbf{E}_T\Big) = 0, \end{array} \right. \tag{2.8}$$

with the continuous bilinear forms

$$\left\{ \begin{array}{ll} \mathbf{m}\Big(\mathbf{E}_T, \widetilde{\mathbf{E}}_T\Big) := \displaystyle\int_\Omega \varepsilon\, \mathbf{E}_T \cdot \widetilde{\mathbf{E}}_T, & m\Big(E_3, \widetilde{E}_3\Big) := \displaystyle\int_\Omega \varepsilon\, E_3\, \widetilde{E}_3, \\ \mathbf{k}_T\Big(\mathbf{E}_T, \widetilde{\mathbf{E}}_T\Big) := \displaystyle\int_\Omega \mu^{-1}\, \mathrm{rot}_T \mathbf{E}_T\, \mathrm{rot}_T \widetilde{\mathbf{E}}_T, & k_T\Big(E_3, \widetilde{E}_3\Big) := \displaystyle\int_\Omega \mu^{-1}\, \nabla_T E_3 \cdot \nabla_T \widetilde{E}_3, \\ \mathbf{k}_3\Big(\mathbf{E}_T, \widetilde{\mathbf{E}}_T\Big) := \displaystyle\int_\Omega \mu^{-1}\, \partial_3 \mathbf{E}_T \cdot \partial_3 \widetilde{\mathbf{E}}_T, & c_{3T}\Big(E_3, \mathbf{E}_T\Big) := \displaystyle\int_\Omega \mu^{-1}\, \nabla_T E_3 \cdot \partial_3 \mathbf{E}_T. \end{array} \right. \tag{2.9}$$

The stiffness bilinear forms $\mathbf{k}_T, k_T$ and $\mathbf{k}_3$ do not couple transverse and longitudinal fields. We use bold letters when they apply to transverse fields. The index T means that only transverse derivatives are involved while the index 3 means that only x_3 derivatives are involved. Oppositely, the bilinear form c_{3T} couple the transverse and longitudinal fields and mixes the x_3 and transverse derivatives. We shall call it the coupling bilinear form. Note that, with the exception of c_{3T}, these bilinear forms are symmetric and positive. The coupling term can easily be controlled thanks to the Cauchy-Schwarz inequality

$$|c_{3T}\Big(E_3, \mathbf{E}_T\Big)| \leq k_T\Big(E_3, E_3\Big)^{\frac{1}{2}}\, \mathbf{k}_3\Big(\mathbf{E}_T, \mathbf{E}_T\Big)^{\frac{1}{2}}. \tag{2.10}$$

We now deal with the space discretization. For the presentation, we find useful to treat successively the discretization in x_3 first (Section 2.4.1) then in the transverse variables $\mathbf{x}_T$ (Section 2.4.2), which is by the way justified by the "cylindrical structure" of Ω. However, we can reinterpret the result of these two steps as the result of direct 3D discretization (Section 2.4.3).

2.4.1 Semi-discretization in x_3.

For the longitudinal discretization, we decompose the cable Ω into small cylindrical cells

$$\mathcal{C}_{j+\frac{1}{2}} = \{(\mathbf{x}_T, x_3) \in \Omega \ / \ jh \leq x_3 \leq (j+1)h\}, \quad j \in \mathbb{Z} \tag{2.11}$$

These cells of size h in the x_3 direction (h is the longitudinal space step) are separated by transverse cross sections $S_j, j \in \mathbb{Z}$ (see Figure 2.2) where, by definition, $\mathcal{S}_\nu = \{(\mathbf{x}_T, \nu h), \mathbf{x}_T \in S\}$, For all $\nu \in \mathbb{R}$.

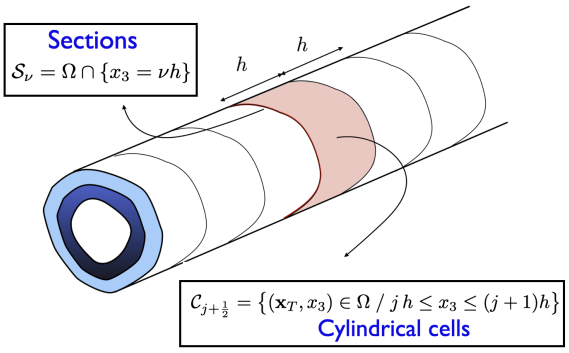

FIGURE 2.2 – Schematic of the sections and the cells of the cable.

We now describe $\mathbf{V}_h$ the approximation space of the 3D space $H(\mathbf{rot};\Omega)$, it is the product space

$$\mathbf{V}_h := \mathbf{V}_{h,T} \times V_{h,\ell} \subset H(\mathbf{rot};\Omega), \tag{2.12}$$

where the approximation of transverse field $\mathbf{E}_T$ lives in $\mathbf{V}_{h,T}$, whereas the approximation of the longitudinal variable E_3 lives in $V_{h,\ell}$. On the one hand, $\mathbf{V}_{h,T}$ is made of $\mathbb{P}_1$ continuous functions in three directions with values in the 2D $H(\mathrm{rot}_T, S)$ space

$$\mathbf{V}_{h,T} := \Big\{\mathbf{E}_{T,h} \in C^0\Big(\mathbb{R}; H(\mathrm{rot}_T, S)\Big) \ / \ \mathbf{E}_T|_{\mathcal{C}_{j+\frac{1}{2}}} \in \mathbb{P}_1\Big(\mathbb{R}; H(\mathrm{rot}_T, S)\Big) \text{ For all } j\Big\}, \tag{2.13}$$

where, $H(\mathrm{rot}_T; S) := \Big\{\mathbf{E}_T \in L^2(\Omega)^2 \times L^2(\Omega) \,/\, \mathrm{rot}_T \mathbf{E}_T \in L^2(\Omega)\Big\}$.

In other words, for any $\mathbf{E}_T \in \mathbf{V}_{h,T}$, denoting $\mathbf{E}_{T,j} = \mathbf{E}_T|_{S_j} \in H(\mathrm{rot}_T, S)$, we have

$$\mathbf{E}_T(\mathbf{x}_T, x_3) = \sum_{j\in\mathbb{Z}} \mathbf{E}_{T,j}(\mathbf{x}_T)\, w_j(x_3), \tag{2.14}$$

where w_j is the usual hat function associated with $x_3 = jh$ (see Figure 2.3).

On the other hand, the space $V_{h,\ell}$ is made of piecewise constant ($\mathbb{P}_0$) functions in x_3 with values in $H^1(S)$

$$V_{h,\ell} := \{E_3 : \Omega \to \mathbb{R} \ / \ E_3|_{\mathcal{C}_{j+\frac{1}{2}}} \in \mathbb{P}_0\Big(\mathbb{R}; H^1(S)\Big) \text{ For all } j\Big\}. \tag{2.15}$$

In other words, for any $E_3 \in V_{h,\ell}$, there exists $E_{3,j+\frac{1}{2}} \in H^1(S), j \in \mathbb{Z}$ such that

$$E_3(\mathbf{x}_T, x_3) = \sum_{j\in\mathbb{Z}} E_{3,j+\frac{1}{2}}(\mathbf{x}_T)\, \chi_{j+\frac{1}{2}}(x_3), \quad E_{3,j+\frac{1}{2}} = E_3|_{S_{j+\frac{1}{2}}} \tag{2.16}$$

where $\chi_{j+\frac{1}{2}}$ is the characteristic function of the interval $(jh, (j+1)h]$ (see Figure 2.3).

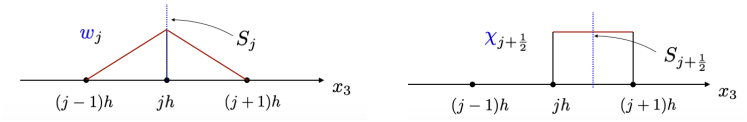

FIGURE 2.3 – The 1D basis functions w_j (left) and $\chi_{j+\frac{1}{2}}$ (right)

The semi-discrete problem is obtained essentially by rewriting the variational formulation (2.8) after replacing the continuous space by the semi-discrete space $\mathbf{V}_h$. More precisely, this problem reads :

Find $\Big(\mathbf{E}_{T,h}, E_{3,h}\Big) \in \mathbf{V}_h := \mathbf{V}_{h,T} \times V_{h,\ell}$ such that for any $\Big(\widetilde{\mathbf{E}}_{T,h}, \widetilde{E}_{3,h}\Big) \in \mathbf{V}_h$,

$$\left|\begin{array}{l} \dfrac{d^2}{dt^2}\, \mathbf{m}_h\Big(\mathbf{E}_{T,h}, \widetilde{\mathbf{E}}_{T,h}\Big) + \mathbf{k}_3\Big(\mathbf{E}_{T,h}, \widetilde{\mathbf{E}}_{T,h}\Big) + \mathbf{k}_{T,h}\Big(\mathbf{E}_{T,h}, \widetilde{\mathbf{E}}_{T,h}\Big) - c_{3T}\Big(E_{3,h}, \widetilde{\mathbf{E}}_{T,h}\Big) = 0, \\ \dfrac{d^2}{dt^2}\, m\Big(E_{3,h}, \widetilde{E}_{3,h}\Big) + k_T\Big(E_{3,h}, \widetilde{E}_{3,h}\Big) - c_{3T}\Big(\widetilde{E}_{3,h}, \mathbf{E}_{T,h}\Big) = 0. \end{array}\right. \tag{2.17}$$

Apart from the functional spaces, there is another difference between (2.8) and (2.17) which makes our approximation non-conforming in the finite element sense. This ingredient is in fact very important for the efficiency of the method and to end up with numerical schemes which will be explicit in x_3. More precisely, we approximate the two bilinear forms that involve transverse fields and do not involve x_3 derivatives, namely $\Big(\mathbf{m}$ and $\mathbf{k}_T\Big)$, by using a quadrature formula in the x_3 direction, transforming them into $\Big(\mathbf{m}_h$ and $\mathbf{k}_{T,h}\Big)$. More precisely, with respect to the definition (2.9) of the exact bilinear forms

$$\Big(\mathbf{m}, \mathbf{k}_T\Big) \quad \longrightarrow \quad \Big(\mathbf{m}_h, \mathbf{k}_{T,h}\Big) \quad \text{via} \quad \int_\Omega \varepsilon\, f \to \oint_\Omega \varepsilon\, f, \quad \int_\Omega \mu^{-1}\, f \to \oint_\Omega \mu^{-1}\, f, \tag{2.18}$$

where $\oint_\Omega \varepsilon\, f$ (resp. $\oint_\Omega \mu^{-1}\, f$) refers to a nodal quadrature formula in x_3, well adapted to the measure $\varepsilon\, d\mathbf{x}$ (resp. $\mu^{-1}\, d\mathbf{x}$). More precisely, for $f \in C^0\Big(\mathbb{R}; L^1(S)\Big) \cap L^1\Big(\Omega\Big)$, we set

$$\oint_\Omega \varepsilon\, f = h \sum_j \int_S \varepsilon_{j+\frac{1}{2}} \left(\frac{f_{j+1} + f_j}{2}\right) d\mathbf{x}_T, \quad f_j = f|_{S_j}, \tag{2.19}$$

where $\varepsilon_{j+\frac{1}{2}}(\mathbf{x}_T)$ holds for the 1D mean value of ε in $S_{j+\frac{1}{2}}$,

$$\text{a.e. } \mathbf{x}_T \in S, \quad \varepsilon_{j+\frac{1}{2}}(\mathbf{x}_T) = \frac{1}{h} \int_{jh}^{(j+1)h} \varepsilon(\mathbf{x}_T, x_3)\, dx_3, \tag{2.20}$$

Remark 2.4.1. *One has the Fubini-like formula*

$$\oint_\Omega \varepsilon\, f = \int_S \Big(\oint_{\mathbb{R}} \varepsilon(\mathbf{x}_T, x_3)\, f(\mathbf{x}_T, x_3)\, dx_3 \Big) d\mathbf{x}_T, \tag{2.21}$$

with the 1D quadrature formula, for any $g \in L^1(\mathbb{R}) \cap C^0(\mathbb{R})$,

$$\oint_{\mathbb{R}} \varepsilon(\mathbf{x}_T, x_3)\, g(x_3)\, dx_3 := h \sum_j \varepsilon_{j+\frac{1}{2}}(\mathbf{x}_T) \Big(\frac{g((j+1)h) + g(jh)}{2}\Big). \tag{2.22}$$

Note that this formula can also be written as

$$\oint_{\mathbb{R}} \varepsilon(\mathbf{x}_T, x_3)\, g(x_3)\, dx_3 := \int_{\mathbb{R}} \varepsilon_h(\mathbf{x}_T, x_3)\, \pi_{1,h} g(x_3)\, dx_3. \tag{2.23}$$

where ε_h *is the piecewise constant approximation of* ε *with its mean value inside each interval*
$(jh, (j+1)h]$ *and* $\pi_{1,h} g$ *is the* $\mathbb{P}_1$*-interpolate of* g.

One has the fundamental property (1D mass lumping) about hat functions

$$\oint_{\mathbb{R}} \varepsilon(\mathbf{x}_T, x_3)\, w_j(x_3)\, w_\ell(x_3)\, dx_3 := 0, \ \textit{for all } \ell \neq j. \tag{2.24}$$

For what follows, it will be useful to have an expanded version of the bilinear forms appearing in (2.17), when acting on the semi-discrete spaces. Since functions in $V_{h,\ell}$ are piecewise constant, the bilinear forms m and k_T are naturally "block diagonal". More precisely, using the decomposition (2.16),

$$\begin{aligned} m\Big(E_{3,h}, \widetilde{E}_{3,h}\Big) &= \sum_{j\in\mathbb{Z}} m_{j+\frac{1}{2}}\Big(E_{3,j+\frac{1}{2}}, \widetilde{E}_{3,j+\frac{1}{2}}\Big) \equiv h \sum_{j\in\mathbb{Z}} \int_{S_{j+\frac{1}{2}}} \varepsilon\, E_{3,j+\frac{1}{2}}\, \widetilde{E}_{3,j+\frac{1}{2}}, \\ k_T\Big(E_{3,h}, \widetilde{E}_{3,h}\Big) &= \sum_{j\in\mathbb{Z}} k_{j+\frac{1}{2}}\Big(E_{3,j+\frac{1}{2}}, \widetilde{E}_{3,j+\frac{1}{2}}\Big) \equiv h \sum_{j\in\mathbb{Z}} \int_{S_{j+\frac{1}{2}}} \mu^{-1}\, \nabla_T E_{3,j+\frac{1}{2}} \cdot \nabla_T \widetilde{E}_{3,j+\frac{1}{2}}. \end{aligned} \tag{2.25}$$

In the same way, thanks to the quadrature (2.19), the bilinear forms $\mathbf{m}_h$ and $\mathbf{k}_{T,h}$ are block diagonal too. More precisely, using the decomposition (2.14),

$$\begin{aligned} \mathbf{m}_h\Big(\mathbf{E}_{T,h}, \widetilde{\mathbf{E}}_{T,h}\Big) &= \sum_{j\in\mathbb{Z}} \mathbf{m}_{h,j}\Big(\mathbf{E}_{T,j}, \widetilde{\mathbf{E}}_{T,j}\Big) \equiv h \sum_{j\in\mathbb{Z}} \int_{S_j} \varepsilon\, \mathbf{E}_{T,j} \cdot \widetilde{\mathbf{E}}_{T,j}, \\ \mathbf{k}_{T,h}\Big(\mathbf{E}_{T,h}, \widetilde{\mathbf{E}}_{T,h}\Big) &= \sum_{j\in\mathbb{Z}} \mathbf{k}_{h,j}\Big(\mathbf{E}_{T,j}, \widetilde{\mathbf{E}}_{T,j}\Big) \equiv h \sum_{j\in\mathbb{Z}} \int_{S_j} \mu^{-1}\, \mathrm{rot}_T \mathbf{E}_{T,j}\, \mathrm{rot}_T \widetilde{\mathbf{E}}_{T,j}. \end{aligned} \tag{2.26}$$

Finally, for the last two bilinear forms, one computes that

$$\begin{aligned} \mathbf{k}_3\Big(\mathbf{E}_{T,h}, \widetilde{\mathbf{E}}_{T,h}\Big) &= h \sum_{j\in\mathbb{Z}} \mu^{-1}_{j+\frac{1}{2}} \int_S \frac{\mathbf{E}_{T,j+1} - \mathbf{E}_{T,j}}{h} \cdot \frac{\widetilde{\mathbf{E}}_{T,j+1} - \widetilde{\mathbf{E}}_{T,j}}{h}, \\ c_{3T}\Big(E_{3,h}, \widetilde{\mathbf{E}}_{T,h}\Big) &= h \sum_{j\in\mathbb{Z}} \mu^{-1}_{j+\frac{1}{2}} \int_S \nabla_T E_{3,j+\frac{1}{2}} \cdot \frac{\widetilde{\mathbf{E}}_{T,j+1} - \widetilde{\mathbf{E}}_{T,j}}{h}, \end{aligned} \tag{2.27}$$

where, as in (2.20), we have defined

$$\mu^{-1}_{j+\frac{1}{2}}(\mathbf{x}_T) = \frac{1}{h} \int_{jh}^{(j+1)h} \mu^{-1}(\mathbf{x}_T, x_3)\, dx_3 \quad \text{a.e. } \mathbf{x}_T \in S. \tag{2.28}$$

2.4.2 Full space discretization

For the discretization in the transverse variables, we introduce a conforming triangular mesh $\mathcal{T}$ (in the usual finite element sense) of S with step size h_T (Figure 2.4), namely the transverse space step. In the sequel, we shall denote N the number of nodes of this mesh and N_e the number of (interior) edges. We shall use the letter $\mathbf{h}$ to denote the set of approximation parameters in space, namely $\mathbf{h} := (h, h_T)$. The fully discrete space, indexed with $\mathbf{h}$ takes the same form of the semi-discrete space as in (2.12),

$$\mathbf{V_h} = \mathbf{V_{h,T}} \times V_{\mathbf{h},\ell}.$$

The transverse field $\mathbf{E_T}$ is searched piecewise linear continuously in x_3 with value in the classical 2D Nedelec space [41],[43] denoted $\mathbf{V}_{h_T}(S)$ (with respect to (2.13), we simply replace $H(\mathrm{rot}_T, S)$ by $\mathbf{V}_{h_T}(S)$).

$$\mathbf{V_{h,T}} := \Big\{ \mathbf{E}_{T,h} \in C^0\Big(\mathbb{R}; \mathbf{V}_{h_T}(S)\Big) \ / \ \mathbf{E}_T|_{\mathfrak{e}_{j+\frac{1}{2}}} \in \mathbb{P}_1\Big(\mathbb{R}; \mathbf{V}_{h_T}(S)\Big) \ \forall\, j \Big\}. \tag{2.29}$$

with
$$\begin{cases} \mathbf{V}_{h_T}(S) := \Big\{ \mathbf{E}_T \in H(\mathrm{rot}_T, S)\Big) \ / \ \forall\, K \in \mathcal{T}, \mathbf{E}_T|_K \in \mathcal{N}_{2D} \Big\}, \\ \mathcal{N}_{2D} := \Big\{ a\,(x_2, -x_1)^t + \mathbf{b}, (a, \mathbf{b}) \in \mathbb{R} \times \mathbb{R}^2 \Big\} \subset \mathbb{P}_1^2. \end{cases} \tag{2.30}$$

The longitudinal field E_3 is searched piecewise constant in x_3 with value in the standard $\mathbb{P}_1$ finite element space for $H^1(S)$ (with respect to (2.15), we simply replace $H^1(S)$ by $V_{h_T}(S)$),

$$\begin{cases} V_{\mathbf{h},\ell} := \Big\{ E_3 : \Omega \to \mathbb{R} \ / \ \forall\, j, \forall\, x_3 \in [jh, (j+1)h] \ \ E_3(\cdot, x_3) = E_{3,j+\frac{1}{2}} \in V_{h_T}(S) \Big\}, \\ V_{h_T}(S) := \Big\{ E_3 \in H^1(S) \ / \ \forall\, K \in \mathcal{T}, \ E_3|_K \in \mathbb{P}_1 \Big\}. \end{cases} \tag{2.31}$$

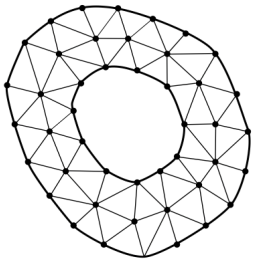

FIGURE 2.4 – Triangular mesh of S with step size h_T

We have thus two types of degrees of freedom for the discrete electric field. The first one, associated to the transverse field, denoted $\mathbb{E}_{T,\mathbf{h}} \equiv \Big\{ \mathbb{E}_{T,j} \Big\}$, $\mathbb{E}_{T,j} \in \mathbb{R}^{N_e}$, is the vector of the tangential components of the discrete transverse electric field along the edges in the cross section S_j. These degrees of freedom are represented with the red arrows in Figure 2.5 (in 2D) and in Figure 2.6 (in 3D).

The second one, for the longitudinal field, is denoted $\mathbb{E}_{3,\mathbf{h}} \equiv \Big\{ \mathbb{E}_{3,j+\frac{1}{2}} \Big\}$, where $\mathbb{E}_{3,j+\frac{1}{2}} \in \mathbb{R}^N$ is the vector of the values of the discrete longitudinal field at the nodes of the mesh. These degrees of freedom are represented with the blue dots in Figure 2.5 (in 2D) and with blue arrows in Figure 2.6 (in 3D).

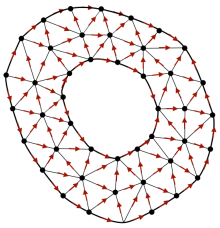

Transverse field in each section S_j

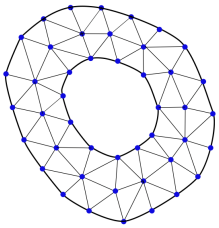

Longitudinal field in each section $S_{j+\frac{1}{2}}$

FIGURE 2.5 – Two types of degrees of freedom

In the end we have the transverse field unknowns $\mathbb{E}_{T,j}$ and longitudinal field unknowns $\mathbb{E}_{3,j+\frac{1}{2}}$ alternate from one cross section to the other (Figure 2.5 and 2.6).

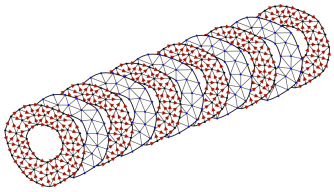

FIGURE 2.6 – Degrees of freedom in the 3D mesh.

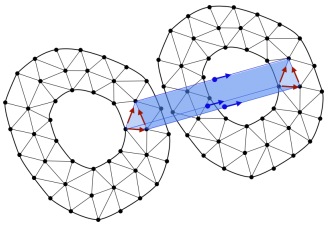

FIGURE 2.7 – Prismatic mesh.

2.4.3 Reinterpretation as prismatic edge elements

It is worthwhile reinterpreting the space as the result of a 3D finite element approximation of $H(\mathbf{rot},\Omega)$ based on a prismatic mesh $\mathcal{T}_{3D}$ of the cable Ω,

$$\mathcal{T}_{3D} := \Big\{\mathcal{P}_{K,j} \;/\; K \in \mathcal{T}, j \in \mathbb{Z}\Big\} \quad \text{such that } \Omega = \bigcup_{K,j} \mathcal{P}_{K,j}, \tag{2.32}$$

where the prim $\mathcal{P}_{K,j}$ is defined as (note that it has only longitudinal or transverse faces, cf. Figure 2.7)

$$\mathcal{P}_{K,j} = K \times [jh, (j+1)h]. \tag{2.33}$$

The space is nothing but a space of prismatic edge elements, namely,

$$\mathbf{V_h} := \Big\{\mathbf{E_h} \in H(\mathbf{rot},\Omega) \;/\; \forall\, \mathcal{P}_{K,j} \in \mathcal{T}_{3D},\ \mathbf{E_h}|_{\mathcal{P}_{K,j}} \in \mathcal{R}\Big\}, \tag{2.34}$$

where $\mathcal{R} = \Big\{\mathbf{E} = (\mathbf{E}_T, E_3) \;/\; \mathbf{E}_T(\cdot,x_3) \in \mathbb{P}_1(\mathbb{R};\mathcal{N}_{2D}),\ E_3(\cdot,x_3) \in \mathbb{P}_0(\mathbb{R};\mathbb{P}_1(\mathbb{R}^2))\Big\} \subset \mathbb{P}_1^3$. Note that the use of edge elements on prisms has been already studied (see [15, 20]), in regard to these works, the originality of our approach lies in the time discretization, that will treat differently in-plane (i.e. in the plane of the sections) and out-of-plane interactions between degrees of freedom.

2.4.4 The semi-discrete scheme and its algebraic form

The fully semi-discrete variational problem reads

Find $\Big(\mathbf{E}_{T,\mathbf{h}}, E_{3,\mathbf{h}}\Big) \in \mathbf{V_h} := \mathbf{V}_{\mathbf{h},T} \times V_{\mathbf{h},\ell}$ such that for any $\Big(\mathbf{E}_{T,\mathbf{h}}, E_{3,\mathbf{h}}\Big) \in \mathbf{V_h}$,

$$\left|\begin{array}{l} \dfrac{d^2}{dt^2}\,\mathbf{m}_h\Big(\mathbf{E}_{T,\mathbf{h}}, \widetilde{\mathbf{E}}_{T,\mathbf{h}}\Big) + \mathbf{k}_3\Big(\mathbf{E}_{T,\mathbf{h}}, \widetilde{\mathbf{E}}_{T,\mathbf{h}}\Big) + \mathbf{k}_{T,h}\Big(\mathbf{E}_{T,\mathbf{h}}, \widetilde{\mathbf{E}}_{T,\mathbf{h}}\Big) - c_{3T}\Big(E_{3,\mathbf{h}}, \widetilde{\mathbf{E}}_{T,\mathbf{h}}\Big) = 0, \\ \dfrac{d^2}{dt^2}\, m\Big(E_{3,\mathbf{h}}, \widetilde{E}_{3,\mathbf{h}}\Big) + k_T\Big(E_{3,\mathbf{h}}, \widetilde{E}_{3,\mathbf{h}}\Big) - c_{3T}\Big(\widetilde{E}_{3,\mathbf{h}}, \mathbf{E}_{T,\mathbf{h}}\Big) = 0. \end{array}\right. \tag{2.35}$$

To write the problem in a more algebraic form, we introduce here the (infinite) vector degrees of freedom namely (with obvious notation)

$$\mathbb{E}_{\mathbf{h}} = \begin{pmatrix} \mathbb{E}_{T,\mathbf{h}} \\ \mathbb{E}_{3,\mathbf{h}} \end{pmatrix} \equiv \begin{pmatrix} \mathbb{E}_{T,j} \\ \mathbb{E}_{3,j+\frac{1}{2}} \end{pmatrix} \in \mathbb{V}_{\mathbf{h}} := \mathbb{V}_{\mathbf{h},T} \times \mathbb{V}_{\mathbf{h},3} \tag{2.36}$$

where $\mathbb{V}_{\mathbf{h},T}$ and $\mathbb{V}_{\mathbf{h},3}$ are the Hilbert spaces

$$\mathbb{V}_{\mathbf{h},T} = \ell^2\Big(\mathbb{Z}, \mathbb{R}^{N_e}\Big), \quad \mathbb{V}_{\mathbf{h},3} = \ell^2(\mathbb{Z}, \mathbb{R}^N).$$

According to the above, it is clear that (2.35) has an equivalent algebraic form,

$$\mathbf{M}_{\mathbf{h}} \frac{d^2\mathbb{E}_{\mathbf{h}}}{dt^2} + \mathbf{K}_{\mathbf{h}}\, \mathbb{E}_{\mathbf{h}} = 0. \tag{2.37}$$

where $\mathbf{M_h}$ and $\mathbf{K_h}$ are the mass and stiffness matrices in $\mathbb{V}_{\mathbf{h}}$ (their obvious and classical definition is omitted here). According to the decomposition of $\mathbf{V_h}$ between transverse and longitudinal fields , the mass matrix $\mathbf{M_h}$ has the following block diagonal form

$$\mathbf{M}_{\mathbf{h}} = \begin{pmatrix} \mathbf{M}_{\mathbf{h}}^T & 0 \\ 0 & M_{\mathbf{h}}^3 \end{pmatrix} \tag{2.38}$$

and, in particular, thanks to numerical quadrature, $\mathbf{M}_{\mathbf{h}}^T$ (resp. $\mathbf{M}_{\mathbf{h}}^3$) is block diagonal by sections with blocks of dimension N_e (resp. N). On the other hand, the stiffness matrix $\mathbf{K_h}$ can be written, according to (2.35) as

$$\mathbf{K}_{\mathbf{h}} = \begin{pmatrix} \mathbf{K}_{3,\mathbf{h}} + \mathbf{K}_{T,\mathbf{h}} & \mathbf{C}_{3T,\mathbf{h}} \\ \mathbf{C}_{3T,\mathbf{h}}^* & K_{T,\mathbf{h}} \end{pmatrix} \tag{2.39}$$

where there are also some block decomposition's by sections. More precisely, the global problem can be rewritten "section by section", separating the roles of the transverse and longitudinal fields as follows

$$\left|\begin{array}{l} \mathbb{M}_j \dfrac{d^2\mathbb{E}_{T,j}}{dt^2} + \mathbb{K}_{T,j}\, \mathbb{E}_{T,j} - \dfrac{1}{h}\left(\mathbb{M}_{j+\frac{1}{2}}\, \dfrac{\mathbb{E}_{T,j+1} - \mathbb{E}_{T,j}}{h} - \mathbb{M}_{j-\frac{1}{2}}\, \dfrac{\mathbb{E}_{T,j} - \mathbb{E}_{T,j-1}}{h}\right) \\ \qquad\qquad + \dfrac{\mathbb{C}_{3T,j+\frac{1}{2}}\, \mathbb{E}_{3,j+\frac{1}{2}} - \mathbb{C}_{3T,j-\frac{1}{2}} \mathbb{E}_{3,j-\frac{1}{2}}}{h} = 0, \\ \mathrm{M}_{j+\frac{1}{2}} \dfrac{d^2\mathbb{E}_{3,j+\frac{1}{2}}}{dt^2} + \mathrm{K}_{T,j+\frac{1}{2}}\, \mathbb{E}_{3,j+\frac{1}{2}} - \mathbb{C}_{3T,j+\frac{1}{2}}^* \dfrac{\mathbb{E}_{T,j+1} - \mathbb{E}_{T,j}}{h} = 0, \end{array}\right. \tag{2.40}$$

which well emphasizes how the various "interface unknowns" are coupled or decoupled. Note that

— The matrices $\mathbb{M}_j$, $\mathbb{M}_{j+\frac{1}{2}}$ and $\mathbb{K}_{T,j}$ are of dimension $N_e \times N_e$: $\mathbb{M}_j$ (resp. $\mathbb{M}_{j+\frac{1}{2}}$) is a 2D (vectorial) mass matrix (which is not diagonal) corresponding to the multiplication by ε (resp. by μ^{-1}) while $\mathbb{K}_{T,j}$ is a 2D stiffness matrix corresponding to the action of the operator $\mathbf{rot}_T(\mu^{-1}\mathrm{rot}_T)$.

— The matrices $\mathrm{M}_{j+\frac{1}{2}}$ and $\mathrm{K}_{T,j+\frac{1}{2}}$ are of dimension $N \times N$: this corresponds to the multiplication by ε while $\mathrm{K}_{T,j+\frac{1}{2}}$ is a 2D stiffness matrix corresponding to the action of the operator $\mathrm{div}_T(\mu^{-1}\nabla_T)$.

— The matrices $\mathbb{C}_{3T,j+\frac{1}{2}}$ are $N \times N_e$ and correspond to the action of the operator $\mu^{-1}\nabla_T$.

— Their transpose corresponds $\mathbb{C}^*_{3T,j+\frac{1}{2}}$ to the action of the operator $-\mathrm{div}_T(\mu^{-1}\cdot)$.

2.5 An explicit/implicit time discretization scheme

Our method will be based on a tricky decomposition of the stiffness matrix $\mathbf{K_h}$ (cf. (2.39))

$$\mathbf{K_h} = \mathbf{K_h^i} + \mathbf{K_h^e} \quad \text{where} \quad \mathbf{K_h^i} = \begin{pmatrix} \mathbf{K}_{T,\mathbf{h}} & 0 \\ 0 & K_{T,\mathbf{h}} \end{pmatrix} \quad \text{and} \quad \mathbf{K_h^e} = \begin{pmatrix} \mathbf{K}_{3,\mathbf{h}} & \mathbf{C}_{3T,\mathbf{h}} \\ \mathbf{C}^*_{3T,\mathbf{h}} & 0 \end{pmatrix}. \tag{2.41}$$

The interest of the decomposition lies in the following double observation

— $\mathbf{K_h^i}$ is adapted to implicit time discretization because the matrix is positive and block diagonal : for this reason it is "easy" to invert (it corresponds to a series 2D problems, see section 2.5.2).

— Oppositely $\mathbf{K_h^e}$ is adapted to explicit time discretization because of the presence of the index "3" which corresponds to the x_3 derivative : this matrix couples all the interfaces and has no sign.

2.5.1 A hybrid implicit-explicit scheme

According to (2.41), we rewrite (2.37) as

$$\mathbf{M_h}\frac{d^2\mathbb{E}_\mathbf{h}}{dt^2} + \mathbf{K_h^e}\,\mathbb{E}_\mathbf{h} + \mathbf{K_h^i}\,\mathbb{E}_\mathbf{h} = 0,$$

and propose a numerical scheme in which $\mathbb{E}_\mathbf{h}$ at time $t^n = n\Delta t$ is approximated differently depending on the fact that it is in factor of $\mathbf{K_h^e}$ or $\mathbf{K_h^i}$. More precisely, and according to what we said in the introduction of this section, we propose the following hybrid implicit-explicit leap frog scheme, in which $\theta \in [0,1]$ is a parameter,

$$\mathbf{M_h}\frac{\mathbb{E}_\mathbf{h}^{n+1} - 2\,\mathbb{E}_\mathbf{h}^n + \mathbb{E}_\mathbf{h}^{n-1}}{\Delta t^2} + \mathbf{K_h^i}\,\{\mathbb{E}_\mathbf{h}^n\}_\theta + \mathbf{K_h^e}\,\mathbb{E}_\mathbf{h}^n = 0, \tag{2.42}$$

where $\{\mathbb{E}_\mathbf{h}^n\}_\theta$ corresponds to the weighted mean value

$$\{\mathbb{E}_\mathbf{h}^n\}_\theta := \theta\,\mathbb{E}_\mathbf{h}^{n+1} + (1-2\theta)\,\mathbb{E}_\mathbf{h}^n + \theta\,\mathbb{E}_\mathbf{h}^{n-1}, \quad \theta \in [0,1]. \tag{2.43}$$

Clearly, this scheme is a mix between the explicit leap frog scheme and the implicit θ-scheme (or centered Newmark scheme). It is obviously second order accurate in Δt whatever θ is. How implicit this scheme is the subject of the next section.

Remark 2.5.1. *The above ideas already appeared in the literature in various contexts and for different purposes. One class of works concerns locally implicit time stepping in which different parts of the computational domain are treated differently : see for instance [45] or more recently [30] for fourth order schemes. In [18], [3], the objective was to treat in a particular way the boundary condition arising from the formulation of elastodynamics by way of potentials introduced for treating separately the two types of waves. In [29], the objective was to treat explicitly the linear part of the model and implicitly the nonlinear one. Here, these are the direction of space differentiation, longitudinal or transverse, which are treated in a different manner. In some sense, except for the fact that we are dealing with a strongly anisotropic problem, our work has some similarities with the ADI schemes proposed by Fornberg and Lee (see [37], [38] and [28] for an analysis).*

2.5.2 Computational complexity

According to the rewriting "section by section" (2.40) of the discrete problem, we can rewrite the scheme

$$\begin{aligned}
&\mathbb{M}_j \frac{\mathbb{E}^{n+1}_{T,j} - 2\mathbb{E}^{n}_{T,j} + \mathbb{E}^{n-1}_{T,j}}{\Delta t^2} + \mathbb{K}_{T,j}\left(\theta\, \mathbb{E}^{n+1}_{T,j} + (1-2\theta)\, \mathbb{E}^{n}_{T,j} + \theta\, \mathbb{E}^{n-1}_{T,j}\right) \\
&-\frac{1}{h}\left(\mathbb{M}_{j+\frac{1}{2}}\, \frac{\mathbb{E}^{n}_{T,j+1} - \mathbb{E}^{n}_{T,j}}{h} - \mathbb{M}_{j-\frac{1}{2}}\, \frac{\mathbb{E}^{n}_{T,j} - \mathbb{E}^{n}_{T,j-1}}{h}\right) + \frac{\mathbb{C}_{3T,j+\frac{1}{2}}\, \mathbb{E}^{n}_{3,j+\frac{1}{2}} - \mathbb{C}_{3T,j-\frac{1}{2}} \mathbb{E}^{n}_{3,j-\frac{1}{2}}}{h} = 0, \\
&\mathrm{M}_{j+\frac{1}{2}} \frac{\mathbb{E}^{n+1}_{3,j+\frac{1}{2}} - 2\mathbb{E}^{n}_{3,j+\frac{1}{2}} + \mathbb{E}^{n-1}_{3,j+\frac{1}{2}}}{\Delta t^2} + \mathrm{K}_{T,j+\frac{1}{2}}\left(\theta\, \mathbb{E}^{n+1}_{3,j+\frac{1}{2}} + (1-2\theta)\, \mathbb{E}^{n}_{3,j+\frac{1}{2}} + \theta\, \mathbb{E}^{n-1}_{3,j+\frac{1}{2}}\right) \\
&\qquad\qquad - \mathbb{C}^{*}_{3T,j+\frac{1}{2}} \frac{\mathbb{E}^{n}_{T,j+1} - \mathbb{E}^{n}_{T,j}}{h} = 0
\end{aligned}$$

Looking at where the superscript $n+1$ appears in the above equations, one sees that at each time step one has to invert (this can be done in parallel) the matrices

$$\mathbb{M}_j + \theta\, \Delta t^2 \mathbb{K}_{T,j} \quad \text{and } \mathrm{M}_{j+\frac{1}{2}} + \theta\, \Delta t^2 \mathrm{K}_{T,j+\frac{1}{2}}.$$

This illustrates the fact that the scheme is implicit only in the transverse direction. This corresponds to solving numerically, using appropriate finite elements,

- a series of coercive 2D vectorial curl-curl problems of the type

$$\gamma\, \mathbf{rot}_T(\mu^{-1}\mathrm{rot}_T \mathbf{u}) + \mathbf{u} = \mathbf{g} \quad \text{in S}, \quad \gamma = \theta\, \Delta t^2\, \varepsilon^{-1} > 0,$$

- a series of coercive 2D scalar div-grad problems of the type

$$-\gamma\, \mathrm{div}_T(\mu^{-1}\nabla_T u) + u = g \quad \text{in S}, \quad \gamma = \theta\, \Delta t^2\, \varepsilon^{-1} > 0.$$

2.6 Stability analysis of the fully discrete scheme

For our main theorem, we need to introduce the function $\alpha_h(\mathbf{x}_T) > 0$ defined by :

$$\alpha_h(\mathbf{x}_T)^2 := \sup_{u_h \in \mathbb{P}_{1,h}} \frac{\int_{\mathbb{R}} \mu(\cdot, \mathbf{x}_T)^{-1} |u_h'|^2}{\oint_{\mathbb{R}} \varepsilon(\cdot, \mathbf{x}_T) |u_h|^2}, \tag{2.44}$$

where

$$\mathbb{P}_{1,h} := \{u_h \in C^0(\mathbb{R}) \cap L^2(\mathbb{R}) \,/\, \forall\, j \in \mathbb{Z},\, u_h|_{[jh,(j+1)h]} \in \mathbb{P}_1\} \tag{2.45}$$

It is also useful to introduce the velocity of electromagnetic waves in Ω

$$\forall\, \mathbf{x} \in \Omega, \quad c(\mathbf{x}) = \varepsilon(\mathbf{x})^{-\frac{1}{2}}\mu(\mathbf{x})^{-\frac{1}{2}}, \quad c^+ := \sup_{\Omega} c(\mathbf{x}). \tag{2.46}$$

Theorem 2.6.1. *The fully discrete scheme (2.42) is stable if* $\theta > \dfrac{1}{4}$ *and*

$$\frac{\Delta t^2}{4}\,\|\alpha_h\|_\infty^2 \le \frac{4\theta - 1}{4\theta} \tag{2.47}$$

with α_h *defined in (2.44). The CFL condition (2.47) is in particular satisfied as soon as*

$$\frac{c^+\Delta t}{h} < \sqrt{\frac{4\theta - 1}{4\theta}}. \tag{2.48}$$

Proof. Since there is no possible ambiguity, and for the sake of simplicity, we shall use the same notation $\big(\cdot,\cdot\big)$ for inner products in $\mathbb{V}_{\mathbf{h},T}$ and $\mathbb{V}_{\mathbf{h},3}$. Below, we refer to (2.36) and the dot is systematically used for the appropriate Euclidean scalar product that may change from one occurrence to the other :

$$\begin{gathered}\Big(\mathbb{U}_{\mathbf{h},T}, \widetilde{\mathbb{U}}_{\mathbf{h},T}\Big) := \sum_{j\in\mathbb{Z}} \mathbb{U}_{T,j}\cdot\widetilde{\mathbb{U}}_{T,j}, \quad \Big(\mathbb{U}_{\mathbf{h},3}, \widetilde{\mathbb{U}}_{\mathbf{h},3}\Big) := \sum_{j\in\mathbb{Z}} \mathbb{U}_{3,j+\frac{1}{2}}\cdot\widetilde{\mathbb{U}}_{3,j+\frac{1}{2}},\\ \Big(\mathbb{U}_{\mathbf{h}}, \widetilde{\mathbb{U}}_{\mathbf{h}}\Big) = \Big(\mathbb{U}_{\mathbf{h},T}, \widetilde{\mathbb{U}}_{\mathbf{h},T}\Big) + \Big(\mathbb{U}_{\mathbf{h},3}, \widetilde{\mathbb{U}}_{\mathbf{h},3}\Big).\end{gathered} \tag{2.49}$$

The proof is done in three steps using an energy approach.

Step 1 : Discrete energy conservation. We use the two key (but standard) identities :

$$\mathbb{E}_{\mathbf{h}}^n = \{\mathbb{E}_{\mathbf{h}}^n\}_{\frac{1}{4}} - \frac{1}{4}\Big(\mathbb{E}_{\mathbf{h}}^{n+1} - 2\,\mathbb{E}_{\mathbf{h}}^n + \mathbb{E}_{\mathbf{h}}^{n-1}\Big), \quad \{\mathbb{E}_{\mathbf{h}}^n\}_\theta = \{\mathbb{E}_{\mathbf{h}}^n\}_{\frac{1}{4}} + \Big(\theta - \frac{1}{4}\Big)\Big(\mathbb{E}_{\mathbf{h}}^{n+1} - 2\,\mathbb{E}_{\mathbf{h}}^n + \mathbb{E}_{\mathbf{h}}^{n-1}\Big).$$

This allows us to rewrite our scheme as a perturbation of the $\dfrac{1}{4}$-scheme.

$$\mathbf{M}_h(\Delta t)\,\frac{\mathbb{E}_{\mathbf{h}}^{n+1} - 2\,\mathbb{E}_{\mathbf{h}}^n + \mathbb{E}_{\mathbf{h}}^{n-1}}{\Delta t^2} + \mathbf{K}_{\mathbf{h}}\,\{\mathbb{E}_{\mathbf{h}}^n\}_{\frac{1}{4}} = 0,$$

where we have set

$$\mathbf{M}_{\mathbf{h}}(\Delta t) = \mathbf{M}_h^i(\Delta t) - \frac{\Delta t^2}{4}\,\mathbf{K}_{\mathbf{h}}^e \quad \text{and} \quad \mathbf{M}_h^i(\Delta t) := \mathbf{M}_{\mathbf{h}} + \Big(\theta - \frac{1}{4}\Big)\,\Delta t^2\,\mathbf{K}_{\mathbf{h}}^i. \tag{2.50}$$

Taking the scalar product (in $\mathbb{V}_{\mathbf{h}} := \mathbb{V}_{\mathbf{h},T} \times \mathbb{V}_{\mathbf{h},3}$) of the above equation with $\dfrac{\mathbb{E}_{\mathbf{h}}^{n+1} - \mathbb{E}_{\mathbf{h}}^{n-1}}{2\Delta t}$ we classically deduce –thanks to the symmetry of all matrices– the conservation of the discrete energy

$$\mathcal{E}_{\mathbf{h}}^{n+\frac{1}{2}} := \frac{1}{2}\left[\left(\mathbf{M}_{\mathbf{h}}(\Delta t)\frac{\mathbb{E}_{\mathbf{h}}^{n+1} - \mathbb{E}_{\mathbf{h}}^n}{\Delta t}, \frac{\mathbb{E}_{\mathbf{h}}^{n+1} - \mathbb{E}_{\mathbf{h}}^n}{\Delta t}\right) + \left(\mathbf{K}_{\mathbf{h}}\Big(\frac{\mathbb{E}_{\mathbf{h}}^{n+1} + \mathbb{E}_{\mathbf{h}}^n}{2}\Big), \frac{\mathbb{E}_{\mathbf{h}}^{n+1} + \mathbb{E}_{\mathbf{h}}^n}{2}\right)\right].$$

Step 2 : Derivation of the sufficient stability condition (2.47).

This will be simply obtained from showing the positivity of the discrete energy $\mathcal{E}_{\mathbf{h}}^{n+\frac{1}{2}}$, that amounts to the positivity of the modified mass matrix $\mathbf{M}_h(\Delta t)$. The idea is first to ensure the positivity of $\mathbf{M}_{\mathbf{h}}^i(\Delta t)$ only choosing adequately θ (typically $\theta > \frac{1}{4}$) then to control $\Delta t^2\,\mathbf{K}_{\mathbf{h}}^e$ by playing with Δt. As we are going to see this can be done by imposing to Δt a lower bound that only sees the longitudinal space step h.

To be more precise, assuming $\theta > \frac{1}{4}$, we first obtain a lower bound of the quadratic form associated with $\mathbf{M}_h^i(\Delta t)$. Recalling that

$$\mathbf{M}_{\mathbf{h}} = \begin{pmatrix} \mathbf{M}_{\mathbf{h}}^T & 0 \\ 0 & M_{\mathbf{h}}^3 \end{pmatrix} \quad \text{and} \quad \mathbf{K}_{\mathbf{h}}^i = \begin{pmatrix} \mathbf{K}_{T,\mathbf{h}} & 0 \\ 0 & K_{T,\mathbf{h}} \end{pmatrix},$$

we drop, in the expression of $\mathbf{M}_{\mathbf{h}}^i(\Delta t)$, the positive blocks associated with $M_{\mathbf{h}}^3$ and $(\theta - \frac{1}{4})\mathbf{K}_{T,\mathbf{h}}$, one deduces that for any $\mathbb{U}_{\mathbf{h}} \in \mathbb{V}_{\mathbf{h}}$,

$$\Big(\mathbf{M}_{\mathbf{h}}^i(\Delta t)\mathbb{U}_{\mathbf{h}}, \mathbb{U}_{\mathbf{h}}\Big) \geq \Big(\mathbf{M}_{\mathbf{h}}^T\,\mathbb{U}_{T,\mathbf{h}}, \mathbb{U}_{T,\mathbf{h}}\Big) + \Big(\theta - \frac{1}{4}\Big)\,\Delta t^2 \Big(K_{T,\mathbf{h}}\mathbb{U}_{3,\mathbf{h}}, \mathbb{U}_{3,\mathbf{h}}\Big), \tag{2.51}$$

where we draw again the attention of the reader to the fact that, according to (2.49) and depending on the context, the notation $(\cdot,\cdot)$ is the scalar product in $\mathbb{V}_{\mathbf{h}}$, $\mathbb{V}_{\mathbf{h},T}$ and $\mathbb{V}_{\mathbf{h},3}$. We now obtain an upper bound for the quadratic form associated with $\mathbf{K}_{\mathbf{h}}^e$. For this, we first remark that inequality (2.10) results in

$$\Big(\mathbf{C}_{3T,\mathbf{h}}\mathbb{U}_{3,\mathbf{h}}, \mathbb{U}_{T,\mathbf{h}}\Big) \equiv \Big(\mathbb{U}_{3,\mathbf{h}}, \mathbf{C}_{3T,\mathbf{h}}^*\mathbb{U}_{T,\mathbf{h}}\Big) \leq \Big(K_{T,\mathbf{h}}\mathbb{U}_{3,\mathbf{h}}, \mathbb{U}_{3,\mathbf{h}}\Big)^{\frac{1}{2}} \Big(\mathbf{K}_{3,\mathbf{h}}\mathbb{U}_{\mathbf{h},T}, \mathbb{U}_{\mathbf{h},T}\Big)^{\frac{1}{2}}, \tag{2.52}$$

so that, from the block decomposition (2.41) of $\mathbf{K}_{\mathbf{h}}^e$, one deduces the inequality

$$\big|\Big(\mathbf{K}_{\mathbf{h}}^e\mathbb{U}_{\mathbf{h}}, \mathbb{U}_{\mathbf{h}}\Big)\big| \leq \Big(\mathbf{K}_{3,\mathbf{h}}\mathbb{U}_{\mathbf{h},T}, \mathbb{U}_{\mathbf{h},T}\Big) + 2\,\Big(K_{T,\mathbf{h}}\mathbb{U}_{3,\mathbf{h}}, \mathbb{U}_{3,\mathbf{h}}\Big)^{\frac{1}{2}} \Big(\mathbf{K}_{3,\mathbf{h}}\mathbb{U}_{\mathbf{h},T}, \mathbb{U}_{\mathbf{h},T}\Big)^{\frac{1}{2}}.$$

Finally, in order to exploit (2.51), we control the matrix $\mathbf{K}_{3,\mathbf{h}}$ with the help of the mass matrix $\mathbf{M}_{\mathbf{h}}^T$ that appears in the lower bound (2.51). This is where the longitudinal space step h will appear via the function α_h.More precisely, let $\mathbf{U}_{h,T} \in \mathbf{V}_{h,T}$ be associated to the vector $\mathbb{U}_{\mathbf{h},T} \in \mathbb{V}_{\mathbf{h},T}$, by definition of $\mathbf{K}_{3,\mathbf{h}}$

$$\Big(\mathbf{K}_{3,\mathbf{h}}\mathbb{U}_{\mathbf{h},T}, \mathbb{U}_{\mathbf{h},T}\Big) = \mathbf{k}_3(\mathbf{U}_{h,T}, \mathbf{U}_{h,T}) = \int_\Omega \mu^{-1}|\partial_3\mathbf{U}_{h,T}|^2.$$

Using the Fubini theorem and $\mathbf{U}_{h,T} = (\mathbf{U}_{h,1}, \mathbf{U}_{h,2})$, we get

$$\Big(\mathbf{K}_{3,\mathbf{h}}\mathbb{U}_{\mathbf{h},T}, \mathbb{U}_{\mathbf{h},T}\Big) = \int_S \Big(\int_{\mathbb{R}} \mu^{-1}(\mathbf{x}_T, x_3)\Big(|\partial_3\mathbf{U}_{h,1}(\mathbf{x}_T, x_3)|^2 + |\partial_3\mathbf{U}_{h,2}(\mathbf{x}_T, x_3)|^2\Big)\,dx_3\Big) d\mathbf{x}_T.$$

Then, by definition (2.44) of the function α_h, and since, for fixed $\mathbf{x}_T$, each function $\mathbf{U}_{h,1}(\mathbf{x}_T,\cdot)$ and $\mathbf{U}_{h,1}(\mathbf{x}_T,\cdot)$ belongs to $\mathbb{P}_{1,h}$ by definition (2.13) of $\mathbf{V}_{h,T}$, we have

$$\Big(\mathbf{K}_{3,\mathbf{h}}\mathbb{U}_{\mathbf{h},T}, \mathbb{U}_{\mathbf{h},T}\Big) \leq \int_S \alpha_h(\mathbf{x}_T)\Big(\oint_{\mathbb{R}} \varepsilon(\mathbf{x}_T, x_3)\Big(|\mathbf{U}_{h,1}(\mathbf{x}_T, x_3)|^2 + |\mathbf{U}_{h,2}(\mathbf{x}_T, x_3)|^2\Big)\,dx_3\Big) d\mathbf{x}_T,$$

so that, referring to the Fubini-like formula (2.21) and the definition of $\mathbf{m}_h$ (see (2.9, 2.18)), we get

$$\Big(\mathbf{K}_{3,\mathbf{h}}\mathbb{U}_{\mathbf{h},T}, \mathbb{U}_{\mathbf{h},T}\Big) \leq \|\alpha_h\|_\infty\, \mathbf{m}_h(\mathbf{U}_{h,T}, \mathbf{U}_{h,T}) \equiv \|\alpha_h\|_\infty\, \Big(\mathbf{M}_{\mathbf{h}}^T\mathbb{U}_{\mathbf{h},T}, \mathbb{U}_{\mathbf{h},T}\Big). \tag{2.53}$$

Finally, joining (2.51) and (2.53) to definition (2.50) of $\mathbf{M_h}(\Delta t)$, we obtain

$$\Big(\mathbf{M_h}(\Delta t)\,\mathbb{U}_\mathbf{h},\mathbb{U}_\mathbf{h}\Big) \geq q(X,Y) := \Big(1-\|\alpha_h\|_\infty^2\,\frac{\Delta t^2}{4}\Big)\,X^2 - \|\alpha_h\|_\infty\,\frac{\Delta t^2}{2}\,XY + \Big(\theta-\frac{1}{4}\Big)\,\Delta t^2\,Y^2, \tag{2.54}$$

where we have set $X = \Big(\mathbf{M}_\mathbf{h}^T\,\mathbb{U}_{\mathbf{h},T},\mathbb{U}_{\mathbf{h},T}\Big)^{\frac12}$ and $Y = \Big(K_{T,\mathbf{h}}\mathbb{U}_{3,\mathbf{h}},\mathbb{U}_{3,\mathbf{h}}\Big)^{\frac12}$.

The stability condition (2.47) is finally obtained by writing that the quadratic $q(X,Y)$ form is positive.

Step 3 : Derivation of the sufficient stability condition (2.48).

With respect to (2.47), (2.48) is a (slightly) stronger but more explicit (thus more useful) sufficient stability condition. It is a direct consequence of the upper bound

$$\|\alpha_h\|_\infty^2 \leq \frac{4\,c_+^2}{h^2}.$$

This estimate is a straightforward consequence of the definition of the weighted quadrature formula (2.22). Indeed, for any $u_h \in P_{1,h}$ and by definition of c^+

$$\int_\mathbb{R} \mu(\cdot,\mathbf{x}_T)^{-1}|u_h'|^2 \leq c_+^2 \int_\mathbb{R} \varepsilon(\cdot,\mathbf{x}_T)|u_h'|^2.$$

However, since u_h' is piecewise constant, we have, with $u_j := u_h(jh)$ and by definition (2.20) of $\varepsilon_{j+\frac12}$,

$$\int_\mathbb{R} \mu(\cdot,\mathbf{x}_T)^{-1}|u_h'|^2 \leq c_+^2 \sum_{j\in Z} \varepsilon_{j+\frac12}\left|\frac{u_{j+1}-u_j}{h}\right|^2.$$

By $|u_{j+1}-u_j|^2 \leq 2\Big(|u_{j+1}|^2+|u_j|^2\Big)$, we deduce,

$$\int_\mathbb{R} \mu(\cdot,\mathbf{x}_T)^{-1}|u_h'|^2 \leq \frac{4\,c_+^2}{h^2}\sum_{j\in Z}\varepsilon_{j+\frac12}\left(\frac{|u_j|^2+|u_{j+1}|^2}{2}\right)h = \frac{4\,c_+^2}{h^2}\oint_\mathbb{R}\varepsilon(\cdot,\mathbf{x}_T)\,|u_h|^2,$$

by definition of the 1D quadrature formula (2.22). ■

2.7 Numerical experiments

2.7.1 The data of the problem

We have chosen to treat two examples : the first one is the case of a cylindrical cable $\widehat\Omega$ with a circular section $\widehat S$, and the second one is the case of a cable Ω with a non-circular section S. More precisely :

$$\Omega = S\times[0,12], \quad \text{and} \quad \widehat\Omega = \widehat S\times[0,12].$$

With $S = F(\widehat S)$, where

$$\widehat S \equiv \{(x_1,x_2)\ /\ 1 \leq (x_1^2+x_2^2)^{\frac12} \leq 2.5\}, \tag{2.55}$$

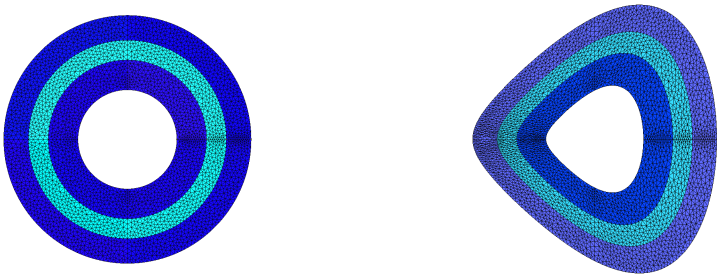

FIGURE 2.8 – Left : the circular section $\widehat{S}$, right : the section S. Each color corresponds to a different material.

and F is the 2D transform defined by

$$F(x_1, x_2) = \left[x_1, \left(\frac{1}{2} \frac{x_1}{\sqrt{x_1^2 + x_2^2}} + 1 \right) x_2 \right]. \tag{2.56}$$

The numerical computations are done in the portion of cable $0 \leq x_3 \leq 12$. For simplicity, periodic boundary conditions will be applied between $x_3 = 0$ and $x_3 = 12$.

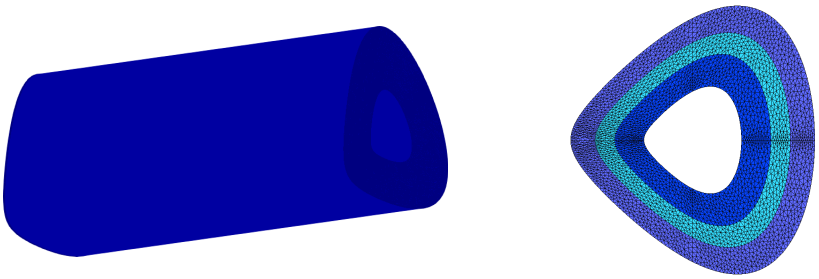

FIGURE 2.9 – Left : the domain Ω, right : the section S of the domain. Each color corresponds to a different material.

Concerning the coefficients of the model, we shall treat the case where the coefficients of the model are invariant by translation in the longitudinal direction,

$$\varepsilon(\mathbf{x}_T, x_3) = \varepsilon^0(\mathbf{x}_T), \quad \mu(\mathbf{x}_T, x_3) = \mu^0(\mathbf{x}_T). \tag{2.57}$$

The cable is however heterogeneous is the cross sections S. More precisely S is made of three layers $S = S_1 \cup S_2 \cup S_3$ and inside S_j, the material is homogeneous (see Figure 2.9),

$$\Big(\varepsilon^0(\mathbf{x}_T), \mu^0(\mathbf{x}_T)\Big) = (\varepsilon_j, \mu_j), \quad \text{in } S_j. \tag{2.58}$$

In our numerical experiments we shall take $(\varepsilon_1, \mu_1) = (2, 1)$, $(\varepsilon_2, \mu_2) = (1, 2)$ and $(\varepsilon_3, \mu_3) = (2, 1)$, so that the velocity of electromagnetic waves, $c(\mathbf{x}) = (\varepsilon\mu)(\mathbf{x})^{-\frac{1}{2}}$ is

$$c(\mathbf{x}) = 1/\sqrt{2} \quad \text{in} \quad \Omega_i := S_i \times \mathbb{R}, \ i = 1, 2, 3. \tag{2.59}$$

We also take initial conditions that are localized near $x_3 = 6$. More precisely, we suppose that $\mathbf{H}_0(\mathbf{x}_T, x_3) = 0$ and

$$\mathbf{E}_0(\mathbf{x}_T, x_3) := \mathcal{E}(x_3)\, \nabla_T \varphi(\mathbf{x}_T), \quad \mathcal{E}(x_3) = e^{-\pi^2 (x_3 - 6)^2}, \tag{2.60}$$

where $\varphi(\mathbf{x}_T)$ is the solution of

$$\begin{cases} \mathrm{div}_T\left(\varepsilon^0 \nabla_T \varphi\right) = 0 & \text{in } S, \\ \varphi = 1 & \text{on } \Gamma_i, \\ \varphi = 0 & \text{on } \Gamma_e, \end{cases}$$

The time interval for the numerical experiments will be $[0, T]$ with $T = 6.75$ so that, taking into account (2.59), implies that the waves will not reach the transverse boundaries $x_3 = 0$ and $x_3 = 12$ before the final time T : in other words, the periodic boundary conditions in x_3 will not play any role.

2.7.2 Discretization parameters

Data for the transverse discretization. The mesh of the cross section will be a triangular mesh represented in Figure 2.8.

Data for the longitudinal discretization. The longitudinal step size h will be taken $h = 0.06$ which is well adapted to the discretization of the Gaussian $\mathcal{E}(x_3)$ (see (2.60)).

Data for the time discretization. The choice of Δt will be constrained by the 3D condition (2.48). We shall take $\theta = 1/3$, in which case (2.48) gives :

$$c^+ \frac{\Delta t}{h} \leq \frac{1}{2}.$$

In practice we shall choose $\Delta t = 0.95\ h/(2\ c^+)$.

Concerning the conductivity, we shall consider two scenarios :

— without any conductivity (*non conductive case.*) : $\sigma = 0$,
— with conductivity (*conductive case.*) : $\sigma = 0.5$.

2.7.3 Numerical results

Example 1 : The cable with circular sections.

In this numerical test we shall use the domain $\widehat{\Omega} = \widehat{S} \times [0, 12]$ (See Figure 2.8).

In the next four pages we represent the results of two numerical experiments via the norm $|\mathbf{E}_T|$ of the transverse field and the longitudinal one E_3 : more precisely we represent color levels of these functions on both interior and exterior boundaries of the cable.

The figures 2.10 (transverse field) and 2.11 (longitudinal field) concern the non conductive case and figures 2.12 (transverse field) and 2.13 (longitudinal field) the conductive case.

- *The non conductive case.*

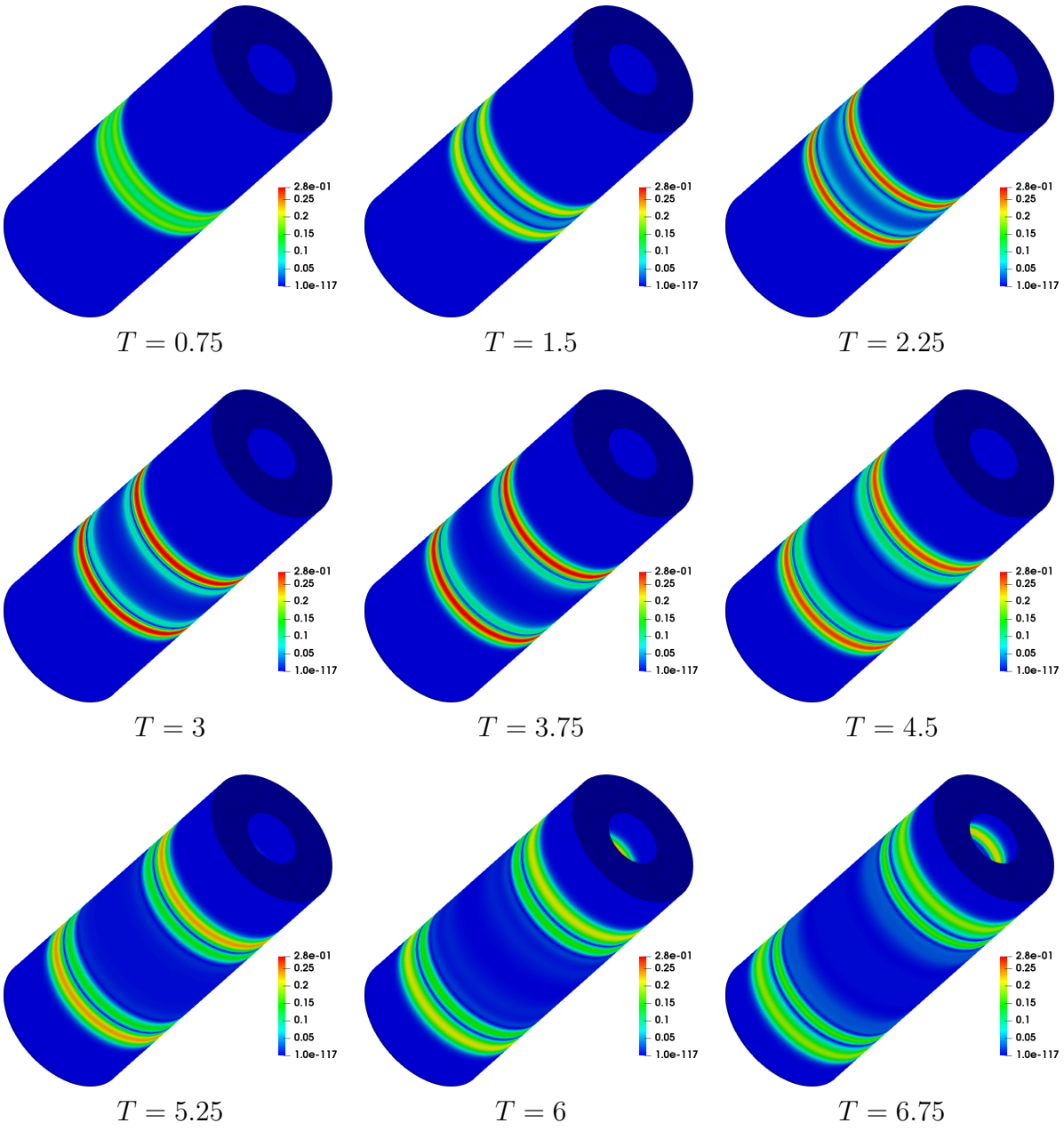

FIGURE 2.10 – The norm of the transverse field $|\mathbf{E}_T|$.

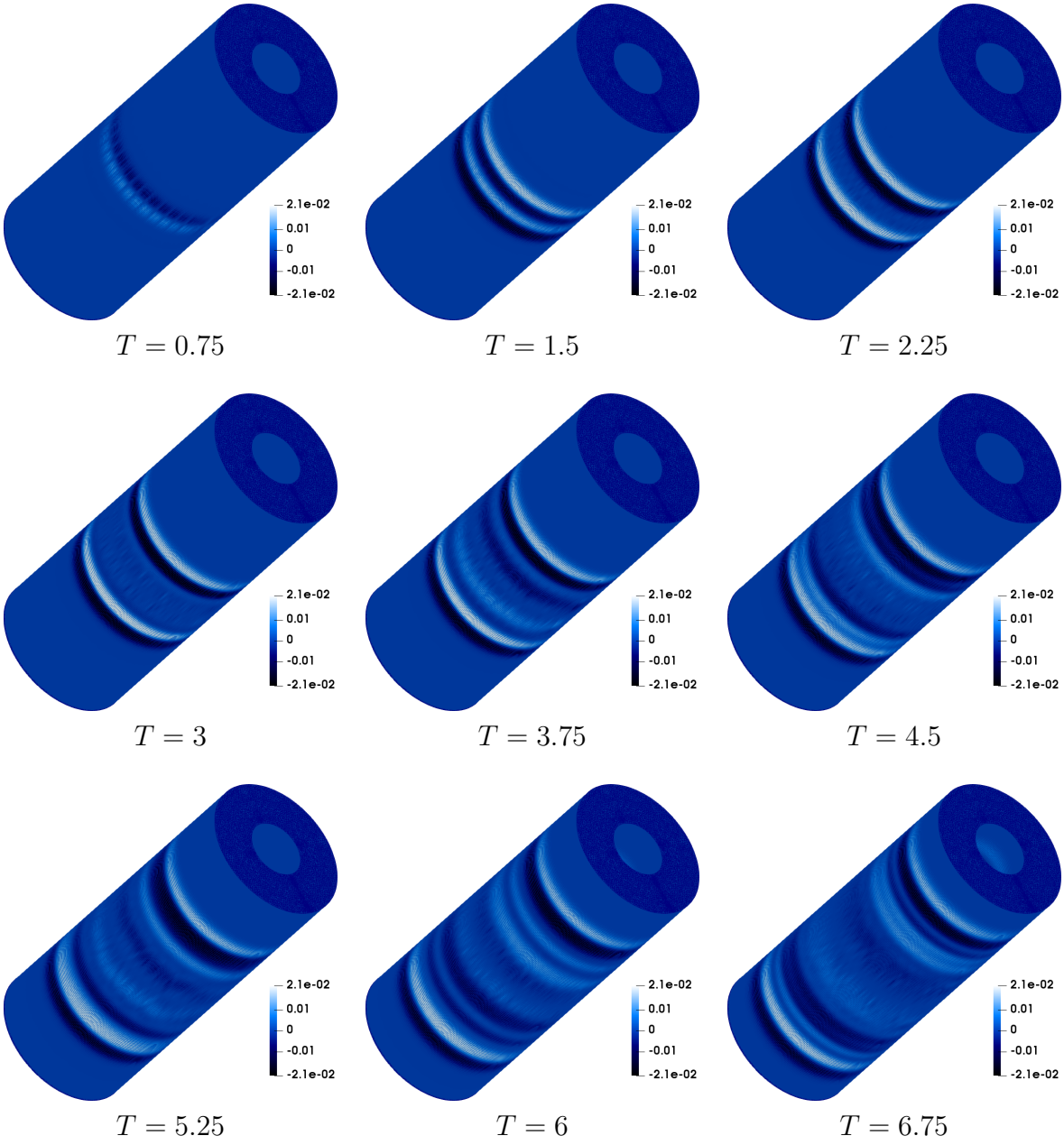

FIGURE 2.11 – The propagation of E_3.

Comment : We essentially observe the propagation of the wave in the longitudinal direction (even though the transverse propagation is also taken into account, but not really visible because of our choice of initial condition).

- *The conductive case.*

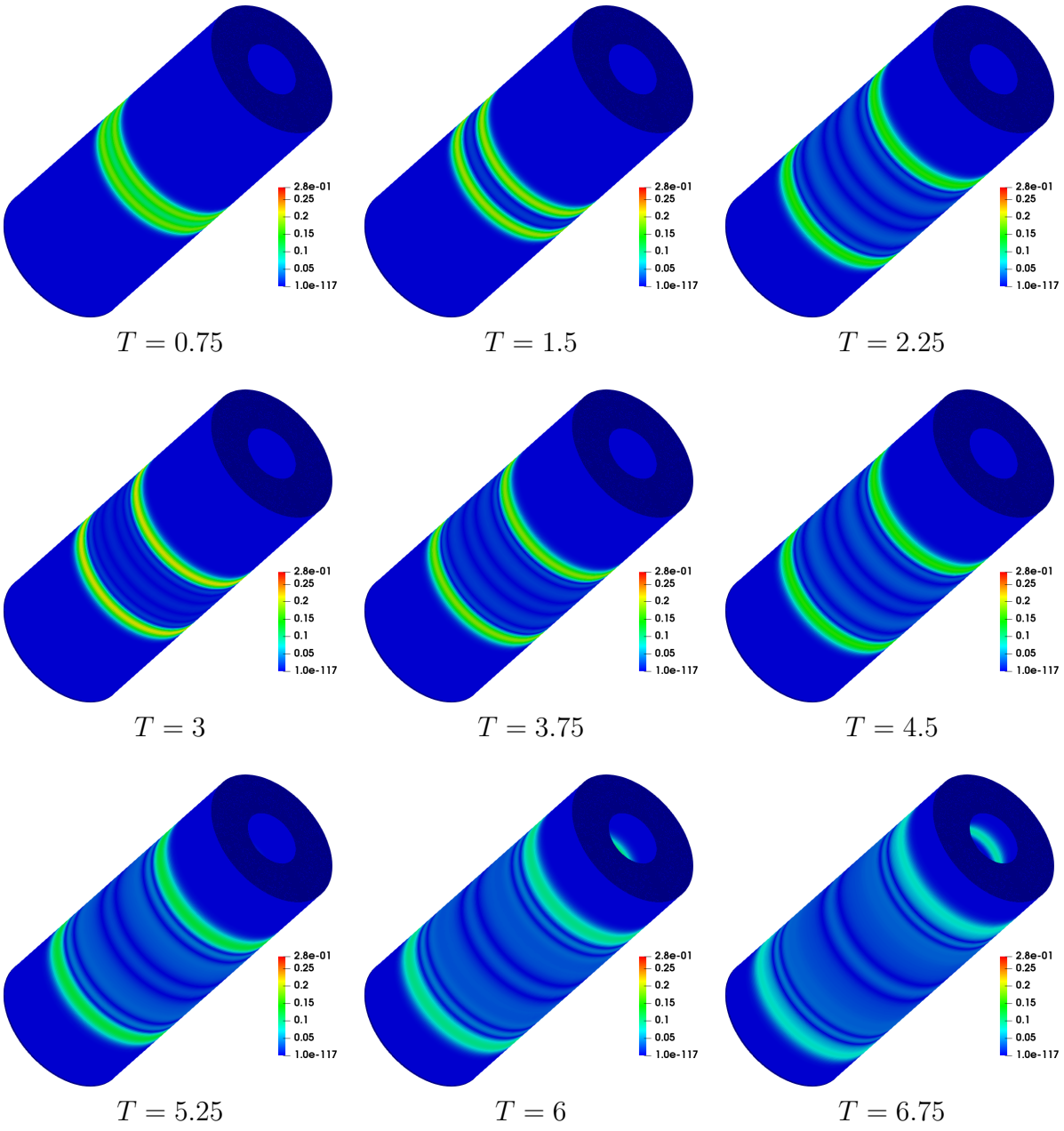

$T = 0.75$ $T = 1.5$ $T = 2.25$

$T = 3$ $T = 3.75$ $T = 4.5$

$T = 5.25$ $T = 6$ $T = 6.75$

FIGURE 2.12 – The norm of the transverse field $|\mathbf{E}_T|$.

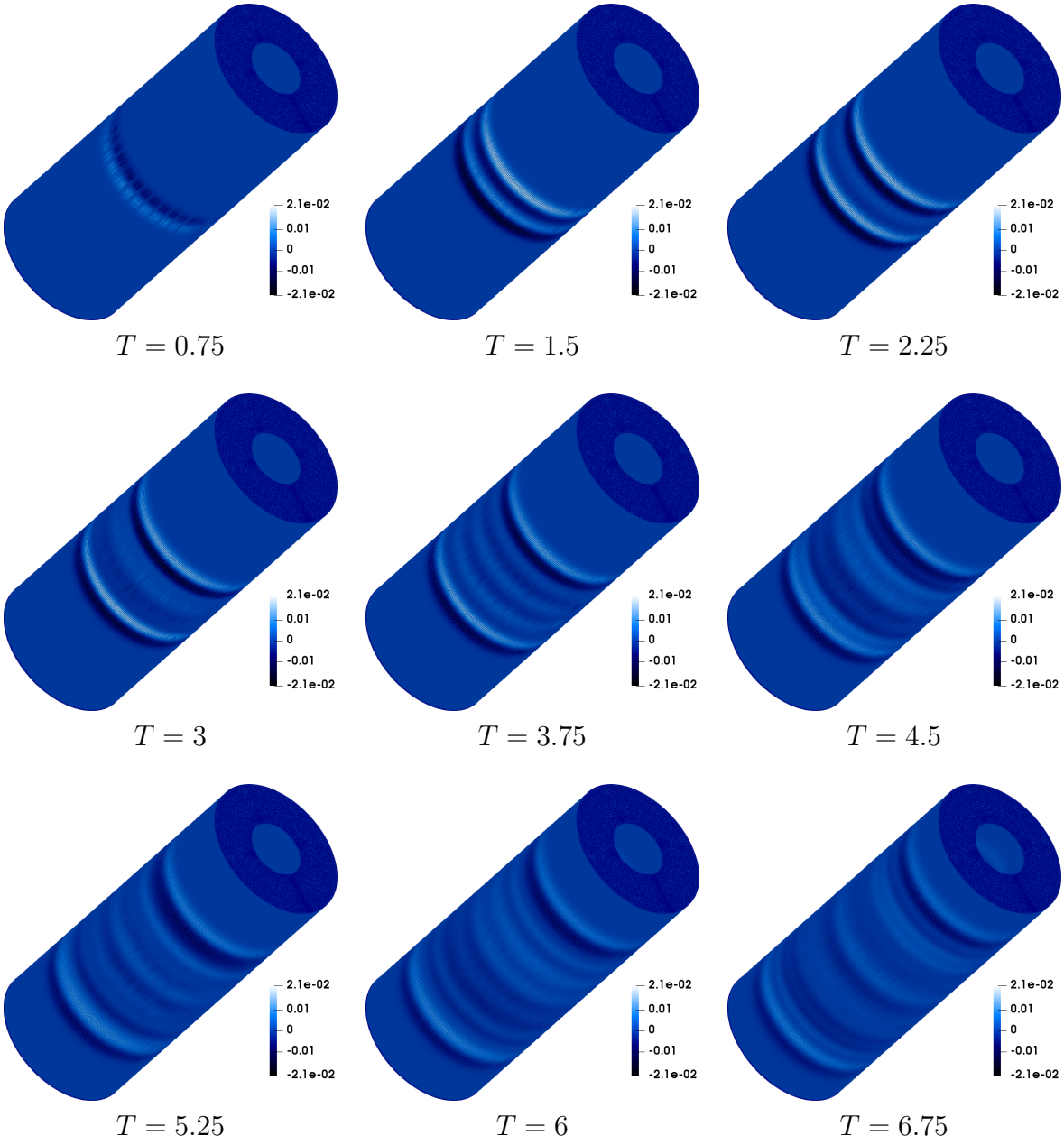

FIGURE 2.13 – The propagation of E_3.

Comment : The comparison of figures 2.12 and 2.13 with figures 2.10 and 2.11 emphasizes, in addition to a pure damping effect visible on the amplituce of the wave, the influence of the presence of the conductivity on the shape (wave form) of the propagating wave.

Example 2 : The cable with non-circular sections.

In this numerical test we shall use the domain $\Omega = S \times [0, 12]$ (See Figure 2.8).

Again, in the next four pages we represent the results of two numerical experiments : figures 2.14 (transverse field) and 2.15 (longitudinal field) concern the non conductive case, figures 2.16 (transverse field) and 2.17 (longitudinal field) concern the conductive case.

- *The non conductive case.*

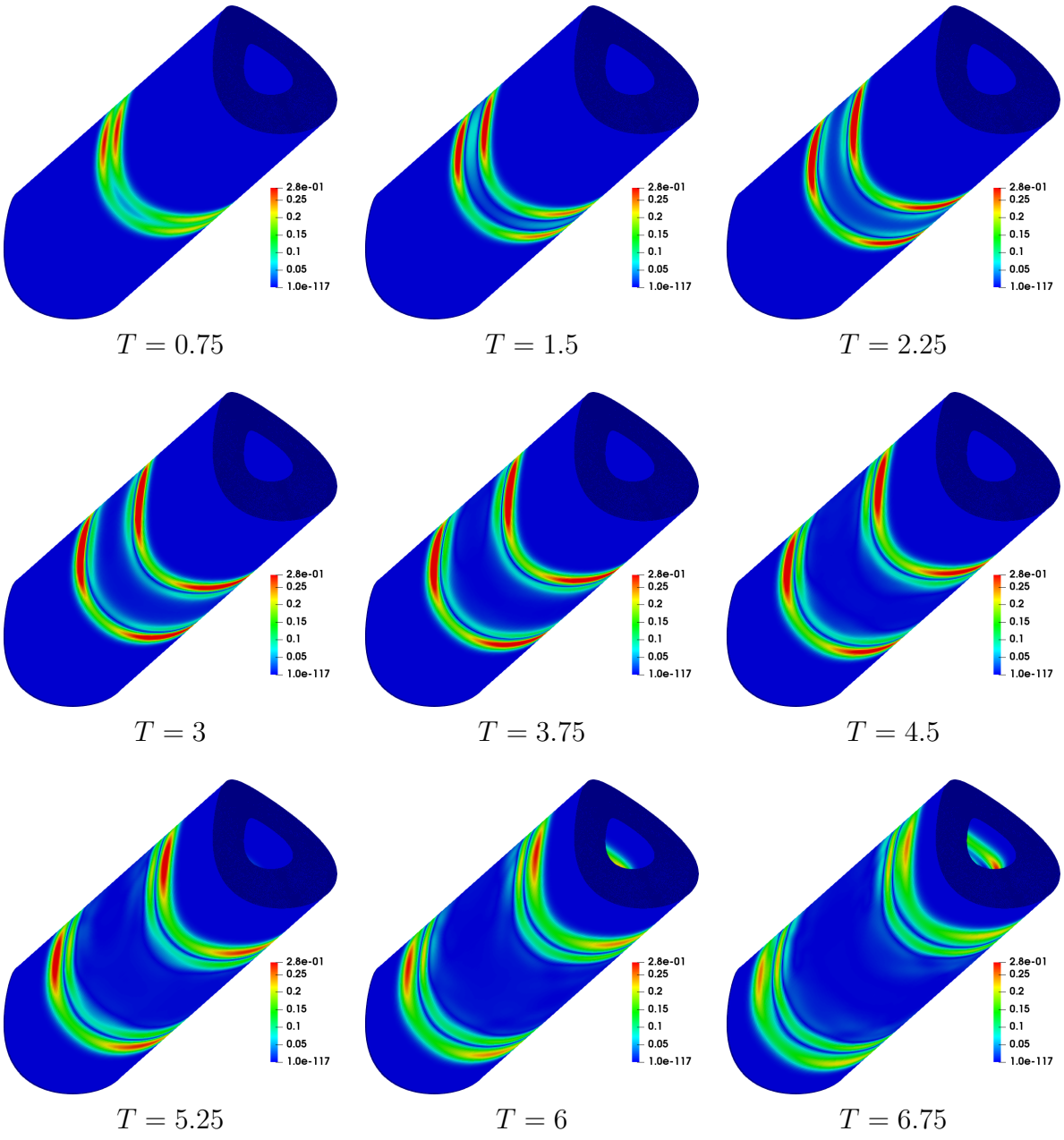

FIGURE 2.14 – The norm of the transverse field $|\mathbf{E}_T|$.

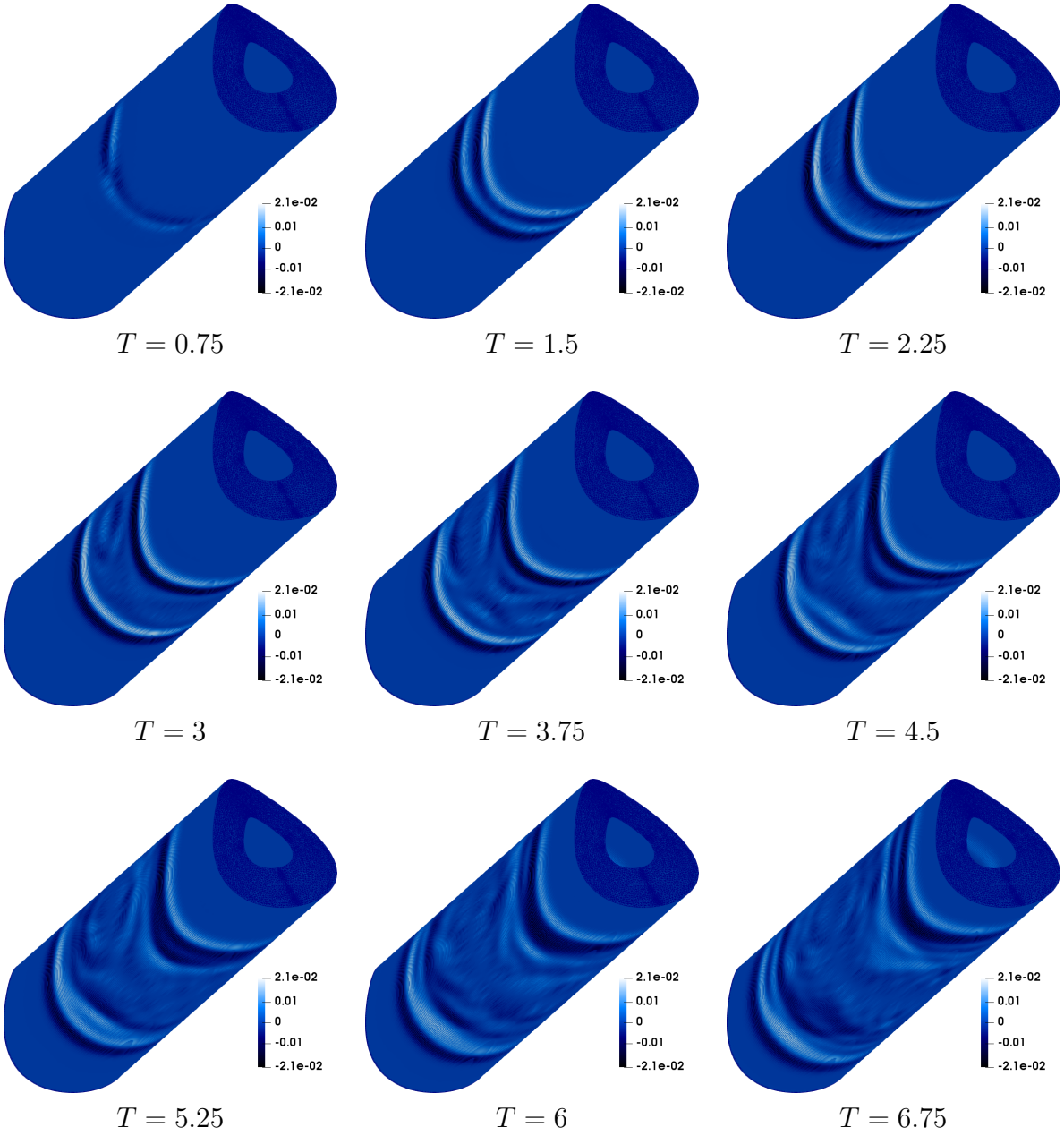

FIGURE 2.15 – The propagation of E_3.

Comment : The comparison of the above figures and figures 2.12 and 2.13 clearly emphasizes the influence of the geometry of the cross section of the cable on the spatial repartition of the electric field.

- *The conductive case.*

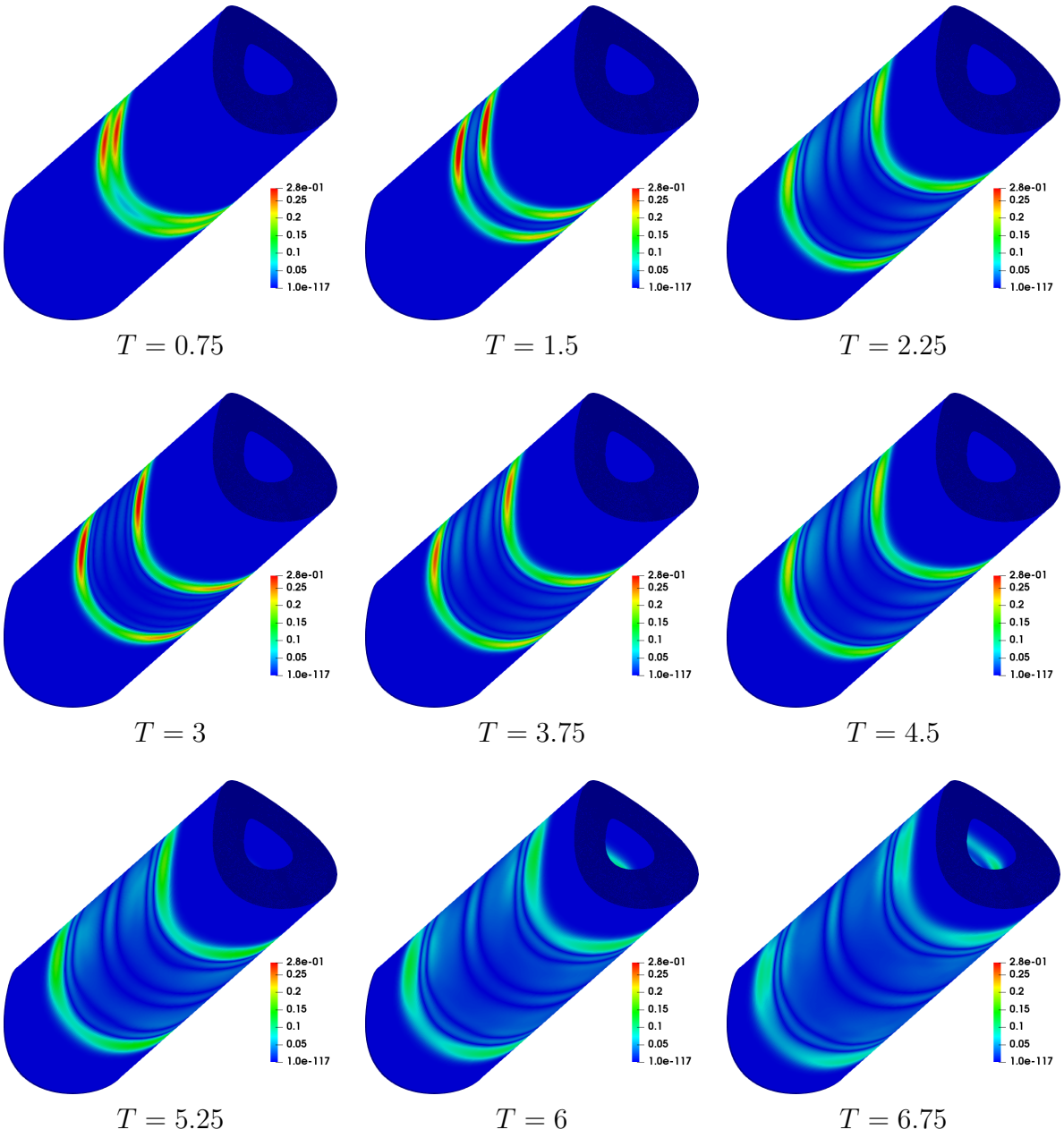

$T = 0.75$ $T = 1.5$ $T = 2.25$

$T = 3$ $T = 3.75$ $T = 4.5$

$T = 5.25$ $T = 6$ $T = 6.75$

FIGURE 2.16 – The norm of the transverse field $|\mathbf{E}_T|$.

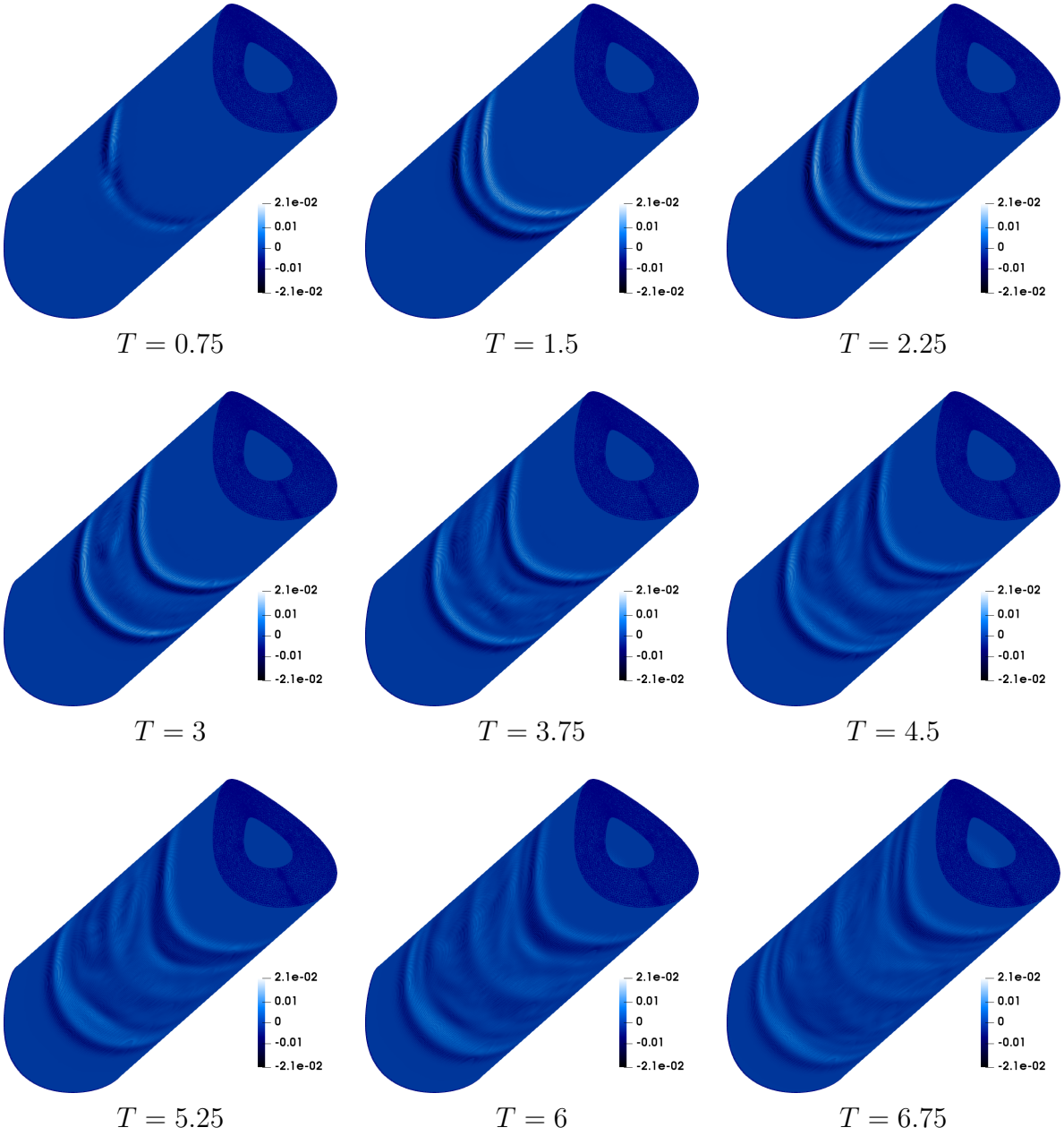

$T = 0.75$ $T = 1.5$ $T = 2.25$

$T = 3$ $T = 3.75$ $T = 4.5$

$T = 5.25$ $T = 6$ $T = 6.75$

FIGURE 2.17 – The propagation of E_3.

2.8 Conclusion

We have presented a hybrid explicit-implicit temporal discretization combined with a spatial discretization of the 3D Maxwell equation based on edge elements on prisms. Note that, since we have shown that our scheme is unconditionally stable with respect to the transverse step size h_T, by employing scaling with respect to the transverse coordinates, one can use the same approach to solve the 3D model in a thin cylindrical coaxial cable. As a result, this approach can be used to validate a 1D limit model that is obtained by an asymptotic analysis applied the the 3D Maxwell's equations. This is the object of the next two chapters.

Chapter 3

The 1D telegrapher limit model and 3D/1D comparison

Contents

3.1 Introduction

In the previous chapter, we have proposed a new efficient numerical method to solve the 3D Maxwell's equations in cylindrical coaxial cables. However, almost all cables are thin, i.e. their transverse dimensions are proportional to a small parameter $\delta \ll 1$. Using a scaling with respect to transverse coordinates our method can be used to solve the 3D model in this configuration. In the other hand, another interesting approach consists in deriving a 1D limit model, called the "the telegrapher limit model", that leads to a good approximation of the solution of our 3D problem, as it has been done in [34] first, and in a more general context in G. Beck Thesis [10]. As a matter of fact, the telegrapher's equations can be found in classical textbooks in electromagnetics [17, 46]. They are justified in the case where the cable is cylindrical has a homogeneous cross section via a modal expansion of the electromagnetic field (see also [21] for a more mathematical presentation). In the case of heterogeneous and varying cross-section, in the possible presence of losses, the telegrapher's equation can be derived and generalized by an asymptotic analysis as in [34] (see also [22] for an alternative, modal-like, approach). It is also worthwhile mentioning that such models can be extended to the multi-conductors case : see [44, 47, 48] in the electromagnetism literature or [12] for a more rigorous approach. Although this type model has been justified from a mathematical point of view by error estimates (in particular when the cable has cylindrical geometry, see [33] and [10]), to the best of our knowledge, there is no existing quantitative numerical comparison between 1D model and 3D Maxwell's theory.

This is the subject of this chapter, in which we will propose a numerical method to solve this 1D limit model and we will validate this 1D model in the case of a cylindrical coaxial cable using 1D/3D comparisons.

This chapter is organized as follows :

We start by presenting briefly (and reminding the formal derivation for the sake of completeness) the "1D" limit model in Section 3.2. Then, we describe in Section 3.3, the method used for the discretization of this 1D model, particularly in the conductive case which involves the appearance of non-local operators in time. Finally, Section 3.4 is dedicated to the validation tests via 3D/1D numerical comparisons.

3.2 Recap about the "1D" limit model

The asymptotic analysis of thin co-axial cables with respect to the small thickness of the cable has been led in [34, 33] (see also [10, 12, 13] for extensions and more elaborated models). What follows is mainly extracted from [34]. Roughly speaking, the 1D model is obtained from a rigorous asymptotic analysis of a family of domains parametrized by a strictly positive scalar $\delta > 0$, which are defined as the result of a *transverse scaling* of a reference cable Ω. More precisely we introduce

$$\Omega^\delta = \mathcal{G}_\delta\big(\Omega\big),$$

where $\mathcal{G}_\delta$ is the transformation $\mathcal{G}_\delta : (x_1, x_2, x_3) \longrightarrow (\delta x_1, \delta x_2, x_3)$. Accordingly, for each $\delta > 0$, we consider $(\varepsilon^\delta, \mu^\delta, \sigma^\delta)$, defined in Ω^δ, respectively the permittivity, permeability and conductivity of the cable Ω^δ obtained from the ones for the reference cable Ω by a simple mapping, namely,

$$\varepsilon^\delta = \varepsilon \circ \mathcal{G}_\delta^{-1}, \quad \mu^\delta = \mu \circ \mathcal{G}_\delta^{-1}, \quad \sigma^\delta = \sigma \circ \mathcal{G}_\delta^{-1},$$

and we consider the family of problems, with unknown $\mathbf{E}^\delta(\mathbf{x}, t) : \Omega^\delta \times \mathbb{R}^+ \to \mathbb{R}^3$,

$$\begin{cases} \varepsilon^\delta\, \partial_t \mathbf{E}^\delta + \sigma^\delta\, \mathbf{E}^\delta - \boldsymbol{\nabla} \times \mathbf{H}^\delta = \mathbf{0}, & \text{in } \Omega^\delta \times \mathbb{R}^+, \\ \mu^\delta\, \partial_t \mathbf{H}^\delta + \boldsymbol{\nabla} \times \mathbf{E}^\delta = \mathbf{0}, & \text{in } \Omega^\delta \times \mathbb{R}^+, \\ \mathbf{E}^\delta \times \mathbf{n} = 0, & \text{on } \partial\Omega^\delta \times \mathbb{R}^+, \end{cases} \tag{3.1}$$

completed with the initial conditions

$$\mathbf{E}^\delta(\cdot, 0) = \mathbf{E}_0^\delta, \quad \mathbf{H}^\delta(\cdot, 0) = \mathbf{H}_0^\delta, \quad \mathbf{E}_0^\delta := \mathbf{E}_0 \circ \mathcal{G}_\delta^{-1}, \quad \mathbf{H}_0^\delta := \mathbf{H}_0 \circ \mathcal{G}_\delta^{-1}. \tag{3.2}$$

In order to state our asymptotic result, we first rescale the fields in the fixed domain Ω setting

$$\widetilde{\mathbf{E}}^\delta(\mathbf{x}, \mathbf{t}) := \mathbf{E}^\delta(\mathcal{G}_\delta \mathbf{x}, \mathbf{t}), \quad \widetilde{\mathbf{H}}^\delta(\mathbf{x}, \mathbf{t}) := \mathbf{H}^\delta(\mathcal{G}_\delta \mathbf{x}, \mathbf{t}), \quad \forall\, \mathbf{x} \in \boldsymbol{\Omega}, \tag{3.3}$$

and it is useful to introduce a cut Σ of the cross S, namely a line $\Sigma \subset \overline{\Omega}$ that joins the interior boundary Γ_i to the exterior boundary Γ_e in such a way that the open set $\Omega \setminus \Gamma$ is simply connected. We then define accordingly,

$$H^1_\Sigma(S) = H^1(S \setminus \Sigma) \quad \text{and} \quad \widetilde{H}^1_\Sigma(\Omega) := \Big\{ u \in H^1_\Sigma(S) \;/\; \int_S u \, d\mathbf{x}_T = 0 \Big\}. \tag{3.4}$$

In what follows, $\Big[u\Big]_\Sigma$ denotes the jump of u across Σ (properly defined in [34], Section 3.1). Then, one can show (see for instance ([33], [10] and [32] in a more general context) that, if the initial data are well-prepared, (cf. (3.12) and remark 3.2.1)

$$\begin{aligned}
&\widetilde{\mathbf{E}}^\delta(\mathbf{x},t) \underset{\delta\to 0}{\sim} \widetilde{\mathbf{E}}^0(\mathbf{x},t) := V(x_3,t)\,\nabla_T\,\varphi_e(\mathbf{x}_T,x_3) + \int_0^t V(x_3,t-s)\,\nabla_T\,\varphi_r(\mathbf{x}_T,x_3,s)\,ds,\\
&\widetilde{\mathbf{H}}^\delta(\mathbf{x},t) \underset{\delta\to 0}{\sim} \widetilde{\mathbf{H}}^0(\mathbf{x},t) := I(x_3,t)\,\nabla_T\,\psi_m(\mathbf{x}_T,x_3),
\end{aligned} \tag{3.5}$$

where, in the formulas (3.5),

(i) the potentials $\varphi_e(\cdot,x_3) \in H^1_0(S)$ and $\psi_m(\cdot,x_3) \in \widetilde{H}^1_\Sigma(S)$ are defined for each x_3 that plays the role of a parameter, as the solutions of the following boundary value problems (see the comments below for more details and subtleties concerning ψ_m),

$$\left\{\begin{array}{ll}
\mathrm{div}_T\Big(\varepsilon(\cdot,x_3)\,\nabla_T\,\varphi_e(\cdot,x_3)\Big)=0 & \text{in } \Omega,\\
\varphi_e(\cdot,x_3)=1 & \text{on } \Gamma_i,\\
\varphi_e(\cdot,x_3)=0 & \text{on } \Gamma_e,
\end{array}\right.
\qquad
\left\{\begin{array}{ll}
\mathrm{div}_T\Big(\mu(\cdot,x_3)\,\nabla_T\,\psi_m(\cdot,x_3)\Big)=0 & \text{in } \Omega\setminus\Sigma,\\
\partial_n\psi_m(\cdot,x_3)=0 & \text{on } \partial S,\\
\Big[\psi_m(\cdot,x_3)\Big]_\Sigma=1,\ \Big[\partial_n\psi_m(\cdot,x_3)\Big]_\Sigma=0 & \text{across } \Sigma,
\end{array}\right. \tag{3.6}$$

(ii) the functions $\varphi_r(\cdot,x_3,\cdot) : S\times\mathbb{R}^+$ are defined for each x_3 by the formula,

$$\varphi_r(\cdot,x_3,t) = e^{-t\,\mathbf{A}(x_3)}\,\varphi_{r,0}(\cdot,x_3) \in C^\infty\Big(\mathbb{R}^+, H^1_0(S)\Big), \tag{3.7}$$

where $\mathbf{A}(x_3)\in\mathcal{L}\Big(H^1_0(S)\Big)$ is the bounded positive definite symmetric operator defined by

$$u := \mathbf{A}(x_3)\,v \quad\Longleftrightarrow\quad u\in H^1_0(S) \text{ and } \mathrm{div}_T\Big(\varepsilon(\cdot,x_3)\nabla_T\,u\Big) = \mathrm{div}_T\Big(\sigma(\cdot,x_3)\nabla_T\,v\Big) \text{ in } S. \tag{3.8}$$

and where $\varphi_{r,0}(\cdot,x_3) := -\mathbf{A}(x_3)\varphi_e \in H^1_0(S)$.

(iii) The voltage $V(x_3,t)$ and the current $I(x_3,t)$ are solution of the generalized telegrapher's equation (this is the 1D limit model)

$$\left\{\begin{array}{l}
C(x_3)\,\partial_t V(x_3,t) + G(x_3)\,V(x_3,t) + \partial_3 I(x_3,t) + \displaystyle\int_0^t k(x_3,t-s)\,V(x_3,s)\,ds = 0,\\
L(x_3)\,\partial_t I(x_3,t) + \partial_3 V(x_3,t) = 0,
\end{array}\right. \tag{3.9}$$

where the effective coefficients $C(x_3)>0, G(x_3)\geq 0$ and $L(x_3)>0$ are given by

$$\left\{\begin{array}{l}
C(x_3) = \displaystyle\int_S \varepsilon(\mathbf{x}_T,x_3)\,|\nabla_T\,\varphi_e(\mathbf{x}_T,x_3)|^2\,d\mathbf{x}_T,\\
G(x_3) = \displaystyle\int_S \sigma(\mathbf{x}_T,x_3)\,|\nabla_T\,\varphi_e(\mathbf{x}_T,x_3)|^2\,d\mathbf{x}_T,\\
L(x_3) = \displaystyle\int_S \mu(\mathbf{x}_T,x_3)\,|\nabla_T\,\psi_m(\mathbf{x}_T,x_3)|^2\,d\mathbf{x}_T,
\end{array}\right. \tag{3.10}$$

and the kernel $k(x,t)$ is given by

$$k(x_3,t) = \int_{S_{x_3}} \sigma(\mathbf{x}_T,x_3)\,\nabla_T\,\varphi_r(\mathbf{x}_T,x_3,t)\cdot\nabla_T\,\varphi_e(\mathbf{x}_T,x_3). \tag{3.11}$$

By well-prepared data we mean that,

$$\begin{cases} \mathbf{E}_0^\delta(\mathbf{x}_T, x_3) = V_0(x_3)\nabla_T\,\varphi_e(\mathbf{x}_T, x_3) + O(\delta), \\ \mathbf{H}_0^\delta(\mathbf{x}_T, x_3) = I_0(x_3)\nabla_T\,\psi_m(\mathbf{x}_T, x_3) + O(\delta), \end{cases} \tag{3.12}$$

and complete the generalized telegrapher's equation (3.9) with the initial conditions

$$V(x_3, 0) = V_0(x_3) \quad \text{and} \quad I(x_3, 0) = I_0(x_3). \tag{3.13}$$

Remark 3.2.1 (Well prepared data)**.** *The reconstruction formulas given in* (3.5) *correspond to well prepared initial conditions* (3.12)*. It is also possible to consider general initial data, i.e.*

$$\begin{cases} \mathbf{E}_0^\delta(\mathbf{x}_T, x_3) = V_0(x_3)\nabla_T\,\varphi_e(\mathbf{x}_T, x_3) + \mathbf{E}_{0,T}^r + O(\delta), \\ \mathbf{H}_0^\delta(\mathbf{x}_T, x_3) = I_0(x_3)\nabla_T\,\psi_m(\mathbf{x}_T, x_3) + \mathbf{H}_{0,T}^r + O(\delta), \end{cases} \tag{3.14}$$

where $\left(\mathbf{E}_{0,T}^r,\ \mathbf{H}_{0,T}^r\right)$ *are purely transverse fields that must satisfy for each* x_3*,*

$$\begin{cases} rot_T\mathbf{E}_{0,T}^r(\cdot, x_3) = 0, & \text{in } \Omega, \\ \mathbf{E}_{0,T}^r(\cdot, x_3) \times n_T = 0, & \text{on } \partial\Omega, \end{cases} \qquad \begin{cases} rot_T\mathbf{H}_{0,T}^r(\cdot, x_3) = 0, & \text{in } \Omega, \\ \mathbf{H}_{0,T}^r(\cdot, x_3) \cdot n_T = 0, & \text{on } \partial\Omega. \end{cases} \tag{3.15}$$

In that case, the asymptotic formula (3.5) *is still valid up to the addition of a quasi-static field that is not propagating. In particular, if the initial data have a compact support, these quasi-static fields vanish outside this support which means that* (3.5) *is still valid outside this support.*

The above asymptotic results and formulas deserve the following comments :

(a) In all above formulas, $\psi_m(\cdot, x_3)$ being discontinuous across Σ, $\nabla_T\,\psi_m(\cdot, x_3) \in L^2(S)^2$ has to be understood in the sense of $\mathcal{D}'(S_\Sigma)$. Let us emphasize that, if $\psi_m(\cdot, x_3)$ depends of course on the choice of the Σ, $\nabla_T\,\psi_m(\cdot, x_3)$ does not ! (see for instance [34], formula (33)).

(b) In the limit $\delta \to 0$, (3.5) shows that the longitudinal fields E_3^δ and H_3^δ vanish. In other words the limit fields are transversely polarized. Moreover, the formula point out the existence of a kind of asymptotic separation of variables between longitudinal and transverse variable. In particular, the time dependency of the limit fields is entirely contained in the 1D (in space) functions $V(x_3, t)$ and $I(x_3, t)$.

(c) It is remarkable that the presence of the conductivity σ induces the apparition of non local effects in time through the presence of the time convolution term appearing in the first equation of (3.9). On the other hand, when $\sigma = 0$, (3.9) is nothing but a 1D wave equation with variable coefficients.

(d) The well posedness and stability of the evolution are ensured by the following positivity property (see Lemma 5.2 in [34]), valid for any $T \geq 0$ and any $\xi \in L^2_{loc}(\mathbb{R}^+)$

$$G(x_3)\int_0^T |\,\xi(t)\,|^2\,dt \;+\; \int_0^T\int_0^t k(x_3, t-s)\,\xi(s)\,\xi(t)\,ds\,dt \;\geq 0. \tag{3.16}$$

(e) We notice that from definition (3.5) of the limit field $\widetilde{\mathbf{E}}^0(\mathbf{x}, t) \equiv \widetilde{\mathbf{E}}_T^0(\mathbf{x}, t)$, one has

$$V(x_3, t) = C(x_3)^{-1}\int_S \varepsilon(\cdot, x_3)\;\widetilde{\mathbf{E}}_T^0(\cdot, x_3, t)\cdot\nabla_T\,\varphi_e(\cdot, x_3)\;d\mathbf{x}_T$$

because, from definition (3.6) of φ_e and form the fact that $\varphi_r(\cdot,t) \in H_0^1(S)$, it follows that

$$\forall\, t>0, \quad \int_S \varepsilon(\cdot,x_3)\, \nabla_T\, \varphi_r(\cdot,x_3,t)\cdot \nabla_T\, \varphi_e(\cdot,x_3)\, d\mathbf{x}_T = 0.$$

This suggests to define a 1D voltage $V^\delta(x_3,t)$ for the 3D problem as

$$V^\delta(x_3,t) = C(x_3)^{-1} \int_S \varepsilon(\cdot,x_3)\, \widetilde{\mathbf{E}}_T^\delta(\cdot,x_3,t)\cdot \nabla_T\, \varphi_e(\cdot,x_3)\, d\mathbf{x}_T. \tag{3.17}$$

3.3 Numerical resolution of the telegrapher's equations

Even though this question is not the main purpose of the present chapter, the main lines of the approach deserve to be explained. These consist of three phases :

(I) Precomputation of the coefficients of the model

It is a preliminary step that only consists in solving 2D problems in the cross section S :

- Numerical computation of the potentials (φ_e,ψ_m) and the coefficients $C(x_3), G(x_3)$ and $L(x_3)$.

  The potentials $(\varphi_e(\cdot,x_3),\psi_m(\cdot,x_3))$ are first approximated thanks to a $\mathbb{P}_1$ finite-elements approximation of the boundary value problems (3.6) with a triangular mesh of the cross section S with step size h_T (this mesh "respects" the cut Σ), producing

  $$(\varphi_{e,h_T}(\cdot,x_3),\psi_{m,h_T}(\cdot,x_3)) \in V_{0,h_T}\times \widetilde{V}_{\Sigma,h_T},$$

  where V_{0,h_T} and $\widetilde{V}_{\Sigma,h_T}$ are the respective Galerkin approximation subspaces for $H_0^1(S)\times H_\Sigma^1(S)$. Then $C(x_3), L(x_3)$ and $L(x_3)$ are approximated, according to (3.10), by

  $$\left\{\begin{array}{l} C_{h_T}(x_3) = \displaystyle\int_S \varepsilon(\mathbf{x}_T,x_3)\, |\nabla_T\, \varphi_{e,h_T}(\mathbf{x}_T,x_3)|^2\, d\mathbf{x_T}, \\ G_{h_T}(x_3) = \displaystyle\int_S \sigma(\mathbf{x}_T,x_3)\, |\nabla_T\, \varphi_{e,h_T}(\mathbf{x}_T,x_3)|^2\, d\mathbf{x_T}, \\ L_{h_T}(x_3) = \displaystyle\int_S \mu(\mathbf{x}_T,x_3)\, |\nabla_T\, \psi_{m,h_T}(\mathbf{x}_T,x_3)|^2\, d\mathbf{x_T}. \end{array}\right. \tag{3.18}$$

  Note that, from well known properties of conforming Galerkin methods one has

  $$C_{h_T}(x_3)\geq C(x_3), \quad G_{h_T}(x_3)\geq G(x_3), \quad L_{h_T}(x_3)\geq L(x_3). \tag{3.19}$$

- Numerical approximation of the function φ_r and kernel $k(x_3,t)$.

  One first realizes a finite dimensional approximation of the operator $\mathbf{A}(x_3)$ via a $\mathbb{P}_1$ finite-elements approximation (using the same mesh as above) of (3.8). This produces

  $$\mathbf{A}_{h_T}(x_3) \in \mathcal{L}\Big(V_{0,h_T}\Big),$$

which is easily proven to be uniformly bounded with respect to h_T. Then, for each x_3, $\varphi_r(\cdot, x_3) \equiv \varphi_r(\mathbf{x}_T, x_3, t)$ is approximated by the solution $\varphi_r(\cdot, t, x_3)$ of the ordinary differential equation

$$\frac{d\varphi_{r,h_T}(\cdot, x_3)}{dt} + \mathbf{A}_{h_T}(x_3)\ \varphi_{r,h_T}(\cdot, x_3) = 0, \quad \varphi_{r,h_T}(\cdot, x_3, 0) = -\mathbf{A}_{h_T}(x_3)\varphi_{e,h_T}(\cdot, x_3).$$

That is consistent with the expression (3.7). The above differential system is not stiff and can thus be efficiently solved numerically with any ODE solver (Euler, Crank-Nicolson, Runge-Kutta, ...). Finally, the convolution kernel $k(x_3)$ is approximated, consistently with (3.11), by

$$k_{h_T}(x_3, t) := \int_S \sigma(\mathbf{x}_T, x_3)\, \nabla_T\, \varphi_{r,h_T}(\mathbf{x}_T, x_3, t) \cdot \nabla_T\, \varphi_{e,h_T}(\mathbf{x}_T, x_3)\ d\mathbf{x}_T. \tag{3.20}$$

(II) Resolution of the 1D evolution problem

The semi-discretization in space does not pose any particular problem : it can be done, for instance, using 1D mixed finite elements (for instance continuous $\mathbb{P}_1$ for V (cf. (2.45)) and discontinuous $\mathbb{P}_0$ for I) and mass lumping with a uniform mesh of step size h. The resulting algebraic problem takes the form

$$\begin{cases} \mathbf{M}_{\mathrm{e},\mathbf{h}}\ \dfrac{\mathrm{d}\mathbb{V}_\mathbf{h}}{\mathrm{d}t} + \mathbf{M}_{\mathrm{c},\mathbf{h}}\ \mathbb{V}_h + \mathbf{D}_\mathbf{h}\ \mathbb{I}_h + \displaystyle\int_0^t \mathbf{K}_\mathbf{h}(t-s)\ \mathbb{V}_h(s)\ ds = 0, \\ \mathbf{M}_{\mathrm{m},\mathbf{h}}\ \dfrac{\mathrm{d}\,\mathbb{I}_\mathbf{h}}{\mathrm{d}t} - \mathbf{D}_\mathbf{h}^*\ \mathbb{V}_h = 0, \end{cases} \tag{3.21}$$

where $\mathbb{V}_\mathbf{h}(t) = \big(V_j(t)\big)$ is the vector of degrees of freedom at time t for the semi-discrete voltage $V_\mathbf{h}(t) \in H^1(\mathbb{R})$ (the nodal values at the points jh), $\mathbb{I}_\mathbf{h}(t) = \big(I_{j+\frac{1}{2}}(t)\big)$ is the vector of degrees of freedom at time t for the current $I_\mathbf{h}(t) \in H^1(\mathbb{R})$ (namely the mean values in the intervals $[jh, (j+1)h]$) and

- $\mathbf{M}_{\mathrm{e},\mathbf{h}} = \mathrm{diag}\big(m_{\mathrm{e},j}\big) > 0$, $\mathbf{M}_{\mathrm{c},\mathbf{h}} = \mathrm{diag}\big(m_{\mathrm{c},j}\big) \geq 0$ and $\mathbf{M}_{\mathrm{m},\mathbf{h}} = \mathrm{diag}\big(m_{\mathrm{m},j+\frac{1}{2}}\big) > 0$ are diagonal mass (like) matrices (divided by h for homogeneity) with

$$m_{\mathrm{e},j} = C_{h_T}(jh), \quad m_{\mathrm{c},j} = C_{h_T}(jh), \quad m_{\mathrm{m},j+\frac{1}{2}} = C_{h_T}((j+\frac{1}{2})h).$$

- $\mathbf{K}_\mathbf{h}(t) = \mathrm{diag}\big(k_j(t)\big)$ is for each t a diagonal matrix with (see (3.20))

$$k_j(t) := \int_S \sigma(\mathbf{x}_T, jh)\ \nabla_T\, \varphi_{r,h_T}(\mathbf{x}_T, jh, t) \cdot \nabla_T\, \varphi_{e,h_T}(\mathbf{x}_T, jh)\ d\mathbf{x}_T.$$

- $\mathbf{D}_\mathbf{h}$ is a rectangular matrix that represents a discrete differentiation operator in x_3 for the current (as well as $-\mathbf{D}_\mathbf{h}^*$ for the voltage).

Concerning the time discretization, it is natural to use a leap-frog (or Stormer-Verlet) scheme with a constant time step and a staggered grid. The only non-standard part is the way one discretizes the convolution involving $\mathbf{K}_\mathbf{h}(t)$. With obvious notation, the resulting

(purely explicit) scheme reads

$$\left\{\begin{array}{l} \mathbf{M}_{\mathrm{e},\mathbf{h}}\,\dfrac{\mathbb{V}_{\mathbf{h}}^{n+1}-\mathbb{V}_{\mathbf{h}}^{n}}{\Delta t}+\mathbf{M}_{\mathrm{c},\mathbf{h}}\,\dfrac{\mathbb{V}_{\mathbf{h}}^{n+1}+\mathbb{V}_{\mathbf{h}}^{n}}{2}+\mathbf{D}_{\mathbf{h}}\,\mathbb{I}_{h}^{n+\frac{1}{2}}+\displaystyle\sum_{m=0}^{n}\mathbf{K}_{\mathbf{h}}^{n-m}\,\dfrac{\mathbb{V}_{\mathbf{h}}^{m+1}+\mathbb{V}_{\mathbf{h}}^{m}}{2}\,\Delta t=0,\\ \mathbf{M}_{\mathrm{m},\mathbf{h}}\,\dfrac{\mathbb{I}_{\mathbf{h}}^{n+\frac{1}{2}}-\mathbb{I}_{\mathbf{h}}^{n-\frac{1}{2}}}{\Delta t}-\mathbf{D}_{\mathbf{h}}^{*}\,\mathbb{V}_{h}^{n}=0, \end{array}\right. \tag{3.22}$$

where the unknowns in the above system are

$$\left\{\begin{array}{ll} \mathbb{V}_{\mathbf{h}}^{n} & \text{is the vector of degrees of freedom of } V_{\mathbf{h}}^{n}\in H^{1}(\mathbb{R}), \quad \text{approximation of } V_{\mathbf{h}}(t^{n}),\\ \mathbb{I}_{\mathbf{h}}^{n+\frac{1}{2}} & \text{is the vector of degrees of freedom of } I_{\mathbf{h}}^{n+\frac{1}{2}}\in L^{2}(\mathbb{R}), \quad \text{approximation of } I_{\mathbf{h}}(t^{n+\frac{1}{2}}), \end{array}\right.$$

and where the matrix $\mathbf{K}_{\mathbf{h}}^{p}$ is defined as follows

$$\mathbf{K}_{\mathbf{h}}^{p}=\mathrm{diag}\big(k_{j}^{p}\big),\quad k_{j}^{p}=\frac{1}{\Delta t^{2}}\int_{0}^{\Delta t}\int_{0}^{\Delta t}k_{e}(jh,r-s+p\Delta t)\,ds\,dr. \tag{3.23}$$

The theoretical interest of choosing $\mathbf{K}_{\mathbf{h}}^{p}$ as defined by (3.23) is clarified by the following lemma, which provides a discrete counter-part to the positivity property (3.16).

Lemma 3.3.1. *For any $j\in\mathbb{Z}$ and any real sequence $\xi^{n},n\in\mathbb{N}$, one has the (discrete) positivity property*

$$G(jh)\sum_{n=0}^{N}|\xi^{n}|^{2}\,\Delta t\;+\sum_{n=0}^{N}\sum_{m=0}^{n}k_{j}^{n-m}\,\xi^{n}\,\xi^{m}\,\Delta t^{2}\;\geq 0. \tag{3.24}$$

Proof. Let w_{j} be the $\mathbb{P}_{1}$ hat function associated to the node jh, we introduce $\xi_{j}^{\Delta t}(t)$ defined by

$$\xi^{\Delta t}(t)=\frac{\xi^{m+1}+\xi^{m}}{2}\ \text{for } t\in\Big[t^{m},t^{m+1}\Big]\ \text{and } 0\leq m\leq n,\quad \xi^{\Delta t}(t)=0\ \text{if } t>t_{n}.$$

Then, one can compute directly that

$$\begin{aligned} &G(jh)\sum_{n=0}^{N}|\xi^{n}|^{2}\,\Delta t\;+\sum_{n=0}^{N}\sum_{m=0}^{n}k_{j}^{n-m}\,\xi^{n}\,\xi^{m}\,\Delta t^{2}=\\ &\qquad G(jh)\int_{0}^{T}|\,\xi^{\Delta t}(t)\,|^{2}\,dt\;+\int_{0}^{T}\int_{0}^{t}k(jh,t-s)\,\xi^{\Delta t}(s)\,\xi^{\Delta t}(t)\,ds\,dt\;\geq 0, \end{aligned}$$

and one concludes with (3.16). ∎

Using Lemma 3.3.1 and standard energy techniques, it is easy to prove the stability result below.

Theorem 3.3.2. *The numerical scheme (3.22) is L^{2}-stable under the sufficient CFL condition*

$$c_{h_{T}}^{+}\,\frac{\Delta t}{h}\leq 1,\quad c_{h_{T}}^{+}=\sup_{x_{3}\in\mathbb{R}}c_{h_{T}}(x_{3}),\quad c_{h_{T}}(x_{3}):=C_{h_{T}}(x_{3})^{-\frac{1}{2}}L_{h_{T}}(x_{3})^{-\frac{1}{2}}, \tag{3.25}$$

where the function $c_{h_{T}}(x_{3})$ satisfies the uniform (in x_{3}) convergence property (see also (3.19))

$$c_{h_{T}}(x_{3})\leq c_{1D}(x_{3}),\quad \lim_{h_{T}\to 0}c_{h_{T}}(x_{3})=c_{1D}(x_{3}),\quad c_{1D}(x_{3}):=C(x_{3})^{-\frac{1}{2}}L(x_{3})^{-\frac{1}{2}}.$$

Remark 3.3.3 (Comparison with the 3D stability condition)**.** *According to Theorem 3.3.2, an asymptotically optimal (when $h_T \to 0$) sufficient CFL condition is*

$$c_{1D}^{+}\,\frac{\Delta t}{h} \leq 1, \quad c_{1D}^{+} := \sup_{x_3 \in \mathbb{R}} c_{1D}(x_3). \tag{3.26}$$

In order to compare with the CFL condition (2.48) for the 3D problem, we need to compare c_{1D}^{+} with c^{+}. However, it is shown in [34] that

$$\forall\, x_3 \in \mathbb{R}, \quad c_{1D}(x_3) \leq \sup_{\mathbf{x}_T \in S} c(\mathbf{x}_T, x_3), \quad \textit{which implies } c_{1D}^{+} < c^{+}.$$

This shows that the 3D CFL condition (2.48) is more restrictive than the 1D condition (3.26). Indeed, if (2.48) holds,

$$c_{1D}^{+}\,\frac{\Delta t}{h} \leq c_{+}\,\frac{\Delta t}{h} \leq \sqrt{\frac{4\theta - 1}{4\theta}} < 1.$$

(III) Reconstruction of the 3D electric field

Once the discrete voltage $V_h^n(x_3)$ is computed, according to (3.5), one can reconstruct the (rescaled) 3D electric field at time as the $\mathbb{P}_1$-interpolant of the following transverse fields, defined for each j, using a discrete convolution formula consistent with the one appearing in (3.22), namely,

$$\widetilde{\mathbf{E}}_j^n(\mathbf{x}_T, jh) = V_h^n(jh)\,\nabla\varphi_e(\mathbf{x}_T, jh) + \sum_{m=0}^{n-1} \frac{V^{m+1}(jh) + V^m(jh)}{2}\,\nabla_T\,\varphi_r(\mathbf{x}_T, jh, t^n - t^m)\,\Delta t. \tag{3.27}$$

3.4 Comparison between 3D and 1D calculations

In this section, we present numerical results aiming at illustrating, and even more quantifying, the asymptotic analysis presented in Section 3.2. This will be done by solving problem (3.1) for several values of δ using the numerical method presented in Chapter 2, thus with the second-order formulation (see (2.5) or equivalently (2.8)). Even more, to allow for a comparison between values of δ, we shall compute the rescaled field (cf. (3.3)) that has the advantage to be defined in the reference geometry, as well as the asymptotic electric field appearing in (3.5). The only difference with respect to (2.8) is the apparition of δ-dependent terms in the equations through the simple substitution

$$\mathrm{rot}_T \to \delta^{-1}\,\mathrm{rot}_T, \quad \mathbf{rot}_T \to \delta^{-1}\,\mathbf{rot}_T, \quad \mathrm{div}_T \to \delta^{-1}\,\mathrm{div}_T, \quad \nabla_T \to \delta^{-1}\,\nabla_T\,,$$

which has no incidence on the numerical method of Chapter 2.

3.4.1 The data of the problem

We have chosen to treat a cable whose geometry has no circular symmetry. This geometry is represented in Figure 3.1. The diameter of S is 4 and its intersection with the half-plane $x_1 > 0$ "coincides" with a circular annulus. More precisely :

$$S \cap \{x_1 > 0\} \equiv \{(x_1, x_2) \;/\; x_1 > 0 \text{ and } 1 \leq (x_1^2 + x_2^2)^{\frac{1}{2}} \leq 2\} \tag{3.28}$$

As the cut for the computation of the potential ψ_m (cf. (3.6)), we shall take the segment

$$\Sigma = [1, 2] \times \{0\}. \tag{3.29}$$

The numerical computations are done in the portion $0 \leq x_3 \leq 10$ of the cable. For simplicity, periodic boundary conditions will be applied between $x_3 = 0$ and $x_3 = 10$.

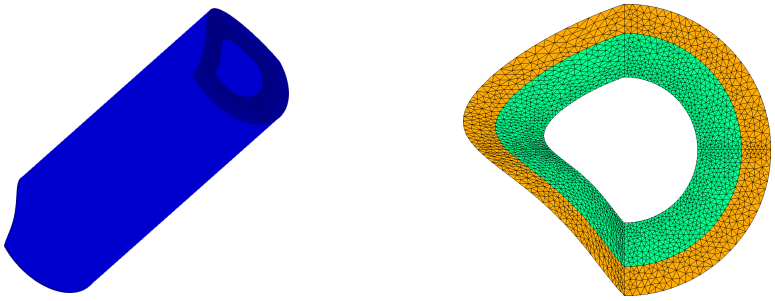

FIGURE 3.1 – Left : the domain Ω, right : the section S of the domain. Each color corresponds to a different material.

Concerning the coefficients of the model, we shall treat two cases

— The *unperturbed* case. This corresponds to the case where the coefficients of the model are invariant by translation in the longitudinal direction,

$$\varepsilon(\mathbf{x}_T, x_3) = \varepsilon^0(\mathbf{x}_T), \quad \mu(\mathbf{x}_T, x_3) = \mu^0(\mathbf{x}_T), \quad \sigma(\mathbf{x}_T, x_3) = \sigma^0(\mathbf{x}_T). \tag{3.30}$$

The cable is however heterogeneous in the cross sections S. More precisely, S is made of two layers $S = S_1 \cup S_2$ and inside S_j, the material is homogeneous (see Figure 3.1),

$$\Big(\varepsilon^0(\mathbf{x}_T), \mu^0(\mathbf{x}_T), \sigma^0(\mathbf{x}_T)\Big) = (\varepsilon_j, \mu_j, \sigma_j) \quad \text{in } S_j. \tag{3.31}$$

In our numerical experiments, we shall take $(\varepsilon_1, \mu_1) = (2, 2)$ and $(\varepsilon_2, \mu_2) = (1, 1)$ so that the velocity of electromagnetic waves, $c(\mathbf{x}) = (\varepsilon\mu)(\mathbf{x})^{-\frac{1}{2}}$ is

$$c(\mathbf{x}) = c_1 = \frac{1}{2} \text{ in } \Omega_1 := S_1 \times \mathbb{R}, \quad c(\mathbf{x}) = c_2 = 1 \text{ in } \Omega_2 := S_2 \times \mathbb{R}. \tag{3.32}$$

Concerning the conductivity, we shall consider two scenarios :

- without any conductivity (*non conductive case.*) : $\sigma_1 = \sigma_2 = 0$,
- with conductivity in Ω_2 (*conductive case.*) : $\sigma_1 = 0,\ \sigma_2 = 0.5$.

— The *perturbed* case. In this case, the translational invariance is broken because the coefficients may vary locally in x_3 near $x_3 = 6$. This can be reinterpreted as a localized damage of the cable. We take,

$$\varepsilon(\mathbf{x}_T, x_3) = \varepsilon^0(\mathbf{x}_T)\ \Big(1 + p(x_3)\Big), \quad \text{and the same for } \mu(\mathbf{x}_T, x_3) \text{ and } \sigma(\mathbf{x}_T, x_3). \tag{3.33}$$

where p is a very localized Gaussian, supported in practice in $[5.75, 6.25]$ (see Figure 3.2),

$$p(x_3) := \pi\, e^{-80\ln(2)(x_3-6)^2}. \tag{3.34}$$

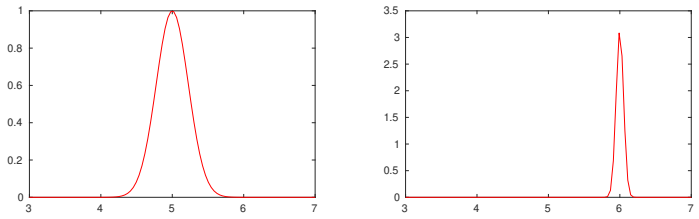

FIGURE 3.2 – The functions $\mathcal{E}(x_3)$ (left) and $p(x_3)$ (right).

We also take initial conditions that are localized near $x_3 = 5$ and are *well prepared* with respect to the expected asymptotic result (3.5). More precisely, $\mathbf{H}_0(\mathbf{x}_T, x_3) = 0$ and

$$\mathbf{E}_0(\mathbf{x}_T, x_3) := \mathcal{E}(x_3)\, \nabla_T\, \varphi_e(\mathbf{x}_T, x_3), \quad \mathcal{E}(x_3) = e^{-\pi^2\,(x_3-5)^2} \tag{3.35}$$

In practice, the initial data are supported in $[4, 6]$ and will generate longitudinal waves with a wavelength $\lambda \simeq 1$. The time interval for the numerical experiments will be $[0, T]$ with $T = 4$ so that, taking into account (3.32), this implies that the waves will not reach the transverse boundaries $x_3 = 0$ and $x_3 = 10$ before the final time T : in other words, the periodic boundary conditions in x_3 will not play any role.

Note that the initial field is transversely polarized. However, due to the heterogeneity of the cable, it will not remain transversely polarized during the time (even in the unperturbed case, separation of variable does not work for Maxwell's equations) as the numerical results will illustrate. Note also that, because of (3.6), $\mathbf{div}(\varepsilon\, \mathbf{E}_0) = 0$.

3.4.2 Discretization parameters

Data for the transverse discretization. The mesh of the cross section will be a triangular mesh represented in Figure 3.1. In particular, there are 20 mesh points along the cut Σ and the typical diameter of each triangle in the mesh is

$$h_T \simeq 0.05.$$

This mesh is used for the 2D transverse problems (3.6,3.7,3.8) for computing the potentials $(\varphi_e, \psi_m, \varphi_r)$ and the coefficients (C, G, L) but also for the 3D computations. Because of the specific form of the coefficients $(\varepsilon, \mu, \sigma)$ for the perturbed case, see (3.33), the potentials $(\varphi_e, \psi_m, \varphi_r)$ coincide with the x_3-independent potentials $(\varphi_e^0, \psi_m^0, \varphi_r^0)$ for the unperturbed case,

$$\varphi_e(\cdot, x_3) = \varphi_e^0(\cdot), \quad \psi_m(\cdot, x_3) = \psi_m^0(\cdot), \quad \varphi_r(\cdot, x_3) = \varphi_r^0(\cdot, t).$$

Thus, only $(\varphi_e^0, \psi_m^0, \varphi_r^0)$ need to be computed numerically. Accordingly, with obvious notation,

$$C(x_3) = \Big(1 + p(x_3)\Big)\, C^0, \quad \text{(the same for } G(x_3), L(x_3), k(x_3, t)).$$

Data for the longitudinal discretization. The longitudinal step size h will be taken as $h = \dfrac{1}{17}$ which is well adapted to the discretization of the Gaussian $\mathcal{E}(x_3)$ (see again Figure 3.2).

This longitudinal mesh will be used for the discretization of the 1D problem (3.22) (cf. (3.9)) but also for the 3D computations.

Data for the time discretization. For facilitating the comparison between the 1D and 3D results, we shall use the same time step Δt for both 1D and 3D computations. According to Remark 3.3.3, the choice of Δt will be constrained by the 3D condition (2.48). For the 3D calculations, we shall take $\theta = \frac{1}{3}$, in which case (2.48) gives : $c^+ \frac{\Delta t}{h} \leq \frac{1}{2}$. In practice we shall choose $\Delta t = 0.95 \frac{h}{2\, c^+}$.

3.4.3 Numerical results

The potentials $(\varphi_e^0, \psi_m^0, \varphi_r^0)$

We present in Figure 3.3 the computed potentials φ_e and ψ_m. The right picture shows at the same time the level lines of φ_e (which are "parallel" to the boundaries) and the ones of ψ_m (which intersect the boundaries). This illustrates that $\Big(\varphi_e(x_1, x_2), \psi_m(x_1, x_2)\Big)$ generalizes polar coordinates inside S.

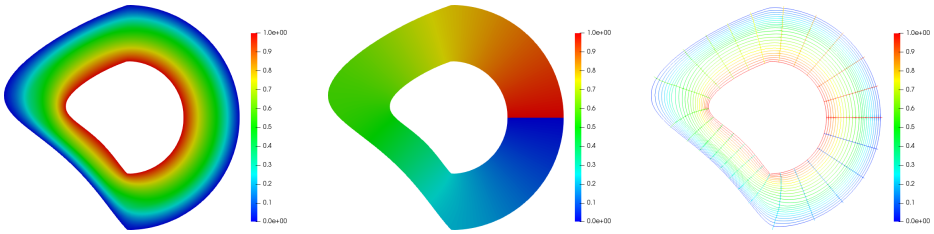

FIGURE 3.3 – Potentials φ_e (left) and ψ_m (center), associated isolines (right).

Figure 3.4 represents, via color levels, the evolution of $\varphi_r(t)$. We observe that $\varphi_r(t)$ tends to 0 when $t \to +\infty$, as expected from its definition (3.7) and the strict positivity of the operator $\mathbf{A}(x_3) \equiv \mathbf{A}$.

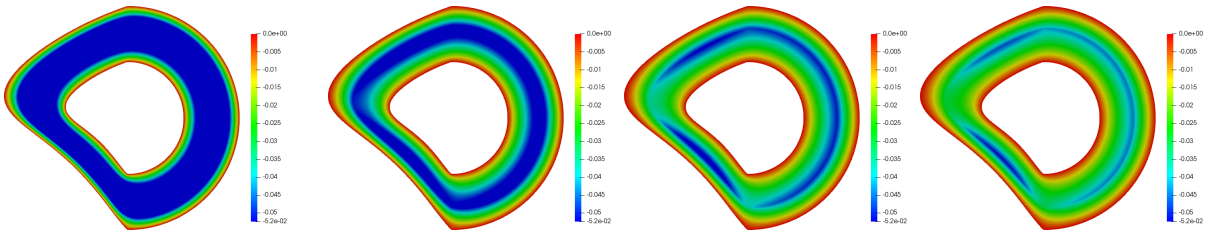

FIGURE 3.4 – Propagation of the $\varphi_r(t)$ field at $t_1 = 0$, $t_2 = 2.43$, $t_3 = 3.47$ and $t_4 = 4$.

Finally, we show in Figure 3.5 the convolution kernel $k(t)$, which is negative (as proven in [34], Lemma 5.2) and tends also to 0 for large t.

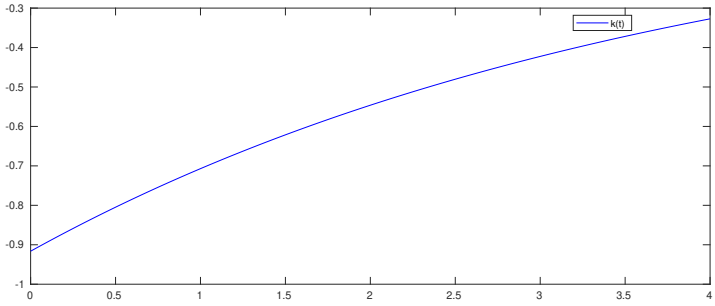

FIGURE 3.5 – The convolution kernel $k(t)$.

3D / 1D comparisons in the unperturbed case.

The non conductive case.

(a) Comparisons of voltages (in 1D). In Figure 3.6, we compare the evolution of the 1D (limit) voltage $V(x_3, t)$ issued from the numerical resolution of the 1D limit model (3.9), to the 1D voltage $V^\delta(x_3, t)$ for the 3D problem, defined by (3.17) and obtained by post-processing the 3D solution $\widetilde{\mathbf{E}}_T^\delta$.

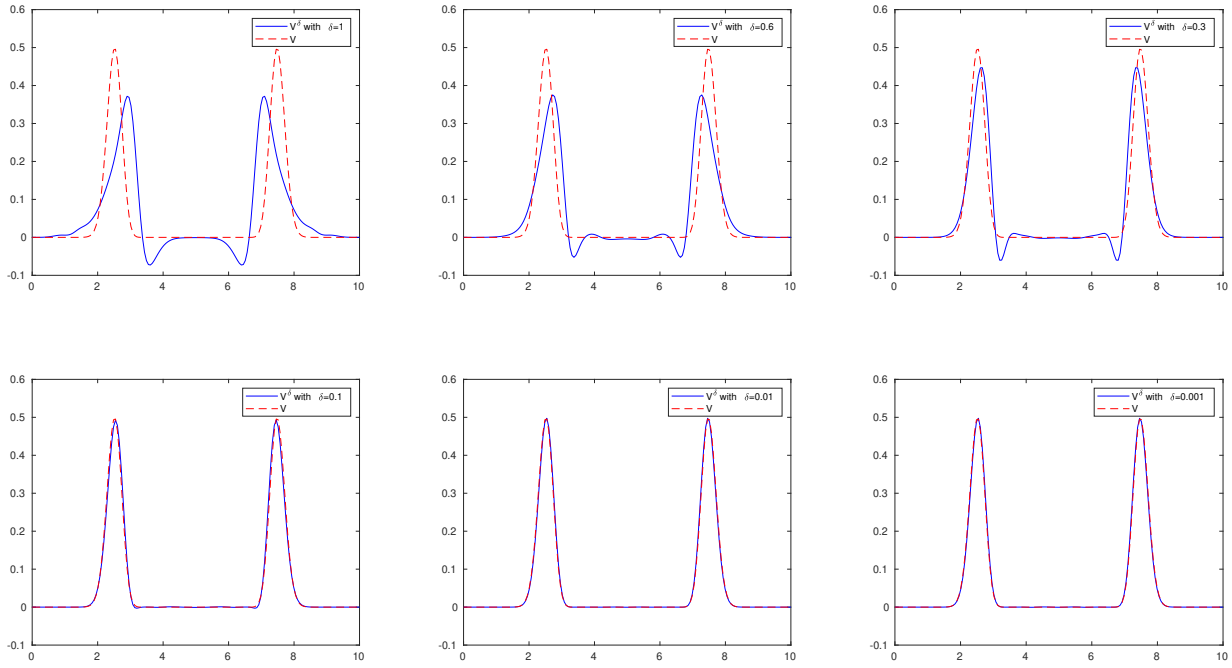

FIGURE 3.6 – The voltages V^δ and V at $t = 4$.

More precisely, we compare the above functions in space at the final time $T = 4$ for δ decreasing from 1 to 10^{-3}. The limit solution $V(x_3, T)$ is in red while $V^\delta(x_3, T)$ is in blue. The numerical results confirm the convergence of $V^\delta(x_3, t)$ towards $V(x_3, t)$. We observe that V and V^δ already almost coincide for $\delta = 0.1$. This corresponds to a cable diameter equal to 0.4, to be compared to the length of the support (in x_3) of the initial condition, which is about 1 according to Figure 3.2.

(b) Comparison of the electric fields in 3D. We now compare, still at the final time $T = 4$, the norm of the electric field for $\delta > 0$ with its limit value. In Figure 3.7, we represent $|\widetilde{\mathbf{E}}_T^\delta|$ on the boundary $\partial\Omega$ of the reference cable for $\delta = 1$ and $\delta = 10^{-3}$ and $\delta = 0$. We observe that the result obtained with $\delta = 10^{-3}$ cannot be distinguished from the one obtained with the limit model while a substantial difference exists for $\delta = 1$. In Figure 3.8, we make the

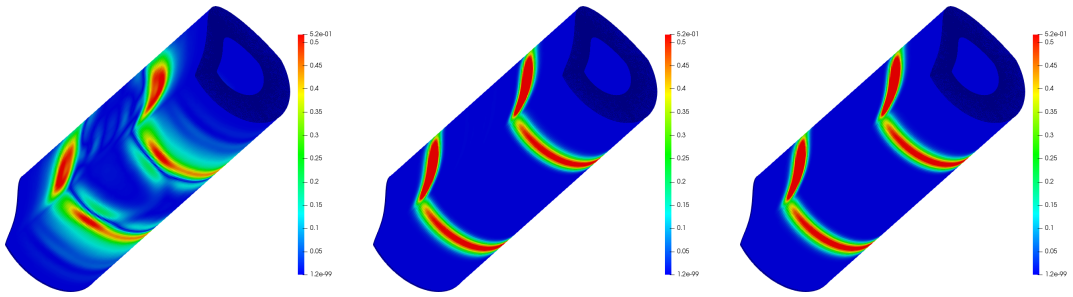

FIGURE 3.7 – Left $|\widetilde{\mathbf{E}}_T^\delta|$ with $\delta = 1$, Center $|\widetilde{\mathbf{E}}_T^\delta|$ with $\delta = 10^{-3}$, Right $|\widetilde{\mathbf{E}}_T^0|$ at $t = 4$.

same comparison in the cross section $x_3 = 2.71$, which roughly corresponds to the position of the wave at time $T = 4$ (see Figure 3.6). Again we observe that the results are very close for $\delta = 10^{-3}$ and $\delta = 0$, themselves quite different from the result obtained for $\delta = 1$.

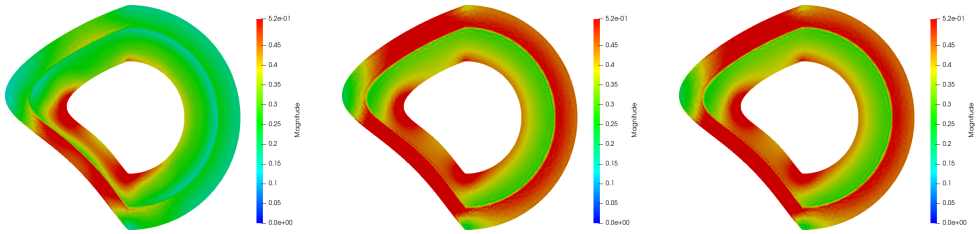

FIGURE 3.8 – Left $|\widetilde{\mathbf{E}}_T^\delta|$ with $\delta = 1$, Center $|\widetilde{\mathbf{E}}_T^\delta|$ with $\delta = 10^{-3}$, Right $|\widetilde{\mathbf{E}}_T^0|$ for $x_3 = 2.71$ and $t = 4$.

Finally, in order to test the asymptotic transverse polarization of the electric field, we represent in Figure 3.9, again along $\partial\Omega$ at time $T = 4$, the longitudinal electric field $\widetilde{E}_3^\delta$. Let us draw the attention of the reader to the fact that the color scale is quite different from the ones in Figures 3.7 and 3.8. We observe that, as expected, the longitudinal field tends to 0 when δ tends to 0. On the other hand, for $\delta = 1$ we see that, as announced previously, the field is really non transversely polarized even though the initial field is (cf.(3.35)) : this confirms that separation of variables does not work.

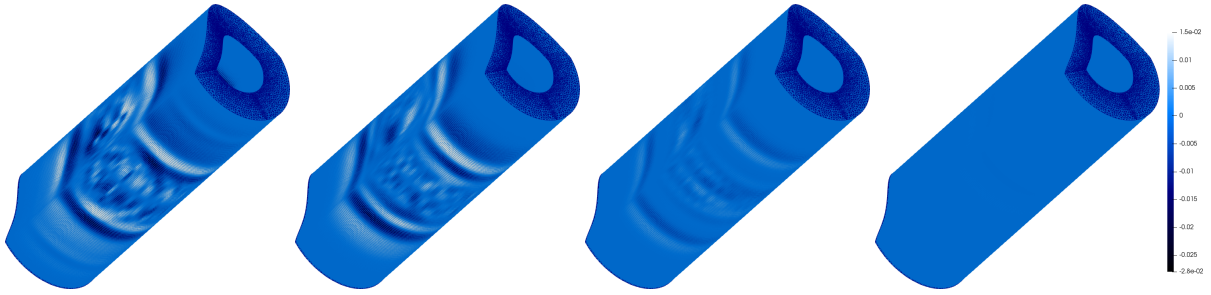

FIGURE 3.9 – E_3^δ with $\delta = 1$, $\delta = 0.5$, $\delta = 0.1$, $\delta = 0.001$ at $t = 4$.

The conductive case.

(a) Comparisons of voltages (in 1D). In figure 3.10, we compare the evolution of the 1D (limit) voltage $V(x_3, t)$ to the 1D voltage $V^\delta(x_3, t)$, exactly as in figure 3.6.

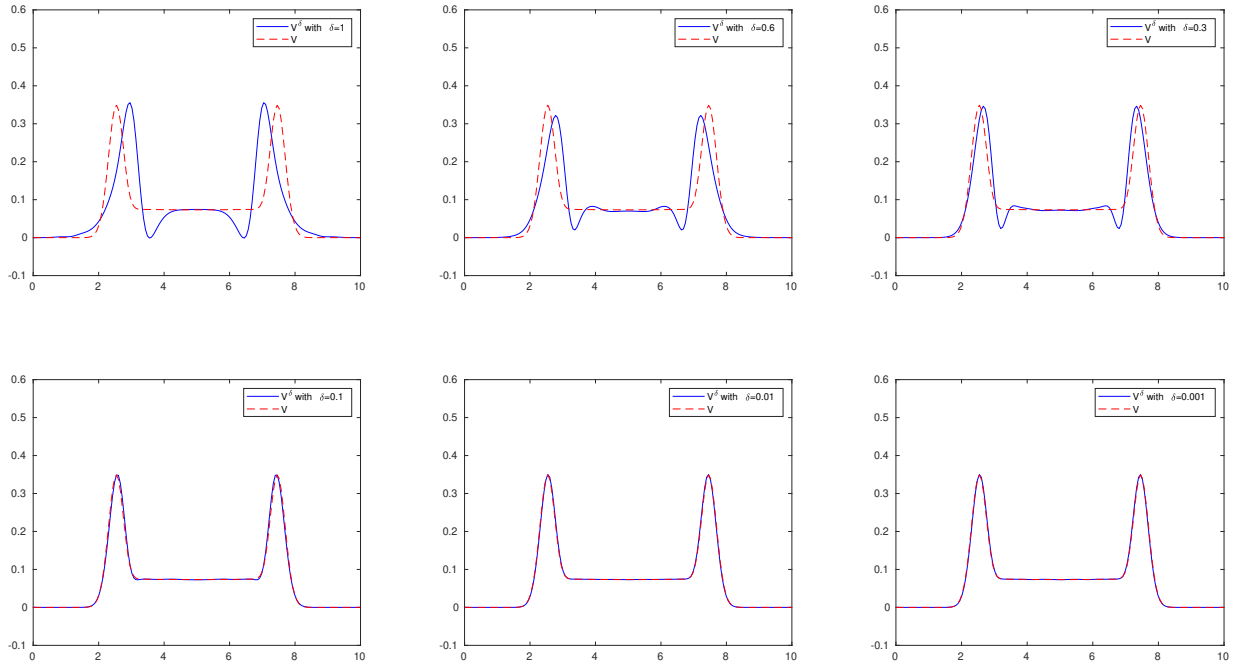

FIGURE 3.10 – The voltages V^δ and V at $t = 4$.

There are two main effects due to the conductivity (clearly visible on the limit blue curves) : the attenuation of the signal (compare Figures 3.6 and 3.10) and the shape of the wave. However, the convergence of $V^\delta(x_3, t)$ towards $V(x_3, t)$ is very similar to the one for the non-conductive case for $\delta \leq 0.1$, but varying δ above 0.1 affects the waveform much more than in the non-conductive case.

(b) Comparison of the electric fields in 3D. We now compare in Figure 3.11, still at the final time $T = 4$ on the boundary $\partial\Omega$, the norm of the electric field for $\delta > 0$ with the one of its limit value, exactly as in Figure 3.7. The conclusions are the same as for the non-conductive case.

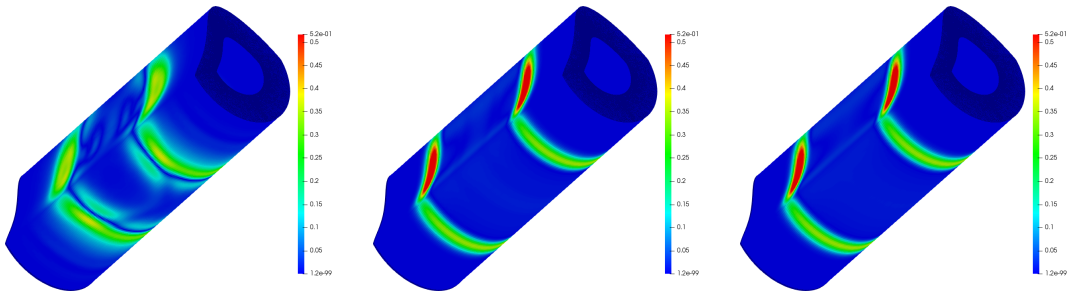

FIGURE 3.11 – Left $|\widetilde{\mathbf{E}}_T^\delta|$ with $\delta = 1$, Center $|\widetilde{\mathbf{E}}_T^\delta|$ with $\delta = 10^{-3}$, Right $|\widetilde{\mathbf{E}}_T^0|$ at $t = 4$.

The perturbed case.

The non-conductive case.

(a) Comparisons of voltages (in 1D). As represented in Figure 3.12, the main effect of the local perturbation is the apparition of reflection phenomena. We observe that the convergence to the limit solution is much slower than in the unperturbed case (compare with Figure 3.6) : for instance, one needs $\delta = 0.01$ to get a correct localization of the reflected waves. This is probably due to the fact that we have considered a strong defect with fast variations and large amplitude.

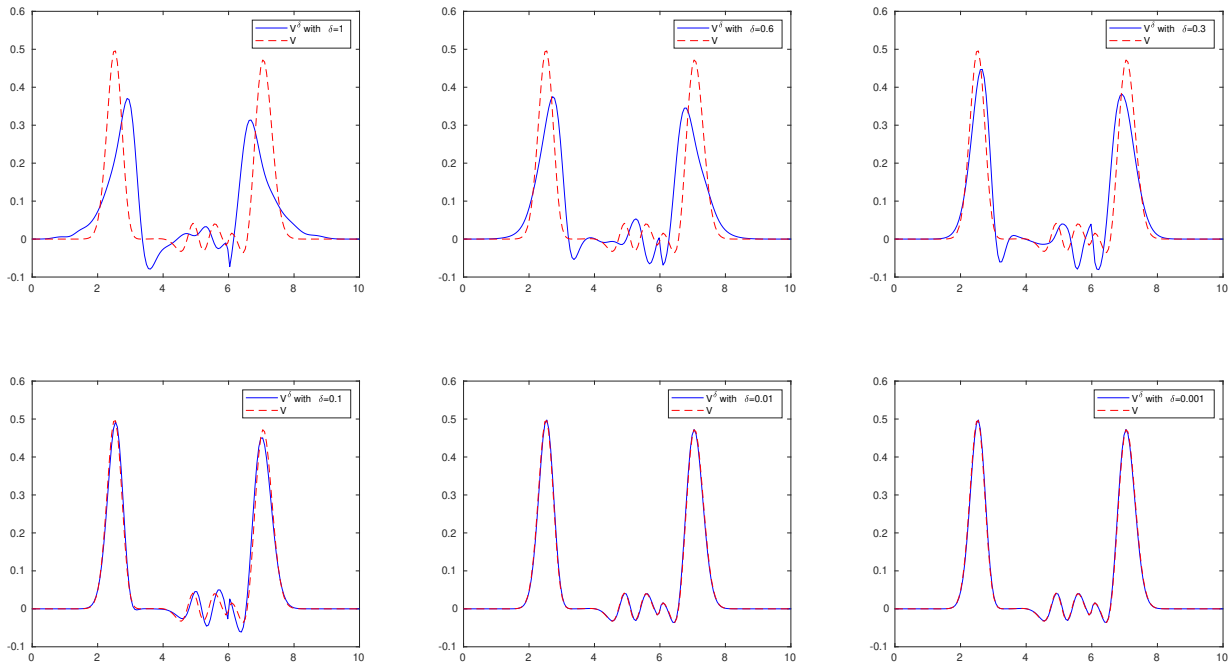

FIGURE 3.12 – The voltages V^δ and V at $t = 4$.

(b) Comparison of the electric fields in 3D. This is the object of Figure 3.13, to be compared with Figure 3.7. In Figure 3.13, we represent the norm $|\widetilde{\mathbf{E}}_T^\delta|$ on the boundary $\partial\Omega$ of the reference cable for $\delta = 1$ and $\delta = 10^{-3}$ and $\delta = 0$. We observe that the norm of the 3D field cannot be distinguished from the one of the limit field $\delta = 10^{-3}$ while a substantial difference exists for $\delta = 1$, and as found in the 1D results, we also observe that the wave is reflected because of the perturbation localized at $x_3 = 6$.

The conductive case.

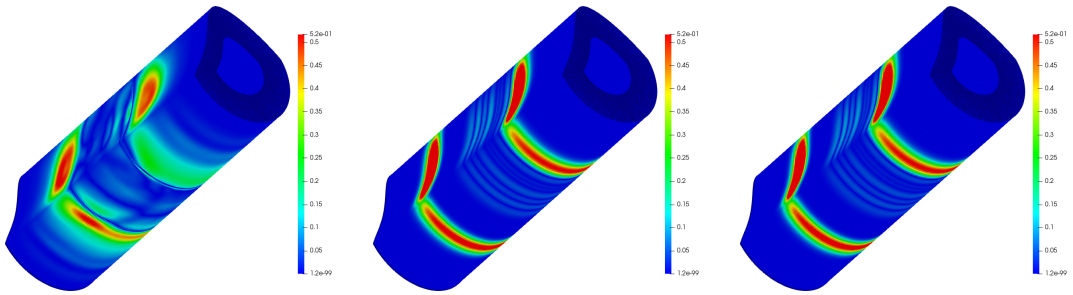

FIGURE 3.13 – Left $|\widetilde{\mathbf{E}}_T^\delta|$ with $\delta = 1$, Center $|\widetilde{\mathbf{E}}_T^\delta|$ with $\delta = 10^{-3}$, Right $|\widetilde{\mathbf{E}}_T^0|$ at $t = 4$.

We repeat in Figures 3.14 and 3.15, the same experiments / comparisons as in Figures 3.10 and 3.11 for the non conductive case, respectively for the 1D voltages and the 3D electric fields. Once again, one observes a big influence of the presence of the conductivity on the shape of the propagating wave. However, this does not affect the speed of convergence towards the limit model, which is quite similar to the one observed in the non conductive case.

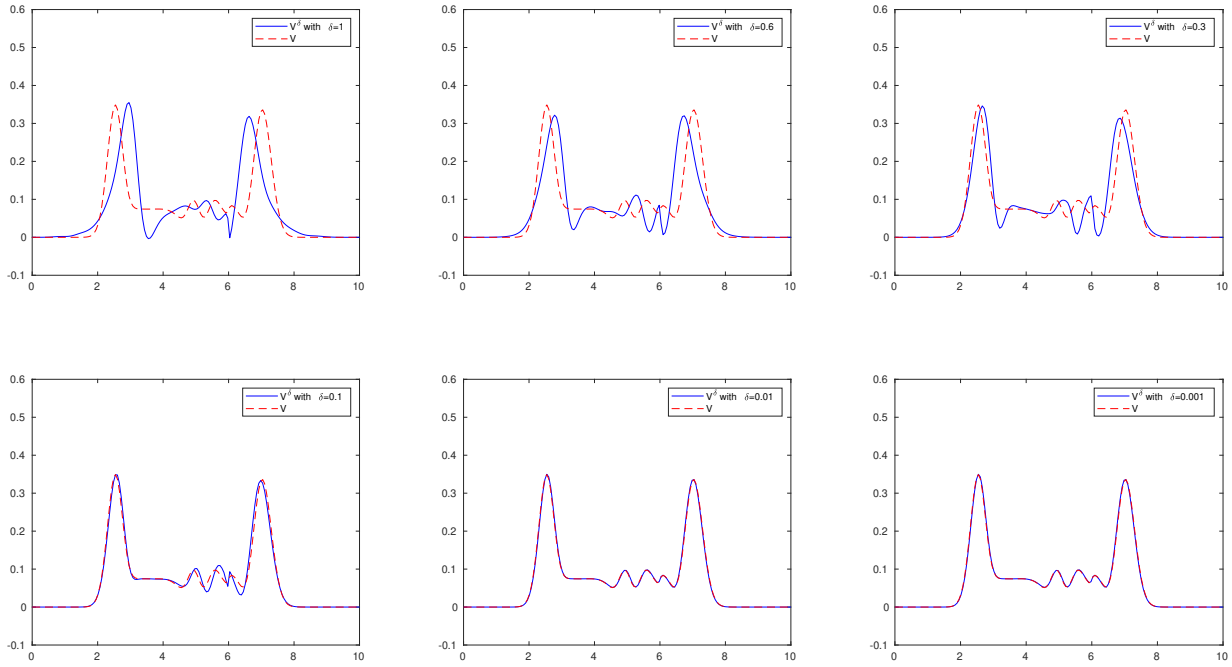

FIGURE 3.14 – The voltages V^δ and V at $t = 4$.

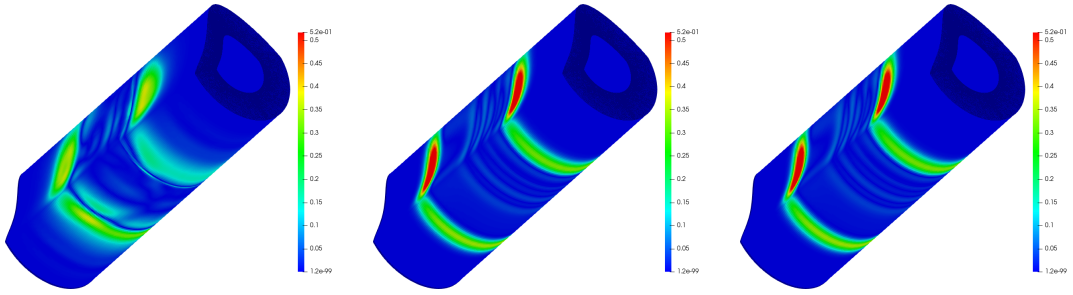

FIGURE 3.15 – Left $|\widetilde{\mathbf{E}}_T^{\delta}|$ with $\delta = 1$, Center $|\widetilde{\mathbf{E}}_T^{\delta}|$ with $\delta = 10^{-3}$, Right $|\widetilde{\mathbf{E}}_T^{0}|$ at $t = 4$.

3.5 Conclusion

In this chapter, we proposed a numerical method to solve the 1D limit model. Then, we used the approach developed in Chapter 1 to validate this 1D limit model. The numerical results showed that the 1D limit model is a good approximation of the 3D model when the thinness δ tends to zero. However, in order to obtain more efficient approximations, it will be interesting to consider a higher order 1D model. This is the subject of the next chapter, in which we will consider the case of the second order 1D model.

Chapter 4

The 1D effective telegrapher's model of order 2 and 3D/1D comparison

Contents

4.1 Introduction

In the previous chapter, we have seen 3D/1D comparisons. In particular, we have shown that the simulation of the full 3D Maxwell's equation and the simulation of the 1D telegrapher's model are very closed when the thinness of the cable is "very small". We recall that the 1D models we used can be obtained through asymptotic analysis with respect to the thinness parameter. In this asymptotic analysis, we have assumed that the electromagnetic fields can be expand in polynoms of power δ where δ is the thinness parameter. In the previous chapter (Chapter 3), we have only consider the first term of this asymptotic expansion. We can also consider higher terms in this expansions. In ([10] Chapter 5), some high-order asymptotic 1D models were derived. This models are more accurate since there are valid even if the thinness is bigger than the one considered in the previous chapter. These models have been rigorously justified, from a mathematical point of view, but there is no numerical validation of their accuracy. In the present chapter, we shall consider the

numerical validation of particular case of the second order model with respect to the thinness parameter, by 1D/3D comparison.

This chapter is organized as follows :

We start in Section 4.2.1 by giving a brief recap of the second-order 1D telegrapher's model in the case of a purely cylindrical cable with heterogeneous cross-sections. Then, in Section 4.2.2, we recall the construction of this second-order 1D model. After that, in Section 4.3, we present a scheme to perform numerical simulations for the obtained 1D model. Finally, we show some comparisons between 1D and 3D computations in Section 4.4.

4.2 A second order effective model for cylindrical cables with piecewise homogeneous cross sections

Second order effective model have been derived for very general cables in the PhD thesis of G. Beck [10]. We restrict ourselves here to describe this model for the class of cables described in the next section (see Definition 4.2.1).

4.2.1 Description of the second order model

In general 1D models of wave propagation in a coaxial cable can be derived by asymptotic analysis from 3D Maxwell's equations for small thinness δ. The reader can refer to Section 3.2 in Chapter 3 for a presentation of Maxwell's equations in a thin cylindrical coaxial cable $\Omega^\delta = \delta S \times \mathbb{R}$ where S is a reference cross section. In this chapter, we will moreover assume that the coaxial cable is cylindrical that the characteristic coefficients of the dielectric material, i.e. ε and μ, do not depend of the longitudinal variable x_3

$$\varepsilon(\mathbf{x}_T, x_3) := \varepsilon(\mathbf{x}_T) \quad \text{and} \quad \mu(\mathbf{x}_T, x_3) := \mu(\mathbf{x}_T) \quad \mathbf{x}_T \in S,\ x_3 \in \mathbb{R}, \tag{4.1}$$

and that there is no electrical conductivity, i.e. $\sigma = 0$. In that context we can consider the following "generalized" telegrapher's equations

$$\begin{cases} \mathbf{C}_\delta(\partial_3)\,\partial_t V^{\delta,2} & + \partial_3\, I^{\delta,2} & = & 0, \\ \mathbf{L}_\delta(\partial_3)\,\partial_t I^{\delta,2} & + \partial_3\, V^{\delta,2} & = & 0, \end{cases} \tag{4.2}$$

where $V^{\delta,2}$ and respectively $I^{\delta,2}$ refers to the electrical voltage and respectively electrical current. We use the notation $\delta, 2$ to emphasize that we consider a more accurate model that the one considered in Section 3.2 of Chapter 3. Indeed, the reader will observe that this model corresponds formally to the limit model presented in Chapter 3 in absence of conductivity, except the fact that the capacitance C and the inductance L appearing in (3.10) become respectively a capacitance and inductance operators (this is the main difference with the limit model (3.9)). More precisely, these are the second order elliptic operator given by

$$\mathbf{C}_\delta(\partial_3) := C - \delta^2\,\gamma_e \partial_3^2, \quad \mathbf{L}_\delta(\partial_3) := L - \delta^2 \gamma_m\,\partial_3^2. \tag{4.3}$$

The new coefficients γ_e and γ_m, respectively the electric and magnetic dispersion coefficients, involve two potentials, namely ψ_e and φ_m which are defined as the solutions of new

elliptic problems in the reference cross section S.

For ψ_e this problem is

$$\begin{cases} \operatorname{div}_T\left(\varepsilon^{-1}\,\nabla_T\,\psi_e\right)=0 & \text{in } S\setminus\Sigma,\\ \partial_n\psi_e=0, & \text{on } \partial S, \qquad \displaystyle\int_S \psi_e\,d\mathbf{x}_T=0,\\ [\psi_e]_\Sigma=1, \quad [\partial_n\psi_e]_\Sigma=0, & \text{through } \Sigma, \end{cases} \tag{4.4}$$

where Σ is a cut of the cross S, and $[u]_\Sigma$ denotes the jump of u across Σ (properly defined in [34], Section 3.1).

For φ_m, it is

$$\begin{cases} \operatorname{div}_T\left(\mu^{-1}\,\nabla_T\,\varphi_m\right)=0, & \text{in } S,\\ \varphi_m=1, \quad \text{on } \Gamma_i, \quad \varphi_m=0, & \text{on } \Gamma_e, \end{cases} \tag{4.5}$$

with Γ_i (resp. Γ_e) is the inner boundary (resp the outer boundary).

The coefficients γ_e and γ_m are then given by

$$\gamma_e=\int_S \varepsilon\,|\varphi_e-\varphi_m|^2\,d\mathbf{x}_T, \quad \gamma_m=\int_S \mu\,|\widetilde{\psi}_e-\widetilde{\psi}_m|^2\,d\mathbf{x}_T, \tag{4.6}$$

where the potentials φ_e and ψ_m have been defined in (3.6), and $\widetilde{\psi}_e$ and $\widetilde{\psi}_m$ are deduced from ψ_e and ψ_m by subtracting their weighted mean value with respect to the weight functions ε and μ :

$$\widetilde{\psi}_e=\psi_e-\langle\psi_e\rangle_\mu, \quad \widetilde{\psi}_m=\psi_m-\langle\psi_m\rangle_\mu, \quad \text{where } \langle g\rangle_\mu=\Big(\int_S \mu\,d\mathbf{x}_T\Big)^{-1}\Big(\int_S \mu\,g\,d\mathbf{x}_T\Big). \tag{4.7}$$

Remark 4.2.1. *In a more general case, i.e. not cylindrical or not longitudinally homogeneous, the 1D effective model still be of the form (4.2) but the capacitance and inductance operators (4.3) will have more complicated expression (see Chapter 5 in [10]).*

If the electromagnetic wave velocity $c=1/\sqrt{\varepsilon\mu}$ is constant, then the dispersion coefficients γ_e and γ_m are null. Indeed in that case, $\varphi_e=\varphi_m$ and $\psi_e=\psi_m$. In the following we shall be interested in cables for which dispersion occurs. One important class or dispersive media is provided by cables whose internal structure is made of finitely many materials structured in an onion-like manner. By this we mean that the coefficients are piecewise constant in successive concentric layers. This is formulated mathematically in the following way.

Definition 4.2.1 (Onion-like piecewise homogeneous cylindrical cables)**.**
An onion-like piecewise homogeneous cylindrical coaxial cable Ω is of the form $\Omega=S\times\mathbb{R}$ such that,

1. *There exists a finite sequence $\{\mathcal{O}_j, j=0,1,\cdots,N\}$ of simply connected open subsets of $\mathbb{R}^2$ such that*

$$\forall\, j\le N-1, \quad \overline{\mathcal{O}}_j\subset\mathcal{O}_{j+1}, \quad \partial\mathcal{O}_0=\Gamma_i, \quad \partial\mathcal{O}_N=\Gamma_e, \tag{4.8}$$

in such a way that $S:=\mathcal{O}_e\setminus\mathcal{O}_i$ is the union of N distinct layers S_j, in the sense that

$$\overline{S}=\bigcup_{j=1}^{N}\overline{S}_i, \quad S_j:=\overline{\mathcal{O}}_j\setminus\mathcal{O}_{j-1}. \tag{4.9}$$

2. *The functions ε and μ are piecewise constant according to the partition (4.9) : there exists positive coefficients (ε_j, μ_j) such that*

$$\varepsilon = \varepsilon_j, \quad \mu = \mu_j \quad in\ S_j, 1 \leq j \leq N. \tag{4.10}$$

In Figure 4.1 an example of the cable Ω when $N = 3$ is given (the cable is made of three concentric layer).

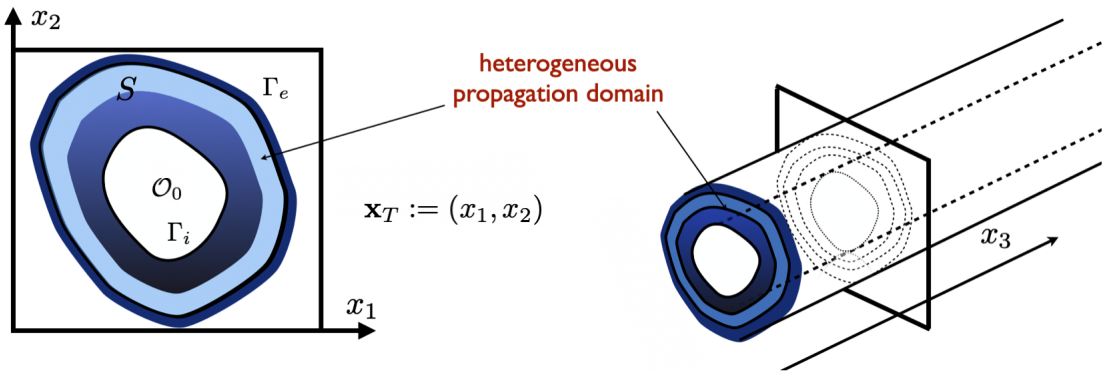

FIGURE 4.1 – Left : the cross-section S of the domain, right : the domain Ω. Each color corresponds to a different material.

Lemma 4.2.1. *The onion-like structure of Definition 4.2.1 implies that $\psi_m = \psi_e$. In particular, any cable with the onion-like structure of Definition 4.2.1 is without magnetic dispersion, i.e. $\gamma_m = 0$.*

Proof.

Step 1 : Onion-like structure cylindrical cable with a circular cross-section.

In the case where the cross section S of the onion-like structure cable is a circular annulus, and ε and μ are radial, one has in polar coordinate system (r, θ) (for more details, see (A.58) in Appendix A)

$$\psi_e = \psi_m = 1 - \frac{\theta}{2\pi}. \tag{4.11}$$

Thus, in the circular annulus case, one has $\gamma_m = 0$.

Step 1 : Onion-like structure cylindrical cable with a non-circular cross-section.

We start by introducing a transformation $\mathcal{T}_v$ to come back to the case of a circular cross-section. More precisely,

$$\mathcal{T}_v =: S \to \widehat{S},$$

with S is the cross-section of the cable Ω, and $\widehat{S}$ is the circular reference cross-section. So using this transformation for each cross-section, we get an onion-like structure cable with a circular annulus (see Figure 4.2).

We will choose this transformation in such a way that it preserves the volume, i.e. map with

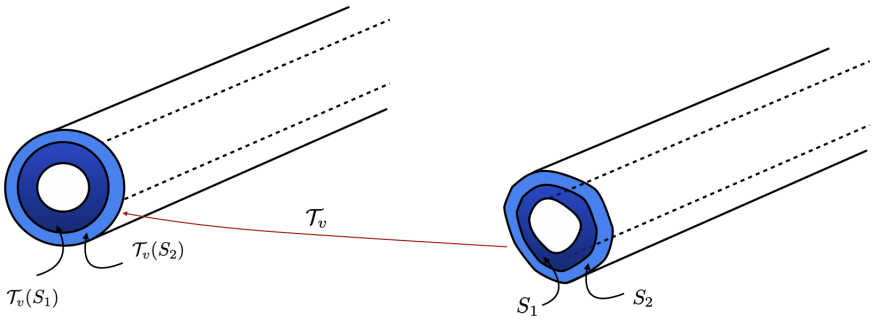

FIGURE 4.2 – Left : the reference cable $\widehat{\Omega} = \widehat{S} \times \mathbb{R}$. Right : the cable $\Omega = S \times \mathbb{R}$.

unitary Jacobian (see [10] Page 154). To to this, we denote by $\mathfrak{v}_n$ the volume of each layer S_n and by $2r_*$ the diameter of S. We can construct a piecewise preserving volume elements mapping $\mathcal{T}_v$ such it restrictions $\mathcal{T}_v^n := \mathcal{T}_v\big|_{S_n}$ transform each layer S_n into an annulus $\widehat{S}_n$, with inner radii r_{n-1} and outer radii r_n, of the same area (see Figure 4.3), where the radii are found through this induction

$$\begin{cases} r_N = r_* \\ r_{n-1} = \sqrt{r_n^2 - \dfrac{\mathfrak{v}_n}{\pi}}. \end{cases}$$

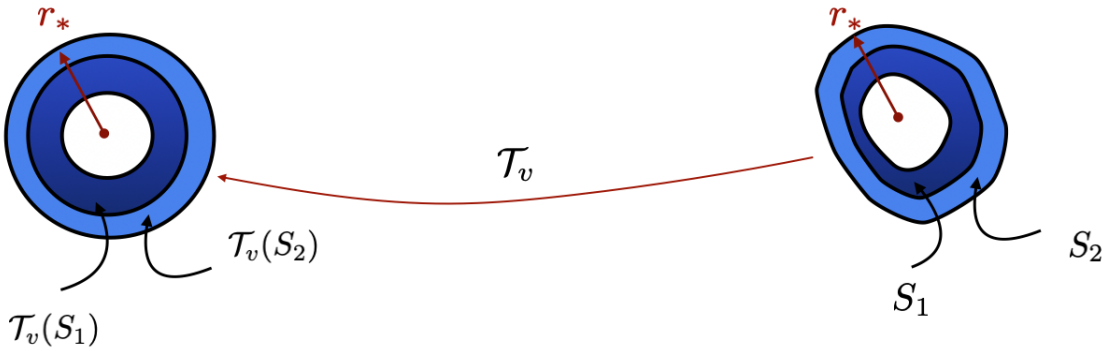

FIGURE 4.3 – The piecewise preserving volume elements mapping $\mathcal{T}_v$.

Thus, using this volume preserving transformation and the definition of γ_m (see (4.6)), one has

$$\gamma_m = \int_{\widehat{S}} \mu \circ \mathcal{T}_v(\mathbf{x}_T) |\widetilde{\psi}_{e,v} - \widetilde{\psi}_{m,v}|,$$

where

$$\widetilde{\psi}_{e,v} = \psi_{e,v} - \langle \psi_{e,v} \rangle_\mu, \quad \widetilde{\psi}_{m,v} = \psi_{m,v} - \langle \psi_{m,v} \rangle_\mu,$$

where the potentials $\psi_{e,v}$ and $\psi_{m,v}$ are the solutions of the following problems,

$$\begin{cases} \operatorname{div}_T \left((\mu \circ \mathcal{T}_v) \nabla_T \psi_{m,v} \right) = 0 & \text{in } \widehat{S} \setminus \mathcal{T}_v(\Sigma), \\ \partial_n \psi_{m,v} = 0, & \text{on } \partial\widehat{S}, \qquad \displaystyle\int_{\widehat{S}} \psi_{m,v} \, d\mathbf{x}_T = 0, \\ [\psi_{m,v}]_{\mathcal{T}_v(\Sigma)} = 1, \quad [\partial_n \psi_{m,v}]_{\mathcal{T}_v(\Sigma)} = 0, & \text{through } \mathcal{T}_v(\Sigma), \end{cases}$$

and

$$\begin{cases} \mathrm{div}_T\left((\varepsilon^{-1}\circ\mathfrak{T}_v)\,\nabla_T\,\psi_{e,v}\right)=0 & \text{in } \widehat{S}\setminus\mathfrak{T}_v(\Sigma),\\ \partial_n\psi_{e,v}=0, & \text{on } \partial\widehat{S}, \qquad \displaystyle\int_{\widehat{S}}\psi_{e,v}\,d\mathbf{x}_T=0.\\ [\psi_{e,v}]_{\mathfrak{T}_v(\Sigma)}=1, \quad [\partial_n\psi_{e,v}]_{\mathfrak{T}_v(\Sigma)}=0, & \text{through } \mathfrak{T}_v(\Sigma), \end{cases}$$

Again, one has in polar coordinates,

$$\psi_{m,v}=\psi_{e,v}=1-\frac{\theta}{2\pi}.$$

this leads us to say that $\gamma_m=0$. ■

In that case, the second order model model (4.2) simplifies into

$$\begin{cases} \mathbf{C}_\delta(\partial_3)\,\partial_t V^{\delta,2} & +\partial_3\,I^{\delta,2} & = & 0,\\ L\,\partial_t I^{\delta,2} & +\partial_3\,V^{\delta,2} & = & 0. \end{cases} \tag{4.12}$$

It is also possible to show that, if moreover the electromagnetic wave velocity $c=1/\sqrt{\varepsilon\mu}$ is not constant, then the dispersive electric coefficient γ_e is positive. We will not give the proof here but the tools are very similar to the one used in the proof of Lemma 4.2.1, namely the used of volume preserving transformation and explicit computation in circular annulus case.

The elimination of $I^{\delta,2}$ in (4.12) results into a dispersive wave equation for $V^{\delta,2}$:

$$\mathbf{C}_\delta(\partial_3)\,\partial_t^2\,V^{\delta,2}-L^{-1}\,\partial_3^2\,V^{\delta,2}=0, \tag{4.13}$$

or equivalently, in more explicit form

$$\partial_t^2 V^{\delta,2}-c^2\,\partial_3^2 V^{\delta,2}-\gamma_e\,C^{-1}\,\partial_3^2\partial_t^2 V^{\delta,2}=0, \text{ with } c^2=C^{-1}L^{-1}.$$

4.2.2 Formal derivation of the second order model

Preliminary material

To derive the second-order 1D telegrapher's model we will need some technical lemmas.

We introduce $\mathcal{E}$ the space defined by :

$$\mathcal{E}=\left\{\mathbf{u}_T\in[L^2(S)]^2\,|\,\mathrm{rot}_T\,\mathbf{u}_T=0, \quad \mathrm{div}_T(\varepsilon\,\mathbf{u}_T)=0, \quad \mathbf{u}_T\times\mathbf{n}_T=0\right\}.$$

Lemma 4.2.2.

We have $\mathcal{E}=$ *span* $\{\nabla_T\widehat{\varphi}_e\}$, *where* $\widehat{\varphi}_e$ *is the unique function solution of the 2D problem*

$$\begin{cases} \mathrm{div}_T\left(\varepsilon\,\nabla_T\,\widehat{\varphi}_e\right)=0, & \textit{in } S,\\ \widehat{\varphi}_e=1, & \textit{on } \Gamma_i,\\ \widehat{\varphi}_e=0, & \textit{on } \Gamma_e. \end{cases} \tag{4.14}$$

Proof. See [34] Page 11. ■

We denote $\mathcal{H}$ the space defined by :

$$\mathcal{H} = \Big\{ \mathbf{u}_T \in [L^2(S)]^2 \,|\, \mathrm{rot}_T\, \mathbf{u}_T = 0, \quad \mathrm{div}_T\,(\mu\, \mathbf{u}_T) = 0, \quad \mathbf{u}_T \cdot \mathbf{n}_T = 0 \Big\}.$$

Lemma 4.2.3.

We have $\mathcal{H} = span\, \left\{ \nabla_T \widehat{\psi}_m \right\}$, *where* $\widehat{\psi}_m$ *is the unique function solution of the 2D boundary value problem*

$$\begin{cases} \mathrm{div}_T \left(\mu\, \nabla_T\, \psi_m \right) = 0 & \text{in } S \setminus \Sigma, \\ \partial_n \psi_m = 0, & \text{on } \partial S, \\ [\psi_m]_\Sigma = 1, \quad [\partial_n \psi_m]_\Sigma = 0, & \text{through } \Sigma, \\ \displaystyle\int_S \psi_m \, d\mathbf{x}_T = 0. \end{cases} \tag{4.15}$$

Proof. See [34] Page 13. ■

Lemma 4.2.4. *Let* $(\varphi_e, \psi_m) \in H^1(S) \times H^1(S \setminus \Sigma)$ *solutions, respectively, of the problems defined in* (3.6). *one has,*

- $\left(\mathbf{rot}_T\, \widehat{\psi}_m, \nabla_T\, \widehat{\varphi}_e \right)_{L^2(S)} = -\left(\mathbf{rot}_T\, \widehat{\varphi}_e, \nabla_T\, \widehat{\psi}_m \right)_{L^2(S)} = 1.$
- $\left(\mathbf{rot}_T\, \widehat{\varphi}_e, \nabla_T\, \widehat{\psi}_m \right)_{L^2(S)} = 0.$
- $\left(\mathbf{rot}_T\, \widehat{\psi}_m, \nabla_T\, \widehat{\varphi}_e \right)_{L^2(S)} = 0.$

Proof. See [34] Page 19. ■

Lemma 4.2.5. *The potentials* (φ_e, ψ_e) *and* (φ_m, ψ_m) *are conjugated in the sense they satisfy the relation*

$$\begin{cases} \varepsilon\, \nabla_T\, \varphi_e = C\, \mathbf{rot}_T\, \psi_e, \\ \mu\, \nabla_T\, \psi_m = -L\, \mathbf{rot}_T\, \varphi_m. \end{cases} \tag{4.16}$$

Proof. See the proof of Lemma 2.4 in [12]. ■

Asymptotic analysis

In order to derive our asymptotic expansion, we first rescale the fields – solution of equations (3.1) in Chapter 3– in the fixed domain $S \times \mathbb{R}$ setting

$$\widetilde{\mathbf{E}}^\delta(\mathbf{x}, \mathbf{t}) := \mathbf{E}^\delta(\delta\, \mathbf{x_T}, \mathbf{x_3}, \mathbf{t}), \quad \widetilde{\mathbf{H}}^\delta(\mathbf{x}, \mathbf{t}) := \mathbf{H}^\delta(\delta\, \mathbf{x_T}, \mathbf{x_3}, \mathbf{t}), \quad \forall\, (\mathbf{x_T}, \mathbf{x_3}) \in \mathbf{S} \times \mathbb{R}. \tag{4.17}$$

As in [12], we postulate an Ansatz for the electromagnetic field of the form of a power series expansion in δ

$$\begin{cases} \widetilde{\mathbf{E}}^\delta(\mathbf{x}_T, x_3) = \displaystyle\sum_{p=0}^{\infty} \delta^p\, \widetilde{\mathbf{E}}^p\, (\mathbf{x}_T, x_3) + O(\delta^\infty), \\ \widetilde{\mathbf{H}}^\delta(x^\delta, x_3^\delta) = \displaystyle\sum_{p=0}^{\infty} \delta^p\, \widetilde{\mathbf{H}}^p\, (\mathbf{x}_T, x_3) + O(\delta^\infty), \end{cases} \quad \text{with} \quad \mathbf{x}_T \in S, x_3 \in \mathbb{R} \tag{4.18}$$

where each coefficients $(\widetilde{\mathbf{E}}^p, \widetilde{\mathbf{H}}^p) : S \times \mathbb{R} \to \mathbb{R}^3$ are given by injecting the Ansatz (4.18) in the Maxwell's equations (3.1) (in Chapter 3). This was done in [10] in Chapter 5. We will just recall the cascade of equations to determine $(\widetilde{\mathbf{E}}^{p+1}, \widetilde{\mathbf{H}}^{p+1})$ from $(\widetilde{\mathbf{E}}^p, \widetilde{\mathbf{H}}^p)$ in the particular case of cable with onion-like structure. We will be interested only in the cases $p = 0, 1, 2$. To do that, we separate for each 3D fields, the tangential component and the longitudinal one

$$\widetilde{\mathbf{E}}^p = \begin{pmatrix} \widetilde{\mathbf{E}}_T^p \\ \widetilde{E}_3^p \end{pmatrix} \quad \text{with} \quad \widetilde{\mathbf{E}}_T^p = \begin{pmatrix} E_1^p \\ E_2^p \end{pmatrix} \quad \text{and so on for } \widetilde{\mathbf{H}}^p.$$

The cascade of equations is :

- Transverse electric fields

$$\begin{cases} \operatorname{div}_T(\varepsilon\ \widetilde{\mathbf{E}}_T^p) = -\partial_3(\varepsilon\ \widetilde{E}_3^{p-1}) & \text{in } S, \\ \operatorname{rot}_T \widetilde{\mathbf{E}}_T^p = -\mu\, \partial_t \widetilde{H}_3^{p-1} & \text{in } S, \\ \widetilde{\mathbf{E}}_T^p \times \mathbf{n} = 0, & \text{on } \partial S. \end{cases} \tag{4.19}$$

- Transverse magnetic fields

$$\begin{cases} \operatorname{div}_T(\mu\ \widetilde{\mathbf{H}}_T^p) = -\partial_3(\mu\ \widetilde{H}_3^{p-1}), & \text{in } S, \\ \operatorname{rot}_T \widetilde{\mathbf{H}}_T^p = \varepsilon\, \partial_t \widetilde{E}_3^{p-1}, & \text{in } S, \\ \widetilde{\mathbf{H}}_T^p \cdot \mathbf{n} = 0, & \text{on } \partial S. \end{cases} \tag{4.20}$$

- Longitudinal electric fields

$$\begin{cases} \mathbf{rot}_T\ \widetilde{E}_3^p = -\mu\, \partial_t \widetilde{\mathbf{H}}_T^{p-1} - \partial_3\,(\mathbf{e}_3 \times \widetilde{\mathbf{E}}_T^{p-1}), & \text{in } S, \\ \widetilde{E}_3^p = 0, & \text{on } \partial S. \end{cases} \tag{4.21}$$

- Longitudinal magnetic fields

$$\begin{cases} \mathbf{rot}_T\ \widetilde{H}_3^p = \varepsilon\, \partial_t \widetilde{\mathbf{E}}_T^{p-1} + \partial_3\,(\mathbf{e}_3 \times \widetilde{\mathbf{H}}_T^{p-1}) & \text{in } S, \\ \displaystyle\int_S \mu \widetilde{H}_3^p = 0. \end{cases} \tag{4.22}$$

With the convention

$$\widetilde{\mathbf{E}}^p = \widetilde{\mathbf{H}}^p = 0 \quad \text{for } p < 0.$$

The zero order terms

∗ *Limit longitudinal field*

Using (4.21) and (4.22) at order 0 ($p = 0$), we get

$$\left| \begin{array}{l} \mathbf{rot}_T\ \widetilde{E}_3^0 = \mathbf{rot}_T\ \widetilde{H}_3^0 = 0, \quad \text{in } S, \\ \widetilde{E}_3^0 = 0, \text{ on } \partial S, \quad \text{and} \quad \displaystyle\int_S \mu \widetilde{H}_3^0 = 0. \end{array} \right.$$

From the first two equalities, the longitudinal fields E_3^0 and H_3^0 are constant in S, and according to the last two equations these constants are zero. Thus, the limit longitudinal electromagnetic field satisfies,

$$\widetilde{E}_3^0 = \widetilde{H}_3^0 = 0.$$

∗ *Limit transverse field*

Using (4.19) and (4.20) with $p = 1$ we get

$$\begin{cases} \operatorname{div}_T(\varepsilon\, \widetilde{\mathbf{E}}_T^0) = 0 & \text{in } S, \\ \operatorname{rot}_T \widetilde{\mathbf{E}}_T^0 = 0 & \text{in } S, \\ \widetilde{\mathbf{E}}_T^0 \times \mathbf{n} = 0 & \text{on } \partial S. \end{cases} \qquad \begin{cases} \operatorname{div}_T(\varepsilon\, \widetilde{\mathbf{H}}_T^0) = 0 & \text{in } S, \\ \operatorname{rot}_T \widetilde{\mathbf{H}}_T^0 = 0 & \text{in } S, \\ \widetilde{\mathbf{H}}_T^0 \times \mathbf{n} = 0 & \text{on } \partial S. \end{cases} \tag{4.23}$$

So, using Lemma 4.2.2 and Lemma 4.2.3, there exist V^0 and I^0 such that,

$$\begin{cases} \widetilde{\mathbf{E}}_T^0(\mathbf{x}_T, x_3, t) = V^0(x_3, t)\nabla_T\, \varphi_e(\mathbf{x}_T), \\ \widetilde{\mathbf{H}}_T^0(\mathbf{x}_T, x_3, t) = I^0(x_3, t)\nabla_T\, \psi_m(\mathbf{x}_T), \end{cases} \tag{4.24}$$

where the potentials φ_e and ψ_m are respectively the solutions of the problems (4.14) and (4.15).

∗ *The 1D limit model*

Now, Using (4.21) and (4.22) at order 1 ($p = 1$) we get

$$\begin{cases} \varepsilon\, \partial_t \widetilde{\mathbf{E}}_T^0 - \partial_3\, (\mathbf{e}_3 \times \widetilde{\mathbf{H}}_T^0) - \mathbf{rot}_T\, \widetilde{H}_3^1 = & \text{in } S, \\ \mu\, \partial_t \widetilde{\mathbf{H}}_T^0 + \partial_3\, (\mathbf{e}_3 \times \widetilde{\mathbf{E}}_T^0) + \mathbf{rot}_T\, \widetilde{E}_3^1 = 0, & \text{in } S, \end{cases} \tag{4.25}$$

We start by replacing the fields $\widetilde{\mathbf{H}}_T^0$ and $\widetilde{\mathbf{E}}_T^0$ in (4.25) by the expressions (4.24). Then, we multiply the first and second equations by $\nabla_T\, \varphi_e$ and $\nabla_T\, \psi_m$ respectively, and we integrate over the section S. Finally, if we use Lemma 4.2.4, we get the 1D limit model as follows

$$\begin{cases} C\, \partial_t V^0(x_3, t) + \partial_3 I^0(x_3, t) = 0, \\ L\, \partial_t I^0(x_3, t) + \partial_3 V^0(x_3, t) = 0, \end{cases} \tag{4.26}$$

where $V^0(x_3, t)$ is the voltage and $I^0(x_3, t)$ is the current.

The first order terms

∗ *The first order longitudinal field*

Using (4.21) and (4.22) at order 1 ($p = 1$) we get

$$\begin{cases} \mathbf{rot}_T\, \widetilde{E}_3^1 = -\mu\, \partial_t \widetilde{\mathbf{H}}_T^0 - \partial_3\, (\mathbf{e}_3 \times \widetilde{\mathbf{E}}_T^0), & \text{in } S, \\ \mathbf{rot}_T\, \widetilde{H}_3^1 = \varepsilon\, \partial_t \widetilde{\mathbf{E}}_T^0 + \partial_3\, (\mathbf{e}_3 \times \widetilde{\mathbf{H}}_T^0) & \text{in } S. \end{cases} \tag{4.27}$$

Now, we inject the formulas (4.24) in (4.27) to get,

$$\begin{cases} \mathbf{rot}_T\ \widetilde{E}_3^1 = -\mu\,\nabla_T\,\psi_m\,\partial_t I^0 - \partial_3\,(\mathbf{e}_3 \times V^0\,\nabla_T\,\varphi_e), & \text{in } S, \\ \mathbf{rot}_T\ \widetilde{H}_3^1 = \varepsilon\,\nabla_T\,\varphi_e\,\partial_t V^0 + \partial_3\,(\mathbf{e}_3 \times I^0\,\nabla_T\,\psi_m), & \text{in } S. \end{cases} \tag{4.28}$$

Using the hypothesis (4.1) we can easily show that the potentials φ_e and ψ_m depend only on the transverse variables $\mathbf{x}_T$. Thus, using Lemma (4.2.5) and the 1D limit model (4.26), we can rewrite the equations (4.28) as

$$\begin{cases} \mathbf{rot}_T\ \widetilde{E}_3^1 = -\partial_3\,V^0\,\mathbf{rot}_T\ \varphi_m + \partial_3\,V^0\,\mathbf{rot}_T\ \varphi_e, & \text{in } S, \\ \mathbf{rot}_T\ \widetilde{H}_3^1 = -\partial_3\,I^0\,\mathbf{rot}_T\ \psi_m + \partial_3\,I^0\,\mathbf{rot}_T\ \psi_e & \text{in } S. \end{cases} \tag{4.29}$$

On the one hand, we have,

$$\mathbf{rot}_T\ \widetilde{E}_3^1 = \mathbf{rot}_T\ (\varphi_e - \varphi_m)\,\partial_3\,V^0,\ \text{in } S,$$

therefore,

$$E_3^1(\mathbf{x},t) = (\varphi_e - \varphi_m)\,\partial_3\,V^0 + C,\ \text{with } C \text{ is a constant.}$$

Since $(\widetilde{E}_3^1)_{|\partial S} = (\varphi_e - \varphi_m)_{|\partial S} = 0$, we get

$$E_3^1(\mathbf{x},t) = (\varphi_e - \varphi_m)\,\partial_3\,V^0.$$

On the other hand, using Lemma 4.2.1, we get $\mathbf{rot}_T\ H_3^0 = 0$, thus H_3^0 does not depend on x_1 and x_2. Thus, since

$$\int_S \mu\widetilde{H}_3^1(\cdot,x_3,t) = \widetilde{H}_3^1(x_3,t)\int_S \mu = 0 \text{ and } \int_S \mu \neq 0,$$

we get $\widetilde{H}_3^1 = 0$.

Finally, we obtain

$$\left|\begin{array}{l} E_3^1(\mathbf{x},t) = (\varphi_e - \varphi_m)\,\partial_3\,V^0, \\ \\ H_3^1(\mathbf{x},t) = 0. \end{array}\right. \tag{4.30}$$

∗ *The first order transverse field*

Using (4.19) and (4.20) with $p = 1$, we get

$$\begin{cases} \mathrm{div}_T(\varepsilon\ \widetilde{\mathbf{E}}_T^1) = 0 & \text{in } S, \\ \mathrm{rot}_T\ \widetilde{\mathbf{E}}_T^1 = 0 & \text{in } S, \\ \widetilde{\mathbf{E}}_T^1 \times \mathbf{n} = 0, & \text{on } \partial S. \end{cases} \quad \begin{cases} \mathrm{div}_T(\varepsilon\ \widetilde{\mathbf{H}}_T^1) = 0 & \text{in } S, \\ \mathrm{rot}_T\ \widetilde{\mathbf{H}}_T^1 = 0 & \text{in } S, \\ \widetilde{\mathbf{H}}_T^1 \cdot \mathbf{n} = 0, & \text{on } \partial S. \end{cases} \tag{4.31}$$

From Lemma 4.2.2 and Lemma 4.2.3, there exist V^1 and I^1 such that,

$$\begin{cases} \widetilde{\mathbf{E}}_T^1(\mathbf{x}_T,x_3,t) = V^1(x_3,t)\nabla_T\,\varphi_e(\mathbf{x}_T), \\ \widetilde{\mathbf{H}}_T^1(\mathbf{x}_T,x_3,t) = I^1(x_3,t)\nabla_T\,\psi_m(\mathbf{x}_T). \end{cases} \tag{4.32}$$

∗ *The first order 1D model*

Using (4.21) and (4.22) at order 2 ($p = 2$), we get

$$\begin{cases} \varepsilon\, \partial_t \widetilde{\mathbf{E}}_T^1 - \partial_3 \left(\mathbf{e}_3 \times \widetilde{\mathbf{H}}_T^1\right) - \mathbf{rot}_T\, \widetilde{H}_3^2 = 0, & \text{in } S, \\ \mu\, \partial_t \widetilde{\mathbf{H}}_T^1 + \partial_3 \left(\mathbf{e}_3 \times \widetilde{\mathbf{E}}_T^1\right) + \mathbf{rot}_T\, \widetilde{E}_3^2 = 0, & \text{in } S. \end{cases} \tag{4.33}$$

We inject the expressions (4.42) of the fields $\widetilde{\mathbf{H}}_T^1$ and $\widetilde{\mathbf{E}}_T^1$ in (4.33). Then, we multiply the first and second equations by $\nabla_T\, \varphi_e$ and $\nabla_T\, \psi_m$ respectively, and we integrate over the section S. Finally, if we use Lemma 4.2.4, we get the 1D model as follows with with the unknowns : the voltage $V^1(x_3, t)$ and the current $I^1(x_3, t)$,

$$\begin{cases} C\, \partial_t V^1(x_3, t) + \partial_3 I^1(x_3, t) = 0, \\ L\, \partial_t I^1(x_3, t) + \partial_3 V^1(x_3, t) = 0, \end{cases} \tag{4.34}$$

with the initial conditions

$$V^1(x_3, 0) = 0 \quad \text{and} \quad I^1(x_3, 0) = 0. \tag{4.35}$$

We can therefore say that the solutions of this model are as follows,

$$V^1(x_3, t) = 0 \quad \text{and} \quad I^1(x_3, t) = 0. \tag{4.36}$$

Thus, one gets

$$\widetilde{\mathbf{E}}_T^1 = \widetilde{\mathbf{H}}_T^1 = 0. \tag{4.37}$$

Second order terms

∗ *The first order longitudinal field*

Using (4.21) and (4.22) at order 2 ($p = 2$) we get

$$\begin{cases} \mathbf{rot}_T\, \widetilde{E}_3^2 = -\mu\, \partial_t \widetilde{\mathbf{H}}_T^1 - \partial_3 \left(\mathbf{e}_3 \times \widetilde{\mathbf{E}}_T^1\right) \underset{(4.37)}{=} 0, & \text{in } S, \\ \mathbf{rot}_T\, \widetilde{H}_3^2 = \varepsilon\, \partial_t \widetilde{\mathbf{E}}_T^1 + \partial_3 \left(\mathbf{e}_3 \times \widetilde{\mathbf{H}}_T^1\right) \underset{(4.37)}{=} 0 & \text{in } S. \end{cases}$$

Thus, the longitudinal fields $\widetilde{E}_3^2$ and $\widetilde{H}_3^2$ are constant in the cross-section S. Since $\widetilde{E}_3^2$ vanishes on ∂S and the mean values of $\mu \widetilde{H}_3^2$ is zero (since the mean values of μ positive), these constants are zeros.

∗ *The second order transverse field*

Using (4.19) and (4.20) with $p = 2$, we get

$$\begin{cases} \mathrm{div}_T(\varepsilon\, \widetilde{\mathbf{E}}_T^2) = -\varepsilon(\varphi_e - \varphi_m)\partial_3^2 V & \text{in } S, \\ \mathrm{rot}_T\, \widetilde{\mathbf{E}}_T^2 = 0 & \text{in } S, \\ \widetilde{\mathbf{E}}_T^2 \times \mathbf{n} = 0, & \text{on } \partial S. \end{cases} \qquad \begin{cases} \mathrm{div}_T(\varepsilon\, \widetilde{\mathbf{H}}_T^2) = 0 & \text{in } S, \\ \mathrm{rot}_T\, \widetilde{\mathbf{H}}_T^2 = \varepsilon(\varphi_e - \varphi_m)\partial_t \partial_3 V^0 & \text{in } S, \\ \widetilde{\mathbf{H}}_T^2 \cdot \mathbf{n} = 0, & \text{on } \partial S. \end{cases} \tag{4.38}$$

First, let us introduce $\xi_{e,2}$ and $\zeta_{m,2}$, respectively the solutions of the following problems :

$$\begin{cases} \mathrm{div}_T(\varepsilon \nabla_T \xi_{e,2}) = -\varepsilon(\varphi_e - \varphi_m), \\ \xi_{e,2} = 0, \end{cases} \qquad \begin{cases} \mathrm{rot}_T \left(\mu^{-1} \mathbf{rot}_T \zeta_{m,2}\right) = \varepsilon(\varphi_e - \varphi_m), & \text{in } S, \\ \zeta_{m,2} = 0, & \text{on } \partial S. \end{cases} \tag{4.39}$$

Then, we define the two fields $\mathbf{G}_T$ and $\mathbf{B}_T$ such that :

$$\begin{aligned} \mathbf{G}_T &:= \widetilde{\mathbf{E}}^2_T(\mathbf{x}_T, x_3, t) - \partial_3^2 V^0(x_3, t)\, \nabla_T \xi_{e,2}(\mathbf{x}_T), \\ \mathbf{B}_T &:= \widetilde{\mathbf{H}}^2_T(\mathbf{x}_T, x_3, t) - \partial_t \partial_3 V^0(x_3, t)\, \mu^{-1}(\mathbf{x}_T)\, \mathbf{rot}_T\, \zeta_{m,2}(\mathbf{x}_T). \end{aligned} \tag{4.40}$$

Using the problems (4.41) and (4.39), we can easily see that the fields $\mathbf{G}_T$ and $\mathbf{B}_T$ are the solutions to the following problems

$$\begin{cases} \mathrm{div}_T(\varepsilon\ \mathbf{G}_T) = 0 & \text{in } S, \\ \mathrm{rot}_T\, \mathbf{G}_T = 0 & \text{in } S, \\ \mathbf{G}_T \times \mathbf{n} = 0, & \text{on } \partial S. \end{cases} \qquad \begin{cases} \mathrm{div}_T(\varepsilon\ \mathbf{B}_T) = 0, & \text{in } S, \\ \mathrm{rot}_T\, \mathbf{B}_T = 0, & \text{in } S, \\ \mathbf{B}_T \cdot \mathbf{n} = 0, & \text{on } \partial S. \end{cases} \tag{4.41}$$

We use again Lemma 4.2.2 and Lemma 4.2.3, thus there exist V^2 and I^2 such that,

$$\begin{cases} \mathbf{G}_T(\mathbf{x}_T, x_3, t) = V^2(x_3, t) \nabla_T \varphi_e(\mathbf{x}_T), \\ \mathbf{B}_T(\mathbf{x}_T, x_3, t) = I^2(x_3, t) \nabla_T \psi_m(\mathbf{x}_T). \end{cases} \tag{4.42}$$

Finally, since (4.40), we get

$$\begin{cases} \widetilde{\mathbf{E}}^2_T(\mathbf{x}_T, x_3, t) = V^2(x_3, t) \nabla_T \varphi_e(\mathbf{x}_T) + \partial_3^2 V^0(x_3, t)\, \nabla_T \xi_{e,2}(\mathbf{x}_T), \\ \widetilde{\mathbf{H}}^2_T(\mathbf{x}_T, x_3, t) = I^2(x_3, t) \nabla_T \psi_m(\mathbf{x}_T) + \partial_t \partial_3 V^0(x_3, t)\, \mu^{-1}(\mathbf{x}_T)\, \mathbf{rot}_T\, \zeta_{m,2}(\mathbf{x}_T), \end{cases} \tag{4.43}$$

∗ *The second order 1D model*

Using (4.21) and (4.22) at order 3 ($p = 3$), we get

$$\begin{cases} \varepsilon\, \partial_t \widetilde{\mathbf{E}}^2_T - \partial_3 \left(\mathbf{e}_3 \times \widetilde{\mathbf{H}}^2_T\right) - \mathbf{rot}_T\, \widetilde{H}^3_3 = 0 & \text{in } S, \\ \mu\, \partial_t \widetilde{\mathbf{H}}^2_T + \partial_3 \left(\mathbf{e}_3 \times \widetilde{\mathbf{E}}^2_T\right) + \mathbf{rot}_T\, \widetilde{E}^3_3 = 0, & \text{in } S. \end{cases} \tag{4.44}$$

We inject the expressions (4.43) of the fields $\widetilde{\mathbf{H}}^2_T$ and $\widetilde{\mathbf{E}}^2_T$ in (4.44),

$$\begin{aligned} \varepsilon\, \partial_t(V^2 \nabla_T \varphi_e) \quad & - \partial_3 \left(\mathbf{e}_3 \times (I^2 \nabla_T \psi_m) - \mathbf{rot}_T\, \widetilde{H}^3_3 \right. \\ & \left. + \varepsilon\, \partial_t(\partial_3^2 V\, \nabla\, \xi_{e,2}) - \partial_3 \left(\mathbf{e}_3 \times (\partial_t \partial_3 V\, \mu^{-1}\, \mathbf{rot}_T\, \zeta_{m,2})\right) = 0, \right. \\ \mu\, \partial_t(I^2 \nabla_T \psi_m) \quad & + \partial_3 \left(\mathbf{e}_3 \times (V^2 \nabla_T \varphi_e) + \mathbf{rot}_T\, \widetilde{E}^3_3 \right. \\ & \left. + \mu\, (\partial_t^2 \partial_3 V\, \mu^{-1}\, \mathbf{rot}_T\, \zeta_{m,2}) + \partial_3 \left(\mathbf{e}_3 \times (\partial_3^2 V\, \nabla\, \xi_{e,2})\right) = 0, \right. \end{aligned} \tag{4.45}$$

Then, we multiply the first and second equations, of (4.45), by $\nabla_T \varphi_e$ and $\nabla_T \psi_m$ respectively, and we integrate over the section S. Finally, if we use again Lemma 4.2.4, we get

$$\begin{cases} C\,\partial_t V^2 + \partial_3 I^2 \;\; + \partial_t \partial_3^2 V^0 \displaystyle\int_S \varepsilon\, \nabla_T \xi_{e,2} \cdot \nabla_T \varphi_e \\ \qquad\qquad\qquad\qquad - \partial_t \partial_3^2 V \displaystyle\int_S (\mathbf{e}_3 \times \mu^{-1}\, \mathbf{rot}_T\, \zeta_{m,2}) \cdot \nabla_T \varphi_e = 0, \\ L\,\partial_t I^2 + \partial_3 V^2 \;\; + \partial_t^2\, \partial_3\, V^0 \displaystyle\int_S \mathbf{rot}_T\, \zeta_{m,2} \cdot \nabla_T \psi_m \\ \qquad\qquad\qquad\qquad + \partial_3^3 V \displaystyle\int_S (\mathbf{e}_3 \times \nabla_T\, \xi_{e,2}) \cdot \nabla_T \psi_m = 0. \end{cases} \tag{4.46}$$

Since Green formula, $(\xi_{e,2})_{|\partial S} = 0$ and using the definition (3.6) of φ_e, we find that

$$\int_S \varepsilon\, \nabla_T\, \xi_{e,2} \cdot \nabla_T\, \varphi_e = -\int_S \xi_{e,2}\, (\mathrm{div}_T\, \varepsilon\, \nabla_T\, \varphi_e) + \int_{\partial S} \xi_{e,2} \varepsilon\, \frac{\partial \varphi_e}{\partial n} = 0$$

Moreover, we have $(\zeta_{m,2})_{|\partial S} = 0$, thus using again the Green formula we get

$$\int_S \mathbf{rot}_T\, \zeta_{m,2} \cdot \nabla_T\, \psi_m = 0.$$

Therefore, the equations (4.47) can rewrite as

$$\begin{cases} C\,\partial_t V^2 + \partial_3 I^2 - \;\partial_t \partial_3^2 V \displaystyle\int_S (\mathbf{e}_3 \times \mu^{-1}\, \mathbf{rot}_T\, \zeta_{m,2}) \cdot \nabla_T\, \varphi_e = 0, \\ L\,\partial_t I^2 + \partial_3 V^2 + \;\partial_3^3 V \displaystyle\int_S (\mathbf{e}_3 \times \nabla_T\, \xi_{e,2}) \cdot \nabla_T\, \psi_m = 0. \end{cases} \tag{4.47}$$

Since $(\zeta_{m,2})_{|\partial S} = 0$, we have

$$\int_S (\mathbf{e}_3 \times \nabla_T\, \xi_{e,2}) \cdot \nabla_T\, \psi_m = -\int_S \mathbf{rot}_T\, \xi_{e,2} \cdot \nabla_T\, \psi_m = 0.$$

In addition, we have

$$\int_S (\mathbf{e}_3 \times \mu^{-1}\, \mathbf{rot}_T\, \zeta_{m,2}) \cdot \nabla_T\, \varphi_e = -\int_S \mu^{-1}\, \nabla_T\, \zeta_{m,2} \cdot \nabla_T\, \varphi_e.$$

Using the definition (4.5) of the potential φ_m, we can say that

$$\int_S \mu^{-1}\, \nabla_T\, \zeta_{m,2} \cdot \nabla_T\, \varphi_m = 0.$$

Thus,

$$\int_S (\mathbf{e}_3 \times \mu^{-1}\, \mathbf{rot}_T\, \zeta_{m,2}) \cdot \nabla_T\, \varphi_e = \int_S \mu^{-1}\, \nabla_T\, \zeta_{m,2} \cdot \nabla_T\, (\varphi_m - \varphi_e). \tag{4.48}$$

Since $(\varphi_e - \varphi_m)_{|\partial S} = (\zeta_{m,2})_{|\partial S} = 0$, by using Green formula we can rewrite (4.49) as

$$\int_S (\mathbf{e}_3 \times \mu^{-1}\, \mathbf{rot}_T\, \zeta_{m,2}) \cdot \nabla_T\, \varphi_e = \int_S \mathrm{div}_T\, (\mu^{-1}\, \nabla_T\, \zeta_{m,2})\, (\varphi_m - \varphi_e),$$

and with definition (4.39) of $\zeta_{m,2}$, we get

$$\int_S (\mathbf{e}_3 \times \mu^{-1}\, \mathbf{rot}_T\, \zeta_{m,2}) \cdot \nabla_T\, \varphi_e = \int_S \varepsilon\, |\varphi_m - \varphi_e)|^2 = \gamma_e. \tag{4.49}$$

Finally, we get the 1D model as follows with the unknowns : the voltage $V^2(x_3,t)$ and the current $I^2(x_3,t)$,

$$\begin{cases} C\ \partial_t V^2(x_3,t) + \partial_3 I^2(x_3,t) - \partial_t\, \gamma_e\, \partial_3^2 V(x_3,t) = 0, \\ L\ \partial_t I^2(x_3,t) + \partial_3 V^2(x_3,t) = 0. \end{cases} \tag{4.50}$$

with the initial conditions

$$V^2(x_3,0) = 0 \quad \text{and} \quad I^2(x_3,0) = 0. \tag{4.51}$$

Derivation of the second order effective telegrapher's model

We want equations that take into account the three equations (4.26), (4.34) and (4.50). It can be done the following formal combination

$$(4.26) + \delta\,(4.50) + \delta^2\,(4.50). \tag{4.52}$$

We can write the equations for $V^0 + \delta\, V^1 + \delta^2\, V^2$ and $I^0 + \delta\, I^1 + \delta^2\, I^2$,

$$\begin{cases} \partial_t\,(C - \gamma_e\, \partial_3^2)\Big(\sum\limits_{p=0}^{2} \delta^p\, V^p\Big) + \partial_3\Big(\sum\limits_{p=0}^{2} \delta^p\, I^p\Big) = \delta^3\, \gamma_e\, \partial_t\, \partial_3^2\,(V^1 + \delta\, V^2), \\ L\ \partial_t \Big(\sum\limits_{p=0}^{2} \delta^p\, I^p\Big) + \partial_3 \Big(\sum\limits_{p=0}^{2} \delta^p\, V^p\Big) = 0. \end{cases} \tag{4.53}$$

Therefore, if we neglect the third and fourth orders we obtain the second order effective telegrapher's model as follows with the unknowns : the second order effective voltage $V^{\delta,2}(x_3,t)$ and current $I^{\delta,2}(x_3,t)$,

$$\begin{cases} C_\delta(\partial_3)\ \partial_t\ V^{\delta,2}(x_3,t) + \partial_3 I^{\delta,2}(x_3,t) = 0, \\ L\ \partial_t I^{\delta,2}(x_3,t) + \partial_3\, V^{\delta,2}(x_3,t) = 0, \end{cases} \tag{4.54}$$

where $C_\delta(\partial_3)$ is the second order elliptic operator given by

$$C_\delta(\partial_3) = (C - \gamma_e\, \partial_3^2).$$

The initial conditions of second order effective telegrapher's model (4.54) are given by

$$V^{\delta,2}(x_3,0) = V^0(x_3,0) = V_0(x_3) \quad \text{and} \quad I^{\delta,2}(x_3,0) = I^0(x_3,0) = I_0(x_3).$$

Approximation of the electromagnetic fields

Using the same formal combination as (4.52) applied to the transverse and longitudinal electromagnetic fields, we can give an approximation of the electromagnetic fields solution

of the rescaled 3D Maxwell's equations (3.1) (in Chapter 3) from $V^{\delta,2}$ and $I^{\delta,2}$ (the solution of the 1D model (4.54)).

$$\left|\begin{array}{l}
\widetilde{\mathbf{E}}_T^{\delta,2}(\mathbf{x}_T,x_3,t) = V^{\delta,2}(x_3,t)\nabla_T\,\varphi_e(\mathbf{x}_T) + \delta^2\,\partial_3^2 V^{\delta,2}(x_3,t)\,\nabla_T\,\xi_{e,2}(\mathbf{x}_T),\\
\widetilde{\mathbf{H}}_T^{\delta,2}(\mathbf{x}_T,x_3,t) = I^{\delta,2}(x_3,t)\nabla_T\,\psi_m(\mathbf{x}_T) + \delta^2\,\partial_t\partial_3 V^{\delta,2}(x_3,t)\,\mu^{-1}(\mathbf{x}_T)\,\mathbf{rot}_T\,\zeta_{m,2}(\mathbf{x}_T),\\
\widetilde{E}_3^{\delta,2}(\mathbf{x}_T,x_3,t) = \delta\,(\varphi_e-\varphi_m)\,\partial_3\,V^{\delta,2},\\
\widetilde{H}_3^{\delta,2}(\mathbf{x}_T,x_3,t) = 0.
\end{array}\right. \tag{4.55}$$

4.3 Numerical resolution of 1D effective telegrapher's model of order 2

4.3.1 Precomputation of the coefficients of the model

First, we must solve a 2D problems in the cross section S, that is to say the numerical computation of the potentials $(\varphi_e,\varphi_m,\psi_m,\psi_m)$ and the coefficients C, L and γ_e.

The potentials $(\varphi_e,\varphi_m,\psi_m,\psi_m)$ are first approximated thanks to a $\mathbb{P}_1$ finite-elements approximation of the boundary value problems (3.6), (4.4) and (4.5) with a triangular mesh of the cross section S with step-size h_T (this mesh "respects" the cut Σ), producing

$$(\varphi_{e,h_T},\varphi_{m,h_T}) \in V_{0,h_T}\times V_{0,h_T}, \qquad (\psi_{m,h_T},\psi_{e,h_T}) \in \widetilde{V}_{\Sigma,h_T}\times \widetilde{V}_{\Sigma,h_T},$$

where V_{0,h_T} and $\widetilde{V}_{\Sigma,h_T}$ are the respective Galerkin approximation sub-spaces for $H^1_0(S)\times H^1_\Sigma(S)$ (where $H^1_\Sigma(S)=H^1(S\backslash\Sigma)$). Then C, L and γ are approximated, according to (3.10) and (4.6), by

$$\left\{\begin{array}{l}
C_{h_T} = \displaystyle\int_S \varepsilon(\mathbf{x}_T)\,|\nabla_T\,\varphi_{e,h_T}(\mathbf{x}_T)|^2\,d\mathbf{x}_T.\\
L_{h_T} = \displaystyle\int_S \mu(\mathbf{x}_T)\,|\nabla_T\,\psi_{m,h_T}(\mathbf{x}_T)|^2\,d\mathbf{x}_T.\\
\gamma_{h_T} = \displaystyle\int_S \varepsilon(\mathbf{x}_T)\,|\varphi_{e,h_T}(\mathbf{x}_T)-\varphi_{m,h_T}(\mathbf{x}_T)|^2\,d\mathbf{x}_T.
\end{array}\right. \tag{4.56}$$

4.3.2 Resolution of the 1D evolution problem

There is no difficulty in tackling the semi-discretization in space of the 1D model (4.13). It can be done, for instance, using 1D finite elements (for instance continuous $\mathbb{P}_1$), and mass lumping with a uniform mesh of step-size h. The resulting algebraic problem takes the form

$$\mathbf{M}_h^\delta\,\frac{\mathrm{d}^2\mathbb{V}_h}{\mathrm{d}t^2} + \mathbf{K}_h\,\mathbb{V}_h = 0, \tag{4.57}$$

where $\mathbb{V}_h(t) = \big(V_j(t)\big)$ is the vector of degrees of freedom at time t for the semi-discrete voltage $V_h(t)\in H^1(\mathbb{R})$ (the nodal values at the points jh), and

$$\mathbf{M}_h^\delta := L_{h_T}\,C_{h_T}\,\mathbf{M}_h + \delta^2\,\gamma_{h_T}\,L_{h_T}\,\mathbf{K}_h,$$

with

- $\mathbf{M}_{e,h} = \mathrm{diag}\big(m_{e,j}\big) > 0$ is diagonal mass (like) matrices with $m_{e,j} = h$.
- $\mathbf{K}_h$ is the stiffness matrix corresponding to the action of the operator ∂_3^2 .

Concerning the time discretization, we use a leap-frog scheme with a constant time step Δt.

$$\mathbf{M}_h^\delta \, \frac{\mathbb{V}_h^{n+1} - 2\,\mathbb{V}_h^n + \mathbb{V}_h^{n-1}}{\Delta t^2} + \mathbf{K}_h \, \mathbb{V}_h^n = 0, \tag{4.58}$$

where $\mathbb{V}_h^n$ is the vector of degrees of freedom of $V_h^n \in H^1(\mathbb{R})$, approximation of $V_h(t^n)$.

Theorem 4.3.1. *The numerical scheme (4.58) is L^2-stable under the sufficient CFL condition*

$$c_{h_T} \, \frac{\Delta t}{h} \le 1, \quad c_{h_T} := C_{h_T}^{-\frac{1}{2}} L_{h_T}^{-\frac{1}{2}}, \tag{4.59}$$

Proof. We shall introduce the notation $\big(\cdot,\cdot\big)$ for inner products in $\mathbb{P}_1$,

$$\big(\mathbb{V}_h, \tilde{\mathbb{V}}_h\big) := \sum_{j\in\mathbb{Z}} \mathbb{V}_j \cdot \tilde{\mathbb{V}}_j. \tag{4.60}$$

and the factor $\alpha_h > 0$ defined by :

$$\alpha_h^2 := \sup_{u_h \in \mathbb{P}_{1,h}} \frac{\int_{\mathbb{R}} |u_h'|^2}{\oint_{\mathbb{R}} |u_h|^2}, \tag{4.61}$$

where

$$\mathbb{P}_{1,h} := \{u_h \in C^0(\mathbb{R}) \cap L^2(\mathbb{R}) \;/\; \forall\, j \in \mathbb{Z},\; u_h|_{[jh,(j+1)h]} \in \mathbb{P}_1\}, \tag{4.62}$$

and $\oint_{\mathbb{R}} f$ refer to a quadrature formula in x_3. More precisely, for $f \in C^0\big(\mathbb{R}\big) \cap L^1\big(\mathbb{R}\big)$, we set

$$\oint_{\mathbb{R}} f = h \sum_j \frac{f_{j+1} + f_j}{2}, \quad f_j = f(jh). \tag{4.63}$$

The proof is done in two steps using an energy approach.

Step 1 : Discrete energy conservation. We use this standard key identity :

$$\mathbb{V}_h^n = \{\mathbb{V}_h^n\}_{\frac{1}{4}} - \frac{1}{4}\big(\mathbb{V}_h^{n+1} - 2\,\mathbb{V}_h^n + \mathbb{V}_h^{n-1}\big), \quad \text{with} \quad \{\mathbb{V}_h^n\}_\theta := \theta\,\mathbb{V}_h^{n+1} + (1-2\,\theta)\,\mathbb{V}_h^n + \theta\,\mathbb{V}_h^{n-1}.$$

This allows us to rewrite our scheme as a perturbation of the $\frac{1}{4}$-scheme.

$$\mathbf{M}_h^\delta(\Delta t) \, \frac{\mathbb{V}_h^{n+1} - 2\,\mathbb{V}_h^n + \mathbb{V}_h^{n-1}}{\Delta t^2} + \mathbf{K}_h \, \{\mathbb{V}_h^n\}_{\frac{1}{4}} = 0,$$

where we have set

$$\mathbf{M}_h^\delta(\Delta t) = \mathbf{M}_h^\delta - \frac{\Delta t^2}{4}\,\mathbf{K}_h. \tag{4.64}$$

Taking the scalar product (in $\mathbb{P}_1$) of the above equation with $\dfrac{\mathbb{V}_h^{n+1} - \mathbb{V}_h^{n-1}}{2\Delta t}$ we classically deduce, thanks to the symmetry of all matrices) the conservation of the discrete energy

$$\mathcal{E}_h^{n+\frac{1}{2}} := \frac{1}{2}\left[\left(\mathbf{M}_h^\delta(\Delta t)\frac{\mathbb{V}_h^{n+1} - \mathbb{V}_h^n}{\Delta t}, \frac{\mathbb{V}_h^{n+1} - \mathbb{V}_h^n}{\Delta t}\right) + \left(\mathbf{K}_h\Big(\frac{\mathbb{V}_h^{n+1} + \mathbb{V}_h^n}{2}\Big), \frac{\mathbb{V}_h^{n+1} + \mathbb{V}_h^n}{2}\right)\right].$$

Step 2 : Derivation of the sufficient stability condition (4.59).

This will be simply obtained from showing the positivity of the discrete energy $\mathcal{E}_h^{n+\frac{1}{2}}$, that amounts to the positivity of the modified mass matrix $\mathbf{M}_h^{\delta}(\Delta t)$.

Since $\mathbf{K}_h$ is positive, we have for any vector $\mathbb{U}_{h,T} \in \mathbb{P}_1$

$$\Big(\mathbf{M}_h^{\delta}\mathbb{U}_{h,T}, \mathbb{U}_{h,T}\Big) \geq L_{x_T} C_{x_T} \Big(\mathbf{M}_h \mathbb{U}_{h,T}, \mathbb{U}_{h,T}\Big). \tag{4.65}$$

We control the matrix $\mathbf{K}_h$ with the help of the mass matrix $\mathbf{M}_h$ that appears in the lower bound (4.65). This is where the space step h will appear via α_h. More precisely, let $\mathbf{U}_{h,T} \in \mathbb{P}_{h,1}$ be associated to the vector $\mathbb{U}_{h,T} \in \mathbb{P}_1$, by definition of $\mathbf{K}_h$

$$\Big(\mathbf{K}_h \mathbb{U}_{h,T}, \mathbb{U}_{h,T}\Big) = \int_{\Omega} |\partial_3 \mathbf{U}_{h,T}|^2.$$

Using $\mathbf{U}_{h,T} = (\mathbf{U}_{h,1}, \mathbf{U}_{h,2})$, we get

$$\Big(\mathbf{K}_h \mathbb{U}_{h,T}, \mathbb{U}_{h,T}\Big) = \int_{\mathbb{R}} \Big(|\partial_3 \mathbf{U}_{h,1}(x_3)|^2 + |\partial_3 \mathbf{U}_{h,2}(x_3)|^2\Big)\, dx_3.$$

Then, by definition (4.61) of the function α_h, and since each function $\mathbf{U}_{h,1}$ and $\mathbf{U}_{h,1}$ belongs to $\mathbb{P}_{1,h}$, we have

$$\Big(\mathbf{K}_h \mathbb{U}_{h,T}, \mathbb{U}_{h,T}\Big) \leq \alpha_h \oint_{\mathbb{R}} \Big(|\mathbf{U}_{h,1}(x_3)|^2 + |\mathbf{U}_{h,2}(x_3)|^2\Big)\, dx_3,$$

so that,

$$\Big(\mathbf{K}_h \mathbb{U}_{h,T}, \mathbb{U}_{h,T}\Big) \leq \alpha_h^2 \Big(\mathbf{M}_h \mathbb{U}_{h,T}, \mathbb{U}_{h,T}\Big). \tag{4.66}$$

Joining (4.65) and (4.66) to definition (4.64) of $\mathbf{M}_h(\Delta t)$, we obtain

$$\Big(\mathbf{M}_h(\Delta t)\, \mathbb{U}_h, \mathbb{U}_h\Big) \geq \Big(L_{x_T} C_{x_T} - \alpha_h^2\, \frac{\Delta t^2}{4}\Big) \Big(\mathbf{M}_h\, \mathbb{U}_{h,T}, \mathbb{U}_{h,T}\Big). \tag{4.67}$$

The stability condition is obtained by writing

$$\Big(L_{x_T} C_{x_T} - \alpha_h^2\, \frac{\Delta t^2}{4}\Big) \geq 0. \tag{4.68}$$

In addition, for any $u_h \in P_{1,h}$, we have u_h' is piecewise constant, and

$$\int_{\mathbb{R}} |u_h'|^2 = \sum_{j \in Z} \left|\frac{u_{j+1} - u_j}{h}\right|^2,$$

with $u_j := u_h(jh)$. By $|u_{j+1} - u_j|^2 \leq 2\Big(|u_{j+1}|^2 + |u_j|^2\Big)$, we deduce,

$$\int_{\mathbb{R}} |u_h'|^2 \leq \frac{4}{h^2} \sum_{j \in Z} \left(\frac{|u_j|^2 + |u_{j+1}|^2}{2}\right) h = \frac{4}{h^2} \oint_{\mathbb{R}} |u_h|^2.$$

thus, we get the upper bound

$$\alpha_h^2 \leq \frac{4}{h^2}. \tag{4.69}$$

Finally, using (4.68) and (4.69), we get the CFL condition (4.59). ■

4.3.3 Reconstruction of the 3D electric field

Once the discrete voltage $V_h^n(x_3)$ is computed, according to (3.5), one can reconstruct the (rescaled) 3D electric field at time t^n as the $\mathbb{P}_1$-interpolant of the following transverse fields, defined for each j, using a discrete convolution formula consistent with the one appearing in (3.22), namely,

$$\begin{aligned}\widetilde{\mathbf{E}}_T^n(\mathbf{x}_T, jh) &= V_h^n(jh)\,\nabla_T\,\varphi_e(\mathbf{x}_T) + \delta^2\,\{\{V_h^n\}\}_j\,\nabla_T\,\xi_{e,2}(\mathbf{x}_T).\\ \widetilde{\mathbf{E}}_3^n(\mathbf{x}_T, (j+\frac{1}{2})h) &= \delta\,(\varphi_e(\mathbf{x}_T) - \varphi_m(\mathbf{x}_T))\,\frac{V^n((j+1)h) - V^n(jh)}{h},\end{aligned} \tag{4.70}$$

Where

$$\{\{V_h^n\}\}_j := \frac{V^n((j+1)h) - 2\,V^n(jh) + V^n((j-1)h)}{h}.$$

4.4 Comparison between 3D and 1D calculations

4.4.1 Problem's data

We have chosen to treat a cylindrical coaxial cable Ω such that,

$$\Omega = S \times [0, 12],$$

This cable is represented in Figure 4.4.

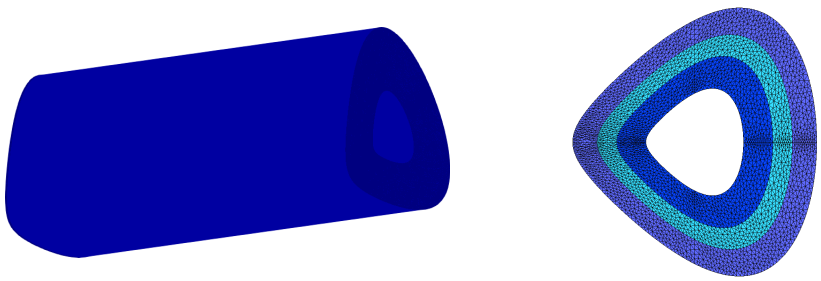

FIGURE 4.4 – Left : the domain Ω, right : the section S of the domain. Each color corresponds to a different material.

For the numerical computations, a periodic boundary conditions will be applied between $x_3 = 0$ and $x_3 = 12$. As the cut for the computation of the potentials ψ_m and ψ_e, we shall take the segment

$$\Sigma = [1, 2.5] \times \{0\}. \tag{4.71}$$

Concerning the coefficients of the model, the cable is heterogeneous (onion-like piecewise homogeneous cylindrical cable). More precisely the cross section S is made of three layers $S = S_1 \cup S_2 \cup S_3$ and inside S_j, the material is homogeneous (see Figure 4.4),

$$\Big(\varepsilon(\mathbf{x}_T), \mu(\mathbf{x}_T)\Big) = (\varepsilon_j, \mu_j) \quad \text{in } S_j. \tag{4.72}$$

In our numerical experiments, we shall take

$$(\varepsilon_1, \mu_1) = (2, 3), \quad (\varepsilon_2, \mu_2) = (1, 2) \quad \text{and} \quad (\varepsilon_3, \mu_3) = (1, 1),$$

so that the velocity of electromagnetic waves, $c(\mathbf{x}) = (\varepsilon\mu)(\mathbf{x})^{-\frac{1}{2}}$ is

$$c(\mathbf{x}) = c_1 = 1/\sqrt{6} \text{ in } S_1 \times \mathbb{R}, \quad c(\mathbf{x}) = c_2 = 1/\sqrt{2} \text{ in } S_2 \times \mathbb{R}, \quad c(\mathbf{x}) = c_3 = 1 \text{ in } S_3 \times \mathbb{R}. \tag{4.73}$$

We also take initial conditions that are localized near $x_3 = 5$ and are *well prepared* with respect to the expected asymptotic result (4.55). More precisely, $\widetilde{\mathbf{H}}_0(\mathbf{x}_T, x_3) = 0$ and

$$\widetilde{\mathbf{E}}_0(\mathbf{x}_T, x_3) := \mathcal{E}(x_3)\, \nabla_T \varphi_e(\mathbf{x}_T, x_3), \quad \mathcal{E}(x_3) = e^{-\pi^2 (x_3-6)^2}. \tag{4.74}$$

The time interval for the numerical experiments will be $[0, T]$ with $T = 6$, so that, taking (4.73) into account, it implies that the waves will not reach the transverse boundaries $x_3 = 0$ and $x_3 = 12$ before the final time T. In other words, the periodic boundary conditions in x_3 will not play any role.

As in the previous chapter, the initial field is transversely polarized. However, due to the heterogeneity of the cable, it will not remain transversely polarized during the time (even in the unperturbed case, separation of variable does not work for Maxwell's equations) as the numerical results will illustrate it.

4.4.2 Discretization parameters

Data for the transverse discretization. The mesh of the cross section will be a triangular mesh represented Figure 4.4. In particular, there are 40 mesh points along the cut Σ and the typical diameter of each triangle in the mesh is

$$h_T \simeq 0.04.$$

This mesh is used for the $2D$ transverse problems (3.6,4.4,4.5) for computing the potentials $(\varphi_e, \varphi_m, \psi_m, \psi_e)$ and the coefficients (C, L, γ_e) but also for the 3D computations.

Data for the longitudinal discretization. The longitudinal step size h will be taken $h = 0.06$ which is well adapted to the discretization of the Gaussian $\mathcal{E}(x_3)$.

This longitudinal mesh will be used for the discretization of the 1D problem (4.58) (cf. (4.13)) but also for the 3D computations (Chapter 2).

Data for the time discretization. For facilitating the comparison between the 1D and 3D results, we shall use the same time step Δt for both 1D and 3D computations. According to Remark 3.3.3, the choice of Δt will be constrained by the 3D condition (2.48). For the 3D computations, we shall take $\theta = 1/3$, in which case (2.48) gives : $c^+\Delta t/h \leq 1/2$. In practice we shall choose $\Delta t = 0.95\ h/(2\, c^+)$.

4.4.3 Numerical results

The potentials $(\varphi_e, \psi_m, \varphi_m, \psi_e)$

We show in Figure 4.5 the computed potentials φ_e and ψ_m. The right picture shows at the same time the level lines of φ_e (which are "parallel" to the boundaries) and the ones of ψ_m (which intersect the boundaries). This illustrates that $\Big(\varphi_e(\mathbf{x}_T), \psi_m(\mathbf{x}_T)\Big)$ generalizes polar coordinates inside S.

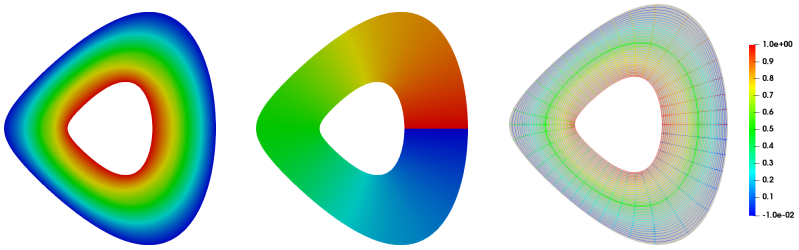

FIGURE 4.5 – Potentials φ_e (left) and ψ_m (center), associated isolines (right).

Similarly, we present in Figure 4.6 the computed potentials φ_m and ψ_e. The right picture shows at the same time the level lines of φ_m (which are "parallel" to the boundaries) and those of ψ_e (which intersect the boundaries).

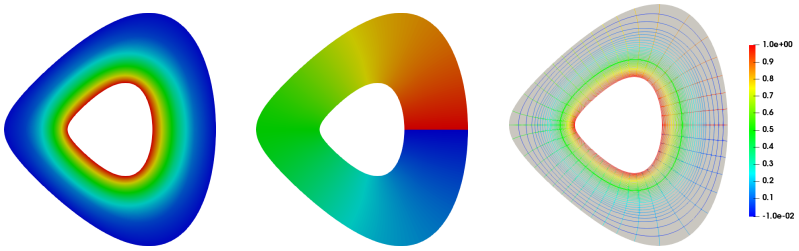

FIGURE 4.6 – Potentials φ_m (left) and ψ_e (center), associated isolines (right).

In Figure 4.7, we present the potentials $\psi_e - \psi_m$, and $\psi_e - \psi_m$. The numerical results proves that $\gamma_e > 0$ and the two potentials ψ_e and ψ_m are equal (this is a numerical interpretation of Lemma 4.2.1).

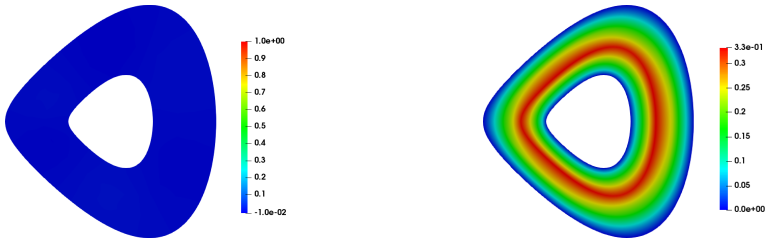

FIGURE 4.7 – Left : the potential $\psi_e - \psi_m$. Right : the potential $\varphi_e - \varphi_m$.

3D / 1D comparisons.

• *Comparisons of voltages (in 1D).*

In Figure 4.8, we compare the evolution of the 1D voltage $V^{\delta,2}(x_3, t)$ issued from the numerical resolution of the 1D model (4.13), to the 1D voltage $V^{\delta}(x_3, t)$ for the 3D problem,

defined by (3.17) and obtained by post-processing the 3D solution $\widetilde{\mathbf{E}}_T^\delta$.

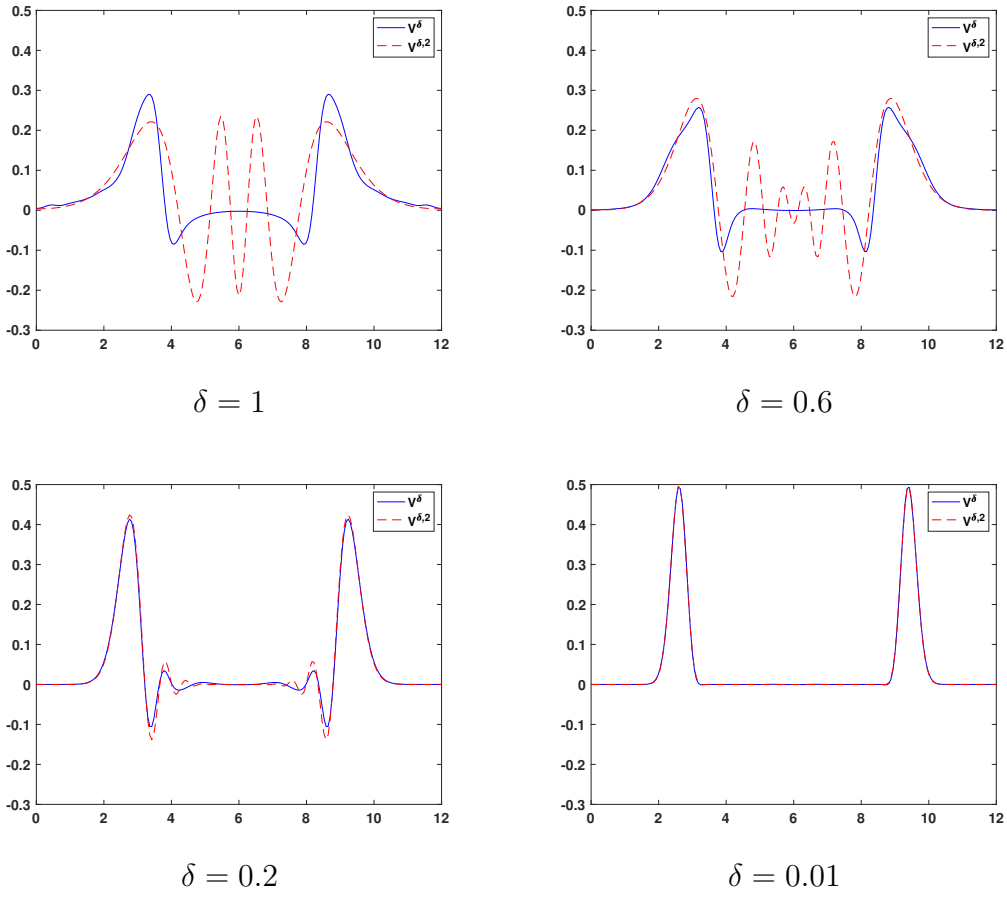

FIGURE 4.8 – The voltages V^δ (in blue) and $V^{\delta,2}$ (in red) at $T = 6$.

More precisely, we compare the above functions in space at the final time $T = 6$ for different values δ. The solution $V^{\delta,2}(x_3, T)$ is in red while $V^\delta(x_3, T)$ is in blue. Numerical results confirm that the approximation of $V^\delta(x_3, t)$ by $V^{\delta,2}(x_3, t)$ improves with the decrease of δ. We observe that $V^{\delta,2}$ and V^δ already almost coincide for $\delta = 0.01$.

• *Comparison of the electric fields in 3D.*

We still at the final time $T = 6$, in Figure 4.9 and Figure 4.10 , we represent respectively $|\widetilde{\mathbf{E}}_T^\delta|$ and $|\widetilde{\mathbf{E}}_T^{\delta,2}|$ on the boundary $\partial\Omega$ of the reference cable for different values of δ.

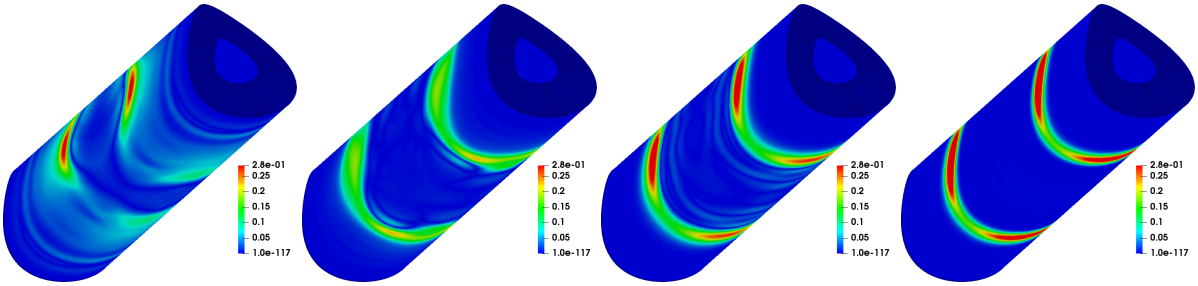

FIGURE 4.9 – $|\widetilde{\mathbf{E}}_T^\delta|$ with $\delta = 1$, $\delta = 0.6$, $\delta = 0.2$, $\delta = 0.01$ at $T = 6$.

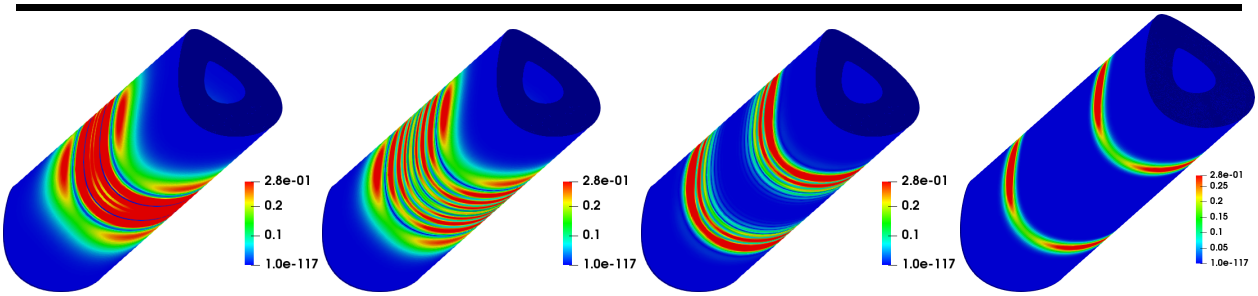

FIGURE 4.10 – $|\widetilde{\mathbf{E}}_T^{\delta,2}|$ with $\delta = 1$, $\delta = 0.6$, $\delta = 0.2$, $\delta = 0.01$ at $T = 6$.

We observe that the result obtained with $\delta = 0.01$ cannot be distinguished from the one obtained with the 1D model ($\widetilde{\mathbf{E}}_T^{\delta,2}$), while a substantial difference exists for $\delta = 1$.

Finally, in order to test the asymptotic transverse polarization of the electric field, we represent in Figures 4.11 and 4.12, again along $\partial\Omega$ at time $T = 6$ the longitudinal electric field $\widetilde{E}_3^{\delta}$ and $\widetilde{E}_3^{\delta,2}$. We observe that the two longitudinal fields tend to 0 when δ tends to 0. On the other hand, for $\delta = 1$ we see that these fields are really non transversely polarized.

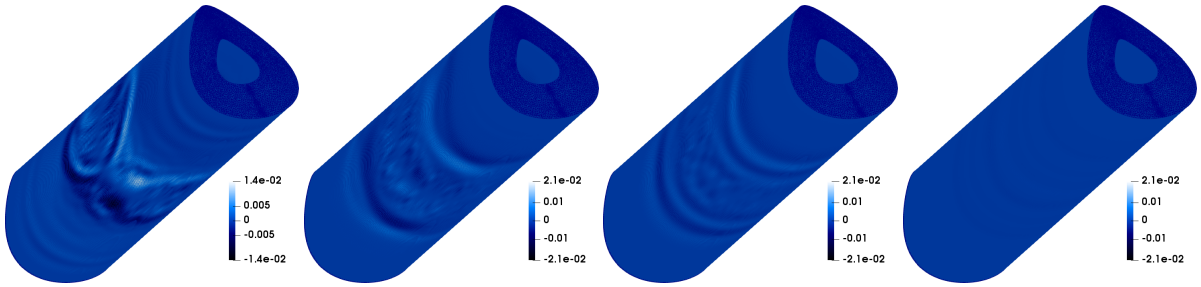

FIGURE 4.11 – E_3^{δ} with $\delta = 1$, $\delta = 0.6$, $\delta = 0.2$, $\delta = 0.01$ at $T = 6$.

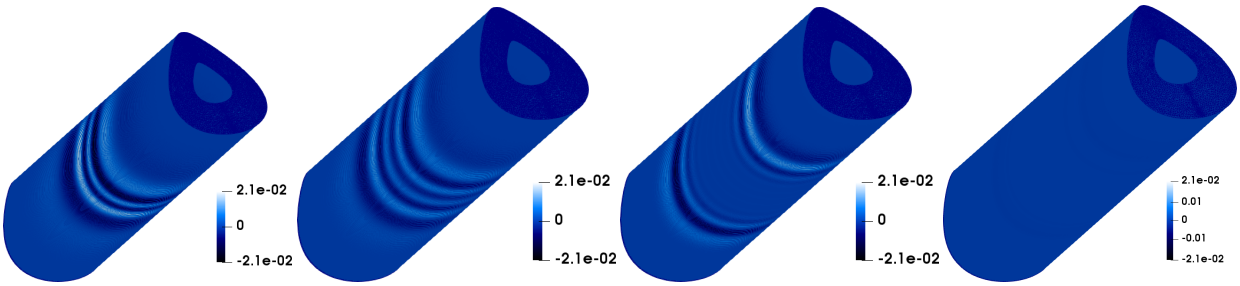

FIGURE 4.12 – $E_3^{\delta,2}$ with $\delta = 1$, $\delta = 0.6$, $\delta = 0.2$, $\delta = 0.01$ at $T = 6$.

We define the relative space-time error as follows :

$$|||V^\delta - V^0||| := \frac{\sup\limits_{t\in[0,T]} \|V^\delta(t) - V^0(t)\|_{L^2([0,L])}}{\sup\limits_{t\in[0,T]} \|V^\delta(t)\|_{L^2([0,L])}}.$$

In Figure 4.13, we present –in red– the relative error between the electric voltage V^δ obtained by the 3D computations with the voltage $V^{\delta,2}$ of the second-order 1D model (4.13), for different values of δ and at different final times T. On the same figures we display –in blue– the relative error between the electric voltage V^δ obtained by the 3D computations with the solution voltage of the 1D limit model V^0 (is the solution of (4.13) when $\delta = 0$). From the numerical results obtained, we can see that when T is small,

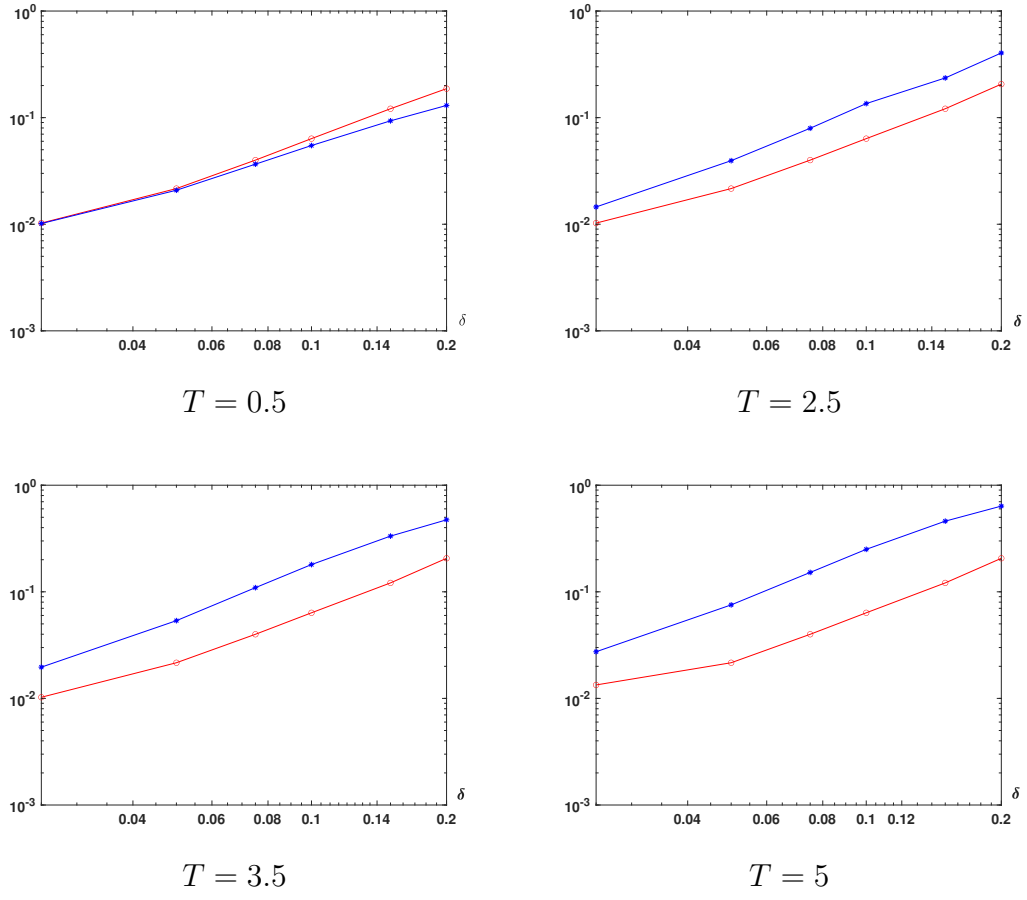

$T = 0.5$ $T = 2.5$

$T = 3.5$ $T = 5$

FIGURE 4.13 – In blue : $|||V^\delta - V^0|||$. In red : $|||V^\delta - V^{\delta,2}|||$. (On the "loglog" scale).

the relative error associated with the 1D limit model is smaller than the one associated with the second order 1D model. This can be explained by the fact that the effect of the dispersion term in the second-order model is negligible for a small value of T, but when the final step T becomes large, this term becomes more important, so the performance of the second-order model becomes better compared to the case of the limit model.

4.5 Conclusion

In this chapter, we presented a second order effective 1D model, developed a stable numerical scheme for its space-time discretization, we carried out and performed the validation of

this new effective model by comparing its results with those obtained for the 3D Maxwell's model for small values of δ. Our numerical results illustrate the interest of this new model compared to the one obtained in the previous chapter. However, it is important to note that all the results obtained in this chapter as well as in the previous chapter are only valid for the case of cylindrical coaxial cables. For this reason, it will be interesting to study the extension of these ideas to the case of non-cylindrical coaxial cables.

Chapter 5

An efficient numerical method for time domain electromagnetic wave propagation in thin co-axial cable with deformation

Contents

5.1 Introduction

In Chapter 2 we have considered the numerical resolution of the 3D time dependent Maxwell's equations in a cylindrical coaxial cable. In order to deal with more realistic situations, it is interesting to extend our approach to the case of non-cylindrical cables. This is the main aim of this chapter in which we will introduce a generalization of the method proposes in Chapter 2 (the case of cylindrical cable).

We propose an approach based on two ingredients. First, the use of a section-by-section

matching technique between the non-cylindrical cable and a cylindrical reference cable. Second, the use of an anisotropic Piola transformation to define the new unknowns in the reference cable.

The new problem obtained in this reference domain includes new terms that depend on the cable geometry (and vanish in the cylindrical case). These terms are not compatible with the finite element approach proposed in Chapter 2. To circumvent this difficulty, we propose a hybrid finite-element/discontinuous-Galerkin approach, with the Discontinuous Galerkin part being used only to handle the new terms. It is found that the resulting method is an extension of the method of Chapter 2 and possesses similar stability properties.

The outline of this chapter is as follows :

In Section 5.2, we will present the 3D Maxwell's problem in a non cylindrical cable, we explain why the classical 3D Piola transform is not adapted to our approach, we propose a modified Piola transform "The anisotropic Piola transform" and finally, we write the weak formulation in the reference domain. Next, in Section 5.3, we applied the Interior Penalty Discontinuous Galerkin approach to the 3D model but only use it in the transverse direction to obtain an Interior Penalty weak formulation. Then, using a mapping approach combined with an anisotropic Piola transform, we rewrite the obtained weak formulation in the reference domain. In Section 5.4 , we derive the spatial discretization of the obtained problem using a hybrid Galerkin finite element/discontinuous approach. Finally, in Section 5.5, we perform the temporal discretization of the problem using an explicit/implicit scheme and study its stability.

5.2 The Maxwell's equations in cables with varying cross-section

5.2.1 Setting of the problem

In this section, we will repeat the setting of our 3D Maxwell's model, found in Chapter 2 (Sections 2.2 and 2.3), but the difference here is that the domain is a non cylindrical cable. More precisely, we consider a cable for which the cross section is dependent of x_3 (see Figure 5.1) and we assume, for simplicity of exposure, that the length L is infinite so that

$$\Omega := \bigcup_{x_3 \in \mathbb{R}} S(x_3). \tag{5.1}$$

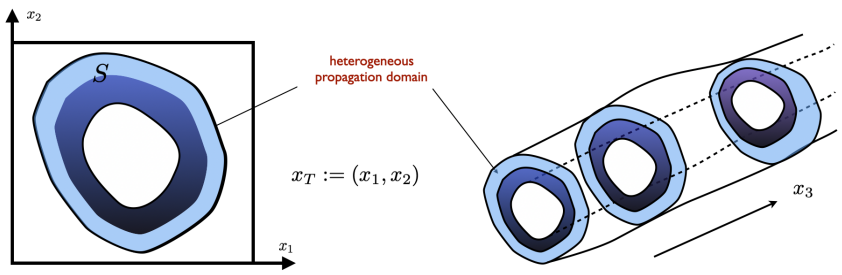

FIGURE 5.1 – Left : slice of the domain, right : the geometry of the domain Ω.

The dielectric material is characterized by the electrical permittivity ε and the magnetic permeability μ which are both function of the space variable $\mathbf{x} \in \Omega$ that satisfy the usual assumptions

$$0 < \mu_- \leq \mu(\mathbf{x}) \leq \mu_+, \quad 0 < \varepsilon_- \leq \varepsilon(\mathbf{x}) \leq \varepsilon_+ \qquad \text{a.e. } \mathbf{x} = (x_1, x_2, x_3) \in \Omega.$$

We shall also consider the possibility that the cable can be, at least locally, conducting, which is modelled through the conductivity σ,

$$0 \leq \sigma(\mathbf{x}) \leq \sigma_+, \qquad \text{a.e. } \mathbf{x} = (x_1, x_2, x_3) \in \Omega. \tag{5.2}$$

The propagation of waves in the cable Ω, through the unknowns $\mathbf{E}(\mathbf{x}, \mathbf{t})$ (the electric field) and $\mathbf{H}(\mathbf{x}, \mathbf{t})$ (the magnetic field) is governed by 3D Maxwell's equations completed with perfectly conducting boundary conditions on $\Gamma := \partial\Omega$,

$$\begin{cases} \varepsilon\, \partial_t \mathbf{E} + \sigma\, \mathbf{E} - \boldsymbol{\nabla} \times \mathbf{H} = \mathbf{0}, & \text{in } \Omega \times \mathbb{R}^+. \\ \mu\, \partial_t \mathbf{H} + \boldsymbol{\nabla} \times \mathbf{E} = \mathbf{0}, & \text{in } \Omega \times \mathbb{R}^+, \\ \mathbf{E} \times \mathbf{n} = 0, & \text{on } \Gamma \times \mathbb{R}^+, \end{cases} \tag{5.3}$$

where t is the time, $\boldsymbol{\nabla}\times$ the 3D curl operator and $\mathbf{n}$ stands for the unit outward normal. the model is completed with initial conditions (for simplicity again we have supposed the absence of source terms, without any loss of generality)

$$\mathbf{E}(\cdot, 0) = \mathbf{E}_0, \quad \mathbf{H}(\cdot, 0) = \mathbf{H}_0. \tag{5.4}$$

Our method will be developed for the second order electric field formulation of the problem, obtained after elimination of the magnetic field,

$$\left| \begin{array}{ll} \varepsilon\, \partial_t^2 \mathbf{E} + \sigma\, \partial_t \mathbf{E} + \boldsymbol{\nabla} \times\, \mu^{-1}\, \boldsymbol{\nabla} \times \mathbf{E} = \mathbf{0}, & \text{in } \Omega \times \mathbb{R}^+, \\ \mathbf{E} \times \mathbf{n} = \mathbf{0}, & \text{on } \Gamma \times \mathbb{R}^+, \\ \mathbf{E}(\cdot, 0) = \mathbf{E}_0, \quad \partial_t \mathbf{E}(\cdot, 0) = \varepsilon^{-1} \left(\boldsymbol{\nabla} \times \mathbf{H}_0 - \sigma\, \mathbf{E}_0 \right) & \text{in } \Omega. \end{array} \right. \tag{5.5}$$

Our approach will be based on a particular rewriting that well separates the roles of the longitudinal and transverse space variables (resp. longitudinal and transverse electric fields).

For simplicity, without any loss generality, we shall present our method in the case $\sigma = 0$. In that case, we recall that the weak formulation of (5.5) is :

Find $\mathbf{E}(\cdot, t) = \left(\mathbf{E}_T(\cdot, t), E_3(\cdot, t) \right) \in H(\mathbf{rot}; \Omega)$ such that, $\forall\, \overline{\mathbf{E}} \in H(\mathbf{rot}; \Omega)$

$$\frac{d^2}{dt^2}\, \mathbf{m}(\mathbf{E}, \overline{\mathbf{E}}) + \mathbf{k}(\mathbf{E}, \overline{\mathbf{E}}) = 0, \tag{5.6}$$

where

$$\begin{cases} \mathbf{m}(\mathbf{E}, \overline{\mathbf{E}}) := \displaystyle\int_\Omega \varepsilon\, \mathbf{E} \cdot \overline{\mathbf{E}}\, d\mathbf{x}, \\ \mathbf{k}(\mathbf{E}, \overline{\mathbf{E}}) := \displaystyle\int_\Omega \mu^{-1}\, \boldsymbol{\nabla} \times \mathbf{E} \cdot \boldsymbol{\nabla} \times \overline{\mathbf{E}}\, d\mathbf{x}. \end{cases} \tag{5.7}$$

Recall of the reformulation of the continuous problem

We introduce the longitudinal and transverse space variables

$$\mathbf{x} := (\mathbf{x}_T, x_3), \quad \mathbf{x}_T := (x_1, x_2)$$

and decompose the electric field into transverse ($\mathbf{E}_T$) and longitudinal (E_3) components,

$$\mathbf{E} = \begin{pmatrix} \mathbf{E}_T \\ \\ E_3 \end{pmatrix} \qquad \text{with} \quad \mathbf{E}_T = \begin{pmatrix} E_1 \\ \\ E_2 \end{pmatrix}.$$

To rewrite (5.5), we shall use the following transverse curl operators and the transverse divergence operator (note that the index T refers to transverse derivatives),

$$\mathrm{rot}_T\, \mathbf{E}_T = \partial_1 E_2 - \partial_2 E_1, \quad \mathbf{rot}_T\, E_3 = \begin{pmatrix} \partial_2 E_3 \\ \\ -\partial_1 E_3 \end{pmatrix}, \quad \mathrm{div}_T\, \mathbf{E}_T = \partial_1 E_1 + \partial_2 E_2. \tag{5.8}$$

The first one is a scalar rotational operator whereas the second is a vectorial rotational operator which can be seen as a "rotated" gradient

$$\mathbf{rot}_T\, E_3 = -\mathbf{e}_3 \times \nabla_T E_3, \quad \text{with} \quad \mathbf{e}_3 \times E_T = \begin{pmatrix} -E_2 \\ \\ E_1 \end{pmatrix} \quad \text{and} \quad \mathbf{e}_3 = (0,0,1)^t. \tag{5.9}$$

These rotational operators are related to the 3D curl operator via

$$\boldsymbol{\nabla} \times \mathbf{E} = \begin{pmatrix} \mathbf{rot}_T E_3 + \mathbf{e}_3 \times \partial_3 \mathbf{E}_T \\ \\ \mathrm{rot}_T\, \mathbf{E}_T \end{pmatrix}. \tag{5.10}$$

Thus, the Maxwell's equations (5.5) rewrite (this is straightforward computations)

$$\left| \begin{array}{l} \varepsilon\, \partial_t^2 \mathbf{E}_T - \partial_3\Big(\mu^{-1} \partial_3 \mathbf{E}_T\Big) + \mathbf{rot}_T\Big(\mu^{-1} \mathrm{rot}_T\, \mathbf{E}_T\Big) + \partial_3\Big(\mu^{-1} \nabla_T E_3\Big) = 0, \\ \varepsilon\, \partial_t^2 E_3 + \mathrm{rot}_T\, \Big(\mu^{-1} \mathbf{rot}_T E_3\Big) + \mathrm{div}_T\Big(\mu^{-1} \partial_3 \mathbf{E}_T\Big) = 0. \end{array} \right. \tag{5.11}$$

From the section above, we will present the novelties of our 3D formulation compared to Chapter 2.

5.2.2 The principle of the mapping approach

In Chapter 2, the propagation domain of electromagnetic waves is a cylindrical cable

$$\widehat{\Omega} := \widehat{S} \times \mathbb{R},$$

with $\widehat{S}$ an invariant cross section in the longitudinal direction. In this section we introduce the case of the variable cross section, and the idea is to come back to the cylindrical case [2], via a mapping

$$F : \ \widehat{\Omega} = \widehat{S} \times \mathbb{R} \quad \longrightarrow \quad \Omega = \bigcup_{x_3 \in \mathbb{R}} S(x_3), \quad F(\widehat{\mathbf{x}}_T, \widehat{\mathbf{x}}_3) = \Big(F_T(\widehat{\mathbf{x}}_T; \widehat{\mathbf{x}}_3), \widehat{\mathbf{x}}_3\Big), \tag{5.12}$$

with $F_T := (F_1, F_2)$ a diffeomorphism,

$$F_T(\cdot\,; x_3) : \widehat{S} \longrightarrow S(x_3). \tag{5.13}$$

The specificity of the mapping F is to keep invariant the transverse planes, so, in some sense, it is a series of 2D transformations from reference cross-section $\widehat{S}$ to each cross-section $S(x_3)$.

Our strategy is then to deduce the solution $\mathbf{E}(\mathbf{x}, t)$ of Maxwell's equations in Ω from an auxiliary unknown $\widehat{\mathbf{E}}(\widehat{\mathbf{x}}, t)$ defined in $\widehat{\Omega}$. More precisely, $\widehat{\mathbf{E}}(\widehat{\mathbf{x}}, t)$ will be defined as the solution of a modified Maxwell-like problem in the reference domain $\widehat{\Omega}$ to which we will apply –more precisely adapt– the method presented in [2]. Then, $\mathbf{E}(\mathbf{x}, t)$ will be deduced via a simple linear transformation

$$\mathbf{E} \circ F(\widehat{\mathbf{x}}, t) = \mathbf{T}(\widehat{\mathbf{x}})\, \widehat{\mathbf{E}}(\widehat{\mathbf{x}}, t) \quad (\mathbf{T} \text{ is a matrix}). \tag{5.14}$$

The key issue is to find the appropriate transformation of the field $\mathbf{E}$ that will allow to adapt the method of cylindrical case [2].

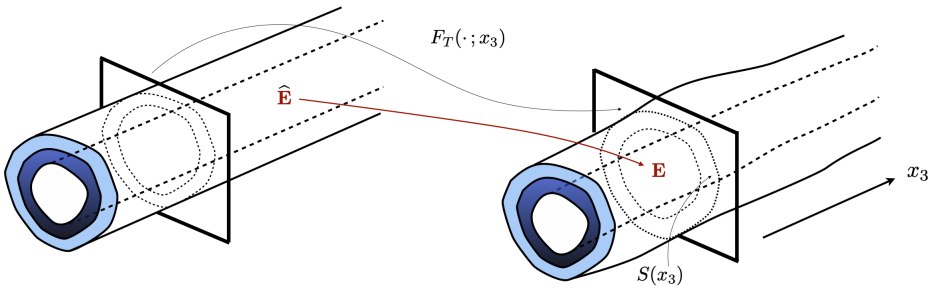

FIGURE 5.2 – An (adapted) mapping approach

5.2.3 Why the usual Piola transformation is not adapted

The mapping approach is inherent, to the finite element theory of Maxwell's equations. In this framework, the most commonly used transformation, the so called 3D Piola transform [2] is given by

$$\mathbf{E}(\mathbf{x}) = \Big(DF(\widehat{\mathbf{x}})^{-1}\Big)^{*}\, \widehat{\mathbf{E}}\Big(\widehat{\mathbf{x}}\Big), \quad \text{for } \widehat{\mathbf{x}} = F(\mathbf{x}), \tag{5.15}$$

where $DF(\widehat{\mathbf{x}})$ is the differential matrix of the mapping F (here, in (5.14) $\mathbf{T} = (DF^{-1})^{*}$).

This transformation is inspired by the usual transformation of the 3D gradient operator $\boldsymbol{\nabla}$ of a scalar field $u(\mathbf{x})$ via the simple change of variable $\mathbf{x} = F(\widehat{\mathbf{x}})$,

$$\boldsymbol{\nabla} u(\mathbf{x}) = \Big(DF(\widehat{\mathbf{x}})^{-1}\Big)^{*}\, \widehat{\boldsymbol{\nabla}} \widehat{u}\Big(\widehat{\mathbf{x}}\Big), \quad \text{if} \quad u(\mathbf{x}) = \widehat{u}(\widehat{\mathbf{x}}).$$

One can show that $\widehat{\mathbf{E}}$ in (5.15) is curl-free, when $\mathbf{E}$ is curl-free. More generally the main interest of the Piola transform is that it preserves the curl operator up to a linear mapping, more precisely,

$$(\boldsymbol{\nabla} \times \mathbf{E})(\mathbf{x}) = J^{-1}(\widehat{\mathbf{x}})\, \Big(DF\ \widehat{\boldsymbol{\nabla}} \times \widehat{\mathbf{E}}\Big)(\widehat{\mathbf{x}}) \text{ for } \mathbf{x} = F(\widehat{\mathbf{x}}), \text{ with } J(\widehat{\mathbf{x}}) = \det\Big(DF(\widehat{\mathbf{x}})\Big). \tag{5.16}$$

In particular, the space $H(\mathbf{rot})$ is preserved by the Piola transformation, this is the reason why it is adapted to finite elements. For the case of the transformation F given in (5.12), the differential DF has the following structure

$$DF(\widehat{\mathbf{x}}_T, x_3) = \begin{pmatrix} D_T F_T(\widehat{\mathbf{x}}_T, x_3) & \partial_3 F_T(\widehat{\mathbf{x}}_T, x_3) \\ 0 & 1 \end{pmatrix}, \tag{5.17}$$

where $D_T F_T$ holds for the partial differential in the transverse variables.

The major difficulty is the presence of the off-diagonal term $\partial_3 F_T$ in (5.17). Indeed, if one defines $\widehat{\mathbf{E}}(\widehat{\mathbf{x}}, t)$ from the solution $\mathbf{E}(\mathbf{x}, t)$ of the Maxwell's system via (5.15) (for each t), it is easy to obtain the weak formulation for $\widehat{\mathbf{E}}(\widehat{\mathbf{x}}, t)$ from (5.6). It suffices to substitute (5.15) in (5.6), the same for the test field $\overline{\mathbf{E}}$, which becomes $\widetilde{\mathbf{E}}$, to use (5.16) for the transformation of the 3D curl operator and $d\mathbf{x} = |J(\widehat{\mathbf{x}})|\, d\widehat{\mathbf{x}}$. One then obtains

Find $\widehat{\mathbf{E}}(\cdot, t) = \big(\widehat{\mathbf{E}}_T(\cdot, t), \widehat{E}_3(\cdot, t)\big) \in H(\mathbf{rot}; \widehat{\Omega})$ such that, $\forall\, \widetilde{\mathbf{E}} \in H(\mathbf{rot}; \widehat{\Omega})$

$$\frac{d^2}{dt^2} \int_{\widehat{\Omega}} \widehat{\varepsilon}\, \mathbf{A}\, \widehat{\mathbf{E}} \cdot \widetilde{\mathbf{E}}\, d\widehat{\mathbf{x}} + \int_{\widehat{\Omega}} \widehat{\mu}^{-1}\, \mathbf{A}^{-1}\, \widehat{\boldsymbol{\nabla}} \times \widehat{\mathbf{E}} \cdot \widehat{\boldsymbol{\nabla}} \times \widetilde{\mathbf{E}}\, d\widehat{\mathbf{x}} = 0.$$

Where the matrix $\mathbf{A}$ ($\mathbf{A} = \mathbf{A}(\widehat{\mathbf{x}})$) is given by $\mathbf{A} = |J|\, DF^{-1}\, (DF^{-1})^*$, and its inverse is written as follows

$$\mathbf{A}^{-1} = |J|^{-1}\, DF^*\, DF = |J|^{-1} \begin{pmatrix} (D_T F_T)^* (D_T F_T) & (D_T F_T)^* \partial_3 F_T \\ (\partial_3 F_T)^* (D_T F_T) & 1 + |\partial_3 F_T|^2 \end{pmatrix}.$$

The problem is the presence, as soon as $\partial_3 F_T \neq 0$, of off diagonal terms in $\mathbf{A}$, and therefore in $\mathbf{A}^{-1}$ which introduces new couplings between the longitudinal and transverse field and longitudinal and transverse derivatives.

The method of Chapter 2 relies on a mass-lumping strategy possible only when the kinetic term do not couple longitudinal and transverse fields. Without mass-lumping, performances are drastically reduced at the point where it is then preferable to use a fully implicit time discretization. To circumvent this problem, we are going to introduce a mapping approach that corresponds to modified Piola transform.

Remark 5.2.1 (Other approaches)**.**

To solve the 3D Maxwell problem in a non-cylindrical coaxial cable, there are other approaches. Among these approaches, we can mention the H^1-formulation with $\mathbb{P}_1$ finite elements by adding in the Maxwell equations a regularization term of form $\boldsymbol{\nabla}(\mathrm{div}\cdot)$. This method is inspired by [16]. There is also the Discontinuous Galerkin method [5][25] [31]. The cable is straight, hence these approaches are not optimal in term of used functional spaces.

5.2.4 Formulation based on an anisotropic Piola transform

An adequate alternative to (5.15) is obtained by treating differently the transverse and longitudinal fields via what we shall call the *anisotropic* Piola transform, $\mathbf{E} = (\mathbf{E}_T, E_3) \to \widehat{\mathbf{E}} = (\widehat{\mathbf{E}}_T, \widehat{E}_3)$ defined as follows : for $\mathbf{x}_T = F_T(\widehat{\mathbf{x}}_T)$,

$$\mathbf{E}(\mathbf{x}_T, x_3) = \big(\mathbf{E}_T, E_3\big)(\mathbf{x}_T, x_3) := \big(D_T F_T^{-*}\, \widehat{\mathbf{E}}_T, \widehat{E}_3\big)(\widehat{\mathbf{x}}_T, x_3), \tag{5.18}$$

where for any invertible matrix $\mathbf{M}$, $\mathbf{M}^{-*} = (\mathbf{M}^{-1})^* \equiv (\mathbf{M}^*)^{-1}$. The formula (5.18) can be rewritten as

$$\mathbf{E}(\mathbf{x}) = (\mathbf{D}^{-1})^* \, \widehat{\mathbf{E}}\big(\widehat{\mathbf{x}}\big), \quad \mathbf{D}\big(\widehat{\mathbf{x}}\big) = \begin{pmatrix} \mathbf{D}_T\big(\widehat{\mathbf{x}}\big) & 0 \\ 0 & 1 \end{pmatrix}, \quad \mathbf{D}_T\big(\widehat{\mathbf{x}}\big) := D_T F_T\big(\widehat{\mathbf{x}}\big). \tag{5.19}$$

In other words,

— the passage from $\mathbf{E}_T$ to $\widehat{\mathbf{E}}_T$ results from a 2D Piola transform,

— the passage from E_3 to $\widehat{E}_3$ results from a simple change of variable.

Remark 5.2.2. *The inverse of the transformation* $\mathbf{E} = (\mathbf{E}_T, E_3) \to \widehat{\mathbf{E}} = (\widehat{\mathbf{E}}_T, \widehat{E}_3)$ *defined by* (5.18) *is as follows : for* $\mathbf{x}_T = F_T(\widehat{\mathbf{x}}_T)$,

$$\widehat{\mathbf{E}}(\widehat{\mathbf{x}}_T, x_3) = \big(\widehat{\mathbf{E}}_T, \widehat{E}_3\big)(\widehat{\mathbf{x}}_T, x_3) = \Big(\mathbf{D}_T(\widehat{\mathbf{x}}_T, x_3)^* \, \mathbf{E}_T\big(\mathbf{x}_T, x_3\big), E_3\big(\mathbf{x}_T, x_3\big)\Big). \tag{5.20}$$

Our next objective is to describe how $\boldsymbol{\nabla} \times \mathbf{E}$ is transformed through the transformation (5.18) for $\mathbf{E}$. For this we shall use the expression (5.10) for $\boldsymbol{\nabla} \times \mathbf{E}$. The next three lemmas 5.2.1, 5.2.2 and 5.2.4 detail how the various terms appearing in (5.10) namely $\mathbf{rot}_T E_3$, $\mathrm{rot}_T \, \mathbf{E}_T$ and $\partial_3 \mathbf{E}_T$. In the following, for shortening the writing, we shall also set,

$$J_T(\widehat{\mathbf{x}}) := \det\big(D_T F_T(\widehat{\mathbf{x}})\big) \equiv \det \, \mathbf{D}_T(\widehat{\mathbf{x}}), \ \mathbf{v}_T(\widehat{\mathbf{x}}) = \partial_3 F_T(\widehat{\mathbf{x}}), \ \mathbf{b}_T(\widehat{\mathbf{x}}) = \mathbf{D}_T^{-1}(\widehat{\mathbf{x}}) \, \mathbf{v}_T(\widehat{\mathbf{x}}). \tag{5.21}$$

$$\mathbf{B}_T := (\partial_3 \mathbf{D}_T^*) \, \mathbf{D}_T^{-*}. \tag{5.22}$$

Remark 5.2.3. *In the reference domain* $\widehat{\Omega}$*, the differential operators have the same definition except that we use the symbol* $\widehat{\cdot}$ *to indicate that they are defined in the reference domain.*

Lemma 5.2.1. *Through the transformation* (5.18)*, the 2D vector curl operator is transform according to*

$$\mathbf{rot}_T \, E_3(\mathbf{x}) = J_T^{-1}(\widehat{\mathbf{x}}) \, \mathbf{D}_T(\widehat{\mathbf{x}}) \, \widehat{\mathbf{rot}}_T \, \widehat{E}_3(\widehat{\mathbf{x}}). \tag{5.23}$$

Proof. By differentiation in the transverse variables (x_1, x_2) of $\widehat{E}_3(\widehat{\mathbf{x}}) = E_3\big(F(\widehat{\mathbf{x}})\big)$, according to the chain rule, we recover that

$$\begin{pmatrix} \partial_2 \widehat{E}_3(\widehat{\mathbf{x}}) \\ -\partial_1 \widehat{E}_3(\widehat{\mathbf{x}}) \end{pmatrix} = \begin{pmatrix} \partial_2 F_2(\widehat{\mathbf{x}}) & -\partial_2 F_1(\widehat{\mathbf{x}}) \\ -\partial_1 F_2(\widehat{\mathbf{x}}) & \partial_1 F_1(\widehat{\mathbf{x}}) \end{pmatrix} \begin{pmatrix} \partial_2 E_3(\mathbf{x}) \\ -\partial_1 E_3(\mathbf{x}) \end{pmatrix},$$

which, by definition (5.8) of $\mathbf{rot}_T$, we can recast as

$$\widehat{\mathbf{rot}}_T \, \widehat{E}_3(\widehat{\mathbf{x}}) = J_T(\widehat{\mathbf{x}}) \, \mathbf{D}_T(\widehat{\mathbf{x}})^{-1} \, \mathbf{rot}_T E_3(\mathbf{x}),$$

that is to say (5.23). ■

Lemma 5.2.2. *Through the transformation* (5.18) *, the 2D scalar curl operator is transformed according to*

$$\mathrm{rot}_T \, \mathbf{E}_T(\mathbf{x}) = J_T^{-1}(\widehat{\mathbf{x}}). \, \widehat{\mathrm{rot}}_T \, \widehat{\mathbf{E}}_T(\widehat{\mathbf{x}}). \tag{5.24}$$

Proof. By definition

$$\mathrm{rot}_T\,\widehat{\mathbf{E}}_T(\widehat{\mathbf{x}}) = (\partial_1\widehat{E}_2 - \partial_2\widehat{E}_1)(\widehat{\mathbf{x}}),$$

while from (5.18), we also have

$$\begin{cases} \widehat{E}_1(\widehat{\mathbf{x}}) = \partial_1 F_1(\widehat{\mathbf{x}})\, E_1(\mathbf{x}) + \partial_1 F_2(\widehat{\mathbf{x}})\, E_2(\mathbf{x}), \\ \widehat{E}_2(\widehat{\mathbf{x}}) = \partial_2 F_1(\widehat{\mathbf{x}})\, E_1(\mathbf{x}) + \partial_2 F_2(\widehat{\mathbf{x}})\, E_2(\mathbf{x}). \end{cases} \tag{5.25}$$

By the chain rule, remembering that $\mathbf{x} = F(\widehat{\mathbf{x}})$, we get

$$\left|\begin{array}{rcl} \partial_1\widehat{E}_2(\widehat{\mathbf{x}}) & = & \partial^2_{12}F_2(\widehat{\mathbf{x}})\, E_2(\mathbf{x}) + \partial^2_{12}F_1(\widehat{\mathbf{x}})\, E_1(\mathbf{x}) \\ & + & (\partial_2 F_1)(\widehat{\mathbf{x}})\Big(\partial_1 F_1(\widehat{\mathbf{x}})\partial_1 E_1(\mathbf{x}) + \partial_1 F_2(\widehat{\mathbf{x}})\partial_2 E_1(\mathbf{x})\Big) \\ & + & (\partial_2 F_2)(\widehat{\mathbf{x}})\Big(\partial_1 F_1(\widehat{\mathbf{x}})\partial_1 E_2(\mathbf{x}) + \partial_1 F_2(\widehat{\mathbf{x}})\partial_2 E_2(\mathbf{x})\Big), \end{array}\right.$$

$$\left|\begin{array}{rcl} \partial_2\widehat{E}_1(\widehat{\mathbf{x}}) & = & \partial^2_{12}F_1(\widehat{\mathbf{x}})\, E_1(\mathbf{x}) + \partial^2_{12}F_2(\widehat{\mathbf{x}})\, E_2(\mathbf{x}) \\ & + & (\partial_1 F_1)(\widehat{\mathbf{x}})\Big(\partial_2 F_1(\widehat{\mathbf{x}})\partial_1 E_1(\mathbf{x}) + \partial_2 F_2(\widehat{\mathbf{x}})\partial_2 E_1(\mathbf{x})\Big) \\ & + & (\partial_1 F_2)(\widehat{\mathbf{x}})\Big(\partial_2 F_1(\widehat{\mathbf{x}})\partial_1 E_2(\mathbf{x}) + \partial_1 F_2(\widehat{\mathbf{x}})\partial_2 E_2(\mathbf{x})\Big). \end{array}\right.$$

By difference the zero order terms in E_1, E_2 cancel, as well as $\partial_1 E_1$ and $\partial_2 E_2$. It remains

$$\mathrm{rot}_T\,\widehat{\mathbf{E}}_T(\widehat{\mathbf{x}}) = \Big(\partial_1 F_1\,\partial_2 F_2 - \partial_1 F_2\,\partial_2 F_1\Big)(\widehat{\mathbf{x}})\;(\partial_1 E_1 - \partial_2 E_2)(\mathbf{x}),$$

which leads to the announced result. ■

For our next result, we shall need the technical lemma below :

Lemma 5.2.3.

$$\forall\, \mathbf{u}_T \in L^2(\widehat{S})^2, \quad \mathbf{e}_3 \times \mathbf{D}_T^{-*}\,\mathbf{u}_T = J_T^{-1}\,\mathbf{D}_T\,\Big(\mathbf{e}_3 \times \mathbf{u}_T\Big). \tag{5.26}$$

Proof. First note that $\mathbf{D}_T^{-*} := \Big(D_T F_T^*\Big)^{-1} = J_T^{-1}\begin{pmatrix} \partial_2 F_2 & -\partial_1 F_2 \\ -\partial_2 F_1 & \partial_1 F_1 \end{pmatrix}$, so that

$$\mathbf{D}_T^{-*}\,\mathbf{u}_T = J_T^{-1}\begin{pmatrix} (\partial_2 F_2)\,u_1 - (\partial_1 F_2)\,u_2 \\ -(\partial_2 F_1)\,u_1 + (\partial_1 F_1)\,u_2 \end{pmatrix}.$$

Thus, using $\mathbf{e_3} \times (v_1, v_2)^t = (-v_2, v_1)^t$, we have

$$\mathbf{e}_3 \times \mathbf{D}_T^{-*}\,\mathbf{u}_T = J_T^{-1}\begin{pmatrix} (\partial_2 F_1)\,u_1 - (\partial_1 F_1)\,u_2 \\ \partial_2 F_2)\,u_1 - (\partial_1 F_2)\,u_2 \end{pmatrix} \equiv \begin{pmatrix} \partial_1 F_1 & \partial_2 F_1 \\ \partial_1 F_2 & \partial_2 F_2 \end{pmatrix}\begin{pmatrix} -u_2 \\ u_1 \end{pmatrix},$$

which is nothing but (5.26) . ■

Lemma 5.2.4. *Through the transformation* (5.18)*, the x_3-derivative is transformed according to*

$$\partial_3\mathbf{E}_T(\mathbf{x}) = \mathbf{D}_T^{-*}\,\partial_3\widehat{\mathbf{E}}_T(\widehat{\mathbf{x}}) - \Big(\mathbf{b}_T \cdot \widehat{\nabla}_T\Big)\Big(\mathbf{D}_T^{-*}\,\widehat{\mathbf{E}}_T\Big) - \mathbf{D}_T^{-*}\,\mathbf{B}_T\,\widehat{\mathbf{E}}_T(\widehat{\mathbf{x}}). \tag{5.27}$$

Proof. By the chain rule and (5.25), one has

$$\left|\begin{array}{rcl} \partial_3 \widehat{E}_1(\widehat{\mathbf{x}}) & = & \partial^2_{31} F_1(\widehat{\mathbf{x}})\, E_1(\mathbf{x}) + \partial^2_{31} F_2(\widehat{\mathbf{x}})\, E_2(\mathbf{x}) \\ & + & (\partial_1 F_1)(\widehat{\mathbf{x}}) \Big(\partial_3 F_1(\widehat{\mathbf{x}}) \partial_1 E_1(\mathbf{x}) + \partial_3 F_2(\widehat{\mathbf{x}}) \partial_2 E_1(\mathbf{x}) + \partial_3 E_1(\mathbf{x})\Big) \\ & + & (\partial_1 F_2)(\widehat{\mathbf{x}}) \Big(\partial_3 F_1(\widehat{\mathbf{x}}) \partial_1 E_2(\mathbf{x}) + \partial_3 F_2(\widehat{\mathbf{x}}) \partial_2 E_2(\mathbf{x}) + \partial_3 E_2(\mathbf{x})\Big), \end{array}\right. \tag{5.28}$$

$$\left|\begin{array}{rcl} \partial_3 \widehat{E}_2(\widehat{\mathbf{x}}) & = & \partial^2_{32} F_1(\widehat{\mathbf{x}})\, E_2(\mathbf{x}) + \partial^2_{32} F_2(\widehat{\mathbf{x}})\, E_1(\mathbf{x}) \\ & + & (\partial_2 F_1)(\widehat{\mathbf{x}}) \Big(\partial_3 F_1(\widehat{\mathbf{x}}) \partial_1 E_1(\mathbf{x}) + \partial_3 F_2(\widehat{\mathbf{x}}) \partial_2 E_1(\mathbf{x}) + \partial_3 E_1(\mathbf{x})\Big) \\ & + & (\partial_2 F_2)(\widehat{\mathbf{x}}) \Big(\partial_3 F_1(\widehat{\mathbf{x}}) \partial_1 E_2(\mathbf{x}) + \partial_3 F_2(\widehat{\mathbf{x}}) \partial_2 E_2(\mathbf{x}) + \partial_3 E_2(\mathbf{x})\Big), \end{array}\right. \tag{5.29}$$

which we can write in vector form as the sum of three vectors

$$\partial_3 \widehat{\mathbf{E}}_T(\widehat{\mathbf{x}}) = \mathbf{a}(\widehat{\mathbf{x}}) + \mathbf{b}(\widehat{\mathbf{x}}) + \mathbf{c}(\widehat{\mathbf{x}}), \tag{5.30}$$

where the vectors $\mathbf{a}(\widehat{\mathbf{x}})$, $\mathbf{b}(\widehat{\mathbf{x}})$ and $\mathbf{c}(\widehat{\mathbf{x}})$ are defined and expressed below.

Definition and expression of $\mathbf{a}(\widehat{\mathbf{x}})$.

This vector is defined from the first lines of (5.28) and (5.29) :

$$\mathbf{a}(\widehat{\mathbf{x}}) := \begin{pmatrix} \partial^2_{31} F_1(\widehat{\mathbf{x}})\, E_1(\mathbf{x}) + \partial^2_{31} F_2(\widehat{\mathbf{x}})\, E_2(\mathbf{x}) \\ \partial^2_{32} F_1(\widehat{\mathbf{x}})\, E_2(\mathbf{x}) + \partial^2_{32} F_2(\widehat{\mathbf{x}})\, E_1(\mathbf{x}) \end{pmatrix}.$$

This can be rewritten as, using (5.19),

$$\mathbf{a}(\widehat{\mathbf{x}}) = \begin{pmatrix} \partial^2_{31} F_1(\widehat{\mathbf{x}}) & \partial^2_{31} F_2(\widehat{\mathbf{x}}) \\ \partial^2_{32} F_1(\widehat{\mathbf{x}}) & \partial^2_{32} F_2(\widehat{\mathbf{x}}) \end{pmatrix} \begin{pmatrix} E_1(\mathbf{x}) \\ E_2(\mathbf{x}) \end{pmatrix} = \Big(\partial_3 \mathbf{D}^*_T\Big)(\widehat{\mathbf{x}})\, \mathbf{E}_T(\mathbf{x}). \tag{5.31}$$

Definition and expression of $\mathbf{b}(\widehat{\mathbf{x}})$.

This vector is defined from the last two lines of (5.28) and (5.29), excluding the last terms in $(\partial_3 E_1,\, \partial_3 E_2)$.

To simplify its writing, we observe that, using (5.21),

$$\partial_3 F_1(\widehat{\mathbf{x}})\, \partial_1 E_j(\mathbf{x}) + \partial_3 F_2(\widehat{\mathbf{x}})\, \partial_2 E_j(\mathbf{x}) = \widehat{\mathbf{v}}_T(\widehat{\mathbf{x}}) \cdot \nabla_T\, E_j(\mathbf{x}).$$

We define

$$\mathbf{b}(\widehat{\mathbf{x}}) := \begin{pmatrix} (\partial_1 F_1)(\widehat{\mathbf{x}})\, \widehat{\mathbf{v}}_T(\widehat{\mathbf{x}}) \cdot \nabla_T\, E_1(\mathbf{x}) + (\partial_1 F_2)(\widehat{\mathbf{x}})\, \widehat{\mathbf{v}}_T(\widehat{\mathbf{x}}) \cdot \nabla_T\, E_1(\mathbf{x}) \\ (\partial_2 F_1)(\widehat{\mathbf{x}})\, \widehat{\mathbf{v}}_T(\widehat{\mathbf{x}}) \cdot \nabla_T\, E_2(\mathbf{x}) + (\partial_2 F_2)(\widehat{\mathbf{x}})\, \widehat{\mathbf{v}}_T(\widehat{\mathbf{x}}) \cdot \nabla_T\, E_2(\mathbf{x}) \end{pmatrix},$$

which we rewrite as

$$\mathbf{b}(\widehat{\mathbf{x}}) = \mathbf{D}^*_T(\widehat{\mathbf{x}}) \begin{pmatrix} \widehat{\mathbf{v}}_T(\widehat{\mathbf{x}}) \cdot \nabla_T E_1(\mathbf{x}) \\ \widehat{\mathbf{v}}_T(\widehat{\mathbf{x}}) \cdot \nabla_T\, E_2(\mathbf{x}) \end{pmatrix}. \tag{5.32}$$

Definition and expression of $\mathbf{c}(\widehat{\mathbf{x}})$.

This vector is defined from the last terms involving $\partial_3 E_1$ and $\partial_3 E_1$ of the last two lines of (5.28) and (5.29).

$$\mathbf{c}(\widehat{\mathbf{x}}) := \begin{pmatrix} \partial_1 F_1(\widehat{\mathbf{x}})\,\partial_3 E_1(\mathbf{x}) + \partial_1 F_2(\widehat{\mathbf{x}})\,\partial_3 E_2(\mathbf{x}) \\ \partial_1 F_2(\widehat{\mathbf{x}})\,\partial_3 E_1(\mathbf{x}) + \partial_2 F_2(\widehat{\mathbf{x}})\,\partial_3 E_2(\mathbf{x}) \end{pmatrix} \equiv \mathbf{D}_T^*(\widehat{\mathbf{x}})\ \partial_3 \mathbf{E}_T(\mathbf{x}). \tag{5.33}$$

Expression of $\partial_3 \widehat{\mathbf{E}}_T(\widehat{\mathbf{x}})$.

Substituting (5.31), (5.32) and (5.33) in (5.30), we get

$$\partial_3 \widehat{\mathbf{E}}_T(\widehat{\mathbf{x}}) = \Big(\partial_3 \mathbf{D}_T^*\Big)(\widehat{\mathbf{x}})\,\mathbf{E}_T(\mathbf{x}) + \mathbf{D}_T^*(\widehat{\mathbf{x}}) \begin{pmatrix} \widehat{\mathbf{v}}_T(\widehat{\mathbf{x}}) \cdot \nabla_T E_1(\mathbf{x}) \\ \widehat{\mathbf{v}}_T(\widehat{\mathbf{x}}) \cdot \nabla_T E_2(\mathbf{x}) \end{pmatrix} + \mathbf{D}_T^*(\widehat{\mathbf{x}})\ \partial_3 \mathbf{E}_T(\mathbf{x}). \tag{5.34}$$

Expression of $\partial_3 \widehat{\mathbf{E}}_T(\widehat{\mathbf{x}})$.

Multiplying (5.34) by $\mathbf{D}_T^{-*}(\widehat{\mathbf{x}})$, we obtain

$$\partial_3 \mathbf{E}_T(\mathbf{x}) = \mathbf{D}_T^{-*}(\widehat{\mathbf{x}}) \left(\partial_3 \widehat{\mathbf{E}}_T(\widehat{\mathbf{x}}) - \Big(\partial_3 \mathbf{D}_T^*\Big)(\widehat{\mathbf{x}})\,\mathbf{E}_T(\mathbf{x})\right) - \begin{pmatrix} \widehat{\mathbf{v}}_T(\widehat{\mathbf{x}}) \cdot \nabla_T E_1(\mathbf{x}) \\ \widehat{\mathbf{v}}_T(\widehat{\mathbf{x}}) \cdot \nabla_T E_2(\mathbf{x}) \end{pmatrix}. \tag{5.35}$$

Next, we express the last terms of (5.35) with respect to $\widehat{\mathbf{E}}_T$. First, using $\mathbf{E}_T(\mathbf{x}) = \mathbf{D}_T^{-*}(\widehat{\mathbf{x}})\widehat{\mathbf{E}}_T(\widehat{\mathbf{x}})$, (cf. (5.18)), we get, by definition of $\mathbf{B}_T$,

$$\partial_3 \mathbf{E}_T(\mathbf{x}) = \mathbf{D}_T^{-*}(\widehat{\mathbf{x}}) \left(\partial_3 \widehat{\mathbf{E}}_T(\widehat{\mathbf{x}}) - \mathbf{B}_T(\widehat{\mathbf{x}})\,\widehat{\mathbf{E}}_T(\widehat{\mathbf{x}})\right) - \begin{pmatrix} \widehat{\mathbf{v}}_T(\widehat{\mathbf{x}}) \cdot \nabla_T E_1(\mathbf{x}) \\ \widehat{\mathbf{v}}_T(\widehat{\mathbf{x}}) \cdot \nabla_T E_2(\mathbf{x}) \end{pmatrix}.$$

Next, we use Lemma 5.2.1, applied to $E_j, j = 1, 2$ instead of E_3, to write

$$\nabla_T E_j(\mathbf{x}) = -\,\mathbf{e}_3 \times \mathbf{rot}_T E_j(\mathbf{x}) = -\,\mathbf{e}_3 \times \Big(J_T^{-1}\mathbf{D}_T\Big)(\widehat{\mathbf{x}})\ \widehat{\mathbf{rot}}_T\ \Big(E_j \circ F(\widehat{\mathbf{x}})\Big).$$

Thus, using Lemma 5.2.3

$$\nabla_T E_j(\mathbf{x}) = -\mathbf{D}_T^{-*}\Big(\mathbf{e}_3 \times \widehat{\mathbf{rot}}_T\ \Big(E_j \circ F(\widehat{\mathbf{x}})\Big)\Big) = \mathbf{D}_T^{-*}\ \widehat{\nabla}_T\Big(E_j \circ F(\widehat{\mathbf{x}})\Big).$$

As a consequence,

$$\begin{aligned} \mathbf{v}_T(\widehat{\mathbf{x}}) \cdot \nabla_T E_j(\mathbf{x}) = \mathbf{v}_T(\widehat{\mathbf{x}}) \cdot \mathbf{D}_T^{-*}\ \widehat{\nabla}_T\Big(E_j \circ F(\widehat{\mathbf{x}})\Big) \ &= \mathbf{D}_T^{-1}\mathbf{v}_T(\widehat{\mathbf{x}}) \cdot \widehat{\nabla}_T\Big(E_j \circ F(\widehat{\mathbf{x}})\Big) \\ &= \Big(\mathbf{b}_T \cdot \widehat{\nabla}_T\Big)\Big(E_j \circ F(\widehat{\mathbf{x}})\Big). \end{aligned}$$

Using the anisotropic Piola transform (5.19), we have $E_j \circ F(\widehat{\mathbf{x}}) = \Big(\mathbf{D}_T^{-*}\,\widehat{\mathbf{E}}_T\Big)_j$. Thus,

$$\mathbf{v}_T(\widehat{\mathbf{x}}) \cdot \nabla_T E_j(\mathbf{x}) = \Big(\mathbf{b}_T \cdot \widehat{\nabla}_T\Big)\Big(\mathbf{D}_T^{-*}\,\widehat{\mathbf{E}}_T\Big)_j.$$

Substituting the above into (5.35), we finally obtain the announced result. ■

Remark 5.2.4. *The "bad" terms for our purpose are the last two terms in formula (5.27), since they involve the x_3-derivative of F_T. These terms disappear when F_T is independent of x_3, that is to say when the cable remains cylindrical after deformation. In such a case, the anisotropic Piola transform (5.18) coincides with the usual one.*

We introduce now the first order matricial transverse differential operator $\mathbf{P}_T(\hat{\mathbf{x}}, \widehat{\nabla}_T)$ that acts on $2D$ tangential vector fields given by (see also Remark 5.2.5) and is given by

$$\mathbf{P}_T(\hat{\mathbf{x}}, \widehat{\nabla}_T)\hat{\mathbf{E}}_T = (\mathbf{b}_T \cdot \widehat{\nabla}_T)\Big(\mathbf{D}_T^{-*}\,\hat{\mathbf{E}}_T\Big) + \mathbf{D}_T^{-*}\,\mathbf{B}_T\,\hat{\mathbf{E}}_T, \tag{5.36}$$

from which we construct (artificially) the first order matricial transverse differential operator $\mathbf{P}(\hat{\mathbf{x}}, \widehat{\nabla}_T)$ that acts this time on 3D tangential vector fields via the block decomposition

$$\mathbf{P}(\hat{\mathbf{x}}, \widehat{\nabla}_T) = \begin{pmatrix} \mathbf{e}_3 \times \mathbf{P}_T(\hat{\mathbf{x}}, \widehat{\nabla}_T) & 0 \\ 0 & 0 \end{pmatrix}. \tag{5.37}$$

Theorem 5.2.5. *Through the transformation (5.18), one has the formula*

$$(\boldsymbol{\nabla} \times \boldsymbol{E})(\mathbf{x}) = J_T(\hat{\mathbf{x}})^{-1}\,\boldsymbol{D}(\hat{\mathbf{x}})\,\Big(\widehat{\boldsymbol{\nabla}} \times \hat{\mathbf{E}}\Big)\,(\hat{\mathbf{x}}) - \boldsymbol{P}(\hat{\mathbf{x}}, \widehat{\nabla}_T)\,\hat{\mathbf{E}}(\hat{\mathbf{x}}) \quad \textit{with } \mathbf{x} = F(\hat{\mathbf{x}}), \tag{5.38}$$

where the matrix $\boldsymbol{D}(\hat{\mathbf{x}})$ is given by (5.19), or equivalently, using (5.10) (with $(\widehat{\boldsymbol{\nabla}}, \widehat{\nabla}_T, \widehat{\mathrm{rot}}_T, \widehat{\mathbf{rot}}_T)$ instead of $(\boldsymbol{\nabla}, \nabla_T, \mathrm{rot}_T, \mathbf{rot}_T)$) and (5.37) - for simplicity, we omit $\mathbf{x}$ and $\hat{\mathbf{x}}$

$$\boldsymbol{\nabla} \times \boldsymbol{E} = J_T^{-1}\,\begin{pmatrix} \boldsymbol{D}_T\Big(\widehat{\mathbf{rot}}_T\,\hat{E}_3 + \mathbf{e}_3 \times \partial_3\hat{\mathbf{E}}_T\Big) - \mathbf{e}_3 \times \boldsymbol{P}_T(\hat{\mathbf{x}}, \widehat{\nabla}_T)\,\hat{\mathbf{E}}_T \Big) \\ \widehat{\mathrm{rot}}_T\,\hat{\mathbf{E}}_T \end{pmatrix}. \tag{5.39}$$

Proof. Our goal is to relate the two 3D curls :

$$\boldsymbol{\nabla} \times \mathbf{E} = \begin{pmatrix} \mathbf{rot}_T E_3 + \mathbf{e}_3 \times \partial_3\mathbf{E}_T \\ \mathrm{rot}_T\,\mathbf{E}_T \end{pmatrix} \quad \text{and} \quad \widehat{\boldsymbol{\nabla}} \times \hat{\mathbf{E}} = \begin{pmatrix} \widehat{\mathbf{rot}}_T\,\hat{E}_3 + \mathbf{e}_3 \times \partial_3\hat{\mathbf{E}}_T \\ \widehat{\mathrm{rot}}_T\,\hat{\mathbf{E}}_T \end{pmatrix}. \tag{5.40}$$

For the first line of $\boldsymbol{\nabla} \times \mathbf{E}$, we first use (5.23), that is to say

$$\mathbf{rot}_T\,E_3(\mathbf{x}) = J_T^{-1}(\hat{\mathbf{x}})\;\mathbf{D}_T(\hat{\mathbf{x}})\;\widehat{\mathbf{rot}}\hat{E}_3(\hat{\mathbf{x}}). \tag{5.41}$$

Next, using (5.27) (Lemma 5.2.4), we also have

$$\mathbf{e}_3 \times \partial_3\mathbf{E}_T(\mathbf{x}) = \mathbf{e}_3 \times \mathbf{D}_T^{-*}\,\partial_3\hat{\mathbf{E}}_T(\hat{\mathbf{x}}) - \mathbf{e}_3 \times \Big(\,\mathbf{D}_T^{-*}\,\mathbf{B}_T\,\hat{\mathbf{E}}_T(\hat{\mathbf{x}}) + (\mathbf{b}_T \cdot \widehat{\nabla}_T)\hat{\mathbf{E}}_T(\hat{\mathbf{x}})\,\Big). \tag{5.42}$$

In order to make appear the first line of $\widehat{\boldsymbol{\nabla}} \times \hat{\mathbf{E}}$, we use Lemma 5.2.3 to make appear $\mathbf{e}_3 \times \partial_3\hat{\mathbf{E}}_T$,

$$\mathbf{e}_3 \times \partial_3\mathbf{E}_T(\mathbf{x}) = J_T^{-1}(\hat{\mathbf{x}})\;\mathbf{D}_T(\hat{\mathbf{x}})\Big(\mathbf{e}_3 \times \partial_3\hat{\mathbf{E}}_T(\hat{\mathbf{x}})\Big) - \mathbf{e}_3 \times \Big(\,\mathbf{D}_T^{-*}\,\mathbf{B}_T\,\hat{\mathbf{E}}_T(\hat{\mathbf{x}}) + (\mathbf{b}_T \cdot \widehat{\nabla}_T)\hat{\mathbf{E}}_T(\hat{\mathbf{x}})\,\Big). \tag{5.43}$$

Since, by (5.23), cf. Lemma 5.2.1, $\mathbf{rot}_T\,E_3(\mathbf{x}) = J_T^{-1}(\hat{\mathbf{x}})\;\mathbf{D}_T(\hat{\mathbf{x}})\;\widehat{\mathbf{rot}}\hat{E}_3(\hat{\mathbf{x}})$. we see that

$$\left|\begin{array}{rcl} \mathbf{rot}_T E_3 + \mathbf{e}_3 \times \partial_3\mathbf{E}_T & = & J_T^{-1}(\hat{\mathbf{x}})\;\mathbf{D}_T(\hat{\mathbf{x}})\Big(\widehat{\mathbf{rot}}_T\,\hat{E}_3 + \mathbf{e}_3 \times \partial_3\hat{\mathbf{E}}_T\Big) \\ & - & \mathbf{e}_3 \times \Big(\mathbf{D}_T^{-*}\,\mathbf{B}_T\,\hat{\mathbf{E}}_T(\hat{\mathbf{x}}) + (\mathbf{b}_T \cdot \widehat{\nabla}_T)\hat{\mathbf{E}}_T(\hat{\mathbf{x}})\Big) \end{array}\right. \tag{5.44}$$

On the other hand, the second line of the expression of $\boldsymbol{\nabla} \times \mathbf{E}$ is directly given by Lemma 5.2.2

$$\mathrm{rot}_T\,\mathbf{E}_T(\mathbf{x}) = J_T^{-1}(\hat{\mathbf{x}}).\;\widehat{\mathrm{rot}}_T\,\hat{\mathbf{E}}_T(\hat{\mathbf{x}}). \tag{5.45}$$

Finally, (5.38) is nothing but the concatenation of (5.44) and (5.45). ■

Remark 5.2.5. *The term* $\boldsymbol{P}(\hat{\mathbf{x}}, \widehat{\nabla}_T)\hat{\mathbf{E}}$ *in* (5.38) *prevents from expressing* $\boldsymbol{\nabla} \times \mathbf{E}$ *from a simple linear transformation of* $\widehat{\boldsymbol{\nabla}} \times \hat{\mathbf{E}}$*. This term can be seen as perturbation term (hence the letter* $\mathbf{P}$*).*

Moreover in the expression (5.36) *of* $\boldsymbol{P}_T(\hat{\mathbf{x}}, \widehat{\nabla}_T)\hat{\mathbf{E}}_T$*, the first term if of order 1 (as a differential operator) while the second one is of order 0. It is clear from the definitions* (5.21) *and* (5.22) *that*

$$\partial_3 F_T(\mathbf{x}) = 0 \quad \Rightarrow \quad \mathbf{b}_T(\mathbf{x}) = 0 \text{ and } \mathbf{B}_T(\mathbf{x}) = 0, \text{ thus } \boldsymbol{P}(\hat{\mathbf{x}}, \widehat{\nabla}_T) = 0. \tag{5.46}$$

In particular $\boldsymbol{P}(\hat{\mathbf{x}}, \widehat{\nabla}_T)$ *vanishes in the cylindrical parts of the cable.*

5.2.5 The weak formulation in the reference domain

The correct functional space to work with for $\hat{\mathbf{E}}$ is

$$\hat{V} := \Big\{\hat{\mathbf{E}} = (\hat{\mathbf{E}}_T, \hat{E}_3) \in L^2(\hat{\Omega})^3 \ / \ \hat{\mathbf{E}} = \mathbf{D}^* \ \mathbf{E} \text{ with } \mathbf{E} = (\mathbf{E}_T, E_3) \in H(\mathbf{rot}, \Omega)\Big\}, \tag{5.47}$$

where $\mathbf{D}$ given by (5.19).

In the definition above, we have used the definition (5.19) of $\hat{\mathbf{E}}$, however, according to Theorem 5.2.5, we have

$$\hat{V} = \Big\{\hat{\mathbf{E}} \in L^2(\hat{\Omega})^3 \ / \ \widehat{\mathrm{rot}}_T \, \hat{\mathbf{E}}_T \in L^2(\hat{\Omega}), \ \mathbf{D}_T\Big(\widehat{\mathbf{rot}}_T \, \hat{E}_3 + \partial_3 \hat{\mathbf{E}}_T\Big) - \mathbf{P}_T(\hat{\mathbf{x}}, \widehat{\nabla}_T) \, \hat{\mathbf{E}}_T \in L^2(\hat{\Omega})^2\Big\}. \tag{5.48}$$

In the cylindrical case, $\mathbf{P}_T(\hat{\mathbf{x}}, \widehat{\nabla}_T) = 0$ and one recovers that

$$\hat{V} = \hat{V}_c := \ \Big\{\hat{\mathbf{E}} \in L^2(\hat{\Omega})^3 \ / \ \widehat{\mathrm{rot}}_T \, \hat{\mathbf{E}}_T \in L^2(\hat{\Omega}), \widehat{\mathbf{rot}}_T \, \hat{E}_3 + \partial_3 \hat{\mathbf{E}}_T \in L^2(\hat{\Omega})^2\Big\}. \tag{5.49}$$

However, in the general case,

$$\hat{V} \neq \hat{V}_c, \tag{5.50}$$

which is the main reason why we can not use the same finite element method as in the cylindrical case. In the following, for shortening the writing, we shall set :

$$\mathbf{A}_T := |J_T| \, \mathbf{D}_T^{-1} \, \mathbf{D}_T^{-*}. \tag{5.51}$$

Theorem 5.2.1 (Weak formulation for the problem in $\hat{\mathbf{E}}$)**.**

If $\mathbf{E}$ *is solution of* (5.6)*,* $\hat{\mathbf{E}}$ *given by* (5.18) *is solution to :*

Find $\hat{\mathbf{E}}(t) = \Big(\hat{\mathbf{E}}_T, \hat{E}_3\Big)(t) \in \hat{V}$ *such that for any test function* $\tilde{\mathbf{E}} = \Big(\tilde{\mathbf{E}}_T, \tilde{E}_3\Big) \in \hat{V}$*, we have*

$$\frac{d^2}{dt^2} \, \widehat{\mathbf{m}}_g\Big(\hat{\mathbf{E}}, \tilde{\mathbf{E}}\Big) + \hat{\mathbf{k}}_g\Big(\hat{\mathbf{E}}, \tilde{\mathbf{E}}\Big) = 0, \tag{5.52}$$

where the global mass bilinear form is given by

$$\begin{cases} \widehat{\mathbf{m}}_g\Big(\hat{\mathbf{E}}, \tilde{\mathbf{E}}\Big) := \widehat{\mathbf{m}}\Big(\hat{\mathbf{E}}_T, \tilde{\mathbf{E}}_T\Big) + \widehat{m}\Big(\hat{E}_3, \tilde{E}_3\Big), \\ \widehat{\mathbf{m}}\Big(\hat{\mathbf{E}}_T, \tilde{\mathbf{E}}_T\Big) := \displaystyle\int_{\widehat{\Omega}} \widehat{\varepsilon}\Big(\mathbf{A}_T \hat{\mathbf{E}}_T \cdot \tilde{\mathbf{E}}_T\Big), \quad \widehat{m}\Big(\hat{E}_3, \tilde{E}_3\Big) := \displaystyle\int_{\widehat{\Omega}} \widehat{\varepsilon} \, |J_T| \, \hat{E}_3 \cdot \tilde{E}_3, \end{cases} \tag{5.53}$$

and the global stiffness bilinear form is given by

$$\widehat{\mathbf{k}}_g(\widehat{\mathbf{E}},\widetilde{\mathbf{E}}) = \int_{\widehat{\Omega}} \widehat{\mu}^{-1}\,|J_T|^{-1}\,\Big(\boldsymbol{D}\Big(\widehat{\boldsymbol{\nabla}}\times\widehat{\mathbf{E}}\Big)-\boldsymbol{P}(\widehat{\mathbf{x}},\widehat{\nabla}_T)\widehat{\mathbf{E}}\Big)\cdot\Big(\boldsymbol{D}\Big(\widehat{\boldsymbol{\nabla}}\times\widetilde{\mathbf{E}}\Big)-\boldsymbol{P}(\widehat{\mathbf{x}},\widehat{\nabla}_T)\widetilde{\mathbf{E}}\Big). \quad (5.54)$$

Moreover, under extra-regularity, namely

$$\widehat{\mathbf{E}} = \Big(\widehat{\mathbf{E}}_T,\widehat{E}_3\Big)\in \widehat{V}\cap\widehat{V}_c \quad \textit{and} \quad \widetilde{\mathbf{E}} = \Big(\widetilde{\mathbf{E}}_T,\widetilde{E}_3\Big)\in \widehat{V}\cap\widehat{V}_c,$$

the above bilinear form can decomposed as

$$\widehat{\mathbf{k}}_g(\widehat{\mathbf{E}},\widetilde{\mathbf{E}}) := \widehat{\mathbf{k}}(\widehat{\mathbf{E}},\widetilde{\mathbf{E}}) + \widehat{\mathbf{k}}_d(\widehat{\mathbf{E}},\widetilde{\mathbf{E}}), \quad (5.55)$$

with

$$\begin{aligned}\widehat{\mathbf{k}}(\widehat{\mathbf{E}},\widetilde{\mathbf{E}}) \;&=\; \int_{\widehat{\Omega}} \widehat{\mu}^{-1}\,\mathbf{A}_T\big(\widehat{\nabla}_T\widehat{E}_3-\partial_3\widehat{\mathbf{E}}_T\big)\cdot\big(\widehat{\nabla}_T\widetilde{E}_3-\partial_3\widetilde{\mathbf{E}}_T\big)\\ &\quad+\int_{\widehat{\Omega}} \widehat{\mu}^{-1}\,|J_T|^{-1}\,\widehat{\mathrm{rot}}_T\,\widehat{\mathbf{E}}_T\cdot\widehat{\mathrm{rot}}_T\,\widetilde{\mathbf{E}}_T,\end{aligned} \quad (5.56)$$

and

$$\left|\begin{aligned}\widehat{\mathbf{k}}_d(\widehat{\mathbf{E}},\widetilde{\mathbf{E}}) \;&=\; \int_{\widehat{\Omega}} \widehat{\mu}^{-1}\,|J_T|\;\boldsymbol{P}_T(\widehat{\mathbf{x}},\widehat{\nabla}_T)\,\widehat{\mathbf{E}}_T\cdot\boldsymbol{P}_T(\widehat{\mathbf{x}},\widehat{\nabla}_T)\,\widetilde{\mathbf{E}}_T\\ &+\; \int_{\widehat{\Omega}} \widehat{\mu}^{-1}\,|J_T|\big(\mathbf{D}_T^{-*}\,\widehat{\nabla}_T\widehat{E}_3-\mathbf{D}_T^{-*}\partial_3\widehat{\mathbf{E}}_T\big)\cdot\boldsymbol{P}_T(\widehat{\mathbf{x}},\widehat{\nabla}_T)\,\widetilde{\mathbf{E}}_T\\ &+\; \int_{\widehat{\Omega}} \widehat{\mu}^{-1}\,|J_T|\big(\mathbf{D}_T^{-*}\,\widehat{\nabla}_T\widetilde{E}_3-\mathbf{D}_T^{-*}\partial_3\widetilde{\mathbf{E}}_T\big)\cdot\boldsymbol{P}_T(\widehat{\mathbf{x}},\widehat{\nabla}_T)\,\widehat{\mathbf{E}}_T,\end{aligned}\right. \quad (5.57)$$

Note that $\widehat{\mathbf{k}}_d$ vanishes when $\partial_3 F_T = 0$.

Proof. The idea is to start from the weak formulation of the original problem in $\mathbf{E}$,

$$\frac{d^2}{dt^2}\int_\Omega \varepsilon\,\mathbf{E}\cdot\overline{\mathbf{E}}\,d\mathbf{x}+\int_\Omega \mu^{-1}\,\boldsymbol{\nabla}\times\mathbf{E}\cdot\boldsymbol{\nabla}\times\overline{\mathbf{E}}\,d\mathbf{x}=0, \quad (5.58)$$

and to use the anisotropic transformation of both the unknown and the test fields

$$\mathbf{E}(\mathbf{x}) = (\mathbf{D}^{-1})^*\,\widehat{\mathbf{E}}\big(\widehat{\mathbf{x}}\big),\quad \overline{\mathbf{E}}(\mathbf{x}) = (\mathbf{D}^{-1})^*\,\widetilde{\mathbf{E}}\big(\widehat{\mathbf{x}}\big),\quad \text{where } \mathbf{x}=F(\widehat{\mathbf{x}}), \quad (5.59)$$

so that the bilinear forms $\widehat{\mathbf{m}}_g$ and $\widehat{\mathbf{k}}_g$ are given by

$$\widehat{\mathbf{m}}_g(\widehat{\mathbf{E}},\widetilde{\mathbf{E}}) = \int_\Omega \varepsilon\,\mathbf{E}\cdot\overline{\mathbf{E}}\,d\mathbf{x},\quad \widehat{\mathbf{k}}_g(\widehat{\mathbf{E}},\widetilde{\mathbf{E}}) = \int_\Omega \mu^{-1}\,\boldsymbol{\nabla}\times\mathbf{E}\cdot\boldsymbol{\nabla}\times\overline{\mathbf{E}}\,d\mathbf{x}.$$

The expressions above are implicit with respect to $(\widehat{\mathbf{E}},\widetilde{\mathbf{E}})$. Our next goal is to give explicit expressions using (5.59).

Step 1. Expression of $\widehat{\mathbf{m}}_g$.

Using (5.59), $d\mathbf{x} = |J_T(\widehat{\mathbf{x}})|\,d\widehat{\mathbf{x}}$, and $\varepsilon\circ F(\widehat{\mathbf{x}}) = \widehat{\varepsilon}(\widehat{\mathbf{x}})$, we get

$$\widehat{\mathbf{m}}_g(\widehat{\mathbf{E}},\widetilde{\mathbf{E}}) = \int_\Omega \varepsilon\,\mathbf{E}\cdot\overline{\mathbf{E}}\,d\mathbf{x} = \int_{\widehat{\Omega}} \widehat{\varepsilon}\,|J_T|\,(\mathbf{D}^{-1})^*\,\widehat{\mathbf{E}}\cdot(\mathbf{D}^{-1})^*\,\widetilde{\mathbf{E}}\,d\widehat{\mathbf{x}}. \quad (5.60)$$

We decompose the 3D electric field $\widehat{\mathbf{E}}$ in transverse field $\widehat{\mathbf{E}}_T$ and longitudinal one $\widehat{E}_3$, and we use the notation (5.51), we obtain,

$$\int_{\widehat{\Omega}} \widehat{\varepsilon}\,|J_T|\,(\mathbf{D}^{-1})^*\,\widehat{\mathbf{E}}\cdot(\mathbf{D}^{-1})^*\,\widetilde{\mathbf{E}}\,d\hat{\mathbf{x}} = \int_{\widehat{\Omega}} \widehat{\varepsilon}\,\mathbf{A}_T\widehat{\mathbf{E}}_T\cdot\widetilde{\mathbf{E}}_T\,d\hat{\mathbf{x}} + \int_{\widehat{\Omega}} \widehat{\varepsilon}\,|J_T|\,\widehat{E}_3\cdot\widetilde{E}_3\,d\hat{\mathbf{x}}. \tag{5.61}$$

Finally, with (5.60) and (5.61) we obtain

$$\widehat{\mathbf{m}}_g\big(\widehat{\mathbf{E}},\widetilde{\mathbf{E}}\big) := \widehat{\mathbf{m}}\big(\widehat{\mathbf{E}}_T,\widetilde{\mathbf{E}}_T\big) + \widehat{m}\big(\widehat{E}_3,\widetilde{E}_3\big).$$

Step 2. Expression of $\widehat{\mathbf{k}}_g$.

Note that the first expression (5.55) is a direct consequence of Theorem 5.2.5 and the change of variable $\mathbf{x} = F(\hat{\mathbf{x}})$.
For the second expression, we shall exploit the fact that, for $\widehat{\mathbf{E}}$ in $\widehat{V}_c \cap \widehat{V}$

$$\big(\widehat{\mathbf{rot}}_T\,\widehat{E}_3 + \partial_3\widehat{\mathbf{E}}_T\big) \in L^2(\widehat{\Omega})^2 \quad \text{and} \quad \mathbf{P}_T(\hat{\mathbf{x}},\widehat{\nabla}_T)\,\widehat{\mathbf{E}}_T \in L^2(\widehat{\Omega})^2,$$

which allows to expand the product inside the integrand of the right and side of (5.55) :

$$\begin{aligned}
&\Big(J_T^{-1}\,\mathbf{D}\,\big(\widehat{\boldsymbol{\nabla}}\times\widehat{\mathbf{E}}\big) - \mathbf{P}(\hat{\mathbf{x}},\widehat{\nabla}_T)\widehat{\mathbf{E}}\Big)\cdot\Big(J_T^{-1}\,\mathbf{D}\,\big(\widehat{\boldsymbol{\nabla}}\times\widetilde{\mathbf{E}}\big) - \mathbf{P}(\hat{\mathbf{x}},\widehat{\nabla}_T)\widetilde{\mathbf{E}}\Big) = \\
&\qquad J_T^{-1}\,\mathbf{D}\,\big(\widehat{\boldsymbol{\nabla}}\times\widehat{\mathbf{E}}\big)\cdot J_T^{-1}\,\mathbf{D}\,\big(\widehat{\boldsymbol{\nabla}}\times\widetilde{\mathbf{E}}\big) + \mathbf{P}(\hat{\mathbf{x}},\widehat{\nabla}_T)\,\widehat{\mathbf{E}}\cdot\mathbf{P}(\hat{\mathbf{x}},\widehat{\nabla}_T)\,\widetilde{\mathbf{E}} \\
&\qquad -J_T^{-1}\,\mathbf{D}\,\big(\widehat{\boldsymbol{\nabla}}\times\widehat{\mathbf{E}}\big)\cdot\mathbf{P}(\hat{\mathbf{x}},\widehat{\nabla}_T)\,\widetilde{\mathbf{E}} - J_T^{-1}\mathbf{D}\,\big(\widehat{\boldsymbol{\nabla}}\times\widetilde{\mathbf{E}}\big)\cdot\mathbf{P}(\hat{\mathbf{x}},\widehat{\nabla}_T)\,\widehat{\mathbf{E}}.
\end{aligned} \tag{5.62}$$

Using the expression

$$\widehat{\boldsymbol{\nabla}}\times\widehat{\mathbf{E}} = \begin{pmatrix} \widehat{\mathbf{rot}}_T\,\widehat{E}_3 + \mathbf{e}_3\times\partial_3\widehat{\mathbf{E}}_T \\ \widehat{\mathrm{rot}}_T\,\widehat{\mathbf{E}}_T \end{pmatrix},$$

the identity $\widehat{\mathbf{rot}}_T\,\widehat{E}_3 = -\mathbf{e}_3\times\widehat{\nabla}_T\widehat{E}_3$ and the Lemma 5.2.3, we get

$$J_T^{-1}\,\mathbf{D}\,\big(\widehat{\boldsymbol{\nabla}}\times\widehat{\mathbf{E}}\big) = \begin{pmatrix} \mathbf{e}_3\times\big(-\mathbf{D}_T^{-*}\,\widehat{\nabla}_T\widehat{E}_3 + \mathbf{D}_T^{-*}\partial_3\widehat{\mathbf{E}}_T\big) \\ J_T^{-1}\,\widehat{\mathrm{rot}}_T\,\widehat{\mathbf{E}}_T \end{pmatrix}, \tag{5.63}$$

Therefore, since $\mathbf{e}_3\times u_T\cdot\mathbf{e}_3\times v_T = u_T\cdot v_T$

$$\begin{aligned}
J_T^{-1}\,\mathbf{D}\,\big(\widehat{\boldsymbol{\nabla}}\times\widehat{\mathbf{E}}\big)\cdot J_T^{-1}\,\mathbf{D}\,\big(\widehat{\boldsymbol{\nabla}}\times\widetilde{\mathbf{E}}\big) &= \big(\mathbf{D}_T^{-*}\,\widehat{\nabla}_T\widehat{E}_3 - \mathbf{D}_T^{-*}\partial_3\widehat{\mathbf{E}}_T\big)\big(\mathbf{D}_T^{-*}\,\widehat{\nabla}_T\widetilde{E}_3 - \mathbf{D}_T^{-*}\partial_3\widetilde{\mathbf{E}}_T\big) \\
&+ J_T^{-2}\,\widehat{\mathrm{rot}}_T\,\widehat{\mathbf{E}}_T\cdot\widehat{\mathrm{rot}}_T\,\widetilde{\mathbf{E}}_T,
\end{aligned}$$

that is to say, since $\mathbf{A}_T = |J_T|\,\mathbf{D}_T^{-1}\mathbf{D}_T^{-*}$ (cf. (5.51)),

$$\begin{aligned}
J_T^{-1}\,\mathbf{D}\,\big(\widehat{\boldsymbol{\nabla}}\times\widehat{\mathbf{E}}\big)\cdot J_T^{-1}\,\mathbf{D}\,\big(\widehat{\boldsymbol{\nabla}}\times\widetilde{\mathbf{E}}\big) &= |J_T|^{-1}\mathbf{A}_T\big(\widehat{\nabla}_T\widehat{E}_3 - \partial_3\widehat{\mathbf{E}}_T\big)\cdot\big(\widehat{\nabla}_T\widetilde{E}_3 - \partial_3\widetilde{\mathbf{E}}_T\big) \\
&+ J_T^{-2}\,\widehat{\mathrm{rot}}_T\,\widehat{\mathbf{E}}_T\cdot\widehat{\mathrm{rot}}_T\,\widetilde{\mathbf{E}}_T.
\end{aligned} \tag{5.64}$$

Obviously, from (5.37),

$$\mathbf{P}(\hat{\mathbf{x}},\widehat{\nabla}_T)\,\widehat{\mathbf{E}}\cdot\mathbf{P}(\hat{\mathbf{x}},\widehat{\nabla}_T)\,\widetilde{\mathbf{E}} = \mathbf{P}_T(\hat{\mathbf{x}},\widehat{\nabla}_T)\,\widehat{\mathbf{E}}_T\cdot\mathbf{P}_T(\hat{\mathbf{x}},\widehat{\nabla}_T)\,\widetilde{\mathbf{E}}_T.$$

Finally, using (5.63) then (5.37), we have that

$$J_T^{-1}\,\mathbf{D}\left(\widehat{\boldsymbol{\nabla}}\times\widehat{\mathbf{E}}\right)\cdot\mathbf{P}(\hat{\mathbf{x}},\widehat{\nabla}_T)\,\widetilde{\mathbf{E}} \;=\; \left(-\mathbf{D}_T^{-*}\,\widehat{\nabla}_T\hat{E}_3+\mathbf{D}_T^{-*}\partial_3\hat{\mathbf{E}}_T\right)\cdot\mathbf{P}_T(\hat{\mathbf{x}},\widehat{\nabla}_T)\,\widetilde{\mathbf{E}}_T.$$

Inverting the roles of $\widehat{\mathbf{E}}$ and $\widetilde{\mathbf{E}}$ we get finally

$$\left|\begin{array}{l} -J_T^{-1}\,\mathbf{D}\left(\widehat{\boldsymbol{\nabla}}\times\widehat{\mathbf{E}}\right)\cdot\mathbf{P}(\hat{\mathbf{x}},\widehat{\nabla}_T)\,\widetilde{\mathbf{E}}-J_T^{-1}\mathbf{D}\left(\widehat{\boldsymbol{\nabla}}\times\widetilde{\mathbf{E}}\right)\cdot\mathbf{P}(\hat{\mathbf{x}},\widehat{\nabla}_T)\,\widehat{\mathbf{E}} \\ \qquad\qquad =\;\left(\mathbf{D}_T^{-*}\,\widehat{\nabla}_T\hat{E}_3-\mathbf{D}_T^{-*}\partial_3\hat{\mathbf{E}}_T\right)\cdot\mathbf{P}_T(\hat{\mathbf{x}},\widehat{\nabla}_T)\,\widetilde{\mathbf{E}}_T \\ \qquad\qquad +\;\left(\mathbf{D}_T^{-*}\,\widehat{\nabla}_T\tilde{E}_3-\mathbf{D}_T^{-*}\partial_3\tilde{\mathbf{E}}_T\right)\cdot\mathbf{P}_T(\hat{\mathbf{x}},\widehat{\nabla}_T)\,\widehat{\mathbf{E}}_T\;\Big). \end{array}\right. \tag{5.65}$$

Using $d\mathbf{x}=|J_T(\hat{\mathbf{x}})|\,d\hat{\mathbf{x}}$, and $\mu\circ F(\hat{\mathbf{x}})=\hat{\mu}(\hat{\mathbf{x}})$, then substituting (5.64) and (5.65) in (5.62), we get (5.55). ■

To use the approach proposed in Chapter 2, it is useful to decompose the two bilinear forms $\widehat{\mathbf{k}}$ and $\widehat{\mathbf{k}}_d$.

Lemma 5.2.1 (Decomposition of the bilinear form $\widehat{\mathbf{k}}$)**.**

$$\begin{array}{rl}\widehat{\mathbf{k}}(\widehat{\mathbf{E}},\widetilde{\mathbf{E}})=&\widehat{\mathbf{k}}_T\left(\widehat{\mathbf{E}}_T,\widetilde{\mathbf{E}}_T\right)+\widehat{\mathbf{k}}_3\left(\widehat{\mathbf{E}}_T,\widetilde{\mathbf{E}}_T\right)-\widehat{c}_{3T}\left(\widehat{E}_3,\widetilde{\mathbf{E}}_T\right)\\ &+k_T\left(E_3,\widetilde{E}_3\right)-\widehat{c}_{3T}\left(\widetilde{E}_3,\widehat{\mathbf{E}}_T\right),\end{array} \tag{5.66}$$

where

$$\left\{\begin{array}{ll}\widehat{\mathbf{k}}_T\left(\widehat{\mathbf{E}}_T,\widetilde{\mathbf{E}}_T\right):=\displaystyle\int_{\widehat{\Omega}}\hat{\mu}^{-1}|J_T|^{-1}\,\widehat{\mathrm{rot}}_T\hat{\mathbf{E}}_T\,\widehat{\mathrm{rot}}_T\tilde{\mathbf{E}}_T, & \widehat{k}_T\left(\widehat{E}_3,\widetilde{E}_3\right):=\displaystyle\int_{\widehat{\Omega}}\hat{\mu}^{-1}\,A_T\widehat{\nabla}_T\hat{E}_3\cdot\widehat{\nabla}_T\tilde{E}_3,\\ \widehat{\mathbf{k}}_3\left(\widehat{\mathbf{E}}_T,\widetilde{\mathbf{E}}_T\right):=\displaystyle\int_{\widehat{\Omega}}\hat{\mu}^{-1}\,A_T\partial_3\hat{\mathbf{E}}_T\cdot\partial_3\tilde{\mathbf{E}}_T, & \widehat{c}_{3T}\left(\widehat{E}_3,\widetilde{\mathbf{E}}_T\right):=\displaystyle\int_{\widehat{\Omega}}\hat{\mu}^{-1}\,A_T\widehat{\nabla}_T\hat{E}_3\cdot\partial_3\tilde{\mathbf{E}}_T.\end{array}\right. \tag{5.67}$$

Remark 5.2.6 (About formulas (5.67))**.**

The stiffness bilinear forms $\widehat{\mathbf{k}}_g,\widehat{k}_T$ and $\widehat{\mathbf{k}}_3$ do not couple transverse and longitudinal fields. We use bold letters when they apply to transverse fields. The index T means that only transverse derivatives are involved while the index 3 means that only x_3-derivatives are involved. Oppositely the bilinear form $\widehat{c}_{3T}$ couple the transverse and longitudinal fields and mixes the x_3 and transverse derivatives. We shall call it the coupling bilinear form. Note that, at the exception of $\widehat{c}_{3T}$, these bilinear forms are symmetric and positive.

Lemma 5.2.2 (Decomposition of the bilinear form $\widehat{\mathbf{k}}_d$)**.**

$$\widehat{\mathbf{k}}_d(\widehat{\mathbf{E}},\widetilde{\mathbf{E}})=\widehat{\mathbf{k}}^d_{TT}\left(\widehat{\mathbf{E}}_T,\widetilde{\mathbf{E}}_T\right)-\widehat{\mathbf{k}}^d_{3T}\left(\widehat{\mathbf{E}}_T,\widetilde{\mathbf{E}}_T\right)+\widehat{c}^d_{TT}\left(\widehat{E}_3,\widetilde{\mathbf{E}}_T\right)+\widehat{c}^d_{TT}\left(\widetilde{E}_3,\widehat{\mathbf{E}}_T\right), \tag{5.68}$$

where

$$\left\{\begin{array}{rcl}\widehat{\mathbf{k}}^d_{TT}\left(\widehat{\mathbf{E}}_T,\widetilde{\mathbf{E}}_T\right) &:=& \displaystyle\int_{\widehat{\Omega}}\mu^{-1}\,|J_T|\;\boldsymbol{P}_T(\hat{\mathbf{x}},\widehat{\nabla}_T)\;\widehat{\mathbf{E}}_T\cdot\boldsymbol{P}_T(\hat{\mathbf{x}},\widehat{\nabla}_T)\;\widetilde{\mathbf{E}}_T,\\ \widehat{\mathbf{k}}^d_{3T}\left(\widehat{\mathbf{E}}_T,\widetilde{\mathbf{E}}_T\right) &:=& \displaystyle\int_{\widehat{\Omega}}\mu^{-1}\,|J_T|\Big(\mathbf{D}_T^{-*}\;\partial_3\hat{\mathbf{E}}_T\cdot\boldsymbol{P}_T(\hat{\mathbf{x}},\widehat{\nabla}_T)\;\widetilde{\mathbf{E}}_T+\mathbf{D}_T^{-*}\;\partial_3\tilde{\mathbf{E}}_T\cdot\boldsymbol{P}_T(\hat{\mathbf{x}},\widehat{\nabla}_T)\;\widehat{\mathbf{E}}_T\Big),\\ \widehat{c}^d_{TT}\left(\widehat{E}_3,\widetilde{\mathbf{E}}_T\right) &:=& \displaystyle\int_{\widehat{\Omega}}\mu^{-1}\,|J_T|\;\mathbf{D}_T^{-*}\,\nabla_T\;\hat{E}_3\cdot\boldsymbol{P}_T(\hat{\mathbf{x}},\widehat{\nabla}_T)\;\widetilde{\mathbf{E}}_T.\end{array}\right. \tag{5.69}$$

Remark 5.2.7 (About formulas (5.69))**.** *The letter d refers to "deformation" . In particular, all these terms vanish if the cross-sections does not vary with respect to x_3, cf. (5.46). We use the bold letters when they apply to transverse fields. Oppositely, the bilinear forms $\widehat{c}^{d}_{TT}$ couple the transverse and longitudinal fields. The index TT means that there are two transverse derivatives involved, while the index $3T$ means that one mixes the x_3 and transverse derivatives.*

The reader will observe that the bilinear form $\widehat{\mathbf{k}}(\widehat{\mathbf{E}}, \widetilde{\mathbf{E}})$ has the same nice structure than the one we had in the cylindrical case. In particular it is continuous in the space $\mathbf{H}(\widehat{\mathbf{rot}}, \widehat{\Omega})$: the only difference lies in the apparition of the matrix $\mathbf{A}_T$ (which is the identity in the absence of deformation) in the first term of its expression and of the coefficient $|J_T|$ (equal to 1 in the absence of deformation) in the second term.

Which prevents us from proceeding as in the cylindrical case for the numerical approximation is the presence of the bilinear form $\widehat{\mathbf{k}}_d(\widehat{\mathbf{E}}, \widetilde{\mathbf{E}})$ which is only due to the presence of deformation, indeed $\mathbf{b}_T$ and $\mathbf{B}_T$ vanish everywhere $\partial_3 F_T$ vanishes. In particular this bilinear form is not continuous in the space $\mathbf{H}(\widehat{\mathbf{rot}}, \widehat{\Omega})$. Therefore, we will use a hybrid Finite Element/Discontinuous Galerkin approach based on Discontinuous Galerkin in the transverse direction and conformal finite elements for longitudinal variables. In the following section, we will start by deriving the Discontinuous Galerkin approach for the transverse variables.

5.3 An Interior Penalty Discontinuous Galerkin approach

Our discretization strategy is based on the use of an Interior Penalty Discontinuous Galerkin approach found in several works in the literature [5][25][26][27][31]. Except that we will apply this approach in a particular case where the cable is discretized with infinite curved prismatic meshes in the longitudinal direction.

5.3.1 Preliminary material

Partitions and broken functions

To prepare Section 5.3.2, we introduce some useful definition.

In the following, if $\mathcal{O}$ denotes an open set of $\mathbb{R}^3$, we denote by $\rho(\mathcal{O}) \in]0, +\infty]$ the largest radius of balls included in $\mathcal{O}$.

$$\rho(\mathcal{O}) = \sup \Big\{ r > 0 \ / \ \exists\, x \in \mathcal{O} \text{ such that } \ B(x, r) \subset \mathcal{O} \Big\}. \tag{5.70}$$

Definition 5.3.1 (Regular partition)**.** *Given $\mathcal{O}$ open set of $\mathbb{R}^3$, a regular partition $\mathcal{P}(\mathcal{O})$ is defined as*

$$P(\mathcal{O}) = \{\mathcal{O}_j \subset \mathcal{O},\ j \in J \subset \mathbb{N}\}, \quad \mathcal{O}_j \text{ open set of } \mathbb{R}^3,$$

satisfying moreover

$$\overline{\mathcal{O}} = \bigcup_{j \in J} \overline{\mathcal{O}}_j, \quad \mathcal{O}_j \cap \mathcal{O}_\ell = \emptyset \text{ for } \ell \neq j, \quad \text{and} \quad \forall\, R > 0, \quad \rho(\mathcal{P}(\mathcal{O})) := \inf_{j \in J} \rho(\mathcal{O}_j) > 0.$$

Note that such a partition is necessarily locally finite, i.e.

$$\forall\, R > 0, \quad \Big\{ j \ / \mathcal{O}_j \cap B(0, R) \neq \emptyset \Big\} \text{ is finite.}$$

With the above definition, we can define broken H^1-functions.

Definition 5.3.2 (Broken H^1-functions)**.** *A function $u \in L^2(\mathcal{O})$ is called a broken H^1-functions, which we shall write $u \in H^1_b(\mathcal{O})$, if there exists a regular partition $\mathcal{P}(\mathcal{O})$ of $\mathcal{O}$ (depending on u) which is u-compatible, meaning that*

$$\forall\, j \in J, \quad u_{|\mathcal{O}_j} \in H^1(\mathcal{O}_j), \quad \text{and} \quad \sum_j \int_{\mathcal{O}_j} |\nabla u|^2 < +\infty.$$

It is not difficult to see that $H^1_b(\mathcal{O})$ is a vector space that we can equip with the norm (the only subtlety is to check the quantity below is independent of the u-compatible partition, we do not claim that it is a Hilbert space)

$$\|u\|^2_{H^1_b(\mathcal{O})} = \|u\|^2_{L^2(\mathcal{O})} + |u|^2_{H^1_b(\mathcal{O})}, \quad |u|^2_{H^1_b(\mathcal{O})} := \sum_j \int_{\mathcal{O}_j} |\nabla u|^2.$$

Finally, we shall denote by $H^1_{b,\rho}(\mathcal{O})$ the subset of functions in $H^1_b(\mathcal{O})$ that admit a ρ-regular partition (note that it is not a vector space).

The important property for us is that, as a consequence on the usual trace theorem in H^1, functions in $H^1_b(\mathcal{O})$ have L^2 traces on any surface included in $\overline{\mathcal{O}}$.

Property 1 (Trace property)**.** *Let $\mathcal{G}$ be any Lipschitz 2d-manifold included in $\overline{\mathcal{O}}$, for any $u \in H^1_b(\mathcal{O})$, the trace $u|_{\mathcal{G}}$ exists and belongs to $L^2(\mathcal{G})$. Moreover, for all functions admitting a compatible partition $\mathcal{P}(\mathcal{O})$ such that $0 < \rho\big(\mathcal{P}(\mathcal{O})\big) \leq \rho$, there exists $C(\rho, \mathcal{G}) > 0$ such that*

$$\forall\, u \in H^1_{b,\rho}(\mathcal{O}), \quad \|u\|_{L^2(\mathcal{G})} \leq C(\rho, \mathcal{G})\, \|u\|_{H^1_b(\mathcal{O})}.$$

Prismatic meshes in the reference cylindrical domain and associated spaces of functions

For the discretization in the transverse variables of the reference cable $\widehat{\Omega}$, we introduce a finite partition of $\mathcal{T}(\widehat{\mathcal{S}})$ (in the sense of Definition 5.3.1 , the set J being finite)

$$\mathcal{T}(\widehat{S}) = \{K \in \mathcal{T}(\widehat{S})\},$$

we assume that $\widehat{S}$ is a polygon, and that $\mathcal{T}(\widehat{S})$ is a triangulation of $\widehat{S}$ with a conformal triangular mesh (in the finite element sense). We denote h_T step-size, namely the transverse space step. In the sequel, we shall denote N the number of nodes of this mesh, N_e the number of (interior) edges and N_t the number of triangles K in this mesh.

Remark 5.3.1. *Implicitly, we should consider, for the numerical analysis, a family of partition $\mathcal{T}(\widehat{\mathcal{S}})$ whose step-size h_T would tend to 0. This means that it would be appropriate to index the partition by h_T. We have chosen not to make appear explicity h_T to avoid too heavy notation.*

Accordingly, we consider a corresponding partition $\mathcal{T}(\widehat{\Omega})$ of $\widehat{\Omega}$ into disjoint infinite elongated prisms $\widehat{P}_K$,

$$\mathcal{T}(\widehat{\Omega}) := \Big\{\widehat{P}_K := K \times \mathbb{R}, K \in \mathcal{T}(\widehat{S})\Big\}. \tag{5.71}$$

In the following, again to avoid heavy notation, we shall often (that is when the context permit) simply denote $\widehat{P}$ (instead of $\widehat{P}_K$) the current element of $\mathcal{T}(\widehat{\Omega})$ (see Figure 5.4).

$$\forall\, \widehat{P} \in \mathcal{T}(\widehat{\Omega}), \quad \exists!\, K \in \mathcal{T}(\widehat{S}) \text{ such that } \widehat{P} = \widehat{P}_K. \tag{5.72}$$

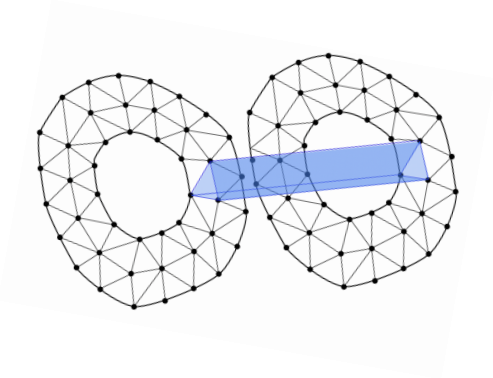

FIGURE 5.3 – Representation of a prismatic element in $\mathcal{T}(\widehat{\Omega})$ (in blue a chunk of the infinite the prism $\widehat{P}$).

In the following, we will denote the interface between two elements $\widehat{P}_K$ and $\widehat{P}_L$ by $\widehat{\Sigma}_{KL}$,

$$\widehat{\Sigma}_{KL} \equiv \widehat{\Sigma}_{LK} := \partial\widehat{P}_K \cap \partial\widehat{P}_L. \tag{5.73}$$

Note that each of these interfaces is included in a plane parallel to the x_3 axis.

We will note $\widehat{\Sigma}$ the skeleton of the partition,

$$\widehat{\Sigma} := \bigcup_{K \neq L} \widehat{\Sigma}_{KL}. \tag{5.74}$$

Finally, for all $K \in \mathcal{T}(\widehat{S})$, it is useful to introduce $\widehat{\mathcal{V}}(K)$ the set of neighbours of P_K

$$\widehat{\mathcal{V}}(K) = \{L \in \mathcal{T}(\widehat{S}) \setminus K \ / \ |\widehat{\Sigma}_{KL}| > 0\}. \tag{5.75}$$

Curved prismatic meshes in the deformed cable

According to the cylindrical partition $\mathcal{T}(\widehat{\Omega})$ of the cylindrical reference cable introduced in the above, we defined a curved prismatic partition of the deformed cable Ω as

$$\mathcal{T}(\Omega) := \Big\{ P = F(\widehat{P}), \widehat{P} \in \mathcal{T}(\widehat{\Omega}) \Big\}. \tag{5.76}$$

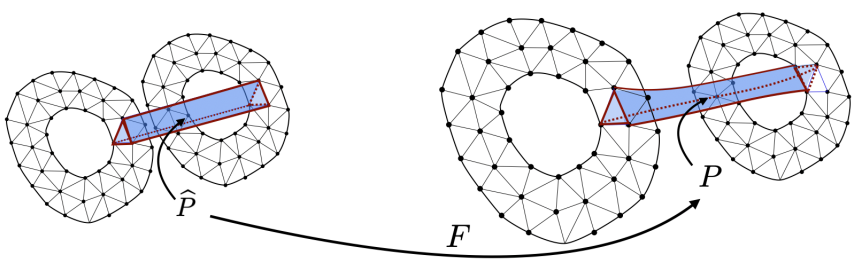

FIGURE 5.4 – The transformation of the infinite reference prisms to an infinite deformed prisms.

In the following, we will denote the interface between two elements P_K and P_L by

$$\Sigma_{KL} := F(\widehat{\Sigma}_{KL}),$$

such that

$$\Sigma_{KL} \equiv \Sigma_{LK} := \partial P_K \cap \partial P_L. \tag{5.77}$$

and we will note Σ the skeleton of the mesh,

$$\Sigma := \bigcup_{K \neq L} \Sigma_{KL}. \tag{5.78}$$

For all $K \in \mathcal{T}(\widehat{S})$, we will denote by $\mathcal{V}(K)$ the set of neighbors of P_K

$$\mathcal{V}(K) = \{L \in \mathcal{T}(\widehat{S}) \setminus K \ / \ |\Sigma_{KL}| > 0\}. \tag{5.79}$$

5.3.2 The Discontinuous Galerkin formulation in the deformed cable

Useful functional spaces

Preliminary notation . For any $\mathbf{u}$ in $L^2(\Omega)^3$, we shall denote $\mathbf{u}_K$ its restriction to P_K, so that $\mathbf{u}$ can be identified to the collection of the $\mathbf{u}_K$'s when K describes $\mathcal{T}(\widehat{S})$.

For any curved prism $P \in \mathcal{T}(\Omega)$ (see (5.76)), we shall define

$$\mathbf{V}(P) = H(\mathbf{rot}, P) \cap H^1_b(P)^3, \tag{5.80}$$

from which we can define

$$\mathbf{V}(\Omega) := \Big\{\mathbf{u} \in L^2(\Omega)^3 \ / \ \forall\, P \in \mathcal{T}(\Omega), \mathbf{u}|_P \in \mathbf{V}(P)\Big\} \subset L^2(\Omega)^3. \tag{5.81}$$

From the trace property (1), we know that vector fields $\mathbf{u}$ in $\mathbf{V}(\Omega)$ have L^2 traces of the interfaces Σ_{KL}. More precisely, on any interface Σ_{KL} we can define the two traces

$$\mathbf{u}_K|_{\Sigma_{KL}} \in L^2(\Sigma_{KL}), \quad \mathbf{u}_L|_{\Sigma_{KL}} \in L^2(\Sigma_{KL}). \tag{5.82}$$

In the following, when it will be clear from the context that we look at traces on Σ_{KL}, we shall often simply write $\mathbf{u}_K$ for the first trace and $\mathbf{u}_L$ for the second one. With this convention we shall define respectively the tangential jump and mean trace of $\mathbf{u}$ on Σ_{KL} by

$$[\mathbf{n} \times \mathbf{u}]_{KL} = \mathbf{n}_K \times \mathbf{u}_K + \mathbf{n}_L \times \mathbf{u}_L, \qquad \{\mathbf{u}\}_{KL} = (\mathbf{u}_K + \mathbf{u}_L)/2. \tag{5.83}$$

where $\mathbf{n}_K$ (resp. $\mathbf{n}_L$) is the unit normal vector along Σ_{KL}, outgoing with respect to P_K (resp. P_L). The reader will observe that the above quantities are invariant under the permutation of K and L. While it is clear that the second quantity in (5.83) is a mean value, the fact that the first one is called a jump is due to the fact that, since $\mathbf{n}_K = -\mathbf{n}_L$, we also have

$$[\mathbf{n} \times \mathbf{u}]_{KL} = \mathbf{n}_K \times \Big(\mathbf{u}_K - \mathbf{u}_L\Big) \equiv \mathbf{n}_L \times \Big(\mathbf{u}_L - \mathbf{u}_K\Big). \tag{5.84}$$

Note that $\mathbf{V}(\Omega)$ is not a subspace of $H(\mathbf{rot}, \Omega)$ since no continuity is imposed through the interfaces Σ_{KL}. Moreover we have the following characterization of $\mathbf{V}(\Omega) \cap H(\mathbf{rot}, \Omega)$:

$$\mathbf{u} \in \mathbf{V}(\Omega) \cap H(\mathbf{rot}, \Omega) \iff \begin{cases} \forall\, P \in \mathcal{T}(\Omega), \quad \mathbf{u} \in \mathbf{V}(P), \\ \\ \forall\, \Sigma_{KL}, \quad [\mathbf{n} \times \mathbf{u}]_{KL} = 0 \quad \text{i. e.} \quad \mathbf{n}_K \times \mathbf{u}_K + \mathbf{n}_L \times \mathbf{u}_L = 0. \end{cases}$$

Indeed, by property (1), functions in $\mathbf{V}(\Omega)$ have well defined traces on $\Gamma = \partial\Omega$ as functions in $L^2(\Gamma)^3$. It is then quite natural to define ($\mathbf{n}$ denoting the unit normal vector to Γ outgoing with respect to Ω)

$$\mathbf{V}_0(\Omega) := \Big\{\mathbf{u} \in \mathbf{V}(\Omega) \ / \ \mathbf{u} \times \mathbf{n} = 0 \text{ on } \Gamma\Big\}. \tag{5.85}$$

Finally, we shall define the space

$$\mathbf{D}(\Omega) := \Big\{\mathbf{u} \in \mathbf{V}(\Omega) \ / \ \mu^{-1}\,\boldsymbol{\nabla} \times \ \mathbf{u} \in \mathbf{V}(\Omega)\Big\}, \tag{5.86}$$

which is also defined as

$$\mathbf{D}(\Omega) := \Big\{\mathbf{u} \in L^2(\Omega)^3 \ / \ \forall\, P \in \mathcal{T}(\Omega), \mathbf{u}|_P \in \mathbf{D}(P)\}. \tag{5.87}$$

where $\mathbf{D}(P)$ is defined as $\mathbf{D}(\Omega)$ (cf. (5.86)).

The Discontinuous Galerkin formulation

In what follows, we assume that the solution $\mathbf{E}$ of (5.5) has the regularity

$$\mathbf{E}(\cdot, t) \in C^2(\mathbb{R}^+; L^2(\Omega)^3) \cap C^0\Big(\mathbb{R}^+, \mathbf{D}(\Omega)\Big). \tag{5.88}$$

The starting point of the weak formulation is the rewriting of (5.5) as an equivalent transmission problem,

$$\left|\begin{array}{ll}
\text{Find } \mathbf{E}(t) : \mathbb{R}^+ \longrightarrow \mathbf{D}(\Omega) \text{ such that for all} (K, L) & \\
\varepsilon\, \partial_t^2 \mathbf{E}_K + \boldsymbol{\nabla} \times \Big(\mu^{-1}\, \boldsymbol{\nabla} \times \mathbf{E}_K\Big) = \mathbf{0}, & \text{in } P_K \times \mathbb{R}^+, \quad (i) \\
\Big(\mu^{-1}\, \boldsymbol{\nabla} \times \mathbf{E}_K\Big) \times \mathbf{n}_K = -\Big(\mu^{-1} \boldsymbol{\nabla} \times \mathbf{E}_L\Big) \times \mathbf{n}_L, & \text{on } \Sigma_{KL} \times \mathbb{R}^+, \quad (ii) \\
\mathbf{n}_K \times \mathbf{E}_K = -\,\mathbf{n}_L \times \mathbf{E}_L, & \text{on } \Sigma_{KL} \times \mathbb{R}^+. \quad (iii)
\end{array}\right. \tag{5.89}$$

Next, we derive a weak formulation of (5.89) of "Discontinuous Galerkin" type.

First, considering any subset P_K of Ω and integrating the equation (i) in (5.89) multiplied (in the sense of the inner product) by a test function $\overline{\mathbf{E}} \in \mathbf{V}(\Omega)$ on P_K, we obtain :

$$\frac{d^2}{dt^2} \int_{P_K} \varepsilon\, \mathbf{E}_K \cdot \overline{\mathbf{E}}_K \, d\mathbf{x} + \int_{P_K} \boldsymbol{\nabla} \times \Big(\mu^{-1}\, \boldsymbol{\nabla} \times \mathbf{E}_K\Big) \cdot \overline{\mathbf{E}}_K \, d\mathbf{x} = 0 \tag{5.90}$$

We then use Green's formula –as in [41] page 59– to transform the second term

$$\begin{aligned}
\int_{P_K} \boldsymbol{\nabla} \times \Big(\mu^{-1}\, \boldsymbol{\nabla} \times \mathbf{E}_K\Big) \cdot \overline{\mathbf{E}}_K \, d\mathbf{x} \ &= \ \int_{P_K} \mu^{-1}\, \boldsymbol{\nabla} \times \mathbf{E}_K \cdot \boldsymbol{\nabla} \times \overline{\mathbf{E}}_K \, d\mathbf{x} \\
&- \ \Big\langle \Big(\mu^{-1}\, \boldsymbol{\nabla} \times \mathbf{E}_K\Big) \times \mathbf{n}_K, \mathbf{n}_K \times (\overline{\mathbf{E}}_K \times \mathbf{n}_K) \Big\rangle_{\partial P_K},
\end{aligned}$$

where we recall that, in the first line, $\Big\langle \cdot, \cdot \Big\rangle_{\partial P_K}$ holds for the duality bracket between

$$H^{-\frac{1}{2}}(\mathrm{div}_\Gamma, \partial P_K) \text{ and } H^{-\frac{1}{2}}(\mathrm{rot}_\Gamma, \partial P_K).$$

Using the L^2-regularity of the traces of $\overline{\mathbf{E}}_K$ (because we chose $\overline{\mathbf{E}} \in \mathbf{V}(\Omega)$) and of $(\mu^{-1}\,\boldsymbol{\nabla}\times\mathbf{E}_K)$ (because, by assumption (5.88), $\mu^{-1}\,\boldsymbol{\nabla}\times\mathbf{E}$ also belongs to $\mathbf{V}(\Omega)$), we can write

$$\begin{aligned}\int_{P_K} \boldsymbol{\nabla}\times\,\mu^{-1}\,\boldsymbol{\nabla}\times\mathbf{E}_K\cdot\overline{\mathbf{E}}_K\,d\mathbf{x} \;&=\; \int_{P_K}\left(\mu^{-1}\,\boldsymbol{\nabla}\times\mathbf{E}_K\right)\cdot\boldsymbol{\nabla}\times\,\overline{\mathbf{E}}_K\,d\mathbf{x}\\ &-\;\int_{\partial P_K}\left((\mu^{-1}\,\boldsymbol{\nabla}\times\mathbf{E}_K)\times\mathbf{n}_K\right)\cdot\left(\mathbf{n}_K\times(\overline{\mathbf{E}}_K\times\mathbf{n}_K)\right)\,d\sigma.\end{aligned}$$

Finally, using the fact that the identity

$$\left((\mu^{-1}\,\boldsymbol{\nabla}\times\mathbf{E}_K)\times\mathbf{n}_K\right)\cdot\left(\mathbf{n}_K\times(\overline{\mathbf{E}}_K\times\mathbf{n}_K)\right)=\left((\mu^{-1}\,\boldsymbol{\nabla}\times\mathbf{E}_K)\times\mathbf{n}_K\right)\cdot\overline{\mathbf{E}}_K.$$

holds in a pointwise sense, we obtain

$$\begin{aligned}\int_{P_K} \boldsymbol{\nabla}\times\,\mu^{-1}\,\boldsymbol{\nabla}\times\mathbf{E}_K\cdot\overline{\mathbf{E}}_K\,d\mathbf{x} \;&=\; \int_{P_K}\left(\mu^{-1}\,\boldsymbol{\nabla}\times\mathbf{E}_K\right)\cdot\boldsymbol{\nabla}\times\,\overline{\mathbf{E}}_K\,d\mathbf{x}\\ &-\;\int_{\partial P_K}\left((\mu^{-1}\,\boldsymbol{\nabla}\times\mathbf{E}_K)\times\mathbf{n}_K\right)\cdot\overline{\mathbf{E}}_K\,d\sigma,\end{aligned}\tag{5.91}$$

that we substitute into (5.90) to obtain

$$\begin{aligned}\frac{d}{dt}\int_{P_K}\varepsilon\,\mathbf{E}_K\cdot\overline{\mathbf{E}}_K\,d\mathbf{x} \;+\; &\int_{P_K}\mu^{-1}\,\boldsymbol{\nabla}\times\mathbf{E}_K\cdot\boldsymbol{\nabla}\times\,\overline{\mathbf{E}}_K\,d\mathbf{x}\\ -\;&\int_{\partial P_K}\left((\mu^{-1}\,\boldsymbol{\nabla}\times\mathbf{E}_K)\times\mathbf{n}_K\right)\cdot\overline{\mathbf{E}}_K\,d\sigma=0.\end{aligned}\tag{5.92}$$

Up to now, all subdomains P_K remain decoupled the ones from the others. This is where we use the decomposition

$$\partial P_K=\bigcup_{L\neq K}\Sigma_{KL}\cup\Gamma_K\quad\text{with}\quad\Gamma_K:=\Gamma\cap\partial K,$$

with Γ_K possibly empty, to rewrite the boundary term as (using that $\overline{\mathbf{E}}_K\times\mathbf{n}_K$ vanishes on Γ_K since $\overline{\mathbf{E}}$ belongs to $\mathbf{V}_0(\Omega)$)

$$\int_{\partial P_K}\left((\mu^{-1}\,\boldsymbol{\nabla}\times\mathbf{E}_K)\times\mathbf{n}_K\right)\cdot\overline{\mathbf{E}}_K\,d\sigma=\sum_{L\in\mathcal{V}(K)}\int_{\Sigma_{KL}}\left((\mu^{-1}\,\boldsymbol{\nabla}\times\mathbf{E}_K)\times\mathbf{n}_K\right)\cdot\overline{\mathbf{E}}_K\,d\sigma.$$

We now use the first transmission condition (5.89)(ii), that we rewrite as (this corresponds to a centered flux in the standard DG vocabulary)

$$(\mu^{-1}\,\boldsymbol{\nabla}\times\mathbf{E}_K)\times\mathbf{n}_K=\frac{1}{2}\,(\mu^{-1}\,\boldsymbol{\nabla}\times\mathbf{E}_K)\times\mathbf{n}_K-\frac{1}{2}\,(\mu^{-1}\boldsymbol{\nabla}\times\mathbf{E}_L)\times\mathbf{n}_L,$$

so that

$$\int_{\Sigma_{KL}}\mu_K^{-1}\,(\boldsymbol{\nabla}\times\mathbf{E}_K)\times\mathbf{n}_K\cdot\overline{\mathbf{E}}_K\,d\sigma=\frac{1}{2}\int_{\Sigma_{KL}}\left(\mu_K^{-1}(\boldsymbol{\nabla}\times\mathbf{E}_K)\times\mathbf{n}_K-\mu_L^{-1}(\boldsymbol{\nabla}\times\mathbf{E}_L)\times\mathbf{n}_L\right)\cdot\overline{\mathbf{E}}_K\,d\sigma.$$

Substituting the above in (5.92)

$$\begin{aligned}\frac{d^2}{dt^2}\int_{P_K}\varepsilon\,\mathbf{E}_K\cdot\overline{\mathbf{E}}_K\,d\mathbf{x} \;+\; &\int_{P_K}\mu^{-1}\,\boldsymbol{\nabla}\times\mathbf{E}_K\cdot\boldsymbol{\nabla}\times\,\overline{\mathbf{E}}_K\,d\mathbf{x}\\ -\;&\frac{1}{2}\int_{\Sigma_{KL}}\left(\mu_K^{-1}(\boldsymbol{\nabla}\times\mathbf{E}_K)\times\mathbf{n}_K-\mu_L^{-1}(\boldsymbol{\nabla}\times\mathbf{E}_L)\times\mathbf{n}_L\right)\cdot\overline{\mathbf{E}}_K\,d\sigma=0.\end{aligned}\tag{5.93}$$

After summation over $K \in \mathcal{T}(S)$, we obtain

$$\frac{d^2}{dt^2}\,\mathbf{m}(\mathbf{E},\overline{\mathbf{E}}) + \mathbf{k}_\Omega(\mathbf{E},\overline{\mathbf{E}}) - \mathbf{c}_\Sigma(\mathbf{E},\overline{\mathbf{E}}) = 0, \quad \forall\, \overline{\mathbf{E}} \in \mathbf{D}^*(\Omega) \tag{5.94}$$

where we have defined

$$\mathbf{m}(\mathbf{E},\overline{\mathbf{E}}) := \int_\Omega \varepsilon\, \mathbf{E}\cdot\overline{\mathbf{E}}\, d\mathbf{x}, \quad \mathbf{k}_\Omega(\mathbf{E},\overline{\mathbf{E}}) := \sum_K \int_{P_K} \mu^{-1}\, \boldsymbol{\nabla}\times\mathbf{E}_K \cdot \boldsymbol{\nabla}\times\overline{\mathbf{E}}_K\, d\mathbf{x}, \tag{5.95}$$

as well as

$$\mathbf{c}_\Sigma(\mathbf{E},\overline{\mathbf{E}}) := \frac{1}{2}\sum_K \sum_{L\in\mathcal{V}(K)} \int_{\Sigma_{KL}} \left(\mu_K^{-1}(\boldsymbol{\nabla}\times\mathbf{E}_K)\times\mathbf{n}_K - \mu_L^{-1}(\boldsymbol{\nabla}\times\mathbf{E}_L)\times\mathbf{n}_L\right)\cdot\overline{\mathbf{E}}_K\, d\sigma. \tag{5.96}$$

Lemma 5.3.1. *With the convention that integrals over Σ_{KL} are 0 when $|\Sigma_{KL}| = 0$, we have*

$$\forall\, (\mathbf{E},\overline{\mathbf{E}}) \in \mathbf{D}(\Omega)^2, \quad \mathbf{c}_\Sigma(\mathbf{E},\overline{\mathbf{E}}) = \frac{1}{2}\sum_{K\neq L} \int_{\Sigma_{KL}} \{\mu^{-1}\,\boldsymbol{\nabla}\times\mathbf{E}\}_{KL}\cdot\left[\overline{\mathbf{E}}\times\mathbf{n}\right]_{KL} d\sigma. \tag{5.97}$$

Proof. With the convention that integrals over Σ_{KL} are 0 when $|\Sigma_{KL}| = 0$, we have

$$\mathbf{c}_\Sigma(\mathbf{E},\overline{\mathbf{E}}) := \frac{1}{2}\sum_{K\neq L} \int_{\Sigma_{KL}} \left(\mu_K^{-1}\,(\boldsymbol{\nabla}\times\mathbf{E}_K)\times\mathbf{n}_K - \mu_L^{-1}\,(\boldsymbol{\nabla}\times\mathbf{E}_L)\times\mathbf{n}_L\right)\cdot\overline{\mathbf{E}}_K\, d\sigma, \tag{5.98}$$

where it is understood that

$$\sum_{K\neq L} a_{KL} = \sum_{(K,L)\in\mathcal{T}(\Sigma)\times\mathcal{T}(\Sigma)} a_{KL} - \sum_{K\in\mathcal{T}(\Sigma)} a_{KK}. \tag{5.99}$$

Inverting the roles of K and L, we also have

$$\mathbf{c}_\Sigma(\mathbf{E},\overline{\mathbf{E}}) := \frac{1}{2}\sum_{K\neq L} \int_{\Sigma_{KL}} \mu^{-1}\left((\boldsymbol{\nabla}\times\mathbf{E}_L)\times\mathbf{n}_L - (\boldsymbol{\nabla}\times\mathbf{E}_K)\times\mathbf{n}_K\right)\cdot\overline{\mathbf{E}}_L\, d\sigma. \tag{5.100}$$

Adding (5.98) and (5.100) we get

$$\mathbf{c}_\Sigma(\mathbf{E},\overline{\mathbf{E}}) := \frac{1}{4}\sum_{K\neq L} \int_{\Sigma_{KL}} \left(\mu_K^{-1}\,(\boldsymbol{\nabla}\times\mathbf{E}_K)\times\mathbf{n}_K - \mu_L^{-1}\,(\boldsymbol{\nabla}\times\mathbf{E}_L)\times\mathbf{n}_L\right)\cdot(\overline{\mathbf{E}}_K - \overline{\mathbf{E}}_L)\, d\sigma. \tag{5.101}$$

Since $\mathbf{n}_K = -\mathbf{n}_L$ on Σ_{KL} We get

$$\mathbf{c}_\Sigma(\mathbf{E},\overline{\mathbf{E}}) := \frac{1}{4}\sum_{K\neq L} \int_{\Sigma_{KL}} \left(\mu_K^{-1}\,(\boldsymbol{\nabla}\times\mathbf{E}_K) + \mu_L^{-1}\,(\boldsymbol{\nabla}\times\mathbf{E}_L)\right)\times\mathbf{n}_K\cdot(\overline{\mathbf{E}}_K - \overline{\mathbf{E}}_L)\, d\sigma. \tag{5.102}$$

Finally, using the fact that $a\cdot(b\times d) = (a\times b)\cdot d$ we obtain

$$\mathbf{c}_\Sigma(\mathbf{E},\overline{\mathbf{E}}) := \frac{1}{4}\sum_{K\neq L} \int_{\Sigma_{KL}} \left(\mu_K^{-1}\,(\boldsymbol{\nabla}\times\mathbf{E}_K) + \mu_L^{-1}\,(\boldsymbol{\nabla}\times\mathbf{E}_L)\right)\cdot\mathbf{n}_K\times(\overline{\mathbf{E}}_K - \overline{\mathbf{E}}_L)\, d\sigma, \tag{5.103}$$

which is nothing but the announced expression using the notation (5.83). ■

With (5.94), we cannot still expect to have equivalence with the problem (5.89) since we still did not use the first transmission condition (5.89)(iii). Moreover, in view of the time discretization, one drawback of the bilinear form $\mathbf{c}_\Sigma(\cdot,\cdot)$ is that it is not symmetric. Fortunately, we remark from the expression (5.97) of $\mathbf{c}_\Sigma(\cdot,\cdot)$ that

$$(5.89)(iii) \quad \Longrightarrow \quad \mathbf{c}_\Sigma(\overline{\mathbf{E}},\mathbf{E}) = 0, \quad \forall\, \overline{\mathbf{E}} \in \mathbf{D}(\Omega), \tag{5.104}$$

so that $\mathbf{E}$ also satisfies

$$\frac{d^2}{dt^2}\,\mathbf{m}(\mathbf{E},\overline{\mathbf{E}}) + \mathbf{k}_\Omega(\mathbf{E},\overline{\mathbf{E}}) - \mathbf{c}_\Sigma(\mathbf{E},\overline{\mathbf{E}}) - \mathbf{c}_\Sigma(\overline{\mathbf{E}},\mathbf{E}) = 0, \tag{5.105}$$

where, now, the stiffness bilinear form $\mathbf{k}_\Omega(\mathbf{E},\overline{\mathbf{E}}) - \mathbf{c}_\Sigma(\mathbf{E},\overline{\mathbf{E}}) - \mathbf{c}_\Sigma(\overline{\mathbf{E}},\mathbf{E})$ are symmetric, this is an essential property for ensuring some energy conservation property after discretization. In addition, to ensure the stability of the method after spatial discretization, we will add to the previous symmetrical weak formulation a jump term as follow,

$$\mathbf{j}_\Sigma(\mathbf{E},\overline{\mathbf{E}}) := \sum_{\Sigma_{KL}\in\Sigma} \int_{\Sigma_{KL}} a\,[\mathbf{E}\times\mathbf{n}]_{KL}\cdot[\overline{\mathbf{E}}\times\mathbf{n}]_{KL}\,d\sigma, \tag{5.106}$$

where $a \in L^\infty(\Sigma)$ is a positive function.

Fortunately, we remark from the expression (5.106) of $\mathbf{j}_\Sigma(\cdot,\cdot)$ that

$$(5.89)(iii) \quad \Longrightarrow \quad \mathbf{j}_\Sigma(\mathbf{E},\overline{\mathbf{E}}) = 0, \quad \forall\, \overline{\mathbf{E}} \in \mathbf{D}(\Omega), \tag{5.107}$$

The interior penalty term $\mathbf{j}_\Sigma(\mathbf{E},\overline{\mathbf{E}})$ penalizes the tangential jumps of $\mathbf{E}$ over the faces, the function a should chosen sufficiently large, as shown later.

Definition 5.3.3 (The Interior Penalty weak formulation)**.**

Find $\mathbf{E} \in \mathbf{D}(\Omega)$ *such that for any test function* $\overline{\mathbf{E}} \in \mathbf{D}(\Omega)$*, we have*

$$\frac{d^2}{dt^2}\,\mathbf{m}\Big(\mathbf{E},\overline{\mathbf{E}}\Big) + \mathbf{k}_\Omega\Big(\mathbf{E},\overline{\mathbf{E}}\Big) + \mathbf{j}^d\Big(\mathbf{E},\overline{\mathbf{E}}\Big) = 0. \tag{5.108}$$

The bilinear forms $\mathbf{m}(\cdot,\cdot)$ *and* $\mathbf{k}(\cdot,\cdot)$ *are defined in* (5.95)*, and* $\mathbf{j}^d$ *is defined as follows,*

$$\mathbf{j}^d\Big(\mathbf{E},\overline{\mathbf{E}}\Big) = -\mathbf{c}_\Sigma(\mathbf{E},\overline{\mathbf{E}}) - \mathbf{c}_\Sigma(\overline{\mathbf{E}},\mathbf{E}) + \mathbf{j}_\Sigma(\mathbf{E},\overline{\mathbf{E}}), \tag{5.109}$$

where $\mathbf{c}_\Sigma(\cdot,\cdot)$ *and* $\mathbf{j}_\Sigma(\cdot,\cdot)$ *are respectively defined in* (5.97) *and* (5.106)*.*

5.3.3 The Discontinuous Galerkin formulation in the reference cylindrical cable

The objective of this section is to rewrite the weak formulation (5.108) in the cylindrical domain. We start by introducing a lemma that is necessary to prove Definition 5.3.4 that summarizes the main results of this section. To do this, we shall recall our anisotropic Piola transform

$$\mathbf{E}(\mathbf{x}_T,x_3) = \Big(\mathbf{E}_T,E_3\Big)(\mathbf{x}_T,x_3) := \Big(\mathbf{D}_T^{-*}\,\widehat{\mathbf{E}}_T,\widehat{E}_3\Big)(\widehat{\mathbf{x}}_T,x_3).$$

Lemma 5.3.2. *If* $\mathbf{E} \in \mathbf{D}(\Omega)$ *(see* (5.86) *for the definition of* $\mathbf{D}(\Omega)$*) and* $\widehat{\mathbf{E}}$ *given by the anisotropic Piola transform, we can write the following relation between the tangential jumps of* $\mathbf{E}$ *and* $\widehat{\mathbf{E}}$*.*

$$[\mathbf{n} \times \mathbf{E}]_{KL} = |(DF^*)^{-1}\widehat{\mathbf{n}}_K|^{-1}\, [[\widehat{\mathbf{E}}]]_{KL}, \tag{5.110}$$

with the notation,

$$[[\mathbf{u}]]_{KL} = \Big((DF^{-1})^*\, \widehat{\mathbf{n}}_K\Big) \times \Big((\mathbf{D}^{-1})^*\, [\mathbf{u}]_{KL}\Big). \tag{5.111}$$

Proof. Using the anisotropic Piola transformation (5.18) and the expression of the outward normal vector on the face of the prism in the reference domain (see [41] page 80)

$$\mathbf{n} \circ F = |(DF^*)^{-1}\widehat{\mathbf{n}}|^{-1}\, (DF^*)^{-1}\widehat{\mathbf{n}},$$

we get

$$\begin{aligned}
[\mathbf{n} \times \mathbf{E}]_{KL} &= \mathbf{n}_K\mathbf{E}_K + \mathbf{n}_L\mathbf{E}_L \\
&= \frac{(DF^{-1})^*\, \widehat{\mathbf{n}}_K}{|(DF^*)^{-1}\widehat{\mathbf{n}}_K|} \times \Big((\mathbf{D}^{-1})^*\, \widehat{\mathbf{E}}_K\Big) + \frac{(DF^{-1})^*\, \widehat{\mathbf{n}}_L}{|(DF^*)^{-1}\widehat{\mathbf{n}}_L|} \times \Big((\mathbf{D}^{-1})^*\, \widehat{\mathbf{E}}_L\Big) \\
&= \frac{(DF^{-1})^*\, \widehat{\mathbf{n}}_K}{|(DF^*)^{-1}\widehat{\mathbf{n}}_K|} \times \Big(\Big((\mathbf{D}^{-1})^*\, \widehat{\mathbf{E}}_K\Big) - \Big((\mathbf{D}^{-1})^*\, \widehat{\mathbf{E}}_L\Big)\Big) \\
&= \frac{(DF^{-1})^*\, \widehat{\mathbf{n}}_K}{|(DF^*)^{-1}\widehat{\mathbf{n}}_K|} \times \Big((\mathbf{D}^{-1})^*\, [\widehat{\mathbf{E}}]_{KL}\Big) \\
&= |(DF^*)^{-1}\widehat{\mathbf{n}}_K|^{-1}\, [[\widehat{\mathbf{E}}]]_{KL}.
\end{aligned} \tag{5.112}$$

■

We now introduce the adequate functional space in which $\mathbf{E}(\cdot,t) = (\mathbf{D}_T^{-*}\, \widehat{\mathbf{E}}_T, \widehat{E}_3)(\cdot,t)$ is sought. Its definition is

$$\widehat{\mathbf{D}}(\widehat{\Omega}) = \Big\{\widehat{\mathbf{E}} = (\widehat{\mathbf{E}}_T, \widehat{E}_3) \in L^2(\widehat{\Omega})^3 \;/\; \mathbf{E} = (\mathbf{E}_T, E_3) \in \mathbf{D}(\Omega),\ \text{where } \mathbf{E} \text{ is given by (5.18)}\Big\}$$

Definition 5.3.4 (Weak formulation for the problem in $\widehat{\mathbf{E}}$)**.**

If $\mathbf{E}(\cdot,t) \in \mathbf{D}(\Omega)$ *is solution of* (5.108)*,* $\widehat{\mathbf{E}}(\cdot,t) \in C^2(\mathbb{R}^+; L^2(\widehat{\Omega})^3) \cap C^0\Big(\mathbb{R}^+, \widehat{\mathbf{D}}(\widehat{\Omega})\Big)$ *given by* (5.18) *is solution of :*

Find $\widehat{\mathbf{E}}(\cdot,t) = \Big(\widehat{\mathbf{E}}_T(\cdot,t), \widehat{E}_3(\cdot,t)\Big) \in \widehat{\mathbf{D}}(\widehat{\Omega})$*, such that for any test function* $\widetilde{\mathbf{E}} \in \widehat{\mathbf{D}}(\widehat{\Omega})$*, we have*

$$\frac{d^2}{dt^2}\, \widehat{\mathbf{m}}_g\Big(\widehat{\mathbf{E}}, \widetilde{\mathbf{E}}\Big) + \widehat{\mathbf{k}}_g\Big(\widehat{\mathbf{E}}, \widetilde{\mathbf{E}}\Big) + \widehat{\mathbf{j}}^d\Big(\widehat{\mathbf{E}}, \widetilde{\mathbf{E}}\Big) = 0, \tag{5.113}$$

where the bilinear forms $\widehat{\mathbf{m}}_g(\cdot,\cdot)$*,* $\widehat{\mathbf{k}}_g(\cdot,\cdot)$*, and* $\widehat{\mathbf{j}}^d(\cdot,\cdot)$ *are defined as follows :*

∗ *The global mass bilinear form :*

$$\begin{cases}
\widehat{\mathbf{m}}_g\Big(\widehat{\mathbf{E}}, \widetilde{\mathbf{E}}\Big) := \widehat{\mathbf{m}}\Big(\widehat{\mathbf{E}}_T, \widetilde{\mathbf{E}}_T\Big) + \widehat{m}\Big(\widehat{E}_3, \widetilde{E}_3\Big), \\
\widehat{\mathbf{m}}\Big(\widehat{\mathbf{E}}_T, \widetilde{\mathbf{E}}_T\Big) := \displaystyle\int_{\widehat{\Omega}} \widehat{\varepsilon}\, \Big(\mathbf{A}_T\widehat{\mathbf{E}}_T \cdot \widetilde{\mathbf{E}}_T\Big), \quad \widehat{m}\Big(\widehat{E}_3, \widetilde{E}_3\Big) := \displaystyle\int_{\widehat{\Omega}} \widehat{\varepsilon}\, |J_T|\, \widehat{E}_3 \cdot \widetilde{E}_3,
\end{cases} \tag{5.114}$$

∗ *The global stiffness bilinear form :*

$$\widehat{\mathbf{k}}_g(\widehat{\mathbf{E}},\widetilde{\mathbf{E}}) = \sum_{K\in\mathcal{T}(\widehat{S})} \int_{\widehat{P}_K} \widehat{\mu}^{-1}\,|J_T|^{-1} \left(\boldsymbol{D}\left(\widehat{\boldsymbol{\nabla}}\times\widehat{\mathbf{E}}_K\right)-\boldsymbol{P}(\hat{\mathbf{x}},\widehat{\nabla}_T)\widehat{\mathbf{E}}_K\right)\cdot\left(\boldsymbol{D}\left(\widehat{\boldsymbol{\nabla}}\times\widetilde{\mathbf{E}}_K\right)-\boldsymbol{P}(\hat{\mathbf{x}},\widehat{\nabla}_T)\widetilde{\mathbf{E}}_K\right). \tag{5.115}$$

∗ *The jump bilinear form :*

$$\begin{aligned}\widehat{\mathbf{j}}\big(\widehat{\mathbf{E}},\widetilde{\mathbf{E}}\big) &= \sum_{\widehat{\Sigma}_{KL}\in\widehat{\Sigma}} \int_{\widehat{\Sigma}_{KL}} \widehat{a}\,|J_T|\,|(DF^*)^{-1}\hat{\mathbf{n}}|^{-1}\,[[\widehat{\mathbf{E}}]]_{KL}\cdot[[\widetilde{\mathbf{E}}]]_{KL}\,d\hat{\sigma}\\ &- \sum_{\widehat{\Sigma}_{KL}\in\widehat{\Sigma}} \int_{\widehat{\Sigma}_{KL}} |J_T|\,[[\widehat{\mathbf{E}}]]_{KL}\cdot\left\{\widehat{\mu}^{-1}\left(J_T^{-1}\,D_TF_T\,\widehat{\nabla}\times\widetilde{\mathbf{E}}-\boldsymbol{P}(\hat{\mathbf{x}},\widehat{\nabla}_T)\,\widetilde{\mathbf{E}}\right)\right\}_{KL} d\hat{\sigma}\\ &- \sum_{\widehat{\Sigma}_{KL}\in\widehat{\Sigma}} \int_{\widehat{\Sigma}_{KL}} |J_T|\,[[\widetilde{\mathbf{E}}]]_{KL}\cdot\left\{\widehat{\mu}^{-1}\left(J_T^{-1}\,D_TF_T\,\widehat{\nabla}\times\widehat{\mathbf{E}}-\boldsymbol{P}(\hat{\mathbf{x}},\widehat{\nabla}_T)\,\widehat{\mathbf{E}}\right)\right\}_{KL} d\hat{\sigma},\end{aligned} \tag{5.116}$$

where $\boldsymbol{P}(\hat{\mathbf{x}},\widehat{\nabla}_T)$ *is given by* (5.36).

Proof. The idea is to start from the weak formulation (5.108)

$$\frac{d^2}{dt^2}\,\mathbf{m}\big(\mathbf{E},\overline{\mathbf{E}}\big)+\mathbf{k}_\Omega\big(\mathbf{E},\overline{\mathbf{E}}\big)+\mathbf{j}^d\big(\mathbf{E},\overline{\mathbf{E}}\big)=0,$$

and to use the anisotropic Piola transformation (5.18) of both the unknown and the test field

$$\mathbf{E}(\mathbf{x})=(\mathbf{D}^{-1})^*\,\widehat{\mathbf{E}}\big(\hat{\mathbf{x}}\big),\quad \overline{\mathbf{E}}(\mathbf{x})=(\mathbf{D}^{-1})^*\,\widetilde{\mathbf{E}}\big(\hat{\mathbf{x}}\big),\qquad \text{for } \mathbf{x}=F(\hat{\mathbf{x}}).$$

The bilinear forms $\widehat{\mathbf{m}}_g$ and $\widehat{\mathbf{k}}_g$ appears as in the proof of the Theorem 5.2.1, where as the bilinear form $\widehat{\mathbf{j}}$, can be expressed as follows : we recall that

$$\begin{aligned}\mathbf{j}^d\big(\mathbf{E},\overline{\mathbf{E}}\big) = &-\sum_{\Sigma_{KL}\in\Sigma}\int_{\Sigma_{KL}}\Big([\mathbf{n}\times\mathbf{E}]_{KL}\cdot\{\mu^{-1}\nabla\times\overline{\mathbf{E}}\}_{KL}+[\mathbf{n}\times\overline{\mathbf{E}}]_{KL}\cdot\{\mu^{-1}\nabla\times\mathbf{E}\}_{KL}\Big)\,d\sigma\\ &+\sum_{\Sigma_{KL}\in\Sigma}\int_{\Sigma_{KL}} a\,[\mathbf{n}\times\mathbf{E}]_{KL}\cdot[\mathbf{n}\times\overline{\mathbf{E}}]_{KL}\,d\sigma.\end{aligned}$$

Using $d\sigma=|J_T|\,|(DF^*)^{-1}\hat{\mathbf{n}}|\,d\hat{\sigma}$, $\mu\circ F(\hat{\mathbf{x}})=\widehat{\mu}(\hat{\mathbf{x}})$, and $a\circ F(\hat{\mathbf{x}})=\widehat{a}(\hat{\mathbf{x}})$, the expression of the jump in the reference domain (5.110) and the 3D curl operator (5.38), we can write that

$$\begin{aligned}\mathbf{j}^d\big(\mathbf{E},\overline{\mathbf{E}}\big) &= \sum_{\widehat{\Sigma}_{KL}\in\widehat{\Sigma}} \int_{\widehat{\Sigma}_{KL}} \widehat{a}\,|J_T|\,|(DF^*)^{-1}\hat{\mathbf{n}}|^{-1}\,[[\widehat{\mathbf{E}}]]_{KL}\cdot[[\widetilde{\mathbf{E}}]]_{KL}\,d\hat{\sigma}\\ &- \sum_{\widehat{\Sigma}_{KL}\in\widehat{\Sigma}} \int_{\widehat{\Sigma}_{KL}} |J_T|\,[[\widehat{\mathbf{E}}]]_{KL}\cdot\left\{\widehat{\mu}^{-1}\left(J_T^{-1}\,D_TF_T\,\widehat{\nabla}\times\widetilde{\mathbf{E}}-\mathbf{P}(\hat{\mathbf{x}},\widehat{\nabla}_T)\,\widetilde{\mathbf{E}}\right)\right\}_{KL} d\hat{\sigma}\\ &- \sum_{\widehat{\Sigma}_{KL}\in\widehat{\Sigma}} \int_{\widehat{\Sigma}_{KL}} |J_T|\,[[\widetilde{\mathbf{E}}]]_{KL}\cdot\left\{\widehat{\mu}^{-1}\left(J_T^{-1}\,D_TF_T\,\widehat{\nabla}\times\widehat{\mathbf{E}}-\mathbf{P}(\hat{\mathbf{x}},\widehat{\nabla}_T)\,\widehat{\mathbf{E}}\right)\right\}_{KL} d\hat{\sigma}.\end{aligned}$$

■

5.4 Space discretization

At this moment, the domain is meshed but the problem is always of infinite dimension. To overcome this problem, we will make a discretization of the space : we will start with a transverse semi-discrete discretization, then a longitudinal discretization will be performed. And we will use the same discrete-spaces as in the cylindrical case [2].

5.4.1 The transverse semi-discretization.

We introduce the finite-element semi-discrete space $\widehat{\mathbf{V}}_{h_T} \subset \widehat{\mathbf{D}}(\widehat{\Omega})$ such that,

$$\widehat{\mathbf{V}}_{h_T}(\widehat{\Omega}) = \Big\{ \widehat{\mathbf{E}} = (\widehat{\mathbf{E}}_T, E_3) \ \in H^1\Big(\mathbb{R}, \widehat{\mathbf{V}}_{h_T}(\widehat{S})\Big) \times L^2(\mathbb{R}, \widehat{V}_{h_T}(\widehat{S}))\Big\}, \tag{5.117}$$

with

$$\begin{cases} \widehat{\mathbf{V}}_{h_T}(\widehat{S}) := \Big\{ \widehat{\mathbf{E}}_T \in H^1(\widehat{S})^2 \ / \ \forall\ K \in \mathcal{T}(\widehat{S}), \widehat{\mathbf{E}}_T|_K \in \mathcal{N}_{2D} \Big\}, \\ \mathcal{N}_{2D} := \Big\{ a\,(x_2, -x_1)^t + \mathbf{b}, (a, \mathbf{b}) \in \mathbb{R} \times \mathbb{R}^2 \Big\} \subset \mathbb{P}_1^2. \\ \widehat{V}_{h_T}(\widehat{S}) := \Big\{ \widehat{E}_3 \in H^1(\widehat{S}) \ / \ \forall\ K \in \mathcal{T}(\widehat{S}),\ E_3|_K \in \mathbb{P}_1 \Big\}. \end{cases} \tag{5.118}$$

Definition 5.4.1.

Find $\widehat{\mathbf{E}}(\cdot, t) = \Big(\widehat{\mathbf{E}}_{T,h_T}(\cdot, t), \widehat{E}_{3,h_T}(\cdot, t)\Big) \in \widehat{\mathbf{V}}_{h_T}(\widehat{\Omega})$, *such that* $\forall\ \widetilde{\mathbf{E}} \in \widehat{\mathbf{V}}_{h_T}(\widehat{\Omega})$, *we have*

$$\frac{d^2}{dt^2}\, \widehat{\mathbf{m}}_g\Big(\widehat{\mathbf{E}}, \widetilde{\mathbf{E}}\Big) + \widehat{\mathbf{k}}_g\Big(\widehat{\mathbf{E}}, \widetilde{\mathbf{E}}\Big) + \widehat{\mathbf{j}}^d\Big(\widehat{\mathbf{E}}, \widetilde{\mathbf{E}}\Big) = 0, \tag{5.119}$$

The bilinear forms $\widehat{\mathbf{m}}_g(\cdot,\cdot)$ *and* $\widehat{\mathbf{k}}_g(\cdot,\cdot)$ *are defined in* (5.114) *and* (5.115), *and* $\widehat{\mathbf{j}}^d$ *is defined in* (5.116).

Let us draw the attention of the reader that if $\widehat{u}$ in $\widehat{\mathbf{V}}_{h_T}(\widehat{\Omega})$ then the expression of the tangential jump term $[[\widehat{u}]]_{KL}$ becomes simpler. To see this, we introduce the Lemma 5.4.1,

Lemma 5.4.1.

$$\forall\ \mathbf{u}_T \in L^2(\widehat{\Omega})^2 \ \textit{and}\ \mathbf{v}_T \in L^2(\widehat{\Omega})^2, \quad \Big(\mathbf{D}_T^{-*}\,\mathbf{u}_T\Big) \times \Big(\mathbf{D}_T^{-*}\,\mathbf{v}_T\Big) = J_T^{-1}\,(\mathbf{u}_T \times \mathbf{v}_T). \tag{5.120}$$

Proof. using the definition of $\mathbf{D}_T^{-*}$

$$\mathbf{D}_T^{-*} = J_T^{-1} \begin{pmatrix} \partial_2 F_2(\widehat{\mathbf{x}}) & -\partial_2 F_1(\widehat{\mathbf{x}}) \\ -\partial_1 F_2(\widehat{\mathbf{x}}) & \partial_1 F_1(\widehat{\mathbf{x}}) \end{pmatrix}.$$

we get,

$$\begin{aligned} \Big(\mathbf{D}_T^{-*}\,\mathbf{u}_T\Big) \times \Big(\mathbf{D}_T^{-*}\,\mathbf{v}_T\Big) &= J_T^{-2} \begin{pmatrix} \partial_2 F_2(\widehat{\mathbf{x}})\,u_1 - \partial_2 F_1(\widehat{\mathbf{x}})\,u_2 \\ -\partial_1 F_2(\widehat{\mathbf{x}})\,u_1 \partial_1 F_1(\widehat{\mathbf{x}})\,u_2 \end{pmatrix} \times \begin{pmatrix} \partial_2 F_2(\widehat{\mathbf{x}})\,v_1 - \partial_2 F_1(\widehat{\mathbf{x}})\,v_2 \\ -\partial_1 F_2(\widehat{\mathbf{x}})\,v_1 \partial_1 F_1(\widehat{\mathbf{x}})\,v_2 \end{pmatrix} \\ &= J_T^{-2}\,(\partial_1 F_1(\widehat{\mathbf{x}})\,\partial_2 F_2(\widehat{\mathbf{x}}) \ - \partial_2 F_1(\widehat{\mathbf{x}})\,\partial_1 F_2(\widehat{\mathbf{x}})\,)\Big(u_1 v_2 - u_2 v_1\Big) \\ &= J_T^{-1}\,\Big(\mathbf{u}_T \times \mathbf{v}_T\Big). \end{aligned}$$

■

The lemma 5.4.1 is very important to prove the following lemma in which we present a simplified expression for the jump term $[[\widehat{u}]]_{KL}$.

Lemma 5.4.2. *If* $\widehat{\mathbf{u}} = \left(\widehat{\mathbf{u}}_T, \widehat{u}_3\right) \in \widehat{\mathbf{V}}_{h_T}(\widehat{\Omega})$, *then*

$$[[\widehat{\mathbf{u}}]]_{KL} = \begin{pmatrix} e_3 \times \left(\mathbf{D}_T^{-*}(d_{3T}\widehat{\mathbf{n}}_T[\widehat{\mathbf{u}}_T]_{KL})\right) \\ 0 \end{pmatrix} \quad \textit{with} \quad d_{3T} := -(\partial_3 F_T)^* \, \mathbf{D}_T^{-*}. \tag{5.121}$$

Proof. We have

$$[[\mathbf{u}]]_{KL} = \left((DF^{-1})^* \, \widehat{\mathbf{n}}\right) \times \left((\mathbf{D}^{-1})^* \, [\mathbf{u}]_{KL}\right).$$

The outward normal vector on $\widehat{\Sigma}_{KL}$ is $\widehat{\mathbf{n}} = \begin{pmatrix} \widehat{\mathbf{n}}_T \\ 0 \end{pmatrix}$, so that we get

$$(DF^{-1})^* \, \widehat{\mathbf{n}} = \begin{pmatrix} \mathbf{D}_T^{-*} \, \mathbf{n}_T \\ -\partial_3 \, F_T^* \, \mathbf{D}_T^{-*} \, \mathbf{n}_T \end{pmatrix} \quad \text{and} \quad (\mathbf{D}^{-1})^* \, \mathbf{u} = \begin{pmatrix} \mathbf{D}_T^{-*} \, \mathbf{u}_T \\ u_3 \end{pmatrix}. \tag{5.122}$$

By definition, we have

$$\forall \, \mathbf{u} = (\mathbf{u}_T, u_3) \in L^2(\widehat{\Omega})^3 \text{ and } \mathbf{v} = (\mathbf{v}_T, v_3) \in L^2(\widehat{\Omega})^3, \quad \mathbf{u} \times \mathbf{v} = \begin{pmatrix} \mathbf{e}_3 \times \left(u_3 \mathbf{v}_T - v_3 \mathbf{u}_T\right) \\ \mathbf{u}_T \times \mathbf{v}_T \end{pmatrix} \tag{5.123}$$

We denote $d_{3T} := -\partial_3 \, F_T^* \, \mathbf{D}_T^{-*}$, So using (5.122) and (5.123), we get

$$[[\widehat{\mathbf{u}}]]_{KL} = \begin{pmatrix} e_3 \times \left(\mathbf{D}_T^{-*}(d_{3T}\widehat{\mathbf{n}}_T[\widehat{\mathbf{u}}_T]_{KL} - [\widehat{u}_3]_{KL}\widehat{\mathbf{n}}_T)\right) \\ \left(\mathbf{D}_T^{-*} \, \widehat{\mathbf{u}}_T\right) \times \left(\mathbf{D}_T^{-*} \, \widehat{\mathbf{v}}_T\right) \end{pmatrix},$$

that is to say, using Lemma 5.4.1,

$$[[\widehat{\mathbf{u}}]]_T = \begin{pmatrix} e_3 \times \left(\mathbf{D}_T^{-*}(d_{3T}\widehat{\mathbf{n}}_T[\widehat{\mathbf{u}}_T]_{KL} - [\widehat{u}_3]_{KL}\widehat{\mathbf{n}}_T)\right) \\ J_T^{-1} \, (\widehat{\mathbf{n}}_T \times [\widehat{\mathbf{u}}_T]_{KL}) \end{pmatrix}.$$

Since $\widehat{\mathbf{u}} = \left(\widehat{\mathbf{u}}_T, \widehat{u}_3\right) \in \widehat{\mathbf{V}}_{h_T}(\widehat{\Omega})$ we have that

$$(\widehat{\mathbf{n}}_T \times [\widehat{\mathbf{u}}_T]_{KL}) = 0 \quad \text{and} \quad [\widehat{u}_3]_{KL} = 0.$$

We finally obtain the announced result,

$$[[\widehat{\mathbf{u}}]]_T = \begin{pmatrix} e_3 \times \left(\mathbf{D}_T^{-*}(d_{3T}\widehat{\mathbf{n}}_T[\widehat{\mathbf{u}}_T]_{KL})\right) \\ 0 \end{pmatrix}.$$

■

Theorem 5.4.1 (Weak formulation for the problem in $\widehat{\mathbf{E}}$)**.**

If $\mathbf{E}$ *is solution of* (5.6), $\widehat{\mathbf{E}}$ *given by* (5.18) *is solution to :*

Find $\widehat{\mathbf{E}}_{h_T}(\cdot,t) = \big(\widehat{\mathbf{E}}_{T,h_T}(\cdot,t), \widehat{E}_{3,h_T}(\cdot,t)\big) \in \widehat{\mathbf{V}}_{h_T}(\widehat{\Omega})$, *such that* $\forall\ \widetilde{\mathbf{E}}_{h_T} \in \widehat{\mathbf{V}}_{h_T}(\widehat{\Omega})$, *we have*

$$\frac{d^2}{dt^2}\,\widehat{\mathbf{m}}_g\big(\widehat{\mathbf{E}}_{h_T},\widetilde{\mathbf{E}}_{h_T}\big) + \widehat{\mathbf{k}}_g\big(\widehat{\mathbf{E}}_{h_T},\widetilde{\mathbf{E}}_{h_T}\big) + \widehat{\mathbf{j}}^d\big(\widehat{\mathbf{E}}_{h_T},\widetilde{\mathbf{E}}_{h_T}\big) = 0. \tag{5.124}$$

The bilinear forms $\widehat{\mathbf{m}}_g(\cdot,\cdot)$ *and* $\widehat{\mathbf{k}}_g(\cdot,\cdot)$ *are defined in* (5.114) *and* (5.115), *and* $\widehat{\mathbf{j}}^d$ *is defined as follows,*

$$\widehat{\mathbf{j}}^d\big(\widehat{\mathbf{E}},\widetilde{\mathbf{E}}\big) = \widehat{\mathbf{j}}^d_T\big(\widehat{\mathbf{E}}_T,\widetilde{\mathbf{E}}_T\big) + \widehat{\mathbf{r}}^d_T\big(\widehat{\mathbf{E}}_T,\widetilde{\mathbf{E}}_T\big) + \widehat{\mathbf{r}}^d_3\big(\widehat{\mathbf{E}}_T,\widetilde{\mathbf{E}}_T\big) + \widehat{r}^d_T\big(\widehat{\mathbf{E}}_T,\widetilde{E}_3\big) + \widehat{r}^d_T\big(\widetilde{\mathbf{E}}_T,\widehat{E}_3\big), \tag{5.125}$$

where

$$\begin{aligned}
\widehat{\mathbf{j}}^d_T\big(\widehat{\mathbf{E}}_T,\widetilde{\mathbf{E}}_T\big) &= \sum_{\widehat{\Sigma}_{KL}\in\widehat{\Sigma}_{\mathbf{h}}} \int_{\widehat{\Sigma}_{KL}} \widehat{a}\,|(DF^*)^{-1}\widehat{\mathbf{n}}|^{-1}\,\mathbf{A}_T\Big((d_{3T}\widehat{\mathbf{n}}_T[\widehat{\mathbf{E}}_T])\Big)\cdot\Big((d_{3T}\widehat{\mathbf{n}}_T[\widetilde{\mathbf{E}}_T])\Big)\,d\widehat{\sigma}\\
\widehat{\mathbf{r}}^d_T\big(\widehat{\mathbf{E}}_T,\widetilde{\mathbf{E}}_T\big) &= \sum_{\widehat{\Sigma}_{KL}\in\widehat{\Sigma}_{\mathbf{h}}} \int_{\widehat{\Sigma}_{KL}} |J_T|\,\Big(\mathbf{D}_T^{-*}(d_{3T}\widehat{\mathbf{n}}_T[\widehat{\mathbf{E}}_T])\Big)\cdot\Big(\{\widehat{\mu}^{-1}\,\boldsymbol{P}_T(\widehat{\mathbf{x}},\widehat{\nabla}_T)\,\widetilde{\mathbf{E}}_T\}\Big)\,d\widehat{\sigma}\\
&\quad + \int_{\widehat{\Sigma}_{KL}} |J_T|\,\Big(\mathbf{D}_T^{-*}(d_{3T}\widehat{\mathbf{n}}_T[\widetilde{\mathbf{E}}_T])\Big)\cdot\Big(\{\widehat{\mu}^{-1}\,\boldsymbol{P}_T(\widehat{\mathbf{x}},\widehat{\nabla}_T)\,\widehat{\mathbf{E}}_T\}\Big)\,d\widehat{\sigma}\\
\widehat{\mathbf{r}}^d_3\big(\widehat{\mathbf{E}}_T,\widetilde{\mathbf{E}}_T\big) &= -\sum_{\widehat{\Sigma}_{KL}\in\widehat{\Sigma}_{\mathbf{h}}} \int_{\widehat{\Sigma}_{KL}} |J_T|\,\Big(\mathbf{D}_T^{-*}(d_{3T}\widehat{\mathbf{n}}_T[\widehat{\mathbf{E}}_T])\Big)\cdot\Big(\{\widehat{\mu}^{-1}\,\mathbf{D}_T^{-*}\,\partial_3\widetilde{\mathbf{E}}_T\}\Big)\,d\widehat{\sigma}\\
&\quad + \int_{\widehat{\Sigma}_{KL}} |J_T|\,\Big(\mathbf{D}_T^{-*}(d_{3T}\widehat{\mathbf{n}}_T[\widetilde{\mathbf{E}}_T])\Big)\cdot\Big(\{\widehat{\mu}^{-1}\,\mathbf{D}_T^{-*}\,\partial_3\widehat{\mathbf{E}}_T\}\Big)\,d\widehat{\sigma}\\
\widehat{r}^d_T\big(\widehat{\mathbf{E}}_T,\widetilde{E}_3\big) &= \sum_{\widehat{\Sigma}_{KL}\in\widehat{\Sigma}_{\mathbf{h}}} \int_{\widehat{\Sigma}_{KL}} \mathbf{A}_T\,\Big((d_{3T}\widehat{\mathbf{n}}_T[\widehat{\mathbf{E}}_T])\Big)\cdot\Big(\{\widehat{\mu}^{-1}\widehat{\nabla}_T\widetilde{E}_3\}\Big)\,d\widehat{\sigma}.
\end{aligned} \tag{5.126}$$

Proof. The result of this theorem is a consequence of the expression for the bilinear jump term (5.116) and Lemma 5.4.2. ■

5.4.2 Full space discretization

For the longitudinal discretization, we consider the mesh $\widehat{\mathcal{T}}_h$, which is a partition of the reference domain $\widehat{\Omega}$. This partition is composed of cylindrical cells parametrized by h,

$$\widehat{\mathcal{T}}_h = \bigcup_{j\in\mathbb{Z}} \mathcal{C}_{j+\frac{1}{2}}, \tag{5.127}$$

where

$$\mathcal{C}_{j+\frac{1}{2}} = \{(\mathbf{x}_T,x_3)\in\Omega\ /\ jh\le x_3\le (j+1)h\},\quad j\in\mathbb{Z}. \tag{5.128}$$

These cells of size h in the x_3 direction (h is the longitudinal space step) are separated by transverse cross section $S_j, j\in\mathbb{Z}$ (see Figure 5.5) where, by definition

$$\forall\ \nu\in\mathbb{R},\quad \mathcal{S}_\nu = \{(\mathbf{x}_T,\nu h), \mathbf{x}_T\in S\}. \tag{5.129}$$

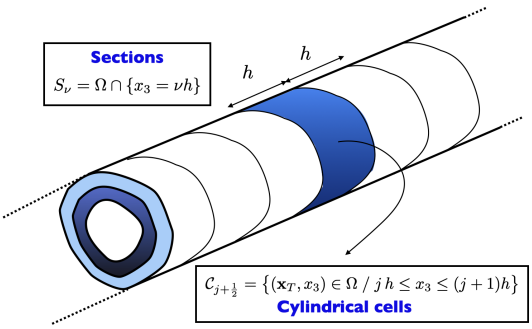

FIGURE 5.5 – Schematic of the sections and the cells of the cable $\widehat{\Omega}$.

Based upon the transverse discretization (5.71) and the longitudinal discretization (5.127), we introduce a 3D prismatic partition $\mathcal{T}_{3D}$ of the cable Ω,

$$\mathcal{T}_{3D} := \Big\{ P_{K,j} \;/\; K \in \mathcal{T}(\widehat{S}), j \in \mathbb{Z} \Big\}, \quad \text{such that } \Omega = \bigcup_{K,j} P_{K,j}, \tag{5.130}$$

where the prism $P_{K,j}$ is defined as (note that it has only longitudinal or transverse faces, cf. Figure 5.3)

$$P_{K,j} = K \times [jh, (j+1)h]. \tag{5.131}$$

As in Chapter 2, we shall use the letter $\mathbf{h}$ to denote the set of approximation parameters in space, namely

$$\mathbf{h} := (h, h_T). \tag{5.132}$$

The fully discrete space, indexed with $\mathbf{h}$ takes the following form,

$$\widehat{\mathbf{V}}_{\mathbf{h}} = \widehat{\mathbf{V}}_{\mathbf{h},T} \times \widehat{V}_{\mathbf{h},\ell},$$

where on the one hand, the transverse field $\widehat{\mathbf{E}}_{\mathbf{T}} \in \widehat{\mathbf{V}}_{\mathbf{h},\mathbf{T}}$ is searched piecewise linear continuous in x_3 with value in the 2D Discontinuous Nedelec space [41],[43].

$$\widehat{\mathbf{V}}_{\mathbf{h},T} := \Big\{ \widehat{\mathbf{E}}_{T,h} \in C^0\Big(\mathbb{R}; \widehat{\mathbf{V}}_{h_T}(\widehat{S})\Big) \;/\; \forall\, j,\; \widehat{\mathbf{E}}_T|_{\mathcal{C}_{j+\frac{1}{2}}} \in \mathbb{P}_1\Big(\mathbb{R}; \widehat{\mathbf{V}}_{h_T}(\widehat{S})\Big) \Big\}, \tag{5.133}$$

where $\widehat{\mathbf{V}}_{h_T}(\widehat{S})$ is defined in (5.118). In other words, for any $\widehat{\mathbf{E}}_T \in \widehat{\mathbf{V}}_{h,T}$, denoting $\widehat{\mathbf{E}}_{T,j} = \widehat{\mathbf{E}}_T|_{\widehat{S}_j} \in \widehat{\mathbf{V}}_{h_T}(\widehat{S})$, we have

$$\widehat{\mathbf{E}}_T(\mathbf{x}_T, x_3) = \sum_{j \in \mathbb{Z}} \widehat{\mathbf{E}}_{T,j}(\mathbf{x}_T)\, w_j(x_3), \tag{5.134}$$

where w_j is the usual hat function associated with $x_3 = jh$ (see Figure 5.6).

On the other hand, the longitudinal field $E_3 \in \widehat{V}_{\mathbf{h},\ell}$ is searched piecewise constant in x_3 with value in the standard $\mathbb{P}_1$ finite element space.

$$\widehat{V}_{\mathbf{h},\ell} := \Big\{ \widehat{E}_3 : \Omega \to \mathbb{R} \;/\; \forall\, j,\, \forall\, x_3 \in [jh, (j+1)h]\;\; \widehat{E}_3(\cdot, x_3) = E_{3,j+\frac{1}{2}} \in \widehat{V}_{h_T}(\widehat{S}) \Big\}, \tag{5.135}$$

with $\widehat{V}_{h_T}(\widehat{S})$ is defined in (5.118). In other words, for any $\widehat{E}_3 \in V_{h,\ell}$, there exists $\widehat{E}_{3,j+\frac{1}{2}} \in \widehat{V}_{h_T}(\widehat{S})$, $j \in \mathbb{Z}$ such that

$$\widehat{E}_3(\mathbf{x}_T, x_3) = \sum_{j \in \mathbb{Z}} \widehat{E}_{3,j+\frac{1}{2}}(\mathbf{x}_T)\, \chi_{j+\frac{1}{2}}(x_3), \quad \widehat{E}_{3,j+\frac{1}{2}} = \widehat{E}_3|_{\widehat{S}_{j+\frac{1}{2}}} \tag{5.136}$$

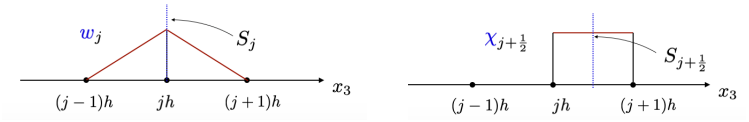

FIGURE 5.6 – The 1D basis functions w_j (left) and $\chi_{j+\frac{1}{2}}$ (right).

where $\chi_{j+\frac{1}{2}}$ is the characteristic function of the interval $[jh, (j+1)h]$ (see Figure 5.6).

We have thus two types of degrees of freedom for the discrete electric field. The first ones, associated to the transverse field, are denoted $\mathbb{E}_{T,\mathbf{h}} \equiv \left\{ \mathbb{E}_{T,j} \right\}$, $\mathbb{E}_{T,j} \in \mathbb{R}^{N_e}$, is the vector of the tangential components of the discrete transverse electric field along the edges in the cross section S_j.

The second ones, for the longitudinal field, are denoted $\mathbb{E}_{3,\mathbf{h}} \equiv \left\{ \mathbb{E}_{3,j+\frac{1}{2}} \right\}$, where $\mathbb{E}_{3,j+\frac{1}{2}} \in \mathbb{R}^N$ is the vector of the values of the discrete longitudinal field at the nodes of the mesh.

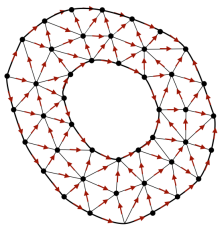

Transverse field in each section S_j

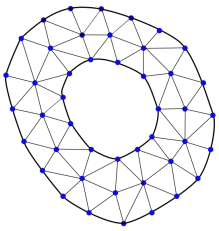

Longitudinal field in each section $S_{j+\frac{1}{2}}$

FIGURE 5.7 – Two types of degrees of freedom.

Reinterpretation as prismatic edge elements

It is worthwhile reinterpreting the space as the result of a 3D finite element approximation of $H(\mathbf{rot}, \Omega)$ based on a prismatic mesh $\mathcal{T}_{3D}$ of the cable Ω,

$$\mathcal{T}_{3D} := \left\{ P_{K,j} \ / \ K \in \mathcal{T}, j \in \mathbb{Z} \right\} \quad \text{such that } \Omega = \bigcup_{k,j} P_{K,j}, \tag{5.137}$$

where the prism $P_{K,j}$ is defined as (note that it has only longitudinal or transverse faces, cf. Figure 5.3)

$$P_{K,j} = K \times [jh, (j+1)h]. \tag{5.138}$$

The discrete scheme in space

The discrete problem in space is obtained essentially by rewriting the variational formulation (5.124) after replacing the semi-discrete space by full space $\widehat{\mathbf{V}}_{\mathbf{h}}$. More precisely, this problem reads,

Find $\widehat{\mathbf{E}}_{\mathbf{h}}(\cdot, t) = \left(\widehat{\mathbf{E}}_{T,\mathbf{h}}(\cdot, t), \widehat{E}_{3,\mathbf{h}}(\cdot, t) \right) \in \widehat{\mathbf{V}}_{\mathbf{h}}(\widehat{\Omega})$, such that $\forall\, \widetilde{\mathbf{E}}_{\mathbf{h}} \in \widehat{\mathbf{V}}_{\mathbf{h}}(\widehat{\Omega})$, we have

$$\frac{d^2}{dt^2} \widehat{\mathbf{m}}_g\left(\widehat{\mathbf{E}}_{\mathbf{h}}, \widetilde{\mathbf{E}}_{\mathbf{h}}\right) + \widehat{\mathbf{k}}_g\left(\widehat{\mathbf{E}}_{\mathbf{h}}, \widetilde{\mathbf{E}}_{\mathbf{h}}\right) + \widehat{\mathbf{j}}^d\left(\widehat{\mathbf{E}}_{\mathbf{h}}, \widetilde{\mathbf{E}}_{\mathbf{h}}\right) = 0. \tag{5.139}$$

For stability analysis reasons, we will rewrite the weak formulation (5.139) in $(\widehat{\mathbf{E}}_T, \widehat{E}_3)$.

Theorem 5.4.2 (Weak formulation for the problem in $(\widehat{\mathbf{E}}_T, \widehat{E}_3)$)**.**
If $(\mathbf{E}_T, E_3)$ *is solution of* (5.6), $\widehat{\mathbf{E}}$ *given by* (5.18) *is solution of :*

Find $\Big(\widehat{\mathbf{E}}_{T,\mathbf{h}}, \widehat{E}_{3,\mathbf{h}}\Big) \in \widehat{\mathbf{V}}_{\mathbf{h}} := \widehat{\mathbf{V}}_{\mathbf{h},T} \times \widehat{V}_{\mathbf{h},\ell}$ *such that for any* $\Big(\widehat{\mathbf{E}}_{T,\mathbf{h}}, \widehat{E}_{3,\mathbf{h}}\Big) \in \widehat{\mathbf{V}}_{\mathbf{h}}$,

$$\left\{\begin{array}{l} \dfrac{d^2}{dt^2}\,\widehat{\mathbf{m}}_h\Big(\widehat{\mathbf{E}}_{T,h}, \widetilde{\mathbf{E}}_{T,h}\Big) + \widehat{\mathbf{k}}_{T,h}\Big(\widehat{\mathbf{E}}_{T,h}, \widetilde{\mathbf{E}}_{T,h}\Big) + \widehat{\mathbf{k}}_3\Big(\widehat{\mathbf{E}}_{T,h}, \widetilde{\mathbf{E}}_{T,h}\Big) - \widehat{c}_{3T}\Big(\widehat{E}_{3,h}, \widetilde{\mathbf{E}}_{T,h}\Big) \\ \qquad\qquad + \widehat{\mathbf{k}}^d_{TT,h}\Big(\widehat{\mathbf{E}}_{T,h}, \widetilde{\mathbf{E}}_{T,h}\Big) - \widehat{\mathbf{k}}^d_{3T,h}\Big(\widehat{\mathbf{E}}_{T,h}, \widetilde{\mathbf{E}}_{T,h}\Big) + \widehat{c}^d_{TT,h}\Big(\widehat{E}_{3,h}, \widetilde{\mathbf{E}}_{T,h}\Big) \\ \qquad\qquad + \widehat{\mathbf{j}}^d_{T,h}\Big(\widehat{\mathbf{E}}_{T,h}, \widetilde{\mathbf{E}}_{T,h}\Big) + \widehat{\mathbf{r}}^d_{T,h}\Big(\widehat{\mathbf{E}}_{T,h}, \widetilde{\mathbf{E}}_{T,h}\Big) + \widehat{r}^d_{T,h}\Big(\widetilde{\mathbf{E}}_{T,h}, \widehat{E}_{3,h}\Big) = 0, \\ \dfrac{d^2}{dt^2}\,\widehat{m}\Big(\widehat{E}_{3,h}, \widetilde{E}_{3,h}\Big) + k_T\Big(\widehat{E}_{3,h}, \widetilde{E}_{3,h}\Big) - \widehat{c}_{3T}\Big(\widetilde{E}_{3,h}, \widehat{\mathbf{E}}_{T,h}\Big) \\ \qquad\qquad + \widehat{c}^d_{TT,h}\Big(\widetilde{E}_{3,h}, \widehat{\mathbf{E}}_{T,h}\Big) + \widehat{r}^d_{T,h}\Big(\widehat{\mathbf{E}}_{T,h}, \widetilde{E}_{3,h}\Big) = 0. \end{array}\right. \tag{5.140}$$

Apart from the functional spaces, there is another difference between (5.124) and (5.140) which makes our approximation non-conforming in the finite element sense. This ingredient is in fact very important for the efficiency of the method and to end up with numerical schemes, that will be explicit in x_3. More precisely, we approximate the two bilinear forms that involve transverse fields and do not involve x_3-derivatives, namely $\widehat{\mathbf{m}}$, $\widehat{\mathbf{k}}_T$ and $\widehat{\mathbf{k}}_d$, by using a quadrature formula in the x_3 direction, transforming them into $\widehat{\mathbf{m}}_h$, $\widehat{\mathbf{k}}_{T,h}$ and $\widehat{\mathbf{k}}_{d,h}$. More precisely, with respect to the definitions (5.53) (5.67) and (5.69) of the exact bilinear forms

$$\Big(\widehat{\mathbf{m}}, \widehat{\mathbf{k}}_T, \widehat{\mathbf{k}}_d\Big) \quad \longrightarrow \quad \Big(\widehat{\mathbf{m}}_h, \widehat{\mathbf{k}}_{T,h}, \widehat{\mathbf{k}}_{d,h}\Big) \quad \text{via} \quad \int_{\widehat{\Omega}} \varepsilon\, f \to \oint_{\widehat{\Omega}} \varepsilon\, f, \quad \int_{\widehat{\Omega}} \mu^{-1}\, f \to \oint_{\widehat{\Omega}} \mu^{-1}\, f, \tag{5.141}$$

where $\oint_{\widehat{\Omega}} \varepsilon\, f$ (resp. $\oint_{\widehat{\Omega}} \mu^{-1}\, f$) refers to a nodal quadrature formula in x_3, well adapted to the measure $\varepsilon\, d\mathbf{x}$ (resp. $\mu^{-1}\, d\mathbf{x}$). More precisely, for $f \in C^0\Big(\mathbb{R}; L^1(\widehat{S})\Big) \cap L^1\Big(\widehat{\Omega}\Big)$, we set

$$\oint_{\widehat{\Omega}} \varepsilon\, f = h \sum_j \int_{\widehat{S}} \varepsilon_{j+\frac{1}{2}} \left(\frac{f_{j+1} + f_j}{2}\right) d\mathbf{x}_T, \quad f_j = f|_{\widehat{S}_j}, \tag{5.142}$$

where $\varepsilon_{j+\frac{1}{2}}(\mathbf{x}_T)$ holds for the 1D mean value of ε in $C_{j+\frac{1}{2}}$,

$$\text{a.e. } \mathbf{x}_T \in \widehat{S}, \quad \varepsilon_{j+\frac{1}{2}}(\mathbf{x}_T) = \frac{1}{h} \int_{jh}^{(j+1)h} \varepsilon(\mathbf{x}_T, x_3)\, dx_3. \tag{5.143}$$

Remark 5.4.1. *One has the Fubini-like formula*

$$\oint_{\widehat{\Omega}} \varepsilon\, f = \int_{\widehat{S}} \Big(\oint_{\mathbb{R}} \varepsilon(\mathbf{x_T}, x_3)\, f(\mathbf{x_T}, x_3)\, dx_3 \Big) d\mathbf{x}_T, \tag{5.144}$$

with the 1D quadrature formula, for any $g \in L^1(\mathbb{R}) \cap C^0(\mathbb{R})$,

$$\oint_{\mathbb{R}} \varepsilon(\mathbf{x_T}, x_3)\, g(x_3)\, dx_3 := h \sum_j \varepsilon_{j+\frac{1}{2}}(\mathbf{x_T}) \Big(\frac{g((j+1)h) + g(jh)}{2}\Big). \tag{5.145}$$

Note that this formula can also be written

$$\oint_{\mathbb{R}} \varepsilon(\mathbf{x_T}, x_3)\, g(x_3)\, dx_3 := \int_{\mathbb{R}} \varepsilon_h(\mathbf{x_T}, x_3)\, \pi_{1,h} g(x_3)\, dx_3. \tag{5.146}$$

where ε_h is the piecewise constant approximation of ε with its mean value inside each interval $[jh,(j+1)h]$ and $\pi_{1,h}g$ is the $\mathbb{P}_1$-interpolate of g.

One has the fundamental property (1D mass lumping) about hat functions

$$\forall\, \ell \neq j, \quad \oint_{\mathbb{R}} \varepsilon(\mathbf{x_T}, x_3)\, w_j(x_3)\, w_\ell(x_3)\, dx_3 := 0. \tag{5.147}$$

Well-posedness

We denote the diameter of element $K \in \mathcal{T}(\widehat{S})$ by h_K, and the transverse mesh size h_T is given by

$$h_T = \min_{K\in\mathcal{T}(\widehat{S})} h_K.$$

We assume that the local mesh sizes are of bounded variation, that is, there is a positive constant c depending only on the shape-regularity of the mesh, such that for all neighboring elements K and L

$$c\, h_K \leq h_L \leq c^{-1}\, h_K, \tag{5.148}$$

To define the interior penalty function $\widehat{a} = a \circ F$ we first introduce

$$h_{|KL} := \begin{cases} \min\{h_K, h_L\}, & \text{if } \widehat{\Sigma}_{KL} \in \widehat{\Sigma}^i_{h_T}, \\ h_K, & \text{if } \widehat{\Sigma}_{KL} \in \widehat{\Sigma}^b_{h_T}. \end{cases}$$

$$\widehat{\mu}_{|KL} = \begin{cases} \min\{\widehat{\mu}_K, \widehat{\mu}_L\}, & \text{if } \widehat{\Sigma}_{KL} \in \widehat{\Sigma}^i_{h_T}, \\ \widehat{\mu}_K, & \text{if } \widehat{\Sigma}_{KL} \in \widehat{\Sigma}^b_{h_T}, \end{cases}$$

with, $\widehat{\mu}_K$ is the restriction of the coefficient $\widehat{\mu}$ to element $\widehat{P}_K$, we then set

$$\widehat{a}_{|\Sigma_{KL}} = \kappa\, \widehat{\mu}^{-1}_{|KL}\, h^{-1}_{|KL},$$

where $\kappa > 0$ is chosen sufficiently large, independently of the mesh size and $\widehat{\mu}$.

To discuss the well-posedness of (5.140), we introduce the semi-norm

$$\begin{aligned} |\mathbf{u}|^2_{\mathbf{h}} \;:=\; & \sum_{K\in\mathcal{T}(\widehat{S})} \| \left(\widehat{\mu}^{-1}\,|J_T|\right)^{\frac{1}{2}} \left(J_T^{-1}\, \mathbf{D}\left(\widehat{\boldsymbol{\nabla}} \times \widehat{\mathbf{u}}\right) - \mathbf{P}(\widehat{\mathbf{x}}, \widehat{\nabla}_T)\widehat{\mathbf{u}} \right) \|^2_{0,K} \\ & + \sum_{\widehat{\Sigma}_{KL}\in\widehat{\Sigma}} \| \left(\widehat{a}\,|J_T|\,|(DF^*)^{-1}\widehat{\mathbf{n}}|^{-1}\right)^{\frac{1}{2}} [[\widehat{\mathbf{u}}]]_{KL} \|_{\widehat{\Sigma}_{KL}}. \end{aligned} \tag{5.149}$$

Lemma 5.4.1 (Well-posedness)**.**
Set $\kappa_{min} = 4\, C^2_{inv}$, with C^2_{inv} denoting a constant that only depends on the shap-regularity of the mesh. So if we denote

$$\widehat{a}(\mathbf{u},\mathbf{v}) := \widehat{\mathbf{k}}_g(\mathbf{u},\mathbf{v}) + \widehat{\mathbf{j}}^d(\mathbf{u},\mathbf{v}), \qquad \mathbf{u},\mathbf{v} \in \widehat{\mathbf{V}}_{\mathbf{h}},$$

and we suppose that $\kappa \geq \kappa_{min}$, we get

$$|\widehat{a}(\mathbf{u},\mathbf{v})| \leq \sqrt{2}\,|\mathbf{u}|_{\mathbf{h}}|\mathbf{v}|_{\mathbf{h}}, \qquad |\widehat{a}(\mathbf{u},\mathbf{u})| \geq \frac{1}{2}\,|\mathbf{u}|^2_{\mathbf{h}}, \qquad \mathbf{u},\mathbf{v} \in \widehat{\mathbf{V}}_{\mathbf{h}}. \tag{5.150}$$

Proof. The proof is similar to the proof of Lemma 5 found in Grote et al., 2007 [26]. ■

The algebraic form

To write the problem in a more algebraic form, we introduce here the vector degrees of freedom namely (with obvious notation)

$$\mathbb{E}_{\mathbf{h}} = \begin{pmatrix} \mathbb{E}_{T,\mathbf{h}} \\ \mathbb{E}_{3,\mathbf{h}} \end{pmatrix} \equiv \begin{pmatrix} \mathbb{E}_{T,j} \\ \mathbb{E}_{3,j+\frac{1}{2}} \end{pmatrix} \in \mathbb{V}_{\mathbf{h}} := \mathbb{V}_{\mathbf{h},T} \times \mathbb{V}_{\mathbf{h},3}, \tag{5.151}$$

where $\mathbb{V}_{\mathbf{h},T}$ and $\mathbb{V}_{\mathbf{h},3}$ are the Hilbert spaces

$$\mathbb{V}_{\mathbf{h},T} = \ell^2\big(\mathbb{Z}, \mathbb{R}^{N_e}\big), \quad \mathbb{V}_{\mathbf{h},3} = \ell^2(\mathbb{Z}, \mathbb{R}^N).$$

According to the above, it is clear that (5.139) has an equivalent algebraic form,

$$\mathbf{M}_{\mathbf{h}} \frac{d^2 \mathbb{E}_{\mathbf{h}}}{dt^2} + \mathbf{K}_{\mathbf{h}}\, \mathbb{E}_{\mathbf{h}} = 0, \tag{5.152}$$

where $\mathbf{M}_{\mathbf{h}}$ and $\mathbf{K}_{\mathbf{h}}$ are the mass and stiffness matrices in $\mathbb{V}_{\mathbf{h}}$ (their obvious and classical definition is omitted here). According to the decomposition of $\mathbf{V}_{\mathbf{h}}$ between transverse and longitudinal fields, the mass matrix $\mathbf{M}_{\mathbf{h}}$ has the following block diagonal form

$$\mathbf{M}_{\mathbf{h}} = \begin{pmatrix} \mathbf{M}^T_{\mathbf{h}} & 0 \\ 0 & M^3_{\mathbf{h}} \end{pmatrix}, \tag{5.153}$$

and, in particular, thanks to numerical quadrature, $\mathbf{M}^T_{\mathbf{h}}$ (resp. $\mathbf{M}^3_{\mathbf{h}}$) is block diagonal by sections with blocks of dimension N_e (resp. N). On the other hand, the stiffness matrix $\mathbf{K}_{\mathbf{h}}$ can be written, according (5.140) as

$$\mathbf{K}_{\mathbf{h}} = \begin{pmatrix} \mathbf{K}_{3,\mathbf{h}} + \mathbf{K}_{T,\mathbf{h}} + \mathbf{K}^d_{TT,\mathbf{h}} - \mathbf{K}^d_{3T,\mathbf{h}} + \mathbf{J}^d_{T,\mathbf{h}} + \mathbf{R}^d_{T,\mathbf{h}} + \mathbf{R}^d_{3,\mathbf{h}} & -\mathbf{C}_{3T,\mathbf{h}} + \mathbf{C}^d_{TT,\mathbf{h}} + R^d_{T,\mathbf{h}} \\ -(\mathbf{C}_{3T,\mathbf{h}})^* + (\mathbf{C}^d_{TT,\mathbf{h}})^* + (R^d_{T,\mathbf{h}})^* & K_{T,\mathbf{h}} \end{pmatrix}. \tag{5.154}$$

5.5 Time discretization

Our method will be based on a tricky decomposition of the stiffness matrix $\mathbf{K}_{\mathbf{h}}$ (cf. (5.154)) into two symmetric matrices,

$$\mathbf{K}_{\mathbf{h}} = \mathbf{K}^i_{\mathbf{h}} + \mathbf{K}^e_{\mathbf{h}}, \tag{5.155}$$

where $\mathbf{K}^i_{\mathbf{h}} = \begin{pmatrix} \mathbf{K}_{T,\mathbf{h}} + \mathbf{K}^d_{TT,\mathbf{h}} + \mathbf{J}^d_{T,\mathbf{h}} + \mathbf{R}^d_{T,\mathbf{h}} & \mathbf{C}^d_{TT,\mathbf{h}} \\ (\mathbf{C}^d_{TT,\mathbf{h}})^* & K_{T,\mathbf{h}} \end{pmatrix}$,

and $\mathbf{K}^e_{\mathbf{h}} = \begin{pmatrix} \mathbf{K}_{3,\mathbf{h}} - \mathbf{K}^d_{3T,\mathbf{h}} + \mathbf{R}^d_{3,\mathbf{h}} & -\mathbf{C}_{3T,\mathbf{h}} + R^d_{T,\mathbf{h}} \\ -(\mathbf{C}_{3T,\mathbf{h}})^* + (R^d_{T,\mathbf{h}})^* & 0 \end{pmatrix}$.

The matrix $\mathbf{K}^i_{\mathbf{h}}$ can be also decomposed into two symmetric matrices

$$\mathbf{K}^i_{\mathbf{h}} = \mathbf{K}^{id}_{\mathbf{h}} + \mathbf{K}^{ic}_{\mathbf{h}},$$

where

$$\mathbf{K}^{id}_{\mathbf{h}} = \begin{pmatrix} \mathbf{K}_{T,\mathbf{h}} + \mathbf{K}^d_{TT,\mathbf{h}} + \mathbf{J}^d_{T,\mathbf{h}} + \mathbf{R}^d_{T,\mathbf{h}} & 0 \\ 0 & K_{T,\mathbf{h}} \end{pmatrix},$$

and

$$\mathbf{K}_{\mathbf{h}}^{ic} = \begin{pmatrix} 0 & \mathbf{C}_{TT,\mathbf{h}}^{d} \\ (\mathbf{C}_{TT,\mathbf{h}}^{d})^{*} & 0 \end{pmatrix}.$$

The interest of the decomposition lies in the following double observation

— $\mathbf{K}_{\mathbf{h}}^{id}$ is adapted to implicit time discretization because the matrix is positive and block diagonal, for this reason it is "easy" to invert (it corresponds to a series 2D problems).

— Oppositely $\mathbf{K}_{\mathbf{h}}^{e}$ and $\mathbf{K}_{\mathbf{h}}^{ic}$ are adapted to explicit time discretization because of the presence of the "3" index that corresponds to the x_3 derivative, these matrices couples all the interfaces and has no sign.

The matrix $\mathbf{K}_{\mathbf{h}}^{e}$ can be also decomposed into two symmetric matrices

$$\mathbf{K}_{\mathbf{h}}^{e} = \mathbf{K}_{\mathbf{h}}^{e,+} + \mathbf{R}_{\mathbf{h}}^{e},$$

where

$$\mathbf{K}_{\mathbf{h}}^{e,+} = \begin{pmatrix} \mathbf{K}_{3,\mathbf{h}} & 0 \\ 0 & 0 \end{pmatrix} \quad \text{and} \quad \mathbf{R}_{\mathbf{h}}^{e} = \begin{pmatrix} -\mathbf{K}_{3T,\mathbf{h}}^{d} + \mathbf{R}_{3,\mathbf{h}}^{d} & -\mathbf{C}_{3T,\mathbf{h}} + \mathbf{C}_{TT,\mathbf{h}}^{d} + R_{T,\mathbf{h}}^{d} \\ -(\mathbf{C}_{3T,\mathbf{h}})^{*} + (\mathbf{C}_{TT,\mathbf{h}}^{d})^{*} + (R_{T,\mathbf{h}}^{d})^{*} & 0 \end{pmatrix}.$$

This decomposition lies in the following double observation

— $\mathbf{K}_{\mathbf{h}}^{e,+}$ is is positive.

— Oppositely $\mathbf{R}_{\mathbf{h}}^{e}$ has no sign.

This choice of decomposition of these matrices is a reasonable choice. It is well chosen to study the stability of our 3D problem. To do this, we introduce the following two definitions :

Definition 5.5.1. *For* $\widehat{\mathbf{E}} = (\widehat{\mathbf{E}}_T, \widehat{E}_3) \in \widehat{\mathbf{V}}_{\mathbf{h}}$ *we define the following differential operator*

$$\mathbf{G}(\widehat{\mathbf{E}}) := \begin{pmatrix} \mathbf{G}_1(\widehat{\mathbf{E}}) \\ \mathbf{G}_2(\widehat{\mathbf{E}}) \\ \mathbf{G}_3(\widehat{\mathbf{E}}) \end{pmatrix} := \begin{pmatrix} \mathbf{D}_T^{-*}(d_{3T}\widehat{\mathbf{n}}_T[\widehat{\mathbf{E}}_T]_{KL}) \\ \left\{\mu^{-1}\,\boldsymbol{D}_T^{-*}\left(\partial_3\widehat{\mathbf{E}}_T - \widehat{\nabla}_T\widehat{E}_3\right) - \mu^{-1}\,\boldsymbol{P}_T(\widehat{\mathbf{x}},\widehat{\nabla}_T)\,\widehat{\mathbf{E}}_T\right\}_{KL} \\ \begin{pmatrix} \mu^{-\frac{1}{2}}\,\boldsymbol{D}_T^{-*}\left(\partial_3\widehat{\mathbf{E}}_T - \widehat{\nabla}_T\widehat{E}_3\right) - \mu^{-\frac{1}{2}}\,\boldsymbol{P}_T(\widehat{\mathbf{x}},\widehat{\nabla}_T)\,\widehat{\mathbf{E}}_T \\ \mu^{-\frac{1}{2}}\,\widehat{\mathrm{rot}}_T\,\widehat{\mathbf{E}}_T \end{pmatrix} \end{pmatrix}.$$

The operator $\mathbf{G}$ *can decompose in two operators* $\mathbf{G}^i$ *and* $\mathbf{G}^e$ *such that,*

$$\mathbf{G}(\widehat{\mathbf{E}}) = \mathbf{G}^i(\widehat{\mathbf{E}}) + \mathbf{G}^e(\widehat{\mathbf{E}}),$$

where

$$\mathbf{G}^i(\widehat{\mathbf{E}}) := \begin{pmatrix} \mathbf{D}_T^{-*}(d_{3T}\widehat{\mathbf{n}}_T[\widehat{\mathbf{E}}_T]_{KL}) \\ -\left\{\mu^{-1}\,\boldsymbol{P}_T(\widehat{\mathbf{x}},\widehat{\nabla}_T)\,\widehat{\mathbf{E}}_T\right\}_{KL} \\ \begin{pmatrix} -\mu^{-\frac{1}{2}}\,\boldsymbol{D}_T^{-*}\,\widehat{\nabla}_T\widehat{E}_3 - \mu^{-\frac{1}{2}}\,\boldsymbol{P}_T(\widehat{\mathbf{x}},\widehat{\nabla}_T)\,\widehat{\mathbf{E}}_T \end{pmatrix} \\ \mu^{-\frac{1}{2}}\,\widehat{\mathrm{rot}}_T\,\widehat{\mathbf{E}}_T \end{pmatrix},$$

$$\mathbf{G}^e(\widehat{\mathbf{E}}) := \begin{pmatrix} 0 \\ -\left\{\mu^{-1}\,\boldsymbol{D}_T^{-*}\,\widehat{\nabla}_T\widehat{E}_3\right\}_{KL} + \left\{\mu^{-1}\,\boldsymbol{D}_T^{-*}\,\partial_3\widehat{\mathbf{E}}_T\right\}_{KL} \\ \begin{pmatrix} \mu^{-\frac{1}{2}}\,\boldsymbol{D}_T^{-*}\,\partial_3\widehat{\mathbf{E}}_T \end{pmatrix} \\ 0 \end{pmatrix}.$$

Definition 5.5.2. *we define the following scalar product for all* $\widehat{\mathbf{E}} = (\widehat{\mathbf{E}}_T, \widehat{E}_3) \in \widehat{\mathbf{V}}_\mathbf{h}$ *and* $\widetilde{\mathbf{E}} = (\widetilde{\mathbf{E}}_T, \widetilde{E}_3) \in \widehat{\mathbf{V}}_\mathbf{h}$

$$\begin{aligned}\Big(\mathbf{G}(\widehat{\mathbf{E}}),\mathbf{G}(\widetilde{\mathbf{E}})\Big)_g \;:=& \sum_{\widehat{\Sigma}_{KL}\in\widehat{\Sigma}_\mathbf{h}} \int_{\widehat{\Sigma}_{KL}} \widehat{a}\,|J_T|\,|(DF^*)^{-1}\widehat{\mathbf{n}}|^{-1}\,\mathbf{G}_1(\widehat{\mathbf{E}})\cdot\mathbf{G}_1(\widetilde{\mathbf{E}})\,d\widehat{\sigma} \\ &- \sum_{\widehat{\Sigma}_{KL}\in\widehat{\Sigma}_\mathbf{h}} \int_{\widehat{\Sigma}_{KL}} |J_T|\,\mathbf{G}_1(\widehat{\mathbf{E}})\cdot\mathbf{G}_2(\widetilde{\mathbf{E}})\,d\widehat{\sigma} \\ &- \sum_{\widehat{\Sigma}_{KL}\in\widehat{\Sigma}_\mathbf{h}} \int_{\widetilde{\Sigma}_{KL}} |J_T|\,\mathbf{G}_1(\widetilde{\mathbf{E}})\cdot\mathbf{G}_2(\widehat{\mathbf{E}})\,d\widehat{\sigma} + \sum_{K\in\mathcal{T}_{h_T}} \int_{\widehat{P}_K} |J_T|\,\mathbf{G}_3(\widehat{\mathbf{E}})\cdot\mathbf{G}_3(\widetilde{\mathbf{E}})\,d\widehat{\sigma},\end{aligned}$$

where $g = L^2(\widehat{\Sigma}_{h_T})^2 \times L^2(\widehat{\Sigma}_{h_T})^2 \times L^2(\Omega)^3$.

Using Definition 5.5.2, we have the following lemma,

Lemma 5.5.1. *For all* $\widehat{\mathbf{E}} = (\widehat{\mathbf{E}}_T, \widehat{E}_3) \in \widehat{\mathbf{V}}_\mathbf{h}$ *and* $\widetilde{\mathbf{E}} = (\widetilde{\mathbf{E}}_T, \widetilde{E}_3) \in \widehat{\mathbf{V}}_\mathbf{h}$, *we have*

$$\Big(\mathbf{G}(\widehat{\mathbf{E}}),\mathbf{G}(\widetilde{\mathbf{E}})\Big)_g = \widehat{\mathbf{k}}_g\Big(\widehat{\mathbf{E}}_\mathbf{h},\widetilde{\mathbf{E}}_\mathbf{h}\Big) + \widehat{\mathbf{j}}^d\Big(\widehat{\mathbf{E}}_\mathbf{h},\widetilde{\mathbf{E}}_\mathbf{h}\Big).$$

Remark 5.5.1.
Let $\mathbf{U}_h \in \mathbf{V}_h$ *associated to the vector* $\mathbb{U}_\mathbf{h} \in \mathbb{V}_\mathbf{h}$, *by definition of* $\mathbf{K}_\mathbf{h}^i$ *and* $\mathbf{K}_\mathbf{h}^e$

$$\Big(\mathbf{K}_\mathbf{h}^i\mathbb{U}_\mathbf{h},\mathbb{U}_\mathbf{h}\Big) = \Big(\mathbf{G}^i(\mathbf{U}_h),\mathbf{G}^i(\mathbf{U}_h)\Big)_g.$$

$$\Big(\mathbf{K}_\mathbf{h}^{e,+}\mathbb{U}_\mathbf{h},\mathbb{U}_\mathbf{h}\Big) = \Big(\mathbf{G}^e(\mathbf{U}_h),\mathbf{G}^e(\mathbf{U}_h)\Big)_g.$$

$$\Big(\mathbf{K}_\mathbf{h}^e\mathbb{U}_\mathbf{h},\mathbb{U}_\mathbf{h}\Big) = \Big(\mathbf{G}^e(\mathbf{U}_h),\mathbf{G}^e(\mathbf{U}_h)\Big)_g + 2\,\Big(\mathbf{G}^i(\mathbf{U}_h),\mathbf{G}^e(\mathbf{U}_h)\Big)_g.$$

The Remark 5.5.1 is very important because it allows to prove the following lemma,

Lemma 5.5.2. *For* $\mathbb{U}_\mathbf{h} \in \mathbb{V}_\mathbf{h}$ *the quadratic form associated with* $\mathbf{K}_\mathbf{h}^e$ *can be estimated thanks to the Young's inequality*

$$\Big(\mathbf{K}_\mathbf{h}^e\mathbb{U}_\mathbf{h},\mathbb{U}_\mathbf{h}\Big) \le (1+\frac{1}{\alpha})\,\Big(\mathbf{K}_\mathbf{h}^{e,+}\mathbb{U}_\mathbf{h},\mathbb{U}_\mathbf{h}\Big) + \alpha\,\Big(\mathbf{K}_\mathbf{h}^i\mathbb{U}_\mathbf{h},\mathbb{U}_\mathbf{h}\Big),$$

with $\alpha > 0$ *is a parameter.*

Proof. Let $\mathbf{U}_h \in \mathbf{V}_h$ associated to the vector $\mathbb{U}_\mathbf{h} \in \mathbb{V}_\mathbf{h}$, we have

$$\Big(\mathbf{K}^e_\mathbf{h}\mathbb{U}_\mathbf{h}, \mathbb{U}_\mathbf{h}\Big) = \Big(\mathbf{G}^e(\mathbf{U}_h), \mathbf{G}^e(\mathbf{U}_h)\Big)_g + 2\Big(\mathbf{G}^i(\mathbf{U}_h), \mathbf{G}^e(\mathbf{U}_h)\Big)_g.$$

Now using the Young's inequality we get the following bound

$$2\Big(\mathbf{G}^i(\mathbf{U}_h), \mathbf{G}^e(\mathbf{U}_h)\Big)_g \leq \frac{1}{\alpha}\Big(\mathbf{G}^e(\mathbf{U}_h), \mathbf{G}^e(\mathbf{U}_h)\Big)_g + \alpha\Big(\mathbf{G}^i(\mathbf{U}_h), \mathbf{G}^i(\mathbf{U}_h)\Big)_g,$$

with $\alpha > 0$ is a parameter. As a consequence

$$\Big(\mathbf{K}^e_\mathbf{h}\mathbb{U}_\mathbf{h}, \mathbb{U}_\mathbf{h}\Big) \leq (1+\frac{1}{\alpha})\Big(\mathbf{G}^e(\mathbf{U}_h), \mathbf{G}^e(\mathbf{U}_h)\Big)_g + \alpha\Big(\mathbf{G}^i(\mathbf{U}_h), \mathbf{G}^i(\mathbf{U}_h)\Big)_g.$$

Finally using the Remark 5.5.1 we get

$$\Big(\mathbf{K}^e_\mathbf{h}\mathbb{U}_\mathbf{h}, \mathbb{U}_\mathbf{h}\Big) \leq (1+\frac{1}{\alpha})\Big(\mathbf{K}^{e,+}_\mathbf{h}\mathbb{U}_\mathbf{h}, \mathbb{U}_\mathbf{h}\Big) + \alpha\Big(\mathbf{K}^i_\mathbf{h}\mathbb{U}_\mathbf{h}, \mathbb{U}_\mathbf{h}\Big).$$

■

A hybrid implicit-explicit scheme

According to $\mathbf{K}_\mathbf{h}$-decomposition (5.155), we rewrite (5.152) as

$$\mathbf{M}_\mathbf{h}\frac{d^2\mathbb{E}_\mathbf{h}}{dt^2} + \mathbf{K}^e_\mathbf{h}\,\mathbb{E}_\mathbf{h} + \mathbf{K}^i_\mathbf{h}\,\mathbb{E}_\mathbf{h} = 0.$$

and propose a numerical scheme in which $\mathbb{E}_\mathbf{h}$ at time $t^n = n\Delta t$ is approximated differently depending on the fact that it is $\mathbf{K}^e_\mathbf{h}$, $\mathbf{K}^{ic}_\mathbf{h}$ or $\mathbf{K}^{id}_\mathbf{h}$. More precisely, and according to what we said in the introduction of this section, we propose the following hybrid implicit-explicit leap frog scheme (see Chapter 2, in which $\theta \in [0,1]$ is a parameter,

$$\mathbf{M}_\mathbf{h}\frac{\mathbb{E}^{n+1}_\mathbf{h} - 2\,\mathbb{E}^n_\mathbf{h} + \mathbb{E}^{n-1}_\mathbf{h}}{\Delta t^2} + \mathbf{K}^{id}_\mathbf{h}\,\{\mathbb{E}^n_\mathbf{h}\}_\theta + (\mathbf{K}^e_\mathbf{h} + \mathbf{K}^{ic}_\mathbf{h})\,\mathbb{E}^n_\mathbf{h} = 0, \tag{5.156}$$

where $\{\mathbb{E}^n_\mathbf{h}\}_\theta$ corresponds to the weighted mean value

$$\{\mathbb{E}^n_\mathbf{h}\}_\theta := \theta\,\mathbb{E}^{n+1}_\mathbf{h} + (1-2\theta)\,\mathbb{E}^n_\mathbf{h} + \theta\,\mathbb{E}^{n-1}_\mathbf{h}, \quad \theta \in [0,1]. \tag{5.157}$$

Clearly, this scheme is a mix between the explicit leap frog scheme and the implicit θ-scheme (or centered Newmark scheme). It is obviously second order accurate in Δt whatever is θ.

Stability analysis

For our main theorem, we need to introduce the function $\widehat{\alpha}_h(\mathbf{x}_T)$ defined by :

$$\|\widehat{\alpha}_h\|^2_\infty := \sup_{\mathbf{u}_h \in \mathbb{P}_{1,h}} \frac{\displaystyle\int_\mathbb{R} \widehat{\mu}(\cdot, x_T)^{-1}\Big(\mathbf{A}_T(\cdot, x_T)\mathbf{u}'_h \cdot \mathbf{u}'_h\Big)}{\displaystyle\oint_\mathbb{R} \widehat{\varepsilon}(\cdot, x_T)\,\Big(\mathbf{A}_T(\cdot, x_T)\mathbf{u}_h \cdot \mathbf{u}_h\Big)}, \tag{5.158}$$

where

$$\mathbb{P}_{1,h} := \{\mathbf{u}_h \in \Big(C^0(\mathbb{R}) \cap L^2(\mathbb{R})\Big)^2 \,/\, \forall\, j \in \mathbb{Z},\, \mathbf{u}_h|_{[jh,(j+1)h]} \in \mathbb{P}_1 \times \mathbb{P}_1\}. \tag{5.159}$$

It is also useful to introduce the velocity of electromagnetic waves in $\widehat{\Omega}$

$$\forall\, \widehat{\mathbf{x}} \in \widehat{\Omega}, \quad \widehat{c}(\widehat{\mathbf{x}}) = \widehat{\varepsilon}(\widehat{\mathbf{x}})^{-\frac{1}{2}}\widehat{\mu}(\widehat{\mathbf{x}})^{-\frac{1}{2}}, \quad \widehat{c}^+ := \sup_{\widehat{\Omega}} \widehat{c}(\widehat{\mathbf{x}}). \tag{5.160}$$

Theorem 5.5.1. *The fully discrete scheme* (5.156) *is stable if* $\theta > \dfrac{1}{2}$ *and*

$$\frac{\Delta t^2}{4}\,\|\widehat{\alpha}_h\|_\infty^2 \le \frac{2\,\theta+1}{2\,\theta-1}. \tag{5.161}$$

with $\widehat{\alpha}_h$ *defined in* (5.158).

The proof of this theorem is very similar to that of Theorem 2.6.1 in Chapter 2.

Proof. Since there is no possible ambiguity, and for the sake of simplicity, we shall use the same notation $\big(\cdot,\cdot\big)$ for inner products in $\mathbb{V}_{\mathbf{h},T}$ and $\mathbb{V}_{\mathbf{h},3}$. Below, we refer to (5.151) and the dot is systematically used for the appropriate Euclidean scalar product that may change from one occurrence to the other,

$$\begin{gathered}\big(\mathbb{U}_{\mathbf{h},T},\widetilde{\mathbb{U}}_{\mathbf{h},T}\big) := \sum_{j\in\mathbb{Z}} \mathbb{U}_{T,j}\cdot\widetilde{\mathbb{U}}_{T,j}, \quad \big(\mathbb{U}_{\mathbf{h},3},\widetilde{\mathbb{U}}_{\mathbf{h},3}\big) := \sum_{j\in\mathbb{Z}} \mathbb{U}_{3,j+\frac12}\cdot\widetilde{\mathbb{U}}_{3,j+\frac12},\\ \big(\mathbb{U}_{\mathbf{h}},\widetilde{\mathbb{U}}_{\mathbf{h}}\big) = \big(\mathbb{U}_{\mathbf{h},T},\widetilde{\mathbb{U}}_{\mathbf{h},T}\big) + \big(\mathbb{U}_{\mathbf{h},3},\widetilde{\mathbb{U}}_{\mathbf{h},3}\big).\end{gathered} \tag{5.162}$$

The proof is done in two steps using an energy approach.

Step 1 : Discrete energy conservation.

We use the two key (but standard) identities :

$$\mathbb{E}_{\mathbf{h}}^n = \{\mathbb{E}_{\mathbf{h}}^n\}_{\frac14} - \frac14\big(\mathbb{E}_{\mathbf{h}}^{n+1} - 2\,\mathbb{E}_{\mathbf{h}}^n + \mathbb{E}_{\mathbf{h}}^{n-1}\big), \quad \{\mathbb{E}_{\mathbf{h}}^n\}_\theta = \{\mathbb{E}_{\mathbf{h}}^n\}_{\frac14} + \Big(\theta-\frac14\Big)\big(\mathbb{E}_{\mathbf{h}}^{n+1} - 2\,\mathbb{E}_{\mathbf{h}}^n + \mathbb{E}_{\mathbf{h}}^{n-1}\big).$$

This allows us to rewrite our scheme as a perturbation of the $\dfrac14$-scheme.

$$\mathbf{M}_h(\Delta t)\,\frac{\mathbb{E}_{\mathbf{h}}^{n+1} - 2\,\mathbb{E}_{\mathbf{h}}^n + \mathbb{E}_{\mathbf{h}}^{n-1}}{\Delta t^2} + \mathbf{K}_{\mathbf{h}}\,\{\mathbb{E}_{\mathbf{h}}^n\}_{\frac14} = 0,$$

where we have set

$$\mathbf{M}_{\mathbf{h}}(\Delta t) = \mathbf{M}_h^i(\Delta t) - \frac{\Delta t^2}{4}\,(\mathbf{K}_{\mathbf{h}}^e + \mathbf{K}_{\mathbf{h}}^{ic}) \quad \text{and} \quad \mathbf{M}_h^i(\Delta t) := \mathbf{M}_{\mathbf{h}} + \Big(\theta-\frac14\Big)\,\Delta t^2\,\mathbf{K}_{\mathbf{h}}^{id}. \tag{5.163}$$

Taking the scalar product (in $\mathbb{V}_{\mathbf{h}} := \mathbb{V}_{\mathbf{h},T}\times\mathbb{V}_{\mathbf{h},3}$) of the above equation with $(\mathbb{E}_{\mathbf{h}}^{n+1} - \mathbb{E}_{\mathbf{h}}^n)/\Delta t$ we classically deduce –thanks to the symmetry of all matrices– the conservation of the discrete energy

$$\mathcal{E}_{\mathbf{h}}^{n+\frac12} := \left(\mathbf{M}_{\mathbf{h}}(\Delta t)\frac{\mathbb{E}_{\mathbf{h}}^{n+1} - \mathbb{E}_{\mathbf{h}}^n}{\Delta t}, \frac{\mathbb{E}_{\mathbf{h}}^{n+1} - \mathbb{E}_{\mathbf{h}}^n}{\Delta t}\right) + \left(\mathbf{K}_{\mathbf{h}}\Big(\frac{\mathbb{E}_{\mathbf{h}}^{n+1} + \mathbb{E}_{\mathbf{h}}^n}{2}\Big), \frac{\mathbb{E}_{\mathbf{h}}^{n+1} + \mathbb{E}_{\mathbf{h}}^n}{2}\right).$$

Step 2 : Derivation of the sufficient stability condition (5.161).

This will be simply obtained showing the positivity of the discrete energy $\mathcal{E}_{\mathbf{h}}^{n+\frac12}$ when the condition (5.5.1) holds, this amounts to the positivity of the modified mass matrix $\mathbf{M}_h(\Delta t)$. The idea is first to ensure the positivity of $\mathbf{M}_{\mathbf{h}}^i(\Delta t)$ only choosing adequately θ –typically $\theta > 1/4$– then to control $\Delta t^2\,(\mathbf{K}_{\mathbf{h}}^e + \mathbf{K}_{\mathbf{h}}^{ic})$ by choosing adequately Δt. As we are going to see this can be done by imposing to Δt a lower bound that only sees the longitudinal space step h.

To be more precise, we first obtain a lower bound of the quadratic form associated with $\mathbf{K}^e_{\mathbf{h}}$, using the Lemma 5.5.2 we get

$$\Big(\mathbf{K}^e_{\mathbf{h}}\mathbb{U}_{\mathbf{h}},\mathbb{U}_{\mathbf{h}}\Big) \leq (1+\frac{1}{\alpha})\,\Big(\mathbf{K}^{e,+}_{\mathbf{h}}\mathbb{U}_{\mathbf{h}},\mathbb{U}_{\mathbf{h}}\Big) + \alpha\,\Big(\mathbf{K}^{i}_{\mathbf{h}}\mathbb{U}_{\mathbf{h}},\mathbb{U}_{\mathbf{h}}\Big), \quad \text{with} \quad \alpha>0$$

Thus, we can write the following bound of the quadratic form associated with $\mathbf{M}_h(\Delta t)$,

$$\begin{aligned}\Big(\mathbf{M}_h(\Delta t)\mathbb{U}_{\mathbf{h}},\mathbb{U}_{\mathbf{h}}\Big) \geq \Big((\mathbf{M}_{\mathbf{h}} - \frac{\Delta t^2}{4}(1+\frac{1}{\alpha})\,\mathbf{K}^{e,+}_{\mathbf{h}}\mathbb{U}_{\mathbf{h}},\mathbb{U}_{\mathbf{h}}\Big) \;&+\Big((\theta-\frac{1}{4}(1+\alpha))\,\Delta t^2\,\mathbf{K}^{id}_{\mathbf{h}}\mathbb{U}_{\mathbf{h}},\mathbb{U}_{\mathbf{h}}\Big)\\ &-\Big(\frac{\Delta t^2}{4}(1+\alpha)\,\mathbf{K}^{ic}_{\mathbf{h}}\mathbb{U}_{\mathbf{h}},\mathbb{U}_{\mathbf{h}}\Big).\end{aligned} \tag{5.164}$$

For any $\mathbb{U}_{\mathbf{h}}=(\mathbb{U}_{T,\mathbf{h}},\mathbb{U}_{3,\mathbf{h}})\in\mathbb{V}_{\mathbf{h}}$, we use the Young's inequality we get the following bound

$$\Big(\mathbf{K}^{ic}_{\mathbf{h}}\mathbb{U}_{\mathbf{h}},\mathbb{U}_{\mathbf{h}}\Big) \leq \Big(\mathbf{K}^{d}_{TT,\mathbf{h}}\mathbb{U}_{T,\mathbf{h}},\mathbb{U}_{T,\mathbf{h}}\Big) + \Big(K_{T,\mathbf{h}}\mathbb{U}_{3,\mathbf{h}},\mathbb{U}_{3,\mathbf{h}}\Big). \tag{5.165}$$

Using the expression of $\mathbf{K}^{id}_{\mathbf{h}}$ and the inequality (5.165), we can rewrite the inequality (5.164) as follows

$$\Big(\mathbf{M}_h(\Delta t)\mathbb{U}_{\mathbf{h}},\mathbb{U}_{\mathbf{h}}\Big) \geq \Big((\mathbf{M}_{\mathbf{h}} - \frac{\Delta t^2}{4}(1+\frac{1}{\alpha})\,\mathbf{K}^{e,+}_{\mathbf{h}}\mathbb{U}_{\mathbf{h}},\mathbb{U}_{\mathbf{h}}\Big) + \Big((\theta-\frac{1}{2}(1+\alpha))\,\Delta t^2\,\mathbf{K}^{id}_{\mathbf{h}}\mathbb{U}_{\mathbf{h}},\mathbb{U}_{\mathbf{h}}\Big). \tag{5.166}$$

Assuming $\theta>\dfrac{1}{2}$, and by choosing $\alpha=2\,\theta-1$ we get

$$\Big(\mathbf{M}_h(\Delta t)\mathbb{U}_{\mathbf{h}},\mathbb{U}_{\mathbf{h}}\Big) \geq \Big((\mathbf{M}_{\mathbf{h}} - \frac{\Delta t^2}{4}(1+\frac{1}{\alpha})\,\mathbf{K}^{e,+}_{\mathbf{h}}\mathbb{U}_{\mathbf{h}},\mathbb{U}_{\mathbf{h}}\Big), \tag{5.167}$$

Recalling that

$$\mathbf{M}_{\mathbf{h}} = \begin{pmatrix}\mathbf{M}^T_{\mathbf{h}} & 0\\ 0 & M^3_{\mathbf{h}}\end{pmatrix} \quad\text{and}\quad \mathbf{K}^{e,+}_{\mathbf{h}} = \begin{pmatrix}\mathbf{K}_{3,\mathbf{h}} & 0\\ 0 & 0\end{pmatrix},$$

we drop, in (5.167), the positive blocks associated with $M^3_{\mathbf{h}}$, and deduces that for any $\mathbb{U}_{\mathbf{h}}=(\mathbb{U}_{T,\mathbf{h}},\mathbb{U}_{3,\mathbf{h}})\in\mathbb{V}_{\mathbf{h}}$,

$$\Big(\mathbf{M}_h(\Delta t)\mathbb{U}_{\mathbf{h}},\mathbb{U}_{\mathbf{h}}\Big) \geq \Big((\mathbf{M}^T_{\mathbf{h}} - \frac{\Delta t^2}{4}\frac{2\,\theta}{2\,\theta-1}\,\mathbf{K}_{3,\mathbf{h}}\mathbb{U}_{\mathbf{h}},\mathbb{U}_{\mathbf{h}}\Big). \tag{5.168}$$

Finally, we control the matrix $\mathbf{K}_{3,\mathbf{h}}$ with the help of the mass matrix $\mathbf{M}^T_{\mathbf{h}}$. This is where the longitudinal space step h will appear via the function $\widehat{\alpha}_h$. More precisely, let $\mathbf{U}_{h,T}\in\mathbf{V}_{h,T}$ associated to the vector $\mathbb{U}_{\mathbf{h},T}\in\mathbb{V}_{\mathbf{h},T}$, by definition of $\mathbf{K}_{3,\mathbf{h}}$

$$\Big(\mathbf{K}_{3,\mathbf{h}}\mathbb{U}_{\mathbf{h},T},\mathbb{U}_{\mathbf{h},T}\Big) = \mathbf{k}_3(\mathbf{U}_{h,T},\mathbf{U}_{h,T}) = \int_{\widehat{\Omega}} \widehat{\mu}^{-1}\,\mathbf{A}_T\,\partial_3\mathbf{U}_{h,T}\cdot\partial_3\mathbf{U}_{h,T}.$$

Using the Fubini's theorem, we get

$$\Big(\mathbf{K}_{3,\mathbf{h}}\mathbb{U}_{\mathbf{h},T},\mathbb{U}_{\mathbf{h},T}\Big) = \int_{\widehat{S}}\Big(\int_{\mathbb{R}}\widehat{\mu}^{-1}(\mathbf{x}_T,x_3)\Big(\mathbf{A}_T(\mathbf{x}_T,x_3)\,\partial_3\mathbf{U}_{h,T}(\mathbf{x}_T,x_3)\cdot\partial_3\mathbf{U}_{h,T}(\mathbf{x}_T,x_3)\Big)\,dx_3\Big)d\mathbf{x}_T.$$

Then, by definition (5.158) of the function $\widehat{\alpha}_h$, and since, for fixed $\mathbf{x}_T$, the function $\mathbf{U}_{h,T}(\mathbf{x}_T,\cdot)$ belongs to $\mathbb{P}_{1,h}$ by definition of $\mathbf{V}_{h,T}$, we have

$$\Big(\mathbf{K}_{3,\mathbf{h}}\mathbb{U}_{\mathbf{h},T},\mathbb{U}_{\mathbf{h},T}\Big) \leq \int_{\widehat{S}}\widehat{\alpha}_h(\mathbf{x}_T)\Big(\oint_{\mathbb{R}}\widehat{\varepsilon}(\mathbf{x}_T,x_3)\Big(\mathbf{A}_T(\mathbf{x}_T,x_3)\,\mathbf{U}_{h,T}(\mathbf{x}_T,x_3)\cdot\mathbf{U}_{h,T}(\mathbf{x}_T,x_3)\Big)\,dx_3\Big)d\mathbf{x}_T$$

so that, referring to the Fubini-like formula and the definition of $\mathbf{m}_h$, we get

$$\Big(\mathbf{K}_{3,\mathbf{h}}\mathbb{U}_{\mathbf{h},T},\mathbb{U}_{\mathbf{h},T}\Big) \leq \|\widehat{\alpha}_h\|_\infty^2\ \mathbf{m}(\mathbf{U}_{h,T},\mathbf{U}_{h,T}) \equiv \|\widehat{\alpha}_h\|_\infty^2\ \Big(\mathbf{M}_{\mathbf{h}}^T\mathbb{U}_{\mathbf{h},T},\mathbb{U}_{\mathbf{h},T}\Big). \tag{5.169}$$

Finally, joining (5.169) to the inequality (5.168), we obtain

$$\Big(\mathbf{M}_{\mathbf{h}}(\Delta t)\,\mathbb{U}_{\mathbf{h}},\mathbb{U}_{\mathbf{h}}\Big) \ \geq \Big(1-\|\widehat{\alpha}_h\|_\infty^2\,\frac{\Delta t^2}{4}\,\frac{2\,\theta}{2\,\theta-1}\Big)\,\Big(\mathbf{M}_{\mathbf{h}}^T\,\mathbb{U}_{\mathbf{h},T},\mathbb{U}_{\mathbf{h},T}\Big). \tag{5.170}$$

A sufficient stability condition is obtained by writing that

$$\Big(1-\|\widehat{\alpha}_h\|_\infty^2\,\frac{\Delta t^2}{4}\,\frac{2\,\theta}{2\,\theta-1}\Big) \geq 0.$$

■

Computational complexity

According to the weak formulation (5.140) and the implicit-explicit scheme (5.156) , we can write the full discrete problem as a series of 2D problems "section by section" which have the following structure :

$$\begin{aligned}
&\mathbb{M}_j\frac{\mathbb{E}_{T,j}^{n+1}-2\mathbb{E}_{T,j}^{n}+\mathbb{E}_{T,j}^{n-1}}{\Delta t^2}+(\mathbb{K}_{T,j}+\mathbb{K}_{TT,j}^d+\mathbb{J}_{T,j}^d+\mathbb{R}_{T,j}^d)\left(\theta\,\mathbb{E}_{T,j}^{n+1}+(1-2\theta)\,\mathbb{E}_{T,j}^{n}+\theta\,\mathbb{E}_{T,j}^{n-1}\right)\\
&\qquad-\frac{1}{h}\left(\mathbb{M}_{j+\frac12}\,\frac{\mathbb{E}_{T,j+1}^{n}-\mathbb{E}_{T,j}^{n}}{h}-\mathbb{M}_{j-\frac12}\,\frac{\mathbb{E}_{T,j}^{n}-\mathbb{E}_{T,j-1}^{n}}{h}\right)+\frac{\mathbb{C}_{3T,j+\frac12}\,\mathbb{E}_{3,j+\frac12}^{n}-\mathbb{C}_{3T,j-\frac12}\mathbb{E}_{3,j-\frac12}^{n}}{h}\\
&\qquad\qquad+\mathbb{C}_{T,j}^d\,(\mathbb{E}_{3,j+\frac12}^{n}+\mathbb{E}_{3,j-\frac12}^{n})+\mathbb{C}_{TT,j}^d\,(\mathbb{E}_{3,j+\frac12}^{n}+\mathbb{E}_{3,j-\frac12}^{n})=0,
\end{aligned}$$

$$\begin{aligned}
&\mathrm{M}_{j+\frac12}\frac{\mathbb{E}_{3,j+\frac12}^{n+1}-2\mathbb{E}_{3,j+\frac12}^{n}+\mathbb{E}_{3,j+\frac12}^{n-1}}{\Delta t^2}+\mathrm{K}_{T,j+\frac12}\left(\theta\,\mathbb{E}_{3,j+\frac12}^{n+1}+(1-2\theta)\,\mathbb{E}_{3,j+\frac12}^{n}+\theta\,\mathbb{E}_{3,j+\frac12}^{n-1}\right)\\
&\qquad-\mathbb{C}_{3T,j+\frac12}^*\frac{\mathbb{E}_{T,j+1}^{n}-\mathbb{E}_{T,j}^{n}}{h}+\left((\mathbb{C}_{T,j+1}^d)^*\,\mathbb{E}_{T,j+1}^{n}+(\mathbb{C}_{T,j}^d)^*\,\mathbb{E}_{T,j}^{n}\right)\\
&\qquad\qquad+\left((\mathbb{C}_{TT,j+1}^d)^*\,\mathbb{E}_{T,j+1}^{n}+(\mathbb{C}_{TT,j}^d)^*\,\mathbb{E}_{T,j}^{n}\right)=0,
\end{aligned}$$

Looking at where the superscript $n+1$ appears in the above equations, one sees that at each time step one has to invert the matrices

$$\mathbb{M}_j+\theta\,\Delta t^2\,(\mathbb{K}_{T,j}+\mathbb{K}_{TT,j}^d+\mathbb{J}_{T,j}^d+\mathbb{R}_{T,j}^d) \quad\text{ and }\quad \mathrm{M}_{j+\frac12}+\theta\,\Delta t^2\mathrm{K}_{T,j+\frac12}.$$

This illustrates the fact that the scheme is implicit only in the transverse direction.

5.6 Conclusion

In this chapter, we presented an extension of the method developed in chapter 2 for cylindrical cables to the case of non-cylindrical cables : we used a mapping technique combined with an anisotropic Piola transform and a hybrid Finite Element/Discontinuous Galerkin approach for the spatial discretization, and an explicit/implicit scheme for the temporal discretization. The implementation of the obtained scheme is not straightforward because it involves new terms that are not available –under construction– in the Xlife++ software.

Chapitre 6

Construction des couches PML pour les modèles 3D/1D

Sommaire

6.1 Introduction

Pour simuler la propagation d'ondes électromagnétiques dans un câble coaxial non borné dans la direction longitudinale, plusieurs approches existantes dans la littérature peuvent être utilisées. Parmi ces approches nous trouvons la méthode basée sur les couches absorbantes parfaitement adaptées (Perfectly Matched Layer) "PML". Le modèle de PML a été introduit par Bérenger en 1994 [14], il constitue une méthode particulièrement efficace pour formuler des conditions de bord transparentes, et consiste à prolonger le domaine de calcul par un domaine fictif dans lequel les ondes sont atténuées. Dans cette couche on cherche à satisfaire deux objectifs :

— Ne pas avoir de réflexion à l'interface entre le domaine d'intérêt et la couche absorbante.

— Atténuer les ondes entrantes dans la couche PML.

Dans ce chapitre, nous allons utiliser cette méthode pour résoudre le modèle Maxwell 3D présenté au Chapitre 2, puis pour résoudre le modèle télégraphique présenté au chapitre 4.

Pour la construction d'une formulation variationnelle adaptée, nous nous sommes inspirés des travaux de Baffet, Grote, Imperiale et Kachanovska [7] pour le cas de l'équation des ondes. La principale difficulté est d'aboutir à une formulation variationnelle compatible avec les éléments finis présentés au Chapitre 2 (pour le modèle 3D) et au Chapitre 4 (pour le modèle 1D), ce qui repose sur l'introduction astucieuse d'inconnues auxiliaires.

6.2 Construction des couches PML pour les équations de Maxwell 3D

6.2.1 Rappel du modèle 3D dans un câble infini

Notre domaine de travail est un câble coaxial cylindrique Ω, nous supposons qu'il est infini dans la direction longitudinale x_3 (voir Figure 6.1).

$$\Omega = S \times \mathbb{R}, \quad \partial S = \Gamma_e \cup \Gamma_i, \tag{6.1}$$

où S est une section du câble Ω indépendante de x_3.

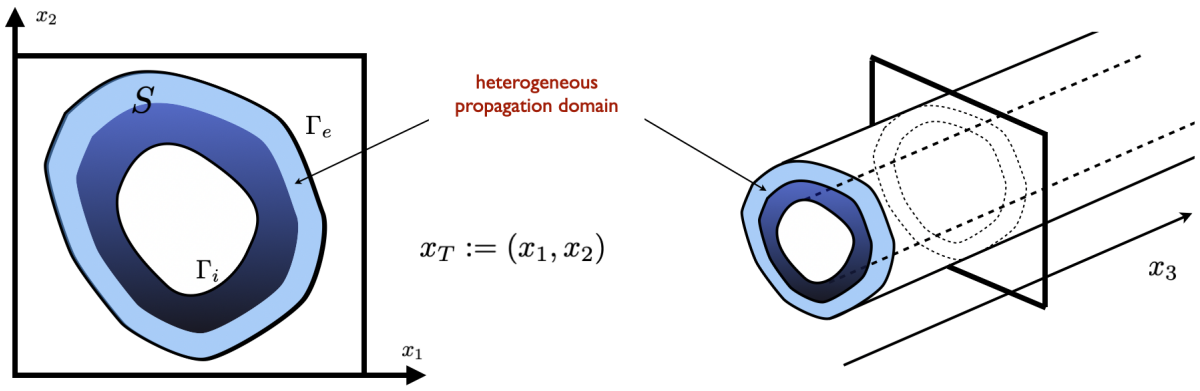

FIGURE 6.1 – Gauche : une section du câble, Droite : le domaine Ω.

La propagation des ondes dans le câble Ω, à travers les inconnues $\mathbf{E}(\mathbf{x}, \mathbf{t})$ (le champ électrique) et $\mathbf{H}(\mathbf{x}, \mathbf{t})$ (le champ magnétique) est régie par les équations de Maxwell 3D complétées par des conditions aux limites parfaitement conductrices sur $\partial\Omega$,

$$\begin{cases} \varepsilon\, \partial_t \mathbf{E} + \sigma\, \mathbf{E} - \boldsymbol{\nabla} \times \mathbf{H} = \mathbf{0}, & \text{dans } \Omega \times \mathbb{R}^+. \\ \mu\, \partial_t \mathbf{H} + \boldsymbol{\nabla} \times \mathbf{E} = \mathbf{0}, & \text{dans } \Omega \times \mathbb{R}^+, \\ \mathbf{E} \times \mathbf{n} = 0, & \text{sur } \partial\Omega \times \mathbb{R}^+, \end{cases} \tag{6.2}$$

où t est le temps, $\boldsymbol{\nabla}\times$ l'opérateur rotationnel 3D et $\mathbf{n}$ représente la normale extérieure unitaire. Les coefficients ε et μ sont respectivement la permittivité électrique et la perméabilité magnétique, et sont toutes deux des fonctions de la variable spatiale $\mathbf{x}_T \in S$ et satisfont aux hypothèses suivantes

$$0 < \mu_- \leq \mu(\mathbf{x}_T) \leq \mu_+, \quad 0 < \varepsilon_- \leq \varepsilon(\mathbf{x}_T) \leq \varepsilon_+ \quad \text{avec} \quad \mathbf{x}_T = (x_1, x_2) \in S.$$

Nous considérerons également la possibilité de la présence de la conductivité σ,

$$0 \leq \sigma(\mathbf{x}_T) \leq \sigma_+, \quad \mathbf{x}_T \in S. \tag{6.3}$$

Le modèle (6.2) est complété par les conditions initiales (pour simplifier, nous supposons l'absence de termes sources, sans aucune perte de généralité).

$$\mathbf{E}(\cdot, 0) = \mathbf{E}_0, \quad \mathbf{H}(\cdot, 0) = \mathbf{H}_0. \tag{6.4}$$

Pour utiliser la méthode développée dans le Chapitre 2, nous considérons la formulation du problème en champ électrique de second ordre, obtenu après élimination du champ magnétique,

$$\left| \begin{array}{ll} \varepsilon\, \partial_t^2 \mathbf{E} + \sigma\, \partial_t \mathbf{E} + \boldsymbol{\nabla} \times\, \mu^{-1}\, \boldsymbol{\nabla} \times \mathbf{E} = \mathbf{0}, & \text{dans } \Omega \times \mathbb{R}^+, \\ \mathbf{E} \times \mathbf{n} = \mathbf{0}, & \text{sur } \partial\Omega \times \mathbb{R}^+, \\ \mathbf{E}(\cdot, 0) = \mathbf{E}_0, \quad \partial_t \mathbf{E}(\cdot, 0) = \varepsilon^{-1} \left(\boldsymbol{\nabla} \times \mathbf{H}_0 - \sigma\, \mathbf{E}_0 \right) & \text{dans } \Omega. \end{array} \right. \tag{6.5}$$

Pour des raisons de simplicité, sans perte de généralité, nous supposons que $\sigma = 0$.

Nous introduisons la décomposition du champ électrique $\mathbf{E}$ en composantes transversale $\mathbf{E}_T$ et longitudinale E_3,

$$\mathbf{E} = \begin{pmatrix} \mathbf{E}_T \\ \\ E_3 \end{pmatrix} \qquad \text{avec} \quad \mathbf{E}_T = \begin{pmatrix} E_1 \\ \\ E_2 \end{pmatrix}.$$

Les équations de Maxwell (6.5) peuvent être réécrites sous la forme suivante :

$$\left| \begin{array}{ll} \varepsilon\, \partial_t^2 \mathbf{E}_T - \partial_3 \left(\mu^{-1} \partial_3\, \mathbf{E}_T \right) + \mathbf{rot}_T \left(\mu^{-1} \mathrm{rot}_T\, \mathbf{E}_T \right) + \partial_3 \left(\mu^{-1} \nabla_T E_3 \right) = 0, & \text{dans } \Omega \times \mathbb{R}^+, \\ \varepsilon\, \partial_t^2 E_3 + \mathrm{rot}_T \left(\mu^{-1} \mathbf{rot}_T E_3 \right) + \mathrm{div}_T \left(\mu^{-1} \partial_3\, \mathbf{E}_T \right) = 0, & \text{dans } \Omega \times \mathbb{R}^+, \\ \mathbf{E}_T \times \mathbf{n}_T = 0, \quad \text{et} \quad E_3 = 0, & \text{sur } \partial\Omega \times \mathbb{R}^+. \end{array} \right. \tag{6.6}$$

Ici ∂_i est la dérivée partielle par rapport à la variable x_i pour $i = 1, 2, 3$, rot_T est l'opérateur de rotation transversal scalaire, $\mathbf{rot}_T$ est l'opérateur de rotation transversal vectorielle, ∇_T est l'opérateur de gradient transversal et div_T est l'opérateur de divergence transversale (notez que l'indice T fait référence aux dérivées transversales) :

$$\begin{aligned} \mathrm{rot}_T \mathbf{E}_T &= \partial_1 E_2 - \partial_2 E_1 \quad \mathbf{rot}_T\, E_3 = \begin{pmatrix} \partial_2 E_3 \\ \\ -\partial_1 E_3 \end{pmatrix} \\ \mathrm{div}_T \mathbf{E}_T &= \partial_1 E_1 - \partial_2 E_2 \quad \nabla_T\, E_3 = \begin{pmatrix} \partial_1 E_3 \\ \\ \partial_2 E_3 \end{pmatrix} \end{aligned} \tag{6.7}$$

6.2.2 Construction des couches PML

Dans cette section, nous allons expliquer comment construire la formulation PML associée à notre modèle (6.6). La première étape consiste à introduire la transformation de Laplace,

$$\widehat{u}(x, s) = \int_0^\infty e^{st}\, u(x, t)\, dt, \quad s \in \mathbb{C}. \tag{6.8}$$

Ensuite, en appliquant cette transformations sur le problème (6.6), nous obtenons

$$\left|\begin{array}{ll} \varepsilon\, s^2\, \widehat{\mathbf{E}}_T - \partial_3 \left(\mu^{-1}\partial_3\, \widehat{\mathbf{E}}_T\right) + \mathbf{rot}_T\Big(\mu^{-1}\mathrm{rot}_T\, \widehat{\mathbf{E}}_T\Big) + \partial_3 \left(\mu^{-1}\nabla_T \widehat{E}_3\right) = 0, & \text{dans } \Omega, s \in \mathbb{C}, \\ \varepsilon\, s^2\, \widehat{E}_3 + \mathrm{rot}_T \left(\mu^{-1}\mathbf{rot}_T \widehat{E}_3\right) + \mathrm{div}_T\Big(\mu^{-1}\partial_3\, \widehat{\mathbf{E}}_T\Big) = 0, & \text{dans } \Omega, s \in \mathbb{C}, \\ \widehat{\mathbf{E}}_T \times \mathbf{n}_T = 0, \text{ et } \quad \widehat{E}_3 = 0, & \text{sur } \partial\Omega, s \in \mathbb{C}, \end{array}\right. \tag{6.9}$$

Soit ξ une fonction positive, qui dépend de la variable longitudinale x_3, et qui s'annule dans un sous-domaine Ω_b borné du Ω, et strictement positive en dehors de Ω_b (voir Figure 6.2), nous introduisons le changement de coordonnée suivant :

$$x_3 \mapsto \widehat{x}_3 = x_3 + \frac{1}{s}\int_0^{x_3} \xi(z)\, dz, \quad x_3 \in \mathbb{R}. \tag{6.10}$$

L'application de ce changement de variable au problème (6.9), et en utilisant le fait que

$$\frac{\partial_{\widehat{x_3}}}{\partial_{x_3}} = \frac{s}{s+\xi},$$

nous conduit au problème suivant :

$$\left\{\begin{array}{l} \varepsilon\, s^2\, \widehat{\mathbf{E}}_T - \dfrac{s}{s+\xi}\, \partial_3 \left(\mu^{-1}\, \dfrac{s}{s+\xi}\, \partial_3 \widehat{\mathbf{E}}_T\right) + \mathbf{rot}_T \left(\mu^{-1}\, \mathrm{rot}_T\, \widehat{\mathbf{E}}_T\right) + \dfrac{s}{s+\xi}\, \partial_3 \left(\mu^{-1}\, \nabla_T\, \widehat{E}_3\right) = 0, \\ \varepsilon\, s^2\, \widehat{E}_3 + \mathrm{rot}_T \left(\mu^{-1}\, \mathbf{rot}_T\, \widehat{E}_3\right) + \mathrm{div}_T\Big(\mu^{-1}\, \dfrac{s}{s+\xi}\, \partial_3\, \widehat{\mathbf{E}}_T\Big) = 0. \end{array}\right. \tag{6.11}$$

Le principe de la méthode des PML consiste à bien choisir la fonction ξ de telle façon à, d'une part, ne pas avoir des réflexions à l'interface entre le domaine d'intérêt Ω_b et les deux couches absorbantes Ω^-_{PML} et Ω^+_{PML}, d'autre part atténuer les ondes entrantes dans les PML. Une fois le système PML construit, on peut tronquer artificiellement le domaine Ω et compléter le problème (6.2.2) par la condition $\mathbf{E} \times \mathbf{n} = 0$ aux extrémités des deux couches PML (voir Figure 6.2).

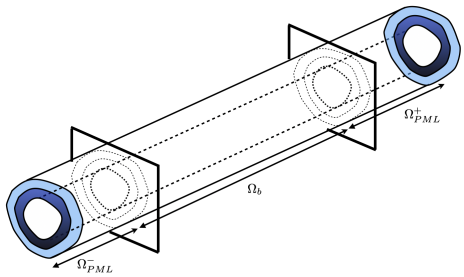

FIGURE 6.2 – Le domaine Ω tronqué par deux couches PML, Ω^+_{PML} et Ω^-_{PML}

Si on multiplie les deux équations (6.2.2) par $1+\dfrac{\xi}{s}$, nous obtenons

$$\begin{cases} \varepsilon\, s^2\,(1+\dfrac{\xi}{s})\,\widehat{\mathbf{E}}_T - \partial_3\left(\mu^{-1}\,\dfrac{s}{s+\xi}\,\partial_3\widehat{\mathbf{E}}_T\right) + \mathbf{rot}_T\left(\mu^{-1}\,(1+\dfrac{\xi}{s})\,\mathrm{rot}_T\,\widehat{\mathbf{E}}_T\right) \\ \qquad\qquad +\partial_3\left(\mu^{-1}\,\nabla_T\,\widehat{E}_3\right) = 0, \\ \varepsilon\, s^2\,(1+\dfrac{\xi}{s})\,\widehat{E}_3 + \mathrm{rot}_T\left(\mu^{-1}\,(1+\dfrac{\xi}{s})\,\mathbf{rot}_T\,\widehat{E}_3\right) + \mathrm{div}_T\left(\mu^{-1}\partial_3\,\widehat{\mathbf{E}}_T\right) = 0. \end{cases} \tag{6.12}$$

Maintenant, nous cherchons à trouver une formulation qui sépare les termes de la formulation (6.9) et les nouveaux termes qui dépendent de ξ et qui expliquent la présence des couches PML. Pour se faire nous utilisons l'égalité suivante

$$\frac{s}{s+\xi} = 1 - \frac{\xi}{s+\xi}.$$

Avec cette remarque, les équations (6.12) se réécrivent comme suit,

$$\begin{cases} \varepsilon\, s^2\ \widehat{\mathbf{E}}_T - \partial_3\left(\mu^{-1}\,\partial_3\,\widehat{\mathbf{E}}_T\right) + \mathbf{rot}_T\left(\mu^{-1}\,\mathrm{rot}_T\,\widehat{\mathbf{E}}_T\right) + \partial_3\left(\mu^{-1}\,\nabla_T\,\widehat{E}_3\right) \\ \qquad\qquad +\varepsilon\,\xi\,s\,\widehat{\mathbf{E}}_T + \partial_3\left(\mu^{-1}\,\dfrac{\xi}{s+\xi}\,\partial_3\,\widehat{\mathbf{E}}_T\right) + \mathbf{rot}_T\left(\mu^{-1}\,\dfrac{\xi}{s}\,\mathrm{rot}_T\,\widehat{\mathbf{E}}_T\right) = 0, \\ \varepsilon\, s^2\ \widehat{E}_3 + \mathrm{rot}_T\left(\mu^{-1}\,\mathbf{rot}_T\,\widehat{E}_3\right) + \mathrm{div}_T\left(\mu^{-1}\partial_3\,\widehat{\mathbf{E}}_T\right) + \varepsilon\,\xi\,s\,\widehat{E}_3 + \mathrm{rot}_T\left(\mu^{-1}\,\dfrac{\xi}{s}\,\mathbf{rot}_T\,\widehat{E}_3\right) = 0. \end{cases}$$

Nous définissons trois nouvelles inconnues,

$$\widehat{\boldsymbol{\phi}} = \frac{\xi}{s+\xi}\,\partial_3\,\widehat{\mathbf{E}}_T, \qquad \widehat{r}_T = \frac{\xi}{s}\,\mathrm{rot}_T\,\widehat{\mathbf{E}}_T, \qquad \widehat{\boldsymbol{r}}_3 = \frac{\xi}{s}\,\mathbf{rot}_T\,\widehat{E}_3, \tag{6.13}$$

et obtenons alors le système,

$$\begin{cases} \varepsilon\, s^2\ \widehat{\mathbf{E}}_T - \partial_3\,\mu^{-1}\,\partial_3\ \widehat{\mathbf{E}}_T + \mathbf{rot}_T\left(\mu^{-1}\,\mathrm{rot}_T\,\widehat{\mathbf{E}}_T\right) + \partial_3\,\mu^{-1}\,\nabla_T\,\widehat{E}_3 \\ \qquad\qquad +\varepsilon\,\xi\,s\,\widehat{\mathbf{E}}_T + \mu^{-1}\,\partial_3\,\widehat{\boldsymbol{\phi}} + \mathbf{rot}_T\left(\mu^{-1}\widehat{r}_T\right) = 0, \\ \varepsilon\, s^2\,\widehat{E}_3 + \mathrm{rot}_T\left(\mu^{-1}\,\mathbf{rot}_T\,\widehat{E}_3\right) + \mathrm{div}_T\left(\mu^{-1}\partial_3\,\widehat{\mathbf{E}}_T\right) + \varepsilon\,\xi\,s\,\widehat{E}_3 + \mathrm{rot}_T\left(\mu^{-1}\,\widehat{\boldsymbol{r}}_3\right) = 0, \\ (s+\xi)\,\widehat{\boldsymbol{\phi}} = \xi\,\partial_3\,\widehat{\mathbf{E}}_T, \\ s\,\widehat{r}_T = \xi\,\mathrm{rot}_T\,\widehat{\mathbf{E}}_T, \\ s\,\widehat{\boldsymbol{r}}_3 = \xi\,\mathbf{rot}_T\,\widehat{E}_3. \end{cases}$$

En utilisant la transformation de Laplace inverse, nous pouvons revenir au régime temporel,

$$\begin{cases} \varepsilon\,\partial_t^2\,E_T - \partial_3\left(\mu^{-1}\,\partial_3\,\widetilde{\mathbf{E}}_T\right) + \mathbf{rot}_T\left(\mu^{-1}\,\mathrm{rot}_T\,E_T\right) + \partial_3\,\mu^{-1}\,\nabla_T\,E_3 \\ \qquad\qquad + \varepsilon\,\xi\;\partial_t\,E_T + \mu^{-1}\,\partial_3\,\boldsymbol{\phi} + \mathbf{rot}_T\left(\mu^{-1} r_T\right) = 0, \\ \varepsilon\,\partial_t^2\,E_3 + \varepsilon\,\xi\;\partial_t\,E_3 + \mathrm{rot}_T\left(\mu^{-1}\,\mathbf{rot}_T\,E_3\right) + \mathrm{rot}_T\left(\mu^{-1}\,\boldsymbol{r}_3\right) + \mathrm{div}_T\left(\mu^{-1}\partial_3\,\widehat{\mathbf{E}}_T\right) = 0, \\ \partial_t\,\boldsymbol{\phi} + \xi\,\boldsymbol{\phi} = \xi\,\partial_3\,E_T, \\ \partial_t\,r_T = \xi\,\mathrm{rot}_T\,E_T, \\ \partial_t\,\boldsymbol{r}_3 = \xi\,\mathbf{rot}_T\,E_3. \end{cases} \tag{6.14}$$

Maintenant, nous allons chercher une méthode de discrétisation en espace et en temps pour résoudre numériquement le modèle obtenu.

6.2.3 Une méthode hybride de discrétisation en espace

Nous allons utiliser une approche Galerkine basée sur la formulation variationnelle de (6.14). Afin de donner la formulation faible de ce problème, nous commençons par introduire l'espace fonctionnel V où nous cherchons le champ électrique transverse $\mathbf{E}_T$ et le champ électrique longitudinal E_3, qui est défini comme suit,

$$\begin{aligned} &H(\mathbf{rot};\Omega) := \Big\{\left(\mathbf{E}_T, E_3\right) \in L^2(\Omega)^2 \times L^2(\Omega) \,/\, \mathbf{rot}_T E_3 \,+\, \mathbf{e}_3 \times \partial_3\,\mathbf{E}_T \in L^2(\Omega)^2, \\ &\qquad\qquad\qquad\qquad\qquad\qquad\qquad\qquad \text{et } \mathrm{rot}_T\,\mathbf{E}_T \in L^2(\Omega)\Big\}, \\ &V := H_0(\mathbf{rot};\Omega) = \Big\{\mathbf{E} \in H(\mathbf{rot};\Omega) \,/\, \mathbf{E}_T \times \mathbf{n}_T = E_3 = 0 \text{ sur } \partial\Omega\Big\}. \end{aligned} \tag{6.15}$$

En utilisant les expressions des nouvelles inconnues (6.13), nous déduisons qu'il faut chercher les inconnues respectivement dans les espaces fonctionnels suivants :

$$\begin{aligned} &\mathbf{W} := L^2\Big(\mathbb{R}, H(\mathrm{rot}_T, S)\Big) = \Big\{\mathbf{u}_T \in L^2(\Omega)^2 \,/\, \forall\, x_3 \in \mathbb{R}, \quad \mathrm{rot}_T\,\mathbf{u}_T(\cdot, x_3) \in L^2(S)\Big\}, \\ &W_T := H^1\Big(\mathbb{R}, L^2(S)\Big) = \Big\{u \in L^2(\Omega) \,/\, \forall\, \mathbf{x}_T \in S, \quad \partial_3\,u(\mathbf{x}_T, \cdot) \in L^2(\mathbb{R})\Big\}, \\ &\mathbf{W}_T := L^2(\Omega)^2, \\ &\mathbf{V} := V \times \mathbf{W} \times W_T \times \mathbf{W}_T. \end{aligned} \tag{6.16}$$

En adaptant ce choix des espaces fonctionnels, nous pouvons introduire la formulation variationnelle du problème (6.14) :

Trouver $\left(\mathbf{E}_T, E_3\right)(t)$ et $\left(\boldsymbol{\phi}, r_T, \boldsymbol{r}_3\right)(t)$ dans $\mathbf{V}$ tel que pour toute fonction test $\left(\widetilde{\mathbf{E}}_T, \widetilde{E}_3\right)$ et

$\big(\widetilde{\boldsymbol{\phi}}, \widetilde{r}_T, \widetilde{\boldsymbol{r}}_3\big)$ dans $\mathbf{V}$, nous avons

$$
\left|\begin{array}{ll}
\dfrac{d^2}{dt^2}\,\mathbf{m}\big(\mathbf{E}_T, \widetilde{\mathbf{E}}_T\big) & + \mathbf{k}_3\big(\mathbf{E}_T, \widetilde{\mathbf{E}}_T\big) + \mathbf{k}_T\big(\mathbf{E}_T, \widetilde{\mathbf{E}}_T\big) - c_{3T}\big(E_3, \widetilde{\mathbf{E}}_T\big) \\
& \quad + \dfrac{d}{dt}\,\mathbf{m}_{\varepsilon\,\xi}\big(\mathbf{E}_T, \widetilde{\mathbf{E}}_T\big) + \mathbf{p}^T_{\mu^{-1}}\big(r_T, , \widetilde{\mathbf{E}}_T\big) - \mathbf{p}^3_{\mu^{-1}}\big(\boldsymbol{\phi}, \widetilde{\mathbf{E}}_T\big) = 0, \\
\dfrac{d^2}{dt^2}\,m\big(E_3, \widetilde{E}_3\big) & + k_T\big(E_3, \widetilde{E}_3\big) - c_{3T}\big(\widetilde{E}_3, \mathbf{E}_T\big) \\
& \quad + \dfrac{d}{dt}\,m_{\varepsilon\,\xi}\big(E_3, \widetilde{E}_3\big) + p^T_{\mu^{-1}}\big(\boldsymbol{r}_3, \widetilde{E}_3\big) = 0, \\
\dfrac{d}{dt}\,\mathbf{m}_1\big(\boldsymbol{\phi}, \widetilde{\boldsymbol{\phi}}\big) & + \mathbf{m}_\xi\big(\boldsymbol{\phi}, \widetilde{\boldsymbol{\phi}}\big) = \mathbf{p}^3_\xi\big(\widetilde{\boldsymbol{\phi}}, \mathbf{E}_T\big), \\
\dfrac{d}{dt}\,m_1\big(r_T, \widetilde{r}_T\big) & = \mathbf{p}^T_\xi\big(\widetilde{r}_T, \mathbf{E}_T\big), \\
\dfrac{d}{dt}\,\mathbf{m}_1\big(\boldsymbol{r}_3, \widetilde{\boldsymbol{r}}_3\big) & = p^T_\xi\big(\widetilde{\boldsymbol{r}}_3, E_3\big).
\end{array}\right. \tag{6.17}
$$

où les formes bilinéaires suivantes ont les mêmes notations et expressions que les formes (2.9) trouvées dans le chapitre (2),

$$
\left|\begin{array}{ll}
\mathbf{m}\big(\mathbf{E}_T, \widetilde{\mathbf{E}}_T\big) := \displaystyle\int_\Omega \varepsilon\,\mathbf{E}_T \cdot \widetilde{\mathbf{E}}_T, & m\big(E_3, \widetilde{E}_3\big) := \displaystyle\int_\Omega \varepsilon\, E_3\, \widetilde{E}_3, \\
\mathbf{k}_T\big(\mathbf{E}_T, \widetilde{\mathbf{E}}_T\big) := \displaystyle\int_\Omega \mu^{-1}\,\mathrm{rot}_T\,\mathbf{E}_T\,\mathrm{rot}_T\,\widetilde{\mathbf{E}}_T, & k_T\big(E_3, \widetilde{E}_3\big) := \displaystyle\int_\Omega \mu^{-1}\,\nabla_T E_3 \cdot \nabla_T \widetilde{E}_3, \\
\mathbf{k}_3\big(\mathbf{E}_T, \widetilde{\mathbf{E}}_T\big) := \displaystyle\int_\Omega \mu^{-1}\,\partial_3\,\mathbf{E}_T \cdot \partial_3\,\widetilde{\mathbf{E}}_T, & c_{3T}\big(E_3, \mathbf{E}_T\big) := \displaystyle\int_\Omega \mu^{-1}\,\nabla_T E_3 \cdot \partial_3\,\mathbf{E}_T.
\end{array}\right. \tag{6.18}
$$

Les nouvelles formes bilinéaires sont les suivantes :

$$
\left|\begin{array}{ll}
\mathbf{p}^3_\alpha\big(\boldsymbol{\phi}, \mathbf{E}_T\big) := \displaystyle\int_\Omega \alpha\,\boldsymbol{\phi} \cdot \partial_{x_3}\,\mathbf{E}_T, & \mathbf{m}_\alpha\big(\boldsymbol{\phi}, \widetilde{\boldsymbol{\phi}}\big) := \displaystyle\int_\Omega \alpha\,\boldsymbol{\phi} \cdot \widetilde{\boldsymbol{\phi}}, \\
\mathbf{p}^T_\alpha\big(r_T, , \mathbf{E}_T\big) := \displaystyle\int_\Omega \alpha\, r_T\,\mathrm{rot}\,\mathbf{E}_T, & m_\alpha\big(r_T, \widetilde{r}_T\big) := \displaystyle\int_\Omega \alpha\, r_T\,\widetilde{r}_T, \\
p^T_\alpha\big(\boldsymbol{r}_3, E_3\big) := \displaystyle\int_\Omega \alpha\,\boldsymbol{r}_3 \cdot \mathbf{rot}_T\, E_3.
\end{array}\right. \tag{6.19}
$$

Remarque 6.2.1 (Les formes bilinéaires (6.19))**.**

Tous ces formes disparaissent en dehors des deux couches de PML. L'indice en bas α signifie que la forme bilinéaire dépend d'un coefficient α. Nous utilisons les lettres en gras (resp. en normale) lorsqu'elles s'appliquent aux champs vectoriels (resp. aux champs scalaires). Pour les formes bilinéaires $\mathbf{p}^3_\alpha$, $\mathbf{p}^T_\alpha$ et p^T_α, l'indice en haut T signifie que la dérivée transversale est impliquée, tandis que l'indice 3 signifie qu'il existe une dérivée par rapport à x_3 dans la forme bilinéaire, et α est une fonction strictement positive.

Nous traitons maintenant de la discrétisation en espace. Nous suivrons la même approche que dans le Chapitre 2 (dans Section 2.4.1 et Section 2.4.2), ainsi nous allons traiter d'abord la discrétisation longitudinale par rapport à x_3, et ensuite une discrétisation transverse par rapport aux variables transversales $\mathbf{x}_T$, ce qui est justifié par la "structure cylindrique" de câble Ω.

Semi-discrétisation longitudinale.

Nous commençons par décomposer le câble Ω en des petits portions cylindriques.

$$\mathcal{C}_{j+\frac{1}{2}} = \{(\mathbf{x}_T, x_3) \in \Omega \ / \ jh \leq x_3 \leq (j+1)h\}, \quad j \in \mathbb{Z} \tag{6.20}$$

Ces portions de taille h dans la direction longitudinale x_3 (h est le pas d'espace longitudinal) sont séparées par des sections transversales $S_j, j \in \mathbb{Z}$ (voir figure 2.2) où, par définition, $S_j = \{(\mathbf{x}_T, jh), \mathbf{x}_T \in S\}$.

Nous introduisons maintenant les sous-espaces semi-discrets des espaces définis dans (6.15) et (6.16), et adaptés à cette semi-discrétisation en espace :

$*$ *Pour l'espace* $H(\mathbf{rot}; \Omega)$

Nous notons $\mathbf{V}_h$ l'espace d'approximation de l'espace 3D $H(\mathbf{rot}; \Omega)$,

$$\mathbf{V}_h := \mathbf{V}_{h,T} \times V_{h,\ell} \subset H(\mathbf{rot}; \Omega), \tag{6.21}$$

où d'une part, $\mathbf{V}_{h,T}$ est constitué de $\mathbb{P}_1$ fonctions continues dans la direction x_3 et à valeurs dans l'espace 2D $H(\mathrm{rot}_T, S)$.

$$\mathbf{V}_{h,T} := \Big\{\mathbf{E}_{T,h} \in C^0\Big(\mathbb{R}; H(\mathrm{rot}_T, S)\Big) \ / \ \mathbf{E}_T|_{\mathcal{C}_{j+\frac{1}{2}}} \in \mathbb{P}_1\Big(\mathbb{R}; H(\mathrm{rot}_T, S)\Big) \, \forall \, j\Big\}, \tag{6.22}$$

avec $H(\mathrm{rot}_T; S) := \Big\{\mathbf{E}_T \in L^2(\Omega)^2 \times L^2(\Omega) \, / \, \mathrm{rot}_T \mathbf{E}_T \in L^2(\Omega)\Big\}$.

En d'autres termes, pour tout $\mathbf{E}_T \in \mathbf{V}_{h,T}$, nous avons

$$\mathbf{E}_T(\mathbf{x}_T, x_3) = \sum_{j \in \mathbb{Z}} \mathbf{E}_{T,j}(\mathbf{x}_T) \, w_j(x_3), \tag{6.23}$$

où w_j est la fonction chapeau habituelle associée à $x_3 = jh$ (voir figure 2.3), et

$$\mathbf{E}_{T,j} = \mathbf{E}_T|_{S_j} \in H(\mathrm{rot}_T, S).$$

D'autre part, l'espace $V_{h,\ell}$ est constitué de fonctions constantes par morceaux $\mathbb{P}_0$ dans la direction x_3 et à valeurs dans $H^1(S)$.

$$V_{h,\ell} := \{E_3 : \Omega \to \mathbb{R} \ / \ E_3|_{\mathcal{C}_{j+\frac{1}{2}}} \in \mathbb{P}_0\Big(\mathbb{R}; H^1(S)\Big) \, \forall \, j\Big\}. \tag{6.24}$$

En d'autres termes, pour tout $E_3 \in V_{h,\ell}$, il existe $E_{3,j+\frac{1}{2}} \in H^1(S), j \in \mathbb{Z}$ tel que

$$E_3(\mathbf{x}_T, x_3) = \sum_{j \in \mathbb{Z}} E_{3,j+\frac{1}{2}}(\mathbf{x}_T) \, \chi_{j+\frac{1}{2}}(x_3), \quad E_{3,j+\frac{1}{2}} = E_3|_{S_{j+\frac{1}{2}}} \tag{6.25}$$

où $\chi_{j+\frac{1}{2}}$ est la fonction caractéristique de l'intervalle $(jh,(j+1)h]$ (voir figure 2.3).

$*$ *Pour l'espace* $\mathbf{W} = L^2\Big(\mathbb{R}, H(\mathrm{rot}_T, S)\Big)$

Nous notons $\mathbf{W}_h$ l'espace d'approximation de l'espace $\mathbf{W}$. Cet espace est constitué de fonctions constantes par morceaux $\mathbb{P}_0$ dans la direction x_3 et à valeurs dans l'espace 2D $H(\mathrm{rot}_T, S)$.

$$\mathbf{W}_h := \Big\{\boldsymbol{\phi} : \Omega \to \mathbb{R}^2 \;/\; \boldsymbol{\phi}|_{\mathcal{C}_{j+\frac{1}{2}}} \in \mathbb{P}_0\Big(\mathbb{R}; H(\mathrm{rot}_T, S)\Big)\, \forall\, j\Big\}. \tag{6.26}$$

En d'autres termes, pour tout $\boldsymbol{\phi} \in \mathbf{W}_h$, il existe $\boldsymbol{\phi}_{j+\frac{1}{2}} \in H(\mathrm{rot}_T, S),\ j \in \mathbb{Z}$ tel que

$$\boldsymbol{\phi}(\mathbf{x}_T, x_3) = \sum_{j\in\mathbb{Z}} \boldsymbol{\phi}_{j+\frac{1}{2}}(\mathbf{x}_T)\, \chi_{j+\frac{1}{2}}(x_3), \quad \boldsymbol{\phi}_{j+\frac{1}{2}} = \boldsymbol{\phi}|_{S_{j+\frac{1}{2}}}. \tag{6.27}$$

$*$ *Pour l'espace* $W_T = H^1\Big(\mathbb{R}, L^2(S)\Big)$

Nous notons $W_{h,T}$ l'espace d'approximation de l'espace W_T. Cet espace est constitué de fonctions constantes par morceaux $\mathbb{P}_1$ dans la direction x_3 et à valeurs dans l'espace $L^2(S)$.

$$W_{h,T} := \Big\{r_T : \Omega \to \mathbb{R} \;/\; r_T|_{\mathcal{C}_{j+\frac{1}{2}}} \in \mathbb{P}_1\Big(\mathbb{R}; L^2(S)\Big)\, \forall\, j\Big\}. \tag{6.28}$$

En d'autres termes, pour tout $r_T \in \mathbf{W}_{h,T}$, il existe $r_{T,j} \in L^2(S)^2,\ j \in \mathbb{Z}$ tel que

$$r_T(\mathbf{x}_T, x_3) = \sum_{j\in\mathbb{Z}} r_{T,j}(\mathbf{x}_T)\, \omega_j(x_3), \quad r_{T,j} = r_T|_{S_j}. \tag{6.29}$$

$*$ *Pour l'espace* $\mathbf{W}_T = L^2(\Omega)^2$

Nous notons $\mathbf{W}_{h,T}$ l'espace d'approximation de l'espace $\mathbf{W}_T$. Cet espace est constitué de fonctions constantes par morceaux $\mathbb{P}_0$ dans la direction x_3 et à valeurs dans l'espace $L^2(S)^2$.

$$\mathbf{W}_{h,T} := \Big\{\boldsymbol{r}_3 : \Omega \to \mathbb{R}^2 \;/\; \boldsymbol{r}_3|_{\mathcal{C}_{j+\frac{1}{2}}} \in \mathbb{P}_0\Big(\mathbb{R}; L^2(S)^2\Big)\, \forall\, j\Big\}. \tag{6.30}$$

En d'autres termes, pour tout $\boldsymbol{r}_3 \in \mathbf{W}_{h,T}$, il existe $\boldsymbol{r}_{3,j+\frac{1}{2}} \in L^2(S)^2,\ j \in \mathbb{Z}$ tel que

$$\boldsymbol{r}_3(\mathbf{x}_T, x_3) = \sum_{j\in\mathbb{Z}} \boldsymbol{r}_{3,j+\frac{1}{2}}(\mathbf{x}_T)\, \chi_{j+\frac{1}{2}}(x_3), \quad \boldsymbol{r}_{3,j+\frac{1}{2}} = \boldsymbol{r}_3|_{S_{j+\frac{1}{2}}}. \tag{6.31}$$

Le problème semi-discret est obtenu essentiellement en réécrivant la formulation variationnelle (6.58) après avoir remplacé les espaces continus par leurs sous-espaces semi-discrets. Plus précisément, ce problème semi-discret s'écrit comme suit :

Trouver $\Big(\mathbf{E}_{T,h}, E_{3,h}\Big) \in \mathbf{V}_h$ et $(\boldsymbol{\phi}_h, r_{T,h}, \boldsymbol{r}_{3,h}) \in \mathbf{W}_h \times \mathbf{W}_{h,T} \times W_{h,3}$ tel que pour toute

fonction test $\Big(\widetilde{\mathbf{E}}_{T,h}, \widetilde{E}_{3,h}\Big) \in V$ et $(\widetilde{\boldsymbol{\phi}}_h, \widetilde{r}_{T,h}, \widetilde{\boldsymbol{r}}_{3,h}) \in \mathbf{W}_h \times \mathbf{W}_{h,T} \times W_{h,3}$, nous avons,

$$
\left|\begin{array}{ll}
\dfrac{d^2}{dt^2}\,\mathbf{m}_h\Big(\mathbf{E}_{T,h}, \widetilde{\mathbf{E}}_{T,h}\Big) & + \mathbf{k}_3\Big(\mathbf{E}_{T,h}, \widetilde{\mathbf{E}}_{T,h}\Big) + \mathbf{k}_{T,h}\Big(\mathbf{E}_{T,h}, \widetilde{\mathbf{E}}_{T,h}\Big) - c_{3T}\Big(E_{3,h}, \widetilde{\mathbf{E}}_{T,h}\Big) \\
& + \dfrac{d}{dt}\,\mathbf{m}_{\varepsilon\,\xi,h}\Big(\mathbf{E}_{T,h}, \widetilde{\mathbf{E}}_{T,h}\Big) + \mathbf{p}^T_{\mu^{-1},h}\Big(r_{T,h}, , \widetilde{\mathbf{E}}_{T,h}\Big) - \mathbf{p}^3_{\mu^{-1}}\Big(\boldsymbol{\phi}_h, \widetilde{\mathbf{E}}_{T,h}\Big) = 0, \\
\dfrac{d^2}{dt^2}\,m\Big(E_{3,h}, \widetilde{E}_{3,h}\Big) & + k_T\Big(E_{3,h}, \widetilde{E}_{3,h}\Big) - c_{3T}\Big(\widetilde{E}_{3,h}, \mathbf{E}_{T,h}\Big) \\
& + \dfrac{d}{dt}\,m_{\varepsilon\,\xi}\Big(E_{3,h}, \widetilde{E}_{3,h}\Big) + p^T_{\mu^{-1}}\Big(\boldsymbol{r}_{3,h}, \widetilde{E}_{3,h}\Big) = 0, \\
\dfrac{d}{dt}\,\mathbf{m}_1\Big(\boldsymbol{\phi}_h, \widetilde{\boldsymbol{\phi}}_h\Big) & + \mathbf{m}_\xi\Big(\boldsymbol{\phi}_h, \widetilde{\boldsymbol{\phi}}_h\Big) = \mathbf{p}^3_\xi\Big(\widetilde{\boldsymbol{\phi}}_h, \mathbf{E}_{T,h}\Big), \\
\dfrac{d}{dt}\,m_{1,h}\Big(r_{T,h}, \widetilde{r}_{T,h}\Big) & = \mathbf{p}^T_{\xi,h}\Big(\widetilde{r}_{T,h}, \mathbf{E}_{T,h}\Big), \\
\dfrac{d}{dt}\,\mathbf{m}_1\Big(\boldsymbol{r}_{3,h}, \widetilde{\boldsymbol{r}}_{3,h}\Big) & = p^T_\xi\Big(\widetilde{\boldsymbol{r}}_{3,h}, E_{3,h}\Big).
\end{array}\right. \tag{6.32}
$$

Comme nous l'avons fait dans le chapitre 2, les formes bilinéaires d'indice h, sont traitées par une formule de quadrature dans la direction x_3. Plus précisément, par rapport à leurs expressions exactes dans (6.18), nous les avons approchées par une formule de quadrature qui est définie comme suit :

$$
\int_\Omega \varepsilon\, f \to \oint_\Omega \varepsilon\, f, \quad \int_\Omega \mu^{-1}\, f \to \oint_\Omega \mu^{-1}\, f, \tag{6.33}
$$

où $\oint_\Omega \varepsilon\, f$ (resp. $\oint_\Omega \mu^{-1}\, f$) correspond à la formule de quadrature dans la direction x_3. Plus précisément, pour $f \in C^0\Big(\mathbb{R}; L^1(S)\Big) \cap L^1\Big(\Omega\Big)$, nous avons :

$$
\oint_\Omega \varepsilon\, f = h \sum_j \int_S \varepsilon_{j+\frac{1}{2}} \left(\frac{f_{j+1} + f_j}{2}\right) d\mathbf{x}_T, \quad f_j = f|_{S_j}, \tag{6.34}
$$

avec pour $\mathbf{x}_T \in S$,

$$
\varepsilon_{j+\frac{1}{2}}(\mathbf{x}_T) = \frac{1}{h} \int_{jh}^{(j+1)h} \varepsilon(\mathbf{x}_T, x_3)\, dx_3. \tag{6.35}
$$

Nous rappelons ici les expressions des formes bilinéaires trouvées au chapitre 2 après avoir utilisé la formule de quadrature,

$$
\begin{aligned}
&m\Big(E_{3,h},\widetilde{E}_{3,h}\Big)=\sum_{j\in\mathbb{Z}} m_{j+\frac12}\Big(E_{3,j+\frac12},\widetilde{E}_{3,j+\frac12}\Big)\equiv\ h\ \sum_{j\in\mathbb{Z}}\int_{S_{j+\frac12}}\varepsilon_j\,E_{3,j+\frac12}\,\widetilde{E}_{3,j+\frac12},\\
&k_T\Big(E_{3,h},\widetilde{E}_{3,h}\Big)=\sum_{j\in\mathbb{Z}} k_{j+\frac12}\Big(E_{3,j+\frac12},\widetilde{E}_{3,j+\frac12}\Big)\equiv\ h\ \sum_{j\in\mathbb{Z}}\int_{S_{j+\frac12}}\mu^{-1}_{j+\frac12}\,\nabla_T E_{3,j+\frac12}\cdot\nabla_T\widetilde{E}_{3,j+\frac12},\\
&\mathbf{m}_h\Big(\mathbf{E}_{T,h},\widetilde{\mathbf{E}}_{T,h}\Big)=\sum_{j\in\mathbb{Z}}\mathbf{m}_{h,j}\Big(\mathbf{E}_{T,j},\widetilde{\mathbf{E}}_{T,j}\Big)\equiv h\sum_{j\in\mathbb{Z}}\int_{S_j}\varepsilon_j\,\mathbf{E}_{T,j}\cdot\widetilde{\mathbf{E}}_{T,j},\\
&\mathbf{k}_{T,h}\Big(\mathbf{E}_{T,h},\widetilde{\mathbf{E}}_{T,h}\Big)=\sum_{j\in\mathbb{Z}}\mathbf{k}_{h,j}\Big(\mathbf{E}_{T,j},\widetilde{\mathbf{E}}_{T,j}\Big)\equiv h\sum_{j\in\mathbb{Z}}\int_{S_j}\mu_j^{-1}\,\mathrm{rot}_T\mathbf{E}_{T,j}\,\mathrm{rot}_T\widetilde{\mathbf{E}}_{T,j},\\
&\mathbf{k}_3\Big(\mathbf{E}_{T,h},\widetilde{\mathbf{E}}_{T,h}\Big)=h\sum_{j\in\mathbb{Z}}\int_S\mu^{-1}_{j+\frac12}\,\frac{\mathbf{E}_{T,j+1}-\mathbf{E}_{T,j}}{h}\cdot\frac{\widetilde{\mathbf{E}}_{T,j+1}-\widetilde{\mathbf{E}}_{T,j}}{h},\\
&c_{3T}\Big(E_{3,h},\widetilde{\mathbf{E}}_{T,h}\Big)=h\sum_{j\in\mathbb{Z}}\int_S\mu^{-1}_{j+\frac12}\,\mu^{-1}_{j+\frac12}\nabla_T E_{3,j+\frac12}\cdot\frac{\widetilde{\mathbf{E}}_{T,j+1}-\widetilde{\mathbf{E}}_{T,j}}{h}.
\end{aligned}
\tag{6.36}
$$

où comme dans (6.35), nous avons défini

$$
\mu^{-1}_{j+\frac12}(\mathbf{x}_T)=\frac1h\int_{jh}^{(j+1)h}\mu^{-1}(\mathbf{x}_T,x_3)\,dx_3\quad\forall\,\mathbf{x}_T\in S.
$$

De même, les formes bilinéaires (6.19) sont réécrites comme suit,

$$
\begin{aligned}
\mathbf{m}_\alpha\Big(\boldsymbol{\phi}_h,\widetilde{\boldsymbol{\phi}}_h\Big)\quad&=\ h\ \sum_{j\in\mathbb{Z}}\int_{S_{j+\frac12}}\alpha_{j+\frac12}\,\boldsymbol{\phi}_{j+\frac12}\cdot\widetilde{\boldsymbol{\phi}}_{j+\frac12},\\
m_{\alpha,h}\Big(r_{T,h},\widetilde{r}_{T,h}\Big)\quad&=\ h\sum_{j\in\mathbb{Z}}\int_{S_j}\alpha_j\,r_{T,j}\,\widetilde{r}_{T,j},\\
\mathbf{p}^3_\alpha\Big(\boldsymbol{\phi},\mathbf{E}_{T,h}\Big)\quad&=h\ \sum_{j\in\mathbb{Z}}\int_{S_{j+\frac12}}\alpha_{j+\frac12}\,\boldsymbol{\phi}_{j+\frac12}\cdot\frac{\mathbf{E}_{T,j+1}-\mathbf{E}_{T,j}}{h},\\
\mathbf{p}^T_{\alpha,h}\Big(r_{T,h},\mathbf{E}_{T,h}\Big)\quad&=\ h\sum_{j\in\mathbb{Z}}\int_{S_j}\alpha_j\,r_{T,j}\,\mathrm{rot}_T\,\mathbf{E}_{T,j},\\
p^T_\alpha\Big(\widetilde{\boldsymbol{r}}_{3,h},E_3\Big)\quad&=\ h\ \sum_{j\in\mathbb{Z}}\int_{S_{j+\frac12}}\alpha_{j+\frac12}\,\boldsymbol{r}_{3,j+\frac12}\cdot\mathbf{rot}_T\,E_{3,j+\frac12},
\end{aligned}
\tag{6.37}
$$

avec la définition,

$$
\alpha_{j+\frac12}(\mathbf{x}_T)=\frac1h\int_{jh}^{(j+1)h}\alpha(\mathbf{x}_T,x_3)\,dx_3\quad\forall\,\mathbf{x}_T\in S.
\tag{6.38}
$$

Discrétisation spatiale globale

Pour la discrétisation transversale, nous introduisons un maillage triangulaire conforme $\mathcal{T}$ (au sens habituel des éléments finis) de S avec un pas transversal h_T.

Dans la suite, nous notons N le nombre de nœuds de ce maillage, N_e le nombre d'arêtes et N_t le nombre de triangles.

Nous introduisons maintenant les espaces totalement discrets, indexés par $\mathbf{h}$ qui prennent les mêmes formes que les espaces semi-discrets.

• Nous notons $\mathbf{V_h}$ l'espace d'approximation de l'espace 3D $H(\mathbf{rot};\Omega)$,

$$\mathbf{V_h} = \mathbf{V_{h,T}} \times V_{\mathbf{h},\ell}.$$

Le champ transverse $\mathbf{E_T}$ est constitué de $\mathbb{P}_1$ fonctions continues dans la direction x_3 et à valeurs dans l'espace classique 2D de Nédélec.

$$\mathbf{V_{h,T}} := \Big\{ \mathbf{E}_{T,h} \in C^0\Big(\mathbb{R}; \mathbf{V}_{h_T}(S)\Big) \ / \ \mathbf{E}_T|_{\mathcal{C}_{j+\frac{1}{2}}} \in \mathbb{P}_1\Big(\mathbb{R}; \mathbf{V}_{h_T}(S)\Big) \ \forall\, j \Big\}, \tag{6.39}$$

avec
$$\begin{cases} \mathbf{V}_{h_T}(S) := \Big\{ \mathbf{E}_T \in H(\mathrm{rot}_T, S)\Big) \ / \ \forall\, K \in \mathcal{T}, \mathbf{E}_T|_K \in \mathcal{N}_{2D} \Big\}, \\ \mathcal{N}_{2D} := \Big\{ a\,(x_2, -x_1)^t + \mathbf{b}, (a,\mathbf{b}) \in \mathbb{R}\times\mathbb{R}^2 \Big\} \subset \mathbb{P}_1 \times \mathbb{P}_1. \end{cases} \tag{6.40}$$

D'autre part, l'espace $V_{h,\ell}$ est constitué de fonctions constantes par morceaux $\mathbb{P}_0$ dans la direction x_3 et à valeurs dans $\mathbb{P}_1$.

$$\begin{cases} V_{\mathbf{h},\ell} := \Big\{ E_3 : \Omega \to \mathbb{R} \ / \ \forall\, j, \forall\, x_3 \in [jh, (j+1)h] \ \ E_3(\cdot, x_3) = E_{3,j+\frac{1}{2}} \in V_{h_T}(S) \Big\}, \\ V_{h_T}(S) := \Big\{ E_3 \in H^1(S) \ / \ \forall\, K \in \mathcal{T}, \ E_3|_K \in \mathbb{P}_1 \Big\}. \end{cases} \tag{6.41}$$

• Nous notons $\mathbf{W_h}$ l'espace d'approximation de l'espace $\mathbf{W}$. Cet espace est constitué de fonctions constantes par morceaux $\mathbb{P}_0$ dans la direction x_3 et à valeurs dans l'espace classique 2D de Nedelec.

$$\mathbf{W}_h := \Big\{ \boldsymbol{\phi} : \Omega \to \mathbb{R}^2 \ / \ \boldsymbol{\phi}|_{\mathcal{C}_{j+\frac{1}{2}}} \in \mathbb{P}_0\Big(\mathbb{R}; \mathbf{V}_{h_T}(S)\Big) \, \forall\, j \Big\}, \tag{6.42}$$

avec $\mathbf{V}_{h_T}(S)$ défini dans (6.40).

• Nous notons $W_{h,T}$ l'espace d'approximation de l'espace W_T. Cet espace est constitué de fonctions constantes par morceaux $\mathbb{P}_1$ dans la direction x_3 et à valeurs dans $\mathbb{P}_0$.

$$W_{h,T} := \Big\{ r_T : \Omega \to \mathbb{R} \ / \ r_T|_{\mathcal{C}_{j+\frac{1}{2}}} \in \mathbb{P}_1\Big(\mathbb{R}; \mathbb{P}_0(S)\Big) \, \forall\, j \Big\}, \tag{6.43}$$

avec $\mathbb{P}_0(S)$ défini par :

$$\mathbb{P}_0(S) := \Big\{ u \in L^2(S) \ / \ \forall\, K \in \mathcal{T}, \ u|_K \in \mathbb{P}_0 \Big\}. \tag{6.44}$$

• Nous notons $\mathbf{W}_{h,T}$ l'espace d'approximation de l'espace $\mathbf{W}_T$. Cet espace est constitué de fonctions constantes par morceaux $\mathbb{P}_0$ dans la direction x_3 et à valeurs dans $\mathbb{P}_0 \times \mathbb{P}_0$.

$$\mathbf{W}_{h,T} := \Big\{ \boldsymbol{r}_3 : \Omega \to \mathbb{R}^2 \ / \ \boldsymbol{r}_3|_{\mathcal{C}_{j+\frac{1}{2}}} \in \mathbb{P}_0\Big(\mathbb{R}; \mathbb{P}_0(S)^2\Big) \, \forall\, j \Big\}, \tag{6.45}$$

avec $\mathbf{V}_{h_T}(S)$ défini dans (6.44).

Le problème discret en espace est obtenu en réécrivant la formulation variationnelle (6.32) après avoir remplacé les espaces semi-discrets par les espaces totalement discrets.
Plus précisément, ce problème semi-discret s'écrit comme suit :

Trouver $\big(\mathbf{E}_{T,\mathbf{h}}, E_{3,\mathbf{h}}\big) \in \mathbf{V_h}$ et $(\boldsymbol{\phi}_\mathbf{h}, r_{T,\mathbf{h}}, \boldsymbol{r}_{3,\mathbf{h}}) \in \mathbf{W_h} \times \mathbf{W}_{\mathbf{h},T} \times W_{\mathbf{h},3}$ tel que pour toute fonction test $\big(\widetilde{\mathbf{E}}_{T,\mathbf{h}}, \widetilde{E}_{3,\mathbf{h}}\big) \in V_\mathbf{h}$ et $(\widetilde{\boldsymbol{\phi}}_\mathbf{h}, \widetilde{r}_{T,\mathbf{h}}, \widetilde{\boldsymbol{r}}_{T,\mathbf{h}}) \in \mathbf{W_h} \times \mathbf{W}_{\mathbf{h},T} \times W_{\mathbf{h},3}$, nous avons,

$$
\left|\begin{array}{ll}
\dfrac{d^2}{dt^2}\,\mathbf{m}_h\big(\mathbf{E}_{T,\mathbf{h}}, \widetilde{\mathbf{E}}_{T,\mathbf{h}}\big) & + \mathbf{k}_3\big(\mathbf{E}_{T,\mathbf{h}}, \widetilde{\mathbf{E}}_{T,\mathbf{h}}\big) + \mathbf{k}_{T,h}\big(\mathbf{E}_{T,\mathbf{h}}, \widetilde{\mathbf{E}}_{T,\mathbf{h}}\big) - c_{3T}\big(E_{3,\mathbf{h}}, \widetilde{\mathbf{E}}_{T,\mathbf{h}}\big) \\
& + \dfrac{d}{dt}\,\mathbf{m}_{\varepsilon\,\xi,h}\big(\mathbf{E}_{T,\mathbf{h}}, \widetilde{\mathbf{E}}_{T,\mathbf{h}}\big) + \mathbf{p}^T_{\mu^{-1},h}\big(r_{T,\mathbf{h}}, , \widetilde{\mathbf{E}}_{T,\mathbf{h}}\big) - \mathbf{p}^3_{\mu^{-1}}\big(\boldsymbol{\phi}_\mathbf{h}, \widetilde{\mathbf{E}}_{T,\mathbf{h}}\big) = 0, \\
\dfrac{d^2}{dt^2}\,m\big(E_{3,\mathbf{h}}, \widetilde{E}_{3,\mathbf{h}}\big) & + k_T\big(E_{3,\mathbf{h}}, \widetilde{E}_{3,\mathbf{h}}\big) - c_{3T}\big(\widetilde{E}_{3,\mathbf{h}}, \mathbf{E}_{T,\mathbf{h}}\big) \\
& + \dfrac{d}{dt}\,m_{\varepsilon\,\xi}\big(E_{3,\mathbf{h}}, \widetilde{E}_{3,\mathbf{h}}\big) + p^T_{\mu^{-1}}\big(\boldsymbol{r}_{3,h}, \widetilde{E}_{3,\mathbf{h}}\big) = 0, \\
\dfrac{d}{dt}\,\mathbf{m}_1\big(\boldsymbol{\phi}_\mathbf{h}, \widetilde{\boldsymbol{\phi}}_\mathbf{h}\big) & + \mathbf{m}_\xi\big(\boldsymbol{\phi}_\mathbf{h}, \widetilde{\boldsymbol{\phi}}_\mathbf{h}\big) = \mathbf{p}^3_\xi\big(\widetilde{\boldsymbol{\phi}}_\mathbf{h}, \mathbf{E}_{T,\mathbf{h}}\big), \\
\dfrac{d}{dt}\,m_{1,h}\big(r_{T,\mathbf{h}}, \widetilde{r}_{T,\mathbf{h}}\big) & = \mathbf{p}^T_{\xi,h}\big(\widetilde{r}_{T,\mathbf{h}}, \mathbf{E}_{T,\mathbf{h}}\big), \\
\dfrac{d}{dt}\,\mathbf{m}_1\big(\boldsymbol{r}_{3,h}, \widetilde{\boldsymbol{r}}_{3,h}\big) & = p^T_\xi\big(\widetilde{\boldsymbol{r}}_{3,h}, E_{3,\mathbf{h}}\big).
\end{array}\right. \tag{6.46}
$$

La forme algébrique

Pour écrire le problème sous une forme algébrique, nous introduisons ici les vecteurs des degrés de liberté,

$$
\bullet\ \mathbb{E}_\mathbf{h} = \begin{pmatrix} \mathbb{E}_{T,\mathbf{h}} \\ \mathbb{E}_{3,\mathbf{h}} \end{pmatrix} \equiv \begin{pmatrix} \{\mathbb{E}_{T,j}\} \\ \{\mathbb{E}_{3,j+\frac{1}{2}}\} \end{pmatrix} \in \mathbb{V}_\mathbf{h} := \mathbb{V}_{\mathbf{h},T} \times \mathbb{V}_{\mathbf{h},3},
$$

où $\mathbb{V}_{\mathbf{h},T}$ et $\mathbb{V}_{\mathbf{h},3}$ sont deux espaces de Hilbert,

$$
\mathbb{V}_{\mathbf{h},T} = \ell^2\big(\mathbb{Z}, \mathbb{R}^{N_e}\big), \quad \mathbb{V}_{\mathbf{h},3} = \ell^2(\mathbb{Z}, \mathbb{R}^N).
$$

$$
\bullet\ \mathbb{R}_\mathbf{h} = \begin{pmatrix} \mathbf{\Phi}_\mathbf{h} \\ \mathbb{R}_{T,\mathbf{h}} \\ \mathbb{R}_{3,\mathbf{h}} \end{pmatrix} \equiv \begin{pmatrix} \{\mathbf{\Phi}_{j+\frac{1}{2}}\} \\ \{\mathbb{R}_{T,j}\} \\ \{\mathbb{R}_{3,j+\frac{1}{2}}\} \end{pmatrix} \in \mathbb{W}_\mathbf{h} \times \mathbb{W}_{\mathbf{h},T} \times \mathbb{W}_{\mathbf{h},3},
$$

où $\mathbb{W}_\mathbf{h}$, $\mathbb{W}_{\mathbf{h},T}$ et $\mathbb{W}_{\mathbf{h},3}$ sont trois espaces de Hilbert,

$$
\mathbb{W}_\mathbf{h} := \ell^2(\mathbb{Z}, \mathbb{R}^{N_e}), \quad \mathbb{W}_{\mathbf{h},T} := \ell^2\big(\mathbb{Z}, \mathbb{R}^{N_t}\big), \quad \mathbb{W}_{\mathbf{h},3} := \ell^2(\mathbb{Z}, \mathbb{R}^{N_t}).
$$

Il est clair que le problème (6.46) a la forme algébrique suivante,

$$\left|\begin{array}{l} \mathbf{M_h}\dfrac{d^2\mathbb{E}_\mathbf{h}}{dt^2} + \mathbf{K_h}\,\mathbb{E}_\mathbf{h} + \mathbf{M}_{\mathbf{h},1}\dfrac{d\,\mathbb{R}_\mathbf{h}}{dt} + \mathbf{P}_{\mathbf{h},1}\,\mathbb{R}_\mathbf{h} = 0, \\ \mathbf{M}_{\mathbf{h},2}\dfrac{d\,\mathbb{R}_\mathbf{h}}{dt} + \mathbf{M}_{\mathbf{h},3}\,\mathbb{R}_\mathbf{h} = \mathbf{P}_{\mathbf{h},2}\,\mathbb{E}_\mathbf{h}, \end{array}\right. \tag{6.47}$$

où $\mathbf{M_h}$ et $\mathbf{K_h}$ sont les matrices de masse et de rigidité. Selon la décomposition de $\mathbb{V}_\mathbf{h}$ entre champs transversaux et longitudinaux, ces matrices ont les formes suivantes :

$$\mathbf{M_h} = \begin{pmatrix} \mathbf{M}_\mathbf{h}^T & 0 \\ 0 & M_\mathbf{h}^3 \end{pmatrix}, \quad \mathbf{K_h} = \begin{pmatrix} \mathbf{K}_{3,\mathbf{h}} + \mathbf{K}_{T,\mathbf{h}} & \mathbf{C}_{3T,\mathbf{h}} \\ \mathbf{C}^*_{3T,\mathbf{h}} & K_{T,\mathbf{h}} \end{pmatrix}. \tag{6.48}$$

Notez que ces matrices ont les mêmes notations que dans le chapitre 2.

Les autres nouvelles matrices signifient la présence de couches PML ont les structures suivantes,

$$\mathbf{M}_{\mathbf{h},1} = \begin{pmatrix} 0 & \mathbf{M}_{\varepsilon\xi,\mathbf{h}} & 0 \\ 0 & 0 & M_{\varepsilon\xi,\mathbf{h}} \end{pmatrix}, \quad \mathbf{P}_{\mathbf{h},1} = \begin{pmatrix} -\mathbf{P}^3_{\mu^{-1},\mathbf{h}} & \mathbf{P}^T_{\mu^{-1},\mathbf{h}} & 0 \\ 0 & 0 & P^T_{\mu^{-1},\mathbf{h}} \end{pmatrix},$$

$$\mathbf{M}_{\mathbf{h},2} = \begin{pmatrix} \mathbf{M}_{1,\mathbf{h}} & 0 & 0 \\ 0 & M_{1,\mathbf{h}} & 0 \\ 0 & 0 & \mathbf{M}_{1,\mathbf{h}} \end{pmatrix}, \quad \mathbf{M}_{\mathbf{h},3} = \begin{pmatrix} \mathbf{M}_{\xi,\mathbf{h}} & 0 & 0 \\ 0 & 0 & 0 \\ 0 & 0 & 0 \end{pmatrix}, \quad \mathbf{P}_{\mathbf{h},2} = \begin{pmatrix} (\mathbf{P}^3_{\xi,\mathbf{h}})^* & 0 \\ (\mathbf{P}^T_{\xi,\mathbf{h}})^* & 0 \\ 0 & (P^T_{\xi,\mathbf{h}})^* \end{pmatrix}.$$

6.2.4 Discrétisation temporelle explicite/implicite

Comme au chapitre 2, nous commençons par la décomposition de la matrice de rigidité K_h en deux matrices : la première est K_h^e adaptée à une discrétisation temporelle explicite, et la seconde est K_h^i adaptée à une discrétisation implicite.

$$\mathbf{K_h} = \mathbf{K_h^i} + \mathbf{K_h^e} \quad \text{où} \quad \mathbf{K_h^i} = \begin{pmatrix} \mathbf{K}_{T,\mathbf{h}} & 0 \\ 0 & K_{T,\mathbf{h}} \end{pmatrix} \quad \text{and} \quad \mathbf{K_h^e} = \begin{pmatrix} \mathbf{K}_{3,\mathbf{h}} & \mathbf{C}_{3T,\mathbf{h}} \\ \mathbf{C}^*_{3T,\mathbf{h}} & 0 \end{pmatrix}. \tag{6.49}$$

En utilisant (6.49), la forme algébrique (6.47) se réécrit comme suit,

$$\left|\begin{array}{l} \mathbf{M_h}\dfrac{d^2\mathbb{E}_\mathbf{h}}{dt^2} + \mathbf{K_h^e}\,\mathbb{E}_\mathbf{h} + \mathbf{K_h^i}\,\mathbb{E}_\mathbf{h} + \mathbf{M}_{\mathbf{h},1}\dfrac{d\,\mathbb{R}_\mathbf{h}}{dt} + \mathbf{P}_{\mathbf{h},1}\,\mathbb{R}_\mathbf{h} = 0, \\ \mathbf{M}_{\mathbf{h},2}\dfrac{d\,\mathbb{R}_\mathbf{h}}{dt} + \mathbf{M}_{\mathbf{h},3}\,\mathbb{R}_\mathbf{h} = \mathbf{P}_{\mathbf{h},2}\,\mathbb{E}_\mathbf{h}, \end{array}\right.$$

Nous allons discrétiser les nouveaux termes apparaissant dans les deux couches PML selon le schéma proposé dans [7] (Page 20), et le reste selon le même schéma proposé dans le chapitre 2. Ainsi, nous proposons le schéma suivant :

$$\left|\begin{array}{l} \mathbf{M_h}\dfrac{\mathbb{E}^{n+1}_\mathbf{h} - 2\,\mathbb{E}^n_\mathbf{h} + \mathbb{E}^{n-1}_\mathbf{h}}{\Delta t^2} + \mathbf{K_h^i}\,\{\mathbb{E}^n_\mathbf{h}\}_\theta + \mathbf{K_h^e}\,\mathbb{E}^n_\mathbf{h} + \mathbf{M}_{\mathbf{h},1}\dfrac{\mathbb{R}^{n+1}_\mathbf{h} - \mathbb{R}^{n-1}_\mathbf{h}}{2\Delta t} + \mathbf{P}_{\mathbf{h},1}\,\mathbb{R}^n_\mathbf{h} = 0, \\ \mathbf{M}_{\mathbf{h},2}\dfrac{\mathbb{R}^{n+1}_\mathbf{h} - \mathbb{R}^n_\mathbf{h}}{\Delta t} + \mathbf{M}_{\mathbf{h},3}\,\dfrac{\mathbb{R}^{n+1}_\mathbf{h} + \mathbb{R}^n_\mathbf{h}}{2} = \mathbf{P}_{\mathbf{h},2}\,\dfrac{\mathbb{E}^{n+1}_\mathbf{h} + \mathbb{E}^n_\mathbf{h}}{2}, \end{array}\right.$$

avec la notation

$$\{\mathbb{E}^n_\mathbf{h}\}_\theta := \theta\,\mathbb{E}^{n+1}_\mathbf{h} + (1-2\theta)\,\mathbb{E}^n_\mathbf{h} + \theta\,\mathbb{E}^{n-1}_\mathbf{h}, \quad \theta \in [0,1].$$

Remarque 6.2.2 (Étude de stabilité)**.** *La question de la stabilité de ce schéma proposé est une question ouverte pour le moment, il est à noter que pour le schéma proposé pour le cas des équations d'ondes avec PML (dans [7]) une étude de stabilité a été réalisée. Comme nous le verrons dans la section suivante, notre schéma devient instable dans le cas où la vitesse est variable.*

6.2.5 Simulations numériques

Les données du problème

Nous traitons un câble cylindrique Ω de longueur $L = 11$, et avec une section circulaire S de rayon intérieur $r_1 = 1$ et de rayon extérieur $r_2 = 2$ (voir Figure 6.3). Plus précisément :

$$\Omega = S \times [0, 11].$$

Ce câble est borné par deux couches PML Ω^+_{PML} et Ω^-_{PML}. Donc on peut le redéfinir comme suit

$$\Omega = \Omega \cup \Omega^+_{PML} \cup \Omega^-_{PML}.$$

avec $\Omega^-_{PML} = S \times [0, 1]$, $\Omega^+_{PML} = S \times [10, 11]$ sont les deux couches PML, et $\Omega_b = S \times [1, 10]$ est le domaine du calcul.

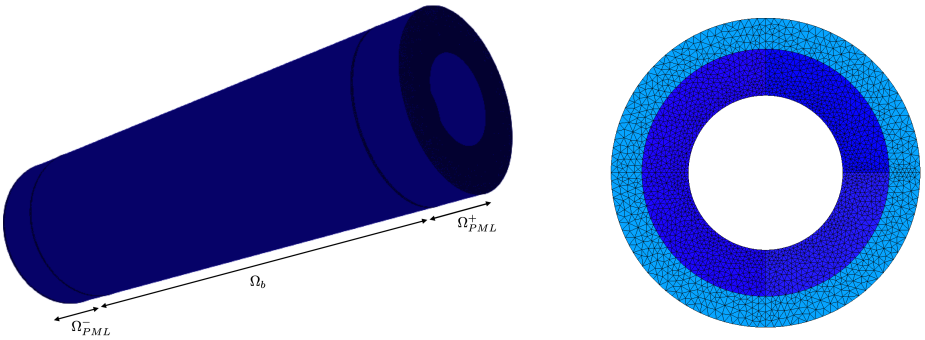

FIGURE 6.3 – À gauche : le domaine Ω, à droite : la section S du domaine. Chaque couleur correspond à un matériau différent.

Le câble est hétérogène au niveau des sections S. Plus précisément S est constituée de deux couches $S = S_1 \cup S_2$ et à l'intérieur de S_j, le matériau est homogène (voir Figure 6.3).

Pour tester les performances de notre méthode, nous allons considérer deux configurations,

— le cas de vitesse de propagation constante : nous allons prendre $(\varepsilon_1, \mu_1) = (2, 1)$ et $(\varepsilon_2, \mu_2) = (1, 2)$. Ainsi, la vitesse de propagation des ondes électromagnétiques est :

$$c(\mathbf{x}) = 1/\sqrt{2} \quad \text{dans} \quad \Omega_i := S_i \times [0, 11],\ i = 1, 2.$$

— le cas de vitesse de propagation variable : nous allons prendre $(\varepsilon_1, \mu_1) = (2, 1)$ et $(\varepsilon_2, \mu_2) = (2, 1)$. Ainsi, la vitesse de propagation des ondes électromagnétiques est :

$$c(\mathbf{x}) = \begin{cases} 1/2 & \text{dans} \quad \Omega_1 := S_1 \times [0, 11], \\ 1 & \text{dans} \quad \Omega_2 := S_2 \times [0, 11]. \end{cases}$$

Nous prenons des données initiales qui sont situées au centre du câble à $x_3 = 5.5$. Plus précisément, nous supposons que $\mathbf{H}_0(\mathbf{x}_T, x_3) = 0$ et que

$$\mathbf{E}_0(\mathbf{x}_T, x_3) := \mathcal{E}(x_3)\ \nabla_T\varphi(\mathbf{x}_T), \quad \mathcal{E}(x_3) = e^{-\pi^2\,(x_3-5.5)^2},$$

avec $\varphi(\mathbf{x}_T)$ est la solution de

$$\begin{cases} \mathrm{div}_T\Big(\varepsilon^0\,\nabla_T\varphi\Big) = 0 & \text{dans } S, \\ \varphi = 1 & \text{sur } \Gamma_i, \\ \varphi = 0 & \text{sur } \Gamma_e. \end{cases}$$

Pour le pas de temps Δt, nous utilisons la condition CFL du problème 3D (voir (2.48), Chapitre 2). En choisissant $\theta = 1/2$, (2.48) donne :

$$c^+\frac{\Delta t}{h} \leq \frac{1}{\sqrt{2}}, \quad \text{avec } c^+ := \sup_{\Omega} c(\mathbf{x}).$$

En pratique, nous choisirons $\Delta t = 0.95\ \ h/\sqrt{2}$, où $h = 0.05$ est le pas d'espace longitudinal. Le choix du terme d'amortissement $\xi(x_3) \geq 0$ est arbitraire. Dans nos simulations, nous utilisons ce choix trouvé dans [24].

$$\xi(x) = \begin{cases} 40\ \left(|x-1| - \dfrac{1}{2\pi}\sin(2\pi\,|x-1|)\right) & \text{si } x \in [0,1], \\ 0 & \text{si } x \in [1,10], \\ 40\ \left(|x-10| - \dfrac{1}{2\pi}\sin(2\pi\,|x-10|)\right) & \text{si } x \in [0,1] \end{cases} \tag{6.50}$$

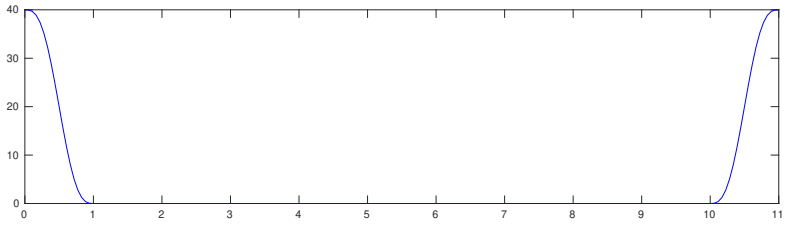

FIGURE 6.4 – Le terme d'amortissement ξ.

Tests numériques

Dans ce paragraphe nous allons présenter les résultats numériques que nous avons obtenus en utilisant la méthode présentée précédemment conjointement avec les données ci-dessus.

Dans cette configuration le champ longitudinal est presque nul (Voir la figure 6.6). Ainsi, nous représentons dans les figures 6.5 et 6.7 uniquement la propagation du champ $|\mathbf{E}_T|$ au cours du temps.

- *Le cas de vitesse de propagation constante.*

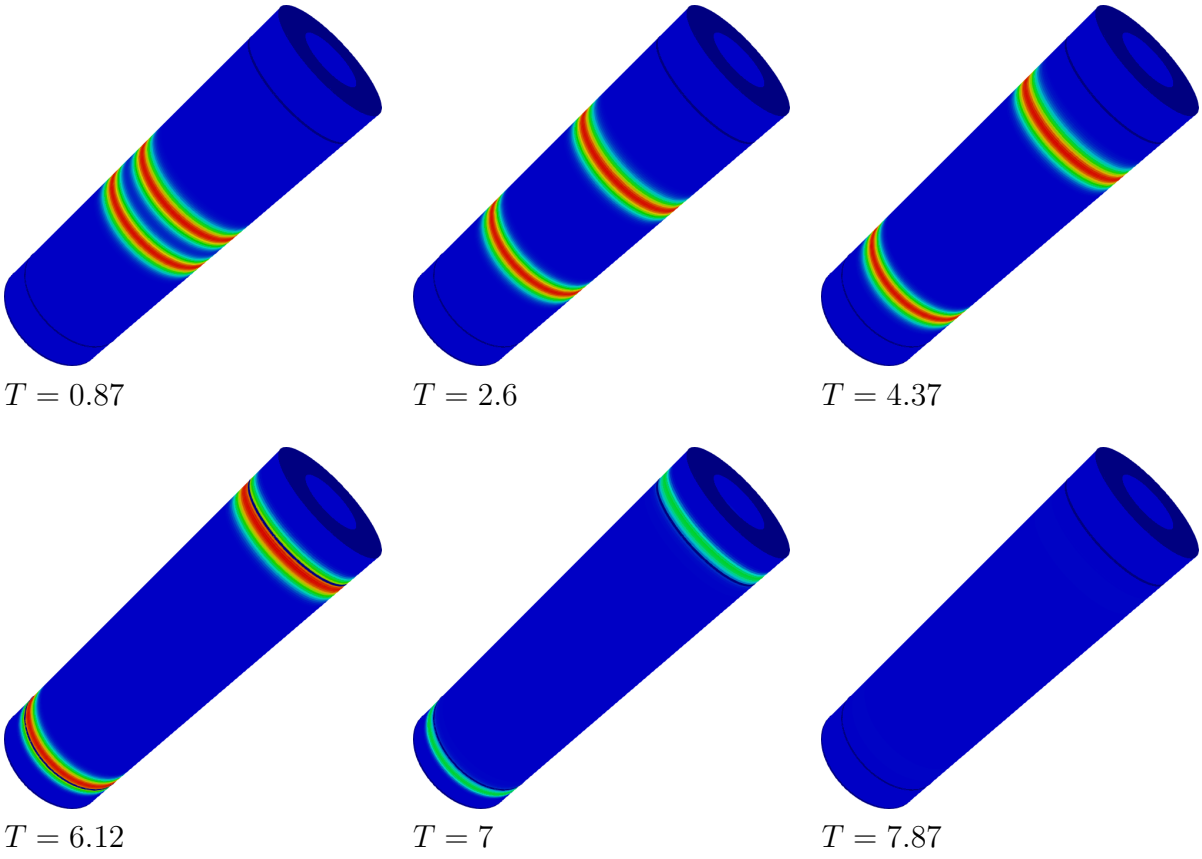

FIGURE 6.5 – La norme du champ transversal $|\mathbf{E}_T|$.

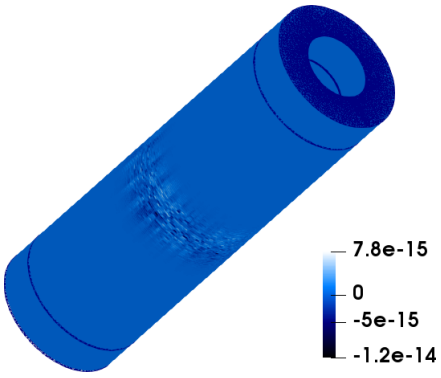

FIGURE 6.6 – Le champ longitudinal E_3 à $T = 0.87$.

- *Le cas de vitesse de propagation variable.*

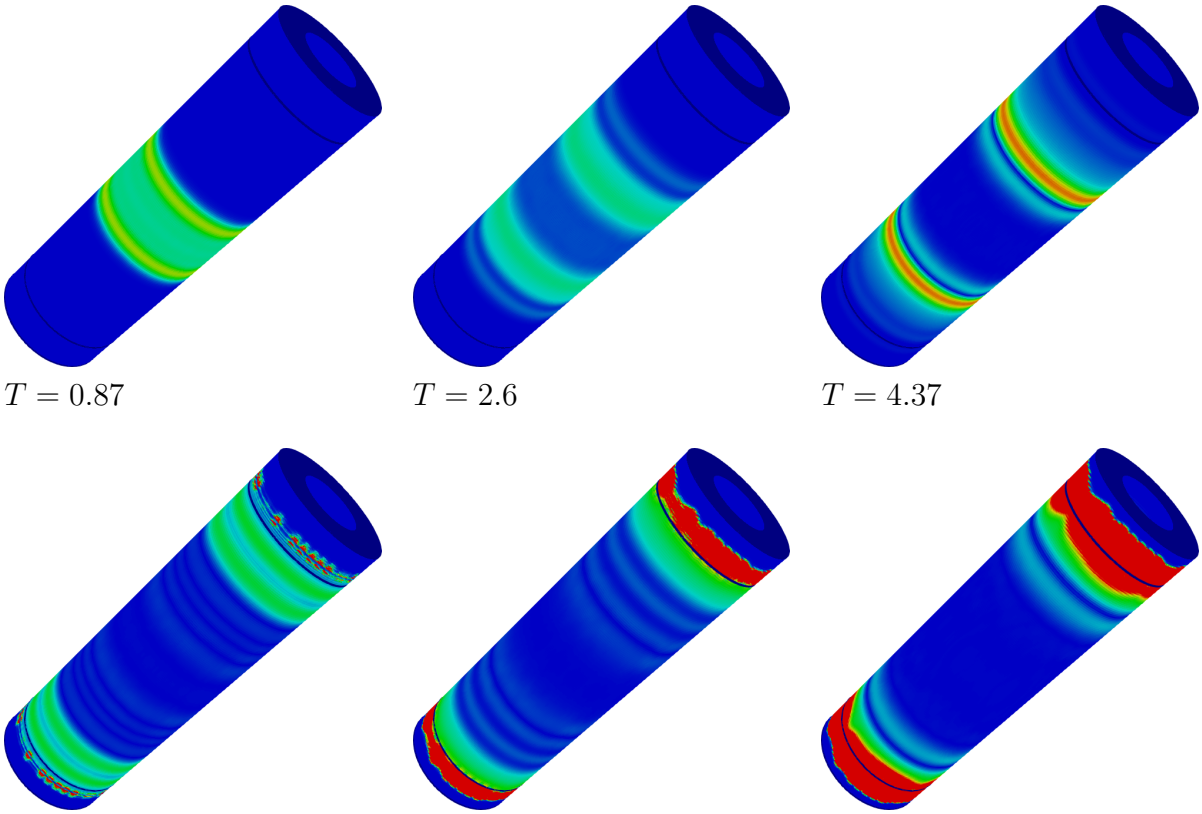

FIGURE 6.7 – La norme du champ transversal $|\mathbf{E}_T|$.

Discussions : Nous constatons que le comportement de la solution est diffèrent entre les deux tests. En effet, dans la première simulation (voir Figure 6.5) l'onde se propage le long du câble et vient s'atténuer dans les deux couches PML sans produire de réflexions parasites significatives : d'où l'efficacité de la méthode de PML dans cette configuration. Par contre lorsque la vitesse devient variable nous constatons que la solution se propage le long du câble mais explose lorsqu'elle atteint les deux couches PML (voir Figure 6.7) : On peut dire que les PML induisent une instabilité du schéma numérique proposé.

Il est à noter que ce phénomène d'instabilité a été déjà observé dans le contexte de la résolution numérique des équations de Maxwell anisotrope dans l'espace libre [9]. Ainsi, avec tous ces éléments, nous conjecturons que l'instabilité est présente sur le modèle continu et ne résulte pas du choix de la discrétisation (ou d'un bug informatique).

6.3 Construction des couches PML pour le modèle Télégraphique 1D d'ordre 2

6.3.1 Rappel du modèle 1D

Dans le chapitre 4, nous avons présenté un modèle dispersif 1D, qui est déduit à l'aide d'une analyse asymptotique appliquée aux équations de Maxwell 3D dans un câble coaxial

cylindrique mince. Nous avons supposé que les coefficients caractéristiques du matériau diélectrique, à savoir ε et μ, ne dépendent pas de la variable longitudinale x_3. Le modèle asymptotique obtenu est un modèle télégraphique du second ordre selon le paramètre δ, dont l'inconnue est V qui désigne la tension électrique. Ce modèle se présente comme suit,

$$(C - \delta^2\,\gamma_e\,\partial_3^2)\,\partial_t^2\,V - L^{-1}\,\partial_3^2\,V = 0, \tag{6.51}$$

avec

$$\gamma_e = \int_S \varepsilon\,|\varphi_e - \varphi_m|^2\,d\mathbf{x}_T, \quad C = \int_S \varepsilon\,|\varphi_e|^2\,d\mathbf{x}_T, \quad \text{et} \quad L = \int_S \mu\,|\psi_m|^2\,d\mathbf{x}_T. \tag{6.52}$$

Ici les potentiels φ_m et φ_e sont les solutions des problèmes suivants :

$$\begin{cases} \mathrm{div}_T\left(\mu^{-1}\,\nabla_T\,\varphi_m\right) = 0, & \text{in } S, \\ \varphi_m = 1, & \text{on } \Gamma_i, \\ \varphi_m = 0, & \text{on } \Gamma_e, \end{cases} \qquad \begin{cases} \mathrm{div}_T\left(\varepsilon\,\nabla_T\,\varphi_e\right) = 0, & \text{in } S, \\ \varphi_e = 1, & \text{on } \Gamma_i, \\ \varphi_e = 0, & \text{on } \Gamma_e, \end{cases} \tag{6.53}$$

et le potentiel ψ_m est la solution du problème suivant :

$$\begin{cases} \mathrm{div}_T\left(\mu\,\nabla_T\,\psi_m\right) = 0 & \text{in } S \setminus \Sigma, \\ \partial_n\psi_m = 0, & \text{on } \partial S, \\ [\psi_m]_\Sigma = 1, \quad [\partial_n\psi_m]_\Sigma = 0, & \text{through } \Sigma, \\ \displaystyle\int_S \psi_m\,d\mathbf{x}_T = 0, \end{cases} \tag{6.54}$$

L'objectif de la section suivante est de construire une formulation PML pour ce modèle asymptotique obtenu. Pour ce faire, nous répétons le même processus que celui effectué dans la section 6.2.2 pour les équations de Maxwell, ce qui fera l'objet de la section suivante.

6.3.2 Construction des couches PML

Nous commençons par appliquer la transformation de Laplace (6.8) à l'équation (6.51).

$$(C - \delta^2\,\gamma_e\,\partial_3^2)\,s^2\,\widehat{V} - L^{-1}\,\partial_3^2\,\widehat{V} = 0, \quad s \in \mathbb{C},\ x_3 \in \mathbb{R}. \tag{6.55}$$

Maintenant on applique le changement de variable (6.10) au problème (6.55), et en utilisant le fait que

$$\partial_{\widehat{x}_3} = \frac{s}{s+\xi}\,\partial_3,$$

nous obtenons le problème suivant

$$s^2\,C\,\widehat{V} - \delta^2\,\gamma_e\,s^2\,\frac{s}{s+\xi}\,\partial_3\,(\frac{s}{s+\xi}\,\partial_3\widehat{V}) - L^{-1}\,\frac{s}{s+\xi}\,\partial_3\,(\frac{s}{s+\xi}\,\partial_3\widehat{V}) = 0.$$

Si on multiplie cette équation par $1 + \dfrac{\xi}{s}$, nous obtenons

$$C\,(s^2 + s\,\xi)\,\widehat{V} - \delta^2\,\gamma_e\,s^2\,\partial_3\,(\frac{s}{s+\xi}\,\partial_3\widehat{V}) - L^{-1}\,\partial_3\,(\frac{s}{s+\xi}\,\partial_3\widehat{V}) = 0,$$

Maintenant, nous cherchons à trouver une formulation qui sépare les termes de la formulation (6.55) et les nouveaux termes qui dépendent de ξ et qui expliquent la présence des couches PML. Pour se faire nous utilisons l'égalité suivante

$$\frac{s}{s+\xi} = 1 - \frac{\xi}{s+\xi}.$$

Donc nous obtenons la formulation suivante :

$$\begin{aligned} & C\, s^2\, \widehat{V} - \delta^2\, \gamma_e\, s^2\, \partial_3^2\, \widehat{V} - L^{-1}\, \partial_3^2\, \widehat{V} \\ & \qquad + C\, s\, \xi\, \widehat{V} + \delta^2\, \gamma_e\, s^2\, \partial_3 \left(\frac{\xi}{s+\xi}\, \partial_3 \widehat{V}\right) + L^{-1}\, \partial_3 \left(\frac{\xi}{s+\xi}\, \partial_3 \widehat{V}\right) = 0. \end{aligned}$$

Nous définissons une nouvelle inconnue,

$$\widehat{U} = \frac{\xi}{s+\xi}\, \partial_3\, \widehat{V}. \tag{6.56}$$

Nous obtenons alors le système suivant,

$$\left| \begin{array}{l} C\, s^2\, \widehat{V} - \delta^2\, \gamma_e\, s^2\, \partial_3^2\, \widehat{V} - L^{-1}\, \partial_3^2\, \widehat{V} \\ \qquad + C\, s\, \xi\, \widehat{V} + \delta^2\, \gamma_e\, s^2\, \partial_3\, \widehat{U} + L^{-1}\, \partial_3\, \widehat{U} = 0, \\ (s+\xi)\, \widehat{U} = \xi\, \partial_3\, \widehat{V}. \end{array} \right.$$

En utilisant la transformation de Laplace inverse, nous pouvons revenir au régime temporel,

$$\left| \begin{array}{l} C\, \partial_t^2\, V - \delta^2\, \gamma_e\, \partial_t^2\, \partial_3^2\, V - L^{-1}\, \partial_3^2\, V \\ \qquad + C\, \xi\, \partial_t\, V + \delta^2\, \gamma_e\, \partial_t^2\, \partial_3\, U + L^{-1}\, \partial_3\, U = 0, \\ \partial_t\, U + \xi\, U = \xi\, \partial_3\, V. \end{array} \right. \tag{6.57}$$

Pour résoudre numériquement ce modèle obtenu, nous allons chercher une méthode de discrétisation en temps et en espace.

6.3.3 Discrétisation spatiale

Nous commençons cette section par donner une la formulation variationnelle du modèle obtenu (6.57). Nous cherchons la tension électrique V dans l'espace $H^1(\mathbb{R})$. Et en utilisant l'expression (6.56) de la nouvelle inconnue U, nous déduisons qu'il faut chercher U dans l'espace $L^2(\mathbb{R})$.

Pour résoudre numériquement ce modèle, nous allons résoudre le problème dans un domaine $[l, L]$, et nous allons borner ce domaine par deux couches PML $[0, l]$ et $[L, L+l]$ dans lesquelles $\xi > 0$ (voir Figure 6.8). les ondes sortantes du domaine du calcul seront atténuées dans les deux couches PML, pour cela nous pouvons tronquer artificiellement le domaine et en compléter le problème (6.57) par une condition de dirichlet homogène aux bout des deux couches PML.

Maintenant, nous pouvons introduire la formulation variationnelle du problème (6.57) :

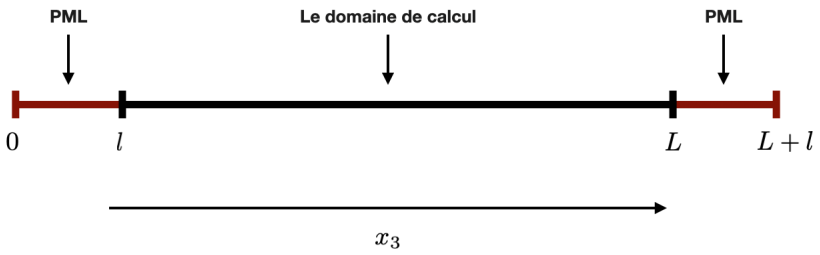

FIGURE 6.8 – Le domaine de calcul borné par deux couches PML.

Trouver $\big(V(t),U(t)\big) \in H_0^1([0,L+l]) \times L^2([0,L+l])$ tel que pour toute fonction test $\big(\widetilde{V},\widetilde{U}\big) \in H_0^1([0,L+l]) \times L^2([0,L+l])$, nous avons :

$$\left|\begin{array}{ll} C\,\dfrac{d^2}{dt^2}\,m\big(V,\widetilde{V}\big) & +\,\delta^2\,\gamma_e\,\dfrac{d^2}{dt^2}\,k\big(V,\widetilde{V}\big) + L^{-1}\,k\big(V,\widetilde{V}\big) \\ & +\,C\,\xi\,\dfrac{d}{dt}\,m\big(V,\widetilde{V}\big) - \delta^2\,\gamma_e\,\dfrac{d^2}{dt^2}\,p\big(U,\widetilde{V}\big) - L^{-1}\,p\big(U,\widetilde{V}\big) = 0, \\ \dfrac{d}{dt}\,m\big(U,\widetilde{U}\big) & +\,\xi\,m\big(U,\widetilde{U}\big) = \xi\,p\big(V,\widetilde{U}\big). \end{array}\right. \tag{6.58}$$

avec les formes bilinéaires continues

$$m\big(V,\widetilde{V}\big) := \int_0^{L+l} V\,\widetilde{V}, \quad k\big(V,\widetilde{V}\big) := \int_0^{L+l} \partial_3 V\,\partial_3 \widetilde{V}, \quad p\big(V,U\big) := \int_0^{L+l} \partial_3 V\,U. \tag{6.59}$$

Nous discrétisons l'intervalle $[0,L+l]$ en m points avec un pas de discrétisation h, et nous définissons les deux sous-espaces de dimensions finis suivants :

$$\mathbb{V} = \{v \in H_0^1([0,L+l]) \quad | \quad v_{|[nh,(n+1)h]} \in \mathbb{P}_1,\ n \in \{0\cdots m-1\}\},$$

$$\mathbb{U} = \{u \in L^2([0,L+l]) \quad | \quad u_{|[nh,(n+1)h]} \in \mathbb{P}_0,\ n \in \{0\cdots m-1\}\}.$$

Nous introduisons alors la formulation variationnelle approchée du problème (6.57) :

Trouver $\big(V_h(t),U_h(t)\big) \in \mathbb{V} \times \mathbb{U}$ tel que pour toute fonction test $\big(\widetilde{V}_h,\widetilde{U}_h\big) \in \mathbb{V} \times \mathbb{U}$, nous avons :

$$\left|\begin{array}{ll} C\,\dfrac{d^2}{dt^2}\,m_h\big(V_h,\widetilde{V}_h\big) & +\,\delta^2\,\gamma_e\,\dfrac{d^2}{dt^2}\,k\big(V_h,\widetilde{V}_h\big) + L^{-1}\,k\big(V_h,\widetilde{V}_h\big) \\ & +\,C\,\xi\,\dfrac{d}{dt}\,m\big(V_h,\widetilde{V}_h\big) - \delta^2\,\gamma_e\,\dfrac{d^2}{dt^2}\,p\big(U_h,\widetilde{V}_h\big) - L^{-1}\,p\big(U_h,\widetilde{V}_h\big) = 0, \\ \dfrac{d}{dt}\,m\big(U_h,\widetilde{U}_h\big) & +\,\xi\,m\big(U_h,\widetilde{U}_h\big) = \xi\,p\big(V_h,\widetilde{U}_h\big). \end{array}\right. \tag{6.60}$$

La forme bilinéaire d'indice h, est traitée par une formule de quadrature dans la direction x_3 (voir (6.34)).

Pour écrire cette formulation variationnelle sous une forme algébrique, nous introduisons les vecteurs de degrés de libertés suivants :

$$\mathbb{V}_h \in \mathbb{V} \text{ et } \mathbb{U}_h \in \mathbb{U}.$$

Ainsi, la forme algébrique du problème (6.57) s'écrit comme suit :

$$\left|\begin{array}{l} \mathbf{M}_h^{\delta}\,\dfrac{d^2\,\mathbb{V}}{dt^2} + C\,\xi\;\mathbf{M}_h\,\dfrac{d\,\mathbb{V}}{dt} + L^{-1}\;\mathbf{K}_h\,\mathbb{V} \\ \qquad\qquad -\delta^2\,\gamma_e\,\mathbf{P}_h\,\dfrac{d^2\,\mathbb{U}}{dt^2} - L^{-1}\,\mathbf{P}_h\,\mathbb{U} = 0, \\ M_h\,\dfrac{d\,\mathbb{U}}{dt} + \xi\,M_h\,\mathbb{U} = \;\xi\,\mathbf{P}_h^{*}\,\mathbb{V}, \end{array}\right. \tag{6.61}$$

avec :

- $\mathbf{M}_h^{\delta} := (C\,\mathbf{M}_h\; + \delta^2\,\gamma_e\,\mathbf{K}_h)$.
- $\mathbf{M}_h$ est une matrice de masse, carré, symétrique et définie positive : $(\mathbf{M}_h)_{i,k} = m_h(\phi_i, \phi_k)$.
- M_h est une matrice de masse, carré, symétrique et définie positive : $(M_h)_{i,k} = m(\psi_i, \psi_k)$.
- $\mathbf{K}_h$ est une matrice de rigidité, carré, symétrique et définie positive : $(\mathbf{K}_h)_{i,k} = k(\phi_i, \phi_k)$.
- $\mathbf{P}_h$ est une matrice rectangulaire : $(\mathbf{P}_h)_{i,k} = p(\psi_i, \phi_k)$.

Les ϕ_i et les ψ_i sont respectivement les fonctions de base de l'espace $\mathbb{V}$ et $\mathbb{U}$.

6.3.4 Discrétisation temporelle

Dans ce qui suit, on va chercher les solutions $(V_h(t), U_h(t))$ du problème (6.60) qui sont déjà discrétisées en espace. Les solutions $(V_h(t), U_h(t))$ seront approchées à différents instants t^n, avec $t^n = n\,\Delta t$, où $\Delta t > 0$ est le pas de temps fixe.

Nous proposons un schéma similaire au schéma proposé pour les équations d'ondes trouvé dans [7] (Page 20).

$$\left|\begin{array}{l} \mathbf{M}_h^{\delta}\,\dfrac{\mathbb{V}^{n+1} - 2\,\mathbb{V}^{n} + \mathbb{V}^{n-1}}{\Delta t^2} + C\,\xi\;\mathbf{M}_h\,\dfrac{\mathbb{V}^{n+1} - \mathbb{V}^{n-1}}{2\Delta t} + L^{-1}\;\mathbf{K}_h\,\mathbb{V}^{n} \\ \qquad\qquad -\delta^2\,\gamma_e\,\mathbf{P}_h\,\dfrac{\mathbb{U}^{n+1} - 2\,\mathbb{U}^{n} + \mathbb{U}^{n-1}}{\Delta t^2} - L^{-1}\,\mathbf{P}_h\,\mathbb{U}^{n} = 0, \\ M_h\,\dfrac{\mathbb{U}^{n+1} - \mathbb{U}^{n}}{\Delta t} + \xi\,M_h\,\dfrac{\mathbb{U}^{n+1} + \mathbb{U}^{n}}{2} = \;\xi\,\mathbf{P}_h^{*}\,\dfrac{\mathbb{V}^{n+1} + \mathbb{V}^{n}}{2}. \end{array}\right. \tag{6.62}$$

6.3.5 Simulations numériques

Les données du problème

Pour calculer les coefficients C, L et γ_e (voir (6.52)), nous supposons que le domaine de référence est un câble cylindrique de longueur $L = 11$, et avec une section circulaire S de rayon intérieur $r_1 = 1$ et de rayon extérieur $r_2 = 2$ (voir Figure 6.3). Plus précisément :

$$\Omega = S \times [0, 11].$$

Nous traitons un cas de vitesse de propagation variable : nous allons prendre $(\varepsilon_1, \mu_1) = (2, 1)$ et $(\varepsilon_2, \mu_2) = (2, 1)$.

Ainsi, en utilisant les expressions des coefficients trouvés dans (6.52) à l'aide du code

Xlife++ nous avons trouvé :

$$C = 13.72, \qquad L = 0.18, \qquad \gamma_e = 0.47.$$

Nous prenons des données initiales comme suit :

$$V(x_3, 0) = e^{-\pi^2 (x_3 - 5.5)^2}, \qquad \partial_t V(x_3, 0) = 0.$$

Pour le pas de temps Δt, nous choisissons $\Delta t = 0.95 \ h/\sqrt{2}$, avec $h = 0.05$ le pas de l'espace. Nous utilisons le choix du terme d'amortissement que nous avons déjà utilisé dans la section 6.2.5.

Tests numériques

Dans ce paragraphe nous allons présenter les résultats numériques que nous avons obtenus en utilisant la méthode présentée précédemment conjointement avec les données ci-dessus.

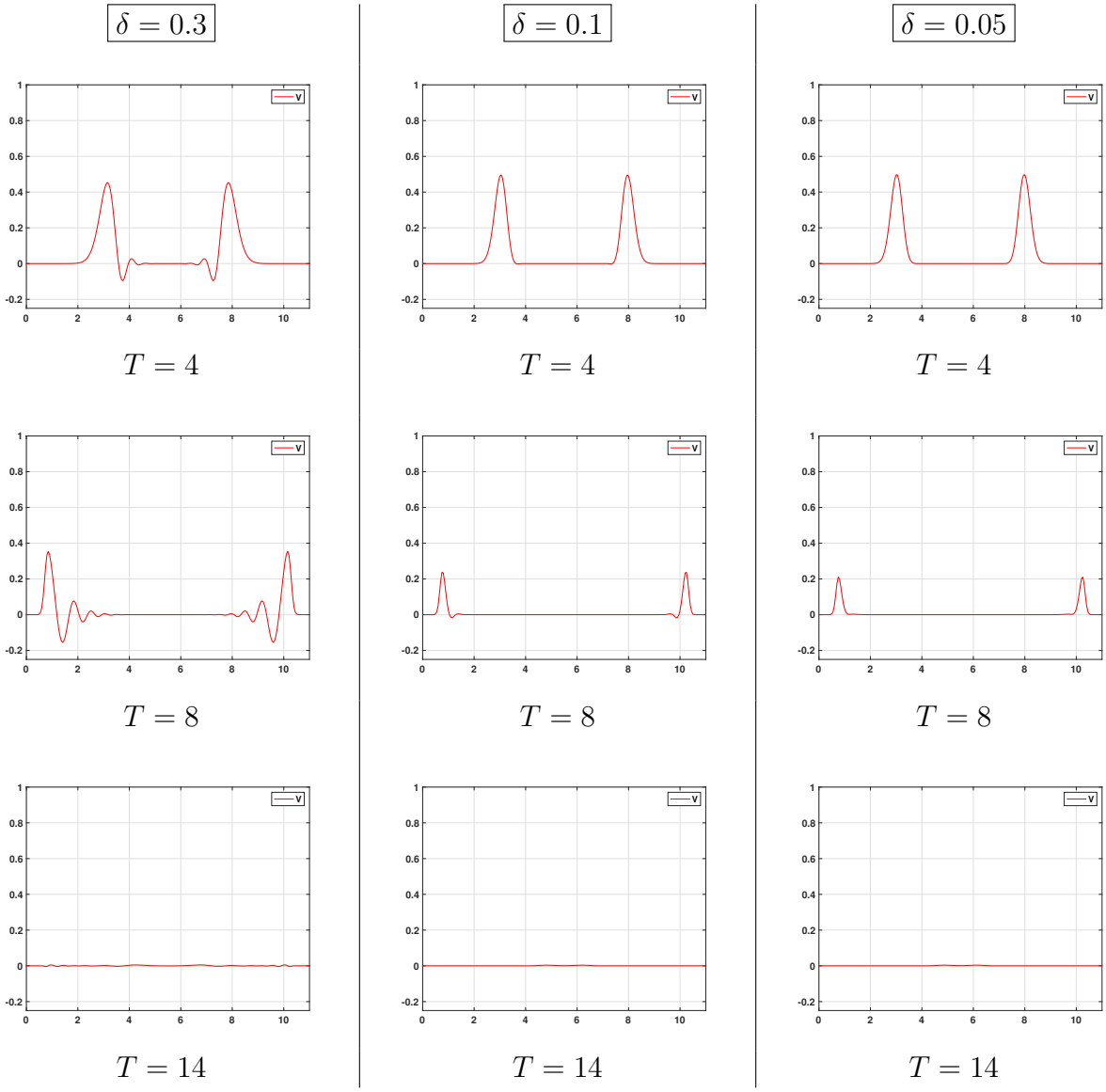

FIGURE 6.9 – La propagation de la tension dans un domaine avec deux couches PML.

Discussions : Nous observons que pour différentes valeurs de δ, l'onde se propage et s'atténue dans les deux couches de PML. Nos simulations montrent que le schéma proposé pour ce modèle 1D proposé est stable.

6.4 Conclusion

Dans ce chapitre, nous avons présenté une méthode numérique basée sur l'utilisation de la méthode des couches absorbantes parfaitement adaptées PML pour résoudre le modèle de Maxwell 3D (Section 6.2) et le modèle de Télégraphiste 1D dispersif (Section 6.3) dans un câble coaxial cylindrique et infini dans la direction longitudinale. Le principe de cette méthode est d'aboutir à une formulation variationnelle qui repose sur l'introduction astucieuse d'inconnues auxiliaires. Nos simulations numériques montrent que cette méthode s'est révélée efficace dans le cas des modèles dispersifs 1D. Cependant, pour le modèle 3D, si les PMLs sont stables dans le cas d'un câble homogène, ce n'est plus le cas dès que la vitesse de propagation des ondes électromagnétiques varie dans la section du câble. La question de la stabilité de la formulation PML 3D n'a pu être abordée que par des simulations numériques, une analyse de stabilité reste une perspective de ce chapitre. Nos expériences numériques nous amènent à penser que cette instabilité est due au modèle continu et non à sa discrétisation.
Pour résumer, la question de la stabilité des PML 3D pour les câbles coaxiaux, et encore plus la construction de PML stables, est largement ouverte et nécessite une analyse approfondie.

Chapitre 7

Conclusion et perspectives

Dans ce dernier chapitre, nous allons résumer la contribution qui a été présentée dans cette thèse, puis nous allons mentionner quelques perspectives qui semblent intéressantes à étudier.

Résultats et principales conclusions

Dans cette thèse, on s'est intéressé principalement à la résolution numérique des équations de Maxwell 3D de second ordre en temps et dont l'inconnue est le champ électrique dans des câbles co-axiaux minces.

Dans le cas d'un câble cylindrique, nous avons proposé une méthode qui vise à exploiter - et non pas subir - la géométrie du problème en distinguant le rôle des variables spatiales transverses et longitudinales, mais aussi celui du champ électrique transverse et du champ électrique longitudinal. Ainsi, la première étape consiste à faire une discrétisation longitudinale du câble, puis une discrétisation transverse de chaque section, enfin une discrétisation en temps. Le champ électrique transverse est alors approché par des éléments d'arête (Nédélec) dans chaque section du câble et par des éléments affines par morceaux selon la direction longitudinale. Par contre le champ électrique longitudinal est approché avec des éléments $\mathbb{P}_1$ dans chaque section et par des éléments $\mathbb{P}_0$ selon la direction longitudinale. Ensuite, on réalise une discrétisation en temps hybride qui est implicite dans les variables transverses, pour ne pas pénaliser la condition CFL, et explicite dans la direction longitudinale, pour maîtriser le coût de calcul. Ainsi, seul le pas de discrétisation longitudinal, en pratique beaucoup plus grand que le pas de discrétisation transverse, intervient dans la condition de stabilité de la méthode.

L'extension de cette méthode au cas non cylindrique est essentielle pour les applications afin de prendre en compte les déformations et les défauts, et présente des difficultés qui ont conduit à proposer une méthode alternative reposant sur une technique de mapping (pour se ramener à une géométrie cylindrique) sur l'utilisation d'une transformation de Piola anisotrope, et finalement sur une stratégie de discrétisation spatiale hybride entre Galerkine discontinu, pour les variables transverses, et éléments finis conformes, pour la variable longitudinale. Grâce à cela, les bonnes propriétés de la méthode dans le cas cylindrique sont préservées. La méthode proposée est en fait une extension de la méthode proposée pour le cas d'un câble cylindrique.

Parmi les principaux objectifs de cette méthode numérique, nous mentionnons la validation

numérique des modèles limites 1D qui prennent en compte la structure complexe du câble. Ceci a été fait dans les deux chapitres 3 et 4.

Nous avons également réussi à la fin de cette thèse (Chapitre 6) à implémenter une formulation PML, mais nous avons constaté que cette formulation n'est valable que pour le cas où la vitesse de propagation des ondes est constante dans tout le domaine.

Perspectives

Ici nous allons présenter quelques pistes de recherche qui peuvent être vues comme une continuation de notre travail.

La liste qui suit présente quelques perspectives du travail entrepris dans cette thèse.

- Mettre en oeuvre la méthode numérique 3D présentée dans le chapitre 5 pour la simulation d'onde électromagnétique dans un câble non cylindrique. Ce travail nécessite l'introduction d'outils numériques différents des outils communément utilisés. En effet il faut pouvoir calculer des termes de sauts et de flux aux interfaces d'éléments de Nédélec. L'implémentation de ce terme est en cours dans le logiciel Xlife++.
- La méthode numérique 3D permettra de valider numériquement des modèles asymptotiques pour des câbles déformés. Ces modèles asymptotiques sont donnés en annexe pour l'ordre 0 et dans la thèse de G. Beck [10] pour les ordres supérieurs.
- L'effet de peau [8] est un phénomène relativement important que nous avons négligé jusqu'à maintenant. La prise en compte de ce phénomène sur le modèle 3D pourrait se faire a priori avec les mêmes outils que ceux développés dans les chapitres 2 et 5 tandis que les modèles asymptotiques ont été obtenus dans [13]. Ces modèles font intervenir des termes non-locaux en temps qui peuvent être traités de la même manière que les modèles développés aux chapitres 3 et 4.
- Une question importante d'analyse numérique reste en suspens : a quel ordre espace-temps converge le schéma proposé au chapitre 2. Il est relativement aisé (bien que cela reste à faire) de proposer une analyse de convergence en espace (sur le problème semi-discret) ou en temps (au sens des systèmes d'ODE) mais une analyse espace-temps est plus difficile, et, dans notre cas, plus difficile que pour l'analyse de schémas saute-mouton standard. Cela s'explique par le fait que le schéma en temps explicite-implicite construit en chapitre 2 dissocie la contribution de l'opérateur rotationnel, faisant apparaître des termes dans l'erreur de consistance qui ne sont pas aisés à contrôler.
- Les simulations du chapitre 6 ont montré des instabilités des PMLs lorsque les paramètres physiques varient dans la section. Ces instabilités sont sûrement des instabilités qui se retrouvent sur le problème continu (cela reste à vérifier). Il serait intéressant d'analyser ces instabilités pour éventuellement y remédier.
- La stratégie de discrétisation en espace et en temps présentée peut être couplée à des modèles 3D de jonctions de câbles. Dans ce cas il apparaît naturel d'utiliser une discrétisation en temps implicite au niveau de la jonction. Le schéma obtenu peut s'avérer efficace pour tester la validité de modèles de jonctions obtenus dans la thèse de G. Beck [10].

Enfin, une perspective plus excitante est d'étudier comment utiliser tous les résultats obtenus ici pour étudier le problème inverse associé : identifier si le câble contient des déformations et les localiser à partir des mesures du champ éclectique.

Annexes

Annexe A

Construction des équations télégraphistes

Sommaire

A.1 Introduction

Dans cette annexe, nous présentons certains des résultats obtenus dans [10, 34, 35] et que nous avons utilisés dans les chapitres 3 et 4. Plus précisément, elle est composée de deux parties : dans la première (Section A.2) nous rappelons comment nous avons obtenu le modèle limite 1D, et dans la deuxième (Section A.3) nous proposons un schéma numérique pour résoudre le modèle limite 1D avec des coefficients calculés explicitement dans le cas d'un câble cylindrique avec une section circulaire, et en présence d'un terme non-local en temps. En particulier, nous présentons deux approches pour traiter ce terme non-local dans cette configuration.

A.2 Le modèle mathématique des câbles coaxiaux

A.2.1 Position du problème

On considère un câble coaxial Ω^δ paramétré par un scalaire strictement positive δ, qui représente l'épaisseur du câble :

$$\Omega^\delta = \bigcup_{x_3 \in \mathbb{R}} S^\delta(x_3),$$

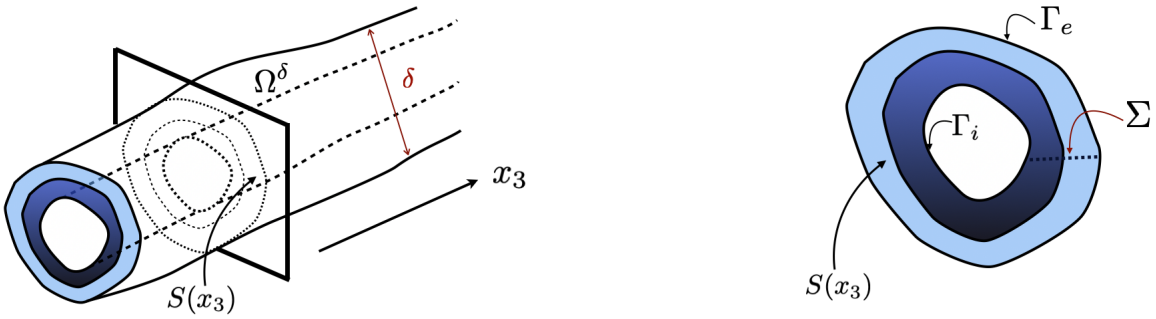

FIGURE A.1 – Droite : le câble Ω^δ. Gauche : une section du câble S^δ.

avec $S^\delta(x_3)$ Lipschitzien de $\mathbb{R}^2$ et n'est pas simplement connexe. Pour simplifier, nous nous limitons au cas où chaque section transversale ne contient qu'un seul trou (voir figure A.1).

Le long du bord du câble $\partial\Omega^\delta$, nous définissons le champ vectoriel 2D des vecteurs normaux unitaires $\mathbf{n}_T : \partial\Omega^\delta \to \mathbb{R}^2$, tel que, le long de $\partial S(x_3)$, $\mathbf{n}_T$ est le vecteur normal unitaire à $\partial S(x_3)$, sortant par rapport à $S(x_3)$. Sur $\partial\Omega^\delta$, un champ de vecteurs normaux à $\partial\Omega^\delta$ (non unitaires), sortant par rapport à Ω^δ, sera défini par

$$\mathbf{n}^\delta := (\mathbf{n}_T^\delta, g^\delta) : \partial\Omega^\delta \to \mathbb{R}^3, \quad \mathbf{n}_T^\delta : \partial\Omega^\delta \to \mathbb{R}^2, \ g^\delta : \partial\Omega^\delta \to \mathbb{R}. \tag{A.1}$$

En d'autres termes, $g^\delta : \partial\Omega^\delta \to \mathbb{R}$ désigne la composante longitudinale du vecteur normal à $\mathbf{n}_T^\delta : \partial\Omega^\delta \to \mathbb{R}^2$ dont la projection sur le plan (x_1, x_2) est $\mathbf{n}_T^\delta$.

Pour décrire la propagation des ondes électromagnétiques dans ce domaine, nous nous reposons sur les équations de Maxwell suivantes,

$$\begin{cases} \varepsilon^\delta \, \partial_t \, \mathbf{E}^\delta + \sigma_e^\delta \, \mathbf{E}^\delta - \boldsymbol{\nabla}_T \times \mathbf{H}^\delta = \mathbf{j}^\delta, \quad \mathbf{x} \in \Omega^\delta, \ t > 0, \\ \mu^\delta \, \partial_t \, \mathbf{H}^\delta + \sigma_m^\delta \, \mathbf{H}^\delta + \boldsymbol{\nabla}_T \times \mathbf{E}^\delta = 0, \quad \mathbf{x} \in \Omega^\delta, \ t > 0, \end{cases} \tag{A.2}$$

où les coefficients $\varepsilon^\delta, \mu^\delta, \sigma_e^\delta$, et σ_m^δ sont des fonctions mesurables de $\mathbf{x} \in \Omega^\delta$ et satisfont, pour tout $\mathbf{x} \in \Omega^\delta$,

$$\begin{aligned} &0 < \varepsilon_- \le \varepsilon^\delta(\mathbf{x}) \le \varepsilon_+, \qquad 0 < \mu_- \le \mu^\delta(\mathbf{x}) \le \mu_+, \\ &0 \le \sigma_{e,-} \le \sigma_e^\delta(\mathbf{x}) \le \sigma_{e,+}, \quad 0 \le \sigma_{m,-} \le \sigma_m^\delta(\mathbf{x}) \le \sigma_{m,+}, \end{aligned} \tag{A.3}$$

et $\mathbf{j}^\delta$ désigne la densité du courant. Pour simplifier, nous supposons que la source $\mathbf{j}^\delta$ de notre modèle est donnée comme suit,

$$\mathbf{j}^\delta = (\mathbf{j}_T^\delta, 0) \text{ avec } \mathrm{div}_T \, \mathbf{j}_T^\delta = 0 \ (\mathrm{div}_T \text{ est l'opérateur de divergence 2D}).$$

Les donnée initiales du problème sont données par

$$\mathbf{E}^\delta(\mathbf{x}, 0) = \mathbf{E}_0^\delta, \qquad \mathbf{H}^\delta(\mathbf{x}, 0) = \mathbf{H}_0^\delta, \qquad \mathbf{x} \in \Omega^\delta,$$

et pour que le problème soit bien posé nous ajoutons les conditions aux bords suivantes le long du câble :

$$\mathbf{E}^\delta \times \mathbf{n}_T = 0, \qquad \mathbf{x} \in \partial\Omega^\delta, \ t > 0. \tag{A.4}$$

Remarque A.2.1. *Si nous prenons la divergence 3D de (A.2), nous obtenons les équations de divergence cachées :*

$$\begin{cases} \operatorname{div}\left(\left(\varepsilon^\delta\,\partial_t+\sigma_e^\delta\right)\mathbf{E}^\delta\right)=0, & \mathbf{x}\in\Omega^\delta,\ t>0,\\ \operatorname{div}\left(\left(\mu^\delta\,\partial_t+\sigma_m^\delta\right)\mathbf{H}^\delta\right)=0, & \mathbf{x}\in\Omega^\delta,\ t>0, \end{cases} \tag{A.5}$$

tel que div *est l'opérateur de divergence 3D.*

On introduit maintenant les composantes tangentielles et les composantes longitudinales de champ électrique $\mathbf{E}^\delta$ et de champ magnétique $\mathbf{H}^\delta$, nous notons alors

- $\mathbf{E}_T^\delta=(E_1^\delta,E_2^\delta)^T,\quad \mathbf{H}_T^\delta=(H_1^\delta,H_2^\delta)^T$: les composantes tangentielles.
- $E_3^\delta,\quad H_3^\delta$: les composantes longitudinales.

nous allons utiliser les opérateurs de rotationnel et de gradient transversaux suivants (nous notons que l'indice T fait référence aux dérivées transversales),

$$\operatorname{rot}_T\mathbf{E}_T=\partial_1E_2-\partial_2E_1,\quad \mathbf{rot}_T\,E_3=\begin{pmatrix}\partial_2E_3\\ -\partial_1E_3\end{pmatrix},\quad \nabla_T\,E_3=\begin{pmatrix}\partial_1E_3\\ \partial_2E_3\end{pmatrix}. \tag{A.6}$$

Le premier terme est un opérateur de rotation scalaire tandis que le second est un opérateur de rotation vectorielle qui peut être vu comme un gradient "tourné",

$$\mathbf{rot}_T\,E_3=-\mathbf{e}_3\times\nabla_TE_3,\quad \text{avec}\quad \mathbf{e}_3\times E_T=\begin{pmatrix}-E_2\\ E_1\end{pmatrix}\quad\text{et}\quad \mathbf{e}_3=(0,0,1)^t. \tag{A.7}$$

L'opérateur rotationnel 3D se réécrit comme suit

$$\boldsymbol{\nabla}_T\times\mathbf{E}=\begin{pmatrix}\mathbf{rot}_TE_3+\mathbf{e}_3\times\partial_3\mathbf{E}_T\\ \operatorname{rot}_T\mathbf{E}_T\end{pmatrix}.$$

Également, grâce à la formule de Green ($\mathrm{d}\sigma$ est la mesure surfacique le long de $\partial S(x_3)$), nous avons pour $(\mathbf{u},\mathbf{v})\in H^1(S(x_3))\times H(\mathbf{rot}_T,S(x_3))$:

$$(\mathbf{rot}_T\,\mathbf{u},\mathbf{v})_{L^2(S(x_3))}=(\mathbf{u},\mathbf{rot}_T\,\mathbf{v})_{L^2(S(x_3))}+\int_{\partial\,S(x_3)}\mathbf{u}\cdot\overline{\mathbf{v}\times\mathbf{n}_T}\,\mathrm{d}\sigma. \tag{A.8}$$

Par suite, nous pouvons réécrire les équations de Maxwell (A.2) comme suit

$$\begin{cases} \varepsilon^\delta\,\partial_t\,\mathbf{E}_T^\delta+\sigma_e^\delta\,\mathbf{E}_T^\delta-\partial_{x_3}\left(\mathbf{e}_3\times\mathbf{H}_T^\delta\right)-\mathbf{rot}_T\,H_3^\delta=\mathbf{j}_T^\delta & \mathbf{x}\in\Omega^\delta,\ t>0,\\ \varepsilon^\delta\,\partial_t\,E_3^\delta+\sigma_e^\delta\,E_3^\delta-\operatorname{rot}_T\mathbf{H}_T^\delta=0, & \mathbf{x}\in\Omega^\delta,\ t>0,\\ \mu^\delta\,\partial_t\,\mathbf{H}_T^\delta+\sigma_m^\delta\,\mathbf{H}_T^\delta+\partial_{x_3}\left(\mathbf{e}_3\times\mathbf{E}_T^\delta\right)+\mathbf{rot}_T\,\mathbf{E}_3^\delta=0, & \mathbf{x}\in\Omega^\delta,\ t>0,\\ \mu^\delta\,\partial_t\,H_3^\delta+\sigma_m^\delta\,H_3^\delta+\operatorname{rot}_T\mathbf{E}_T^\delta=0, & \mathbf{x}\in\Omega^\delta,\ t>0. \end{cases} \tag{A.9}$$

A.2.2 Les équations de Maxwell dans un câble de référence

Nous considérons une famille de domaines (minces) Ω^δ paramétrés par un scalaire δ ($0 < \delta << 1$ est le diamètre de la section transversale d'un câble habituel dans le plan $x_3 = 0$) :

$$\Omega^\delta = \mathcal{G}_\delta(\Omega), \text{ avec } \mathcal{G}_\delta(\mathbf{x}_T, x_3) = (\delta\,\mathbf{x}_T, x_3).$$

où $\mathbf{x}_T = (x_1, x_2)$représente les coordonnées transversales.

Les propriétés matérielles des câbles minces Ω^δ sont définies à partir de celles du câble de référence Ω :

$$\varepsilon^\delta = \varepsilon \circ \mathcal{G}_\delta^{-1}, \quad \sigma_e^\delta = \sigma_e \circ \mathcal{G}_\delta^{-1}, \quad \mu^\delta = \mu \circ \mathcal{G}_\delta^{-1}, \quad \sigma_m^\delta = \sigma_m \circ \mathcal{G}_\delta^{-1}.$$

Nous notons ici que nous pouvons définir la normale $\mathbf{n}^\delta$, qui est défini par (A.1), à partir de la normale à $\partial\Omega$ et sortant par rapport à Ω

$$\mathbf{n}^\delta = \mathbf{n} \circ \mathcal{G}_\delta^{-1}, \qquad \mathbf{n} = (\delta^{-1}\,\mathbf{n}_T, g), \qquad \text{avec } |\mathbf{n}_T| = 1 \text{ et } g : \partial\Omega \to \mathbb{R}. \tag{A.10}$$

Remarque A.2.2. *Dans ce qui suit, nous allons utiliser le passage de Ω^δ à Ω via le changement de variable $\mathcal{G}_\delta$. Et pour plus de clarté, nous allons utiliser la notation $\mathbf{x}$ pour les coordonnées dans Ω^δ et Ω.*

On introduit maintenant le champ électrique $\widetilde{\mathbf{E}}^\delta = (\widetilde{\mathbf{E}}_T^\delta, \widetilde{E}_3^\delta)$, le champ magnétique $\widetilde{\mathbf{H}}^\delta = (\widetilde{\mathbf{H}}_T^\delta, \widetilde{H}_3^\delta)$ et la source $\mathbf{j}_T$ dans le câble de référence et qui sont défini par les expressions suivantes

$$\mathbf{E}^\delta = \widetilde{\mathbf{E}}^\delta \circ \mathcal{G}_\delta^{-1}, \qquad \mathbf{H}^\delta = \widetilde{\mathbf{H}}^\delta \circ \mathcal{G}_\delta^{-1}, \qquad \mathbf{j}_T^\delta = \mathbf{j}_T \circ \mathcal{G}_\delta^{-1}.$$

Les équations de Maxwell (A.9) se réécrivent dans le domaine de référence Ω comme suit

$$\begin{cases} \varepsilon\,\partial_t\,\widetilde{\mathbf{E}}_T^\delta + \sigma_e\,\widetilde{\mathbf{E}}_T^\delta - \partial_{x_3}\left(\mathbf{e}_3 \times \widetilde{\mathbf{H}}_T^\delta\right) - \delta^{-1}\,\mathbf{rot}_T\,\widetilde{H}_3^\delta = \mathbf{j}_T & \mathbf{x} \in \Omega,\ t > 0, \\ \varepsilon\,\partial_t\,\widetilde{E}_3^\delta + \sigma_e\,\widetilde{E}_3^\delta - \delta^{-1}\,\mathrm{rot}_T\,\widetilde{\mathbf{H}}_T^\delta = 0, & \mathbf{x} \in \Omega,\ t > 0, \\ \mu\,\partial_t\,\widetilde{\mathbf{H}}_T^\delta + \sigma_m\,\widetilde{\mathbf{H}}_T^\delta + \partial_{x_3}\left(\mathbf{e}_3 \times \widetilde{\mathbf{E}}_T^\delta\right) + \delta^{-1}\,\mathbf{rot}_T\,\widetilde{\mathbf{E}}_3^\delta = 0, & \mathbf{x} \in \Omega,\ t > 0, \\ \mu\,\partial_t\,\widetilde{H}_3^\delta + \sigma_m\,\widetilde{H}_3^\delta + \delta^{-1}\,\mathrm{rot}_T\,\widetilde{\mathbf{E}}_T^\delta = 0, & \mathbf{x} \in \Omega,\ t > 0, \end{cases} \tag{A.11}$$

avec les conditions aux bords (A.4)

$$\delta^{-1}\,\widetilde{\mathbf{E}}_T^\delta \times \mathbf{n}_T = 0, \qquad \delta^{-1}\,\widetilde{E}_3^\delta\,\mathbf{n}_T - g\,\widetilde{\mathbf{E}}_T^\delta = 0. \tag{A.12}$$

Ces conditions impliquent des conditions aux bords par rapport au champ magnétique $\mathbf{H}$:

$$\delta^{-1}\left((\mu\,\partial_t + \sigma_m)\,\widetilde{\mathbf{H}}_T^\delta\right) \cdot \mathbf{n}_T + g\left((\mu\,\partial_t + \sigma_m)\,\widetilde{H}_3^\delta\right) = 0. \tag{A.13}$$

Pour plus de détails, on renvoie le lecteur à la thèse [10] (page 82).

Remarque A.2.3.
Les équations de divergence (A.5) se réécrivent dans le domaine de référence Ω comme suit,

$$\begin{cases} \delta^{-1}\,\mathrm{div}_T\left((\partial_t\,\varepsilon + \sigma_e)\,\widetilde{\mathbf{E}}_T^\delta\right) + (\partial_t\,\varepsilon + \sigma_e)\,\partial_{x_3}\,\widetilde{E}_3^\delta = 0 & \mathbf{x} \in \Omega,\ t > 0, \\ \delta^{-1}\,\mathrm{div}_T\left((i\,\omega\,\mu + \sigma_m)\,\widetilde{\mathbf{H}}_T^\delta\right) + (i\,\omega\,\mu + \sigma_m)\,\partial_{x_3}\,\widetilde{H}_3^\delta = 0 & \mathbf{x} \in \Omega,\ t > 0, \end{cases} \tag{A.14}$$

avec div_T l'opérateur de divergence $2D$.

A.2.3 Analyse asymptotique

Maintenant, nous nous intéressons au développement asymptotique formel de la solution du problème (A.11) − (A.14) lorsque δ tend vers 0, pour cette raison nous cherchons des solutions sous la forme suivante :

$$\widetilde{\mathbf{E}}_T = \widetilde{\mathbf{E}}_T^0 + \delta\,\widetilde{\mathbf{E}}_T^1 + \delta^2\,\widetilde{\mathbf{E}}_T^2 + \ldots, \quad \widetilde{\mathbf{H}}_T = \widetilde{\mathbf{H}}_T^0 + \delta\,\widetilde{\mathbf{H}}_T^1 + \delta^2\,\widetilde{\mathbf{H}}_T^2 + \ldots,$$

$$\widetilde{E}_3 = \widetilde{E}_3^0 + \delta\,\widetilde{E}_3^1 + \delta^2\,\widetilde{E}_3^2 + \ldots, \quad \widetilde{H}_3 = \widetilde{H}_3^0 + \delta\,\widetilde{H}_3^1 + \delta^2\,\widetilde{H}_3^2 + \ldots.$$

On adopte la méthodologie d'analyse asymptotique habituelle qui consiste à injecter ces solutions dans (A.11), et à identifier la série terme par terme qui commence par les termes en δ^{-1} (en raison des facteurs δ^{-1} dans (A.11)).

Définition A.2.1. *Les champs électromagnétiques à chaque ordre p sont définis comme la solution dans $L^2(\Omega)$ des équations suivantes*

$$\begin{cases} (\varepsilon\,\partial_t + \sigma_e)\,\widetilde{\mathbf{E}}_T^p - \partial_{x_3}\left(\mathbf{e}_3 \times \widetilde{\mathbf{H}}_T^p\right) - \mathbf{rot}_T\,\widetilde{\mathbf{H}}_3^{p+1} = \delta_p^0\,\mathbf{j}_T, \\ (\varepsilon\,\partial_t + \sigma_e)\,\widetilde{E}_3^p - \mathrm{rot}_T\,\widetilde{\mathbf{H}}_T^{p+1} = 0, \\ (\mu\,\partial_t + \sigma_m)\,\widetilde{\mathbf{H}}_T^p + \partial_{x_3}\left(\mathbf{e}_3 \times \widetilde{\mathbf{E}}_T^p\right) + \mathbf{rot}_T\,\widetilde{\mathbf{E}}_3^{p+1} = 0, \\ (\mu\,\partial_t + \sigma_m)\,\widetilde{H}_3^p + \mathrm{rot}_T\,\widetilde{\mathbf{E}}_T^{p+1} = 0, \end{cases} \tag{A.15}$$

avec les conditions aux bords

$$\left| \begin{array}{l} \widetilde{\mathbf{E}}_T^{p+1} \times \mathbf{n}_T = 0, \quad \widetilde{E}_3^{p+1}\,\mathbf{n}_T - g\,\widetilde{\mathbf{E}}_T^p = 0, \\ \left((\mu\,\partial_t + \sigma_m)\,\widetilde{\mathbf{H}}_T^{p+1}\right) \cdot \mathbf{n}_T + g\left((\mu\,\partial_t + \sigma_m)\,\widetilde{H}_3^p\right) = 0. \end{array} \right. \tag{A.16}$$

Nous utilisons également les équations "cachées" de divergence suivantes

$$\begin{cases} \mathrm{div}_T\left((\partial_t\,\varepsilon + \sigma_e)\,\widetilde{\mathbf{E}}_T^{p+1}\right) + (\partial_t\,\varepsilon + \sigma_e)\,\partial_{x_3}\,\widetilde{E}_3^p = 0 & \mathbf{x} \in \Omega,\ t > 0, \\ \mathrm{div}_T\left((\partial_t\,\mu + \sigma_m)\,\widetilde{\mathbf{H}}_T^{p+1}\right) + (\partial_t\,\mu + \sigma_m)\,\partial_{x_3}\,\widetilde{H}_3^p = 0 & \mathbf{x} \in \Omega,\ t > 0. \end{cases} \tag{A.17}$$

Avec la convention :

$$\widetilde{\mathbf{E}}^p = \widetilde{\mathbf{H}}^p = 0, \quad \textit{pour} \quad p < 0, \quad \textit{et} \quad \delta_p^0 = \begin{cases} 1 & \textit{si } p = 0, \\ 0 & \textit{si } p \neq 0. \end{cases}$$

Pour effectuer l'analyse asymptotique, il est utile de passer au régime fréquentiel via une transformée de Fourier temporelle :

$$(\widetilde{\mathbf{E}}, \widetilde{\mathbf{H}}) \mapsto (\widehat{\mathbf{E}}, \widehat{\mathbf{H}}), \quad \partial_t\,\varepsilon + \sigma_e \mapsto \mathrm{i}\,\omega\,\varepsilon + \sigma_e, \quad \partial_t\,\mu + \sigma_m \mapsto \mathrm{i}\,\omega\,\mu + \sigma_m.$$

Définition A.2.2. *Dans le cas où les données initiales sont causales nous pouvons étendre les équations posées en domaine temporel, (A.15) − (A.17), pour des temps négatifs, et à*

l'aide de la transformation de Fourier nous obtenons le problème suivant :

$$\begin{cases} (i\omega\,\varepsilon+\sigma_e)\,\widehat{\mathbf{E}}_T^p-\partial_{x_3}\left(\mathbf{e}_3\times\widehat{\mathbf{H}}_T^p\right)-\mathbf{rot}_T\,\widehat{\mathbf{H}}_3^{p+1}=0,\\ (i\omega\,\varepsilon+\sigma_e)\,\widehat{E}_3^p-\mathrm{rot}_T\,\widehat{\mathbf{H}}_T^{p+1}=0,\\ (i\omega\,\mu+\sigma_m)\,\widehat{\mathbf{H}}_T^p+\partial_{x_3}\left(\mathbf{e}_3\times\widehat{\mathbf{E}}_T^p\right)+\mathbf{rot}_T\,\widehat{\mathbf{E}}_3^{p+1}=0,\\ (i\omega\,\mu+\sigma_m)\,\widehat{H}_3^p+\mathrm{rot}_T\,\widehat{\mathbf{E}}_T^{p+1}=0, \end{cases} \tag{A.18}$$

avec les conditions aux bords

$$\left|\begin{array}{l} \widehat{\mathbf{E}}_T^{p+1}\times\mathbf{n}_T=0,\quad \widehat{E}_3^{p+1}\,\mathbf{n}_T-g\,\widehat{\mathbf{E}}_T^p=0,\\ \left((i\omega\,\mu+\sigma_m)\,\widehat{\mathbf{H}}_T^{p+1}\right)\cdot\mathbf{n}_T+\,g\left((i\omega\,\mu+\sigma_m)\,\widehat{H}_3^p\right)=0. \end{array}\right. \tag{A.19}$$

Les équations de divergence en régime harmonique se réécrivent comme suit

$$\begin{cases} \mathrm{div}_T\left((i\omega\,\varepsilon+\sigma_e)\,\widehat{\mathbf{E}}_T^{p+1}\right)+(i\omega\,\varepsilon+\sigma_e)\,\partial_{x_3}\,\widehat{E}_3^p=0 & \mathbf{x}\in\Omega,\ t>0,\\ \mathrm{div}_T\left((i\omega\,\mu+\sigma_m)\,\widehat{\mathbf{H}}_T^{p+1}\right)+(i\omega\,\mu+\sigma_m)\,\partial_{x_3}\,\widehat{H}_3^p=0 & \mathbf{x}\in\Omega,\ t>0, \end{cases} \tag{A.20}$$

avec la convention :

$$\widehat{\mathbf{E}}^p=\widehat{\mathbf{H}}^p=0,\quad \textit{pour}\quad p<0.$$

A.2.4 Le modèle Télégraphiste limite

Dans cette section, nous allons traiter les termes limites $\widetilde{\mathbf{E}}^0$ et $\widetilde{\mathbf{H}}^0$. Dans ce cadre, nous avons besoin de quelques considérations sur les premiers ordres $\widetilde{\mathbf{E}}^1$ et $\widetilde{\mathbf{H}}^1$.

Notre objectif est donc l'identification des champs limites :

$$\widehat{\mathbf{E}}_T^0,\ \widehat{E}_3^0,\ \widehat{\mathbf{H}}_T^0,\ \widehat{H}_3^0.$$

Les équations en δ^{-1}

L'identification des termes en δ^{-1} dans le problème (A.18) (i.e., nous remplaçons dans ces équations p par -1), nous donne les équations suivantes :

$$\begin{cases} \mathbf{rot}_T\,\widehat{E}_3^0=\mathbf{rot}_T\,\widehat{H}_3^0=0, & \mathbf{x}\in\Omega,\\ \mathrm{rot}_T\,\widehat{\mathbf{E}}_T^0=\mathrm{rot}_T\,\widehat{\mathbf{H}}_T^0=0, & \mathbf{x}\in\Omega. \end{cases} \tag{A.21}$$

De même pour les équations de divergence (A.18), nous obtenons :

$$\begin{cases} \mathrm{div}_T\left((\mathrm{i}\,\omega\,\varepsilon+\sigma_e)\,\widehat{\mathbf{E}}_T^0\right)=0, & \mathbf{x}\in\Omega,\\ \mathrm{div}_T\left((\mathrm{i}\,\omega\,\mu+\sigma_m)\,\widehat{\mathbf{H}}_T^0\right)=0, & \mathbf{x}\in\Omega. \end{cases} \tag{A.22}$$

Pour les conditions aux bords, nous obtenons :

$$\begin{cases} \widehat{\mathbf{E}}_T^0 \times \mathbf{n}_T = 0, & \mathbf{x} \in \partial\Omega, \\ \widehat{E}_3^0 = 0, & \mathbf{x} \in \partial\Omega, \\ \widehat{\mathbf{H}}_T^0 \cdot \mathbf{n}_T = 0, & \mathbf{x} \in \partial\Omega. \end{cases} \tag{A.23}$$

• **Champ électrique longitudinal $\widehat{E}_3^0$**

En utilisant la première équation de (A.23), il est facile de vérifier que $\widehat{E}_3^0$ ne dépend pas de x_1 et x_2, et puisque E_3^0 est nul sur les bords, alors

$$\widehat{E}_3^0 = 0, \quad \mathbf{x} \in \Omega.$$

• **Champ électrique transversal $\widehat{\mathbf{E}}_T^0$**

$\widehat{\mathbf{E}}_T^0$ est la solution du problème suivant :

$$\begin{cases} \mathrm{rot}_T\, \widehat{\mathbf{E}}_T^0 = 0, & \mathbf{x} \in \Omega, \\ \mathrm{div}_T \left((\mathrm{i}\,\omega\,\varepsilon + \sigma_e)\, \widehat{\mathbf{E}}_T^0 \right) = 0, & \mathbf{x} \in \Omega, \\ \widehat{\mathbf{E}}_T^0 \times \mathbf{n}_T = 0, & \mathbf{x} \in \partial\Omega. \end{cases} \tag{A.24}$$

Propriété A.2.1.
Soient $S(x_3)$ un domaine borné, Lipschitz de $\mathbb{R}^2$, et $v \in [L^2(S)]^2$ vérifiant :

$$\begin{cases} \mathrm{rot}_T\, v = 0, & \textit{dans } S, \\ v \times \mathbf{n}_T = 0, & \textit{sur } \partial S(x_3), \end{cases}$$

alors il existe $\varphi \in H^1(S)$ telle que $v = \nabla_T \varphi$.

Nous notons $\mathcal{E}$ l'espace défini par :

$$\mathcal{E} = \left\{ \mathbf{u}_T \in [L^2(S(x_3))]^2 \,|\, \mathrm{rot}_T\, \mathbf{u}_T = 0, \quad \mathrm{div}_T \Big((\mathrm{i}\,\omega\,\varepsilon + \sigma_e)\, \mathbf{u}_T \Big) = 0, \quad \mathbf{u}_T \times \mathbf{n}_T = 0 \right\}.$$

Lemme A.2.1.
L'espace $\mathcal{E}$ est un espace de dimension 1

$$\mathcal{E} = vect\, \{ \nabla_T \widehat{\varphi}_e \},$$

avec $\widehat{\varphi}_e$ l'unique fonction de $H^1(S(x_3))$ solution du problème

$$\begin{cases} \mathrm{div}_T \left((i\omega\,\varepsilon + \sigma_e)\, \nabla_T\, \widehat{\varphi}_e \right) = 0, & \mathbf{x}_T \in S(x_3), \\ \widehat{\varphi}_e = 1, & \Gamma_i, \\ \widehat{\varphi}_e = 0, & \Gamma_e. \end{cases} \tag{A.25}$$

Il est clair que pour tout $x_3 \in \mathbb{R}$ la solution $\widehat{\mathbf{E}}_T^0(.,x_3,\omega)$ du problème (A.24) est dans $\mathcal{E}$, donc nous choisissons de définir $\widehat{V}(x_3,\omega)$ tel que

$$\widehat{\mathbf{E}}_T^0(\mathbf{x}_T,x_3,\omega) = \widehat{V}(x_3,\omega)\,\nabla_T\widehat{\varphi}_e(\mathbf{x}_T,x_3,\omega). \tag{A.26}$$

• **Champ magnétique transversal $\widehat{\mathbf{H}}_T^0$**

$\widehat{\mathbf{H}}_T^0$ est la solution du problème suivant :

$$\begin{cases} \mathrm{rot}_T\,\widehat{\mathbf{H}}_T^0 = 0, & \mathbf{x}\in\Omega,\\ \mathrm{div}_T\,(\mu\partial_t+\sigma_m)\,\widehat{\mathbf{H}}_T^0 = 0, & \mathbf{x}\in\Omega,\\ \widehat{\mathbf{H}}_T^0\cdot\mathbf{n}_T = 0, & \mathbf{x}\in\partial\Omega. \end{cases} \tag{A.27}$$

Propriété A.2.2.
*Soient D un domaine borné, **simplement connexe**, Lipschitz de $\mathbb{R}^2$ et $v\in[L^2(D)]^2$, telle que $\mathrm{rot}_T\,v=0$ dans D, alors il existe $\psi\in H^1(D)$ telle que $v=\nabla_T\psi$.*

Nous définissons un espace $\mathcal{H}$ tel que

$$\mathcal{H} = \Big\{\mathbf{u}_T\in[L^2(S(x_3))]^2\,|\,\mathrm{rot}_T\,\mathbf{u}_T=0,\quad \mathrm{div}_T\Big((\mathrm{i}\,\omega\mu+\sigma_m)\,\mathbf{u}_T\Big)=0,\quad \mathbf{u}_T\cdot\mathbf{n}_T=0\Big\}.$$

Il est clair que pour tout $x_3\in[0,L]$, nous avons $\widehat{\mathbf{H}}_T^0\in\mathcal{H}$.
Afin d'étudier l'espace $\mathcal{H}$ et pour appliquer la propriété précédente, nous introduisons une coupure intérieure notée Σ qui rend $S(x_3)$ simplement connexe, nous notons alors

$$\widetilde{S}(x_3) \;=\; S(x_3)\setminus\Sigma.$$

Lemme A.2.2. *L'espace $\mathcal{H}$ est un espace de dimension 1 :*

$$\mathcal{H} = vect\left\{\nabla_T\widehat{\psi}_m\right\},$$

avec $\widehat{\psi}_m$ l'unique fonction de $H^1(\widetilde{S}(x_3))$ solution du problème

$$\begin{cases} \mathrm{div}_T\Big((i\omega\,\mu+\sigma_m)\,\nabla_T\,\widehat{\psi}_m\Big)=0, & \mathbf{x}_T\in\widetilde{S}(x_3),\\ \nabla_T\,\widehat{\psi}_m\cdot\mathbf{n}_T=0, & \mathbf{x}_T\in\partial S(x_3),\\ [\widehat{\psi}_m]=1, & \mathbf{x}_T\in\Sigma,\\ [(i\omega\,\mu+\sigma_m)\,\nabla_T\,\widehat{\psi}_m]=1, & \mathbf{x}_T\in\Sigma, \end{cases} \tag{A.28}$$

avec

$$[\psi] = \lim_{\substack{y\longrightarrow x\\ y\cdot\mathbf{n}_T<0}}\psi(y) - \lim_{\substack{y\longrightarrow x\\ y\cdot\mathbf{n}_T>0}}\psi(y),\quad x=(x_1,x_2)\in\Sigma.$$

Comme $\widehat{\mathbf{H}}_T^0\in\mathcal{H}$, nous pouvons alors choisir une fonction $\widehat{I}(x_3,\omega)$ telle que

$$\widehat{\mathbf{H}}_T^0(\mathbf{x}_T,x_3,\omega) = \widehat{I}(x_3,\omega)\,\nabla_T\,\widehat{\psi}_m(\mathbf{x}_T,x_3,\omega). \tag{A.29}$$

Les équations en δ^0

L'identification des termes en δ^0 dans le problème (A.18), nous conduit au problème

$$\begin{cases} (\mathrm{i}\,\omega\,\varepsilon+\sigma_e)\,\widehat{\mathbf{E}}_T^0-\partial_{x_3}\left(\mathbf{e}_3\times\widehat{\mathbf{H}}_T^0\right)-\mathbf{rot}_T\,\widehat{\mathbf{H}}_3^1=\widehat{\mathbf{j}}_T,\\ (\mathrm{i}\,\omega\,\varepsilon+\sigma_e)\,\widehat{E}_3^0-\mathrm{rot}_T\,\widehat{\mathbf{H}}_T^1=0,\\ (\mathrm{i}\,\omega\,\mu+\sigma_m)\,\widehat{\mathbf{H}}_T^0+\partial_{x_3}\left(\mathbf{e}_3\times\widehat{\mathbf{E}}_T^0\right)+\mathbf{rot}_T\,\widehat{\mathbf{E}}_3^1=0,\\ (\mathrm{i}\,\omega\,\mu+\sigma_m)\,\widehat{H}_3^0+\mathrm{rot}_T\,\widehat{\mathbf{E}}_T^1=0. \end{cases} \tag{A.30}$$

Ce problème est complété par des conditions aux bords, obtenues en identifiant les termes en δ^0 dans les conditions aux bords

$$\left|\begin{array}{l} \widehat{\mathbf{E}}_T^1\times\mathbf{n}_T=0,\\ \widehat{E}_3^1\,\mathbf{n}_T-g\,\widehat{\mathbf{E}}_T^0=0,\\ \left((\mathrm{i}\,\omega\,\mu+\sigma_m)\,\widehat{\mathbf{H}}_T^1\right)\cdot\mathbf{n}_T+\,g\left((\mathrm{i}\,\omega\,\mu+\sigma_m)\,\widehat{H}_3^0\right)=0. \end{array}\right. \tag{A.31}$$

• **Champ magnétique longitudinal $\widehat{H}_3^0$**

En utilisant la première équation de (A.21), il est facile de vérifier que H_3^0 ne dépend pas de x_1 et x_2. On intègre, la dernière équation de (A.30) sur la surface $S(x_3)$, nous obtenons,

$$\widehat{H}_3^0\int_S \mathrm{i}\,\omega\,\mu+\sigma_m\,\mathrm{d}\mathbf{x}_T+\int_S \mathrm{rot}_T\,\widehat{E}_T^1\,\mathrm{d}\mathbf{x}_T=0.$$

D'après (A.31) nous avons

$$\underline{\mathrm{E}}_T^1\times\mathbf{n}_T=0,\ \forall\mathbf{x}\in\partial\Omega,$$

donc $\displaystyle\int_S \mathrm{rot}_T\,\widehat{E}_T^1\,\mathrm{d}\sigma=0$ et puisque $\displaystyle\int_S \mathrm{i}\,\omega\,\mu+\sigma_m\,\mathrm{d}\mathbf{x}_T\neq 0$, nous obtenons donc

$$\widehat{H}_3^0(\mathbf{x},\omega)=0,\quad \mathbf{x}\in\Omega.$$

Construction des équations télégraphistes

On commence par remplacer les champs $\widehat{\mathbf{H}}_T^0$ et $\widehat{\mathbf{E}}_T^0$ dans la première et la troisième équation de (A.30) par leur expressions en fonction respectivement de $\widehat{I}$ et $\widehat{V}$, nous obtenons alors

$$\begin{cases} (\mathrm{i}\,\omega\,\varepsilon\,+\sigma_e)\,\widehat{V}\,\nabla_T\,\widehat{\varphi}_e-\partial_{x_3}\left(\widehat{I}\,\mathbf{e}_3\times\nabla_T\,\widehat{\psi}_m\right)-\mathbf{rot}_T\,\widehat{H}_3^1=\widehat{\mathbf{j}}_T, & \mathbf{x}\in\Omega,\\ (\mathrm{i}\,\omega\,\mu\,+\sigma_m)\,\widehat{I}\,\nabla_T\,\widehat{\psi}_m+\partial_{x_3}\left(\widehat{V}\,\mathbf{e}_3\times\nabla_T\,\widehat{\varphi}_m(\mathbf{x}_T,\omega)\right)+\mathbf{rot}_T\,\widehat{E}_3^1=0, & \mathbf{x}\in\Omega. \end{cases}$$

Ensuite, nous multiplions la première et la deuxième équation, respectivement, par $\nabla_T\,\widehat{\varphi}_e$ et $\nabla_T\,\widehat{\psi}_m$, et nous passons par l'intégration sur la section $S(x_3)$. Nous obtenons alors le

système suivant :

$$\left|\begin{array}{lcl} (\mathrm{i}\,\omega\,\widehat{C}+\widehat{G})\,\widehat{V} & - & \Big(\partial_{x_3}\Big(\widehat{I}\,\mathbf{e}_3\times\nabla_T\,\widehat{\psi}_m\Big),\nabla_T\,\widehat{\varphi}_e(\cdot,x_3,\omega)\Big)_{L^2(S(x_3))} \\ & - & \Big(\mathbf{rot}_T\,\widehat{H}_3^1,\nabla_T\,\widehat{\varphi}_e(\cdot,x_3,\omega)\Big)_{L^2(S(x_3))}=\widehat{f}(x_3,\omega), \\ (\mathrm{i}\,\omega\,\widehat{L}+\widehat{R})\,\widehat{I} & + & \Big(\partial_{x_3}\Big(\widehat{V}\,\mathbf{e}_3\times\nabla_T\,\widehat{\varphi}_e\Big),\nabla_T\,\widehat{\psi}_m(\cdot,x_3,\omega)\Big)_{L^2(S(x_3))} \\ & + & \Big(\mathbf{rot}_T\,\widehat{E}_3^1,\nabla_T\,\widehat{\psi}_m(\cdot,x_3,\omega)\Big)_{L^2(S(x_3))}=0, \end{array}\right. \tag{A.32}$$

où $(\widehat{C},\widehat{G},\widehat{L},\widehat{R})$ sont des coefficients et $\widehat{f}$ est la nouvelle source qui dépendent de x_3 et ω :

- $\widehat{C}(x_3,\omega):=(\varepsilon\,\nabla_T\,\widehat{\varphi}_e(\cdot,x_3,\omega),\nabla_T\,\widehat{\varphi}_e(\cdot,x_3,\omega))_{L^2(S(x_3))}$,
- $\widehat{G}(x_3,\omega):=(\sigma_e\,\nabla_T\,\widehat{\varphi}_e(\cdot,x_3,\omega),\nabla_T\,\widehat{\varphi}_e(\cdot,x_3,\omega))_{L^2(S(x_3))}$,
- $\widehat{L}(x_3,\omega):=\Big(\mu\,\nabla_T\,\widehat{\psi}_m(\cdot,x_3,\omega),\nabla_T\,\widehat{\psi}_m(\cdot,x_3,\omega)\Big)_{L^2(S(x_3))}$,
- $\widehat{R}(x_3,\omega):=\Big(\sigma_m\,\nabla_T\,\widehat{\psi}_m(\cdot,x_3,\omega),\nabla_T\,\widehat{\psi}_m(\cdot,x_3,\omega)\Big)_{L^2(S(x_3))}$,
- $\widehat{f}(x_3,\omega):=\Big(\sigma_m\,\nabla_T\,\widehat{\mathbf{j}}_T(\cdot,x_3,\omega),\nabla_T\,\widehat{\varphi}_e(\cdot,x_3,\omega)\Big)_{L^2(S(x_3))}$.

Nous utilisons (A.29) et (A.7), nous aurons

$$\begin{aligned}\Big(\partial_{x_3}\Big(\widehat{I}\,\mathbf{e}_3\times\nabla_T\,\widehat{\psi}_m\Big),\nabla_T\,\widehat{\varphi}_e\Big)_{L^2(S(x_3))} = & -\Big(\mathbf{rot}_T\,\widehat{\psi}_m,\nabla_T\,\widehat{\varphi}_e\Big)_{L^2(S(x_3))}\,\partial_{x_3}\,\widehat{I} \\ & -\Big(\partial_{x_3}\,\mathbf{rot}_T\,\widehat{\psi}_m,\nabla_T\,\widehat{\varphi}_e\Big)_{L^2(S(x_3))}\,\widehat{I}.\end{aligned} \tag{A.33}$$

De même, nous utilisons (A.26) et (A.7) pour obtenir l'égalité suivante :

$$\begin{aligned}\Big(\partial_{x_3}\Big(\widehat{V}\,\mathbf{e}_3\times\nabla_T\,\widehat{\varphi}_e\Big),\nabla_T\,\widehat{\psi}_m\Big)_{L^2(S(x_3))} = & -\Big(\mathbf{rot}_T\,\widehat{\varphi}_e,\nabla_T\,\widehat{\psi}_m\Big)_{L^2(S(x_3))}\,\partial_{x_3}\,\widehat{V} \\ & -\Big(\partial_{x_3}\,\mathbf{rot}_T\,\widehat{\varphi}_e,\nabla_T\,\widehat{\psi}_m\Big)_{L^2(S(x_3))}\,\widehat{V}.\end{aligned} \tag{A.34}$$

Maintenant, nous appliquons la formule de Green (A.8), puis nous utilisons le fait que $\mathbf{rot}_T(\nabla_T\,\widehat{\varphi}_e)=0$), et que $\nabla_T\,\widehat{\varphi}_e\times\mathbf{n}_T=0$, nous obtenons

$$\Big(\mathbf{rot}_T\,\widehat{H}_3^1,\nabla_T\,\widehat{\varphi}_e(\cdot,x_3,\omega)\Big)_{L^2(S(x_3))}=\int_{\partial S(x_3)}\widehat{H}_3^1\cdot\nabla_T\,\widehat{\varphi}_e(\cdot,x_3,\omega)\times\mathbf{n}_T\,\mathrm{d}\sigma=0. \tag{A.35}$$

D'une façon similaire, nous utilisons la formule de Green (A.8), la deuxième équation de (A.31) et les expressions (A.26) et (A.7), nous obtenons

$$\begin{aligned}\Big(\mathbf{rot}_T\,\widehat{E}_3^1,\nabla_T\,\widehat{\psi}_m(\cdot,x_3,\omega)\Big)_{L^2(S(x_3))} &= \int_{\partial S(x_3)}\widehat{E}_3^1\cdot\nabla_T\,\widehat{\psi}_m(\cdot,x_3,\omega)\times\mathbf{n}_T\,\mathrm{d}\sigma \\ &= -\int_{\partial S(x_3)} g\,\widehat{\mathbf{E}}_T^0\cdot\mathbf{rot}_T\,\widehat{\psi}_m\,\mathrm{d}\sigma \\ &= -\Big(\int_{\partial S(x_3)} g\,\nabla_T\widehat{\varphi}_e\cdot\,\mathrm{d}\sigma\mathbf{rot}_T\,\widehat{\psi}_m\,\mathrm{d}\sigma\Big)\,\widehat{V}.\end{aligned} \tag{A.36}$$

Par conséquent, nous obtenons le problème suivant :

$$\left|\begin{array}{ll} (\mathrm{i}\,\omega\,\widehat{C}+\widehat{G})\,\widehat{V} & +\Big(\mathbf{rot}_T\,\widehat{\psi}_m,\nabla_T\,\widehat{\varphi}_e\Big)_{L^2(S(x_3))}\,\partial_{x_3}\,\widehat{I} \\ & +\Big(\partial_{x_3}\,\mathbf{rot}_T\,\widehat{\psi}_m,\nabla_T\,\widehat{\varphi}_e\Big)_{L^2(S(x_3))}\,\widehat{I}=\widehat{f}, \\ (\mathrm{i}\,\omega\,\widehat{L}+\widehat{R})\,\widehat{I} & -\Big(\mathbf{rot}_T\,\widehat{\varphi}_e,\nabla_T\,\widehat{\psi}_m\Big)_{L^2(S(x_3))}\,\partial_{x_3}\,\widehat{V} \\ & -\Big(\partial_{x_3}\,\mathbf{rot}_T\,\widehat{\varphi}_e,\nabla_T\,\widehat{\psi}_m\Big)_{L^2(S(x_3))}\,\widehat{V} \\ & -\Big(\displaystyle\int_{\partial S(x_3)} g\,\nabla_T\widehat{\varphi}_e\cdot\,\mathrm{d}\sigma\mathbf{rot}_T\,\widehat{\psi}_m\,\mathrm{d}\sigma\Big)\,\widehat{V}=0. \end{array}\right. \tag{A.37}$$

Propriété A.2.3. *Soient $(\varphi_e,\psi_m)\in H^1(S(x_3))\times H^1(S(x_3)\backslash\Sigma)$ les solutions, respectivement, des problèmes (A.25) et (A.28). Nous avons*

- $\Big(\mathbf{rot}_T\,\widehat{\psi}_m,\nabla_T\,\widehat{\varphi}_e\Big)_{L^2(S(x_3))}=-\Big(\mathbf{rot}_T\,\widehat{\varphi}_e,\nabla_T\,\widehat{\psi}_m\Big)_{L^2(S(x_3))}=1.$
- $\Big(\partial_{x_3}\,\mathbf{rot}_T\,\widehat{\varphi}_e,\nabla_T\,\widehat{\psi}_m\Big)_{L^2(S(x_3))}+\Big(\displaystyle\int_{\partial S(x_3)} g\,\nabla_T\widehat{\varphi}_e\cdot\,\mathbf{rot}_T\,\widehat{\psi}_m\,d\sigma\Big)=0.$
- $\Big(\partial_{x_3}\,\mathbf{rot}_T\,\widehat{\psi}_m,\nabla_T\,\widehat{\varphi}_e\Big)_{L^2(S(x_3))}=0.$

Démonstration. Voir [34] page 19. ■

Finalement, nous obtenons les équations suivantes :

$$\begin{cases} (i\omega\,\widehat{C}(x_3,\omega)+\widehat{G}(x_3,\omega))\,\widehat{V}(x_3,\omega)+\partial_{x_3}\,\widehat{I}(x_3,\omega)=\widehat{f}, & x_3\in\mathbb{R}, \\ (i\omega\,\widehat{L}(x_3,\omega)+\widehat{R}(x_3,\omega)\,\widehat{I}(x_3,\omega)+\partial_{x_3}\,\widehat{V}(x_3,\omega)=0, & x_3\in\mathbb{R}. \end{cases} \tag{A.38}$$

Les coefficients homogénéisés

Lemme A.2.3. *Nous définissons la décomposition suivante :*

$$\widehat{\varphi}_e(\omega)=\widehat{\varphi}_r(\omega)+\varphi.$$

La fonction φ est la limite de $\widehat{\varphi}_e(\omega)$ lorsque $|\omega|\longrightarrow+\infty$, et elle est l'unique solution de

$$\begin{cases} \mathrm{div}_T\,\Big(\varepsilon\,\nabla_T\,\varphi\Big)=0, & dans\,S(x_3), \\ \varphi=1, & sur\,\Gamma_i, \\ \varphi=0, & sur\,\Gamma_e, \end{cases} \tag{A.39}$$

et nous avons que $\widehat{\varphi}_r(\omega)$ est la solution du problème

$$\begin{cases} \mathrm{div}_T\,\Big((i\omega\varepsilon+\sigma_e)\,\nabla_T\,\widehat{\varphi}_r\Big)=-\mathrm{div}_T\,\Big(\sigma_e\,\nabla_T\,\varphi\Big), & dans\,S(x_3), \\ \varphi_r=0, & sur\,\partial S(x_3). \end{cases} \tag{A.40}$$

Lemme A.2.4. *Nous définissons la décomposition suivante :*

$$\widehat{\psi}_m(\omega) = \widehat{\psi}_r(\omega) + \psi.$$

- *ψ est la limite de $\widehat{\psi}_m(\omega)$ lorsque $|\omega| \longrightarrow +\infty$, et elle est l'unique solution de*

$$\begin{cases} \operatorname{div}_T\left(\mu\,\nabla_T\,\psi\right) = 0, & \mathbf{x}_T \in \widetilde{S}(x_3), \\ \nabla_T\,\psi\cdot\mathbf{n}_T = 0, & \mathbf{x}_T \in \partial S(x_3), \\ [\psi] = 1, & \mathbf{x}_T \in \Sigma, \\ [\mu\,\nabla_T\,\psi\cdot\mathbf{n}_T] = 0, & \mathbf{x}_T \in \Sigma. \end{cases} \tag{A.41}$$

- *$\widehat{\psi}_r(\omega)$ est la solution du problème*

$$\begin{cases} \operatorname{div}_T\left((i\omega\mu+\sigma_m)\,\nabla_T\,\widehat{\psi}_r\right) = -\operatorname{div}_T\left(\sigma_m\,\nabla_T\,\psi\right), & \mathbf{x}_T \in \widetilde{S}(x_3), \\ \nabla_T\,\widehat{\psi}_r\cdot\mathbf{n}_T = 0, & \mathbf{x}_T \in \partial S(x_3), \\ [\widehat{\psi}_r] = 0, & \mathbf{x}_T \in \Sigma, \\ [(i\omega\mu+\sigma_m)\,\nabla_T\,\widehat{\psi}_r\cdot\mathbf{n}_T] = -[\sigma_m\,\nabla_T\,\psi\cdot\mathbf{n}_T], & \mathbf{x}_T \in \Sigma. \end{cases} \tag{A.42}$$

Lemme A.2.5. *Les coefficients homogénéisés satisfont*

$$i\omega\,\widehat{C}(x_3,\omega) + \widehat{G}(x_3,\omega) = i\omega\,C + G + \widehat{k}_e(\omega),$$
$$i\omega\,\widehat{L}(x_3,\omega) + \widehat{R}(\omega) = i\omega\,L + R + \widehat{k}_m(\omega),$$

où

- $C = (\varepsilon\,\nabla_T\,\varphi, \nabla_T\,\varphi)_{L^2(S(x_3))}$,
- $L = (\mu\,\nabla_T\,\psi, \nabla_T\,\psi)_{L^2(S(x_3))}$,
- $G = (\sigma_e\,\nabla_T\,\varphi, \nabla_T\,\varphi)_{L^2(S(x_3))}$,
- $R = (\sigma_m\,\nabla_T\,\psi, \nabla_T\,\psi)_{L^2(S(x_3))}$,
- $\widehat{k}_e(\omega) = (\sigma_e\,\nabla_T\,\widehat{\varphi}_r(\omega), \nabla_T\,\varphi)_{L^2(S(x_3))}$,
- $\widehat{k}_m(\omega) = \left(\sigma_m\,\nabla_T\,\widehat{\psi}_r(\omega), \nabla_T\,\psi\right)_{L^2(S(x_3))}$,

et

$$\widehat{k}_e(\omega) \in L(\mathbb{R}) \cup L^2(\mathbb{R}), \quad \widehat{k}_m(\omega) \in L(\mathbb{R}) \cup L^2(\mathbb{R}).$$

Le théorème A.2.5 nous permet de réécrire le problème (A.38) comme suit

$$\begin{cases} (i\omega\,C + G\,\widehat{V}(x_3,\omega) + \partial_{x_3}\,\widehat{I}(x_3,\omega) + \widehat{k}_e(\omega)\,\widehat{V}(x_3,\omega) = \widehat{f}, & x_3 \in \mathbb{R}, \\ (i\omega\,L + R\,\widehat{I}(x_3,\omega) + \partial_{x_3}\,\widehat{V}(x_3,\omega) + \widehat{k}_m(\omega)\,\widehat{I}(x_3,\omega) = 0, & x_3 \in \mathbb{R}. \end{cases} \tag{A.43}$$

Les noyaux de convolutions $k_e(t)$ et $k_m(t)$

Nous notons par $\mathcal{F}^{-1}$ la transformée de Fourier inverse, alors nous avons

$$\blacksquare\ k_e(t) = \mathcal{F}^{-1}\left(\widehat{k}_e(\omega)\right) = \left(\sigma_e\,\nabla_T\,\varphi_r(t), \nabla_T\,\varphi\right)_{L^2(S(x_3))}(t),$$

$$\blacksquare\ k_m(t) = \mathcal{F}^{-1}\left(\widehat{k}_m(\omega)\right) = \left(\sigma_m\,\nabla_T\,\psi_r(t), \nabla_T\,\psi\right)_{L^2(S(x_3))}(t),$$

avec $\varphi_r(t) = \mathcal{F}^{-1}\left(\widehat{\varphi}_r(\omega)\right)$ et $\psi_r(t) = \mathcal{F}^{-1}\left(\widehat{\psi}_r(\omega)\right)$ les solutions des problèmes obtenus après l'application de la transformée de Fourier inverse sur (A.40) et (A.42) :

$$\begin{cases} \mathrm{div}_T\left((\varepsilon\,\partial_t + \sigma_e)\,\nabla_T\,\varphi_r\right) = -\delta_0(t)\,\mathrm{div}_T\left(\sigma_e\,\nabla_T\,\varphi\right), & \text{dans } S(x_3), \quad t \in \mathbb{R}, \\ \varphi_r = 0, & \text{sur } \partial S(x_3), \quad t \in \mathbb{R}, \end{cases} \tag{A.44}$$

et

$$\begin{cases} \mathrm{div}_T\left((\mu\,\partial_t + \sigma_m)\,\nabla_T\,\psi_r\right) = -\delta_0(t)\,\mathrm{div}_T\left(\sigma_m\,\nabla_T\,\psi\right), & \mathbf{x}_T \in \widetilde{S}(x_3), \quad t \in \mathbb{R}, \\ \nabla_T\,\psi_r \cdot \mathbf{n}_T = 0, & \mathbf{x}_T \in \partial S(x_3), \quad t \in \mathbb{R}, \\ [\psi_r] = 0, & \mathbf{x}_T \in \Sigma, \quad t \in \mathbb{R}, \\ [(\mu\,\partial_t + \sigma_m)\,\nabla_T\,\psi_r \cdot \mathbf{n}_T] = -\delta_0(t)\,[\sigma_m\,\nabla_T\,\psi \cdot \mathbf{n}_T], & \mathbf{x}_T \in \Sigma, \quad t \in \mathbb{R}. \end{cases} \tag{A.45}$$

Théorème A.2.1.
Les problèmes (A.44) et (A.45), pour des temps positifs ($t \geqslant 0$), possèdent une unique solution

$$\varphi_r \in C\left(\mathbb{R}^+, H_0^1(S)\right), \quad \psi_r \in C\left(\mathbb{R}^+, H_0^1(S)\right).$$

Pour des temps négatifs ($t < 0$), ces deux problèmes possèdent une unique solution (φ_r, ψ_r) avec φ_r , respectivement ψ_r, est nulle ou exponentiellement croissante lorsque $(-t)$ augmente.

Démonstration. Voir la thèse [35] page 106. ■

Les équations 1D en domaine temporel

Le problème temporel s'obtient en appliquant la transformée de Fourier inverse sur le problème (A.43), et s'écrit comme suit

$$\begin{cases} C\,\partial_t\,V + G\,V + \partial_{x_3}\,I + \displaystyle\int_0^t k_e(t-s)V(s)\,ds = f, & x_3 \in \mathbb{R}^+, \quad t > 0, \\ L\,\partial_t\,I + R\,I - \partial_{x_3}\,V + \displaystyle\int_0^t k_m(t-s)I(s)\,ds = 0, & x_3 \in \mathbb{R}^+, \quad t > 0, \end{cases} \tag{A.46}$$

avec les conditions initiales suivantes

$$V(x_3, 0) = I(x_3, 0) = 0.$$

Remarque A.2.4 (Reconstruction du champ électrique 3D)**.** *Nous supposons que la densité de courant* $\mathbf{j}_T$ *est quelconque. Une fois que la tension discrète* $V_h^n(x_3)$ *est calculée, nous pouvons reconstruire les champs électrique et magnétique 3D en utilisant la formule suivante :*

$$\begin{aligned}\widetilde{\mathbf{E}}^\delta(\mathbf{x},t) \underset{\delta\to 0}{\sim} \widetilde{\mathbf{E}}^0(\mathbf{x},t) &:= V(x_3,t)\,\nabla_T\varphi(\mathbf{x}_T,x_3) + \int_0^t V(x_3,t-s)\,\nabla_T\varphi_r(\mathbf{x}_T,x_3,s) \\ &\qquad +\xi_e^0(\mathbf{x}_T,x_3,t)\,ds,\\ \widetilde{\mathbf{H}}^\delta(\mathbf{x},t) \underset{\delta\to 0}{\sim} \widetilde{\mathbf{H}}^0(\mathbf{x},t) &:= I(x_3,t)\,\nabla_T\psi(\mathbf{x}_T,x_3).\end{aligned} \tag{A.47}$$

Le potentiel électrostatique ξ_e^0 *est la solution du problème suivant :*

$$\begin{cases} \mathrm{div}_T\Big((\varepsilon\,\partial_t+\sigma_e)\,\xi_e^0(\cdot,x_3,t)\Big) = \mathrm{div}_T\,\mathbf{j}_T, & \text{sur } S(x_3), t>0,\\ \xi_e^0 = 0, & \text{sur } \partial S(x_3),\\ \xi_e^0 = 0, & \text{pour } t=0. \end{cases} \tag{A.48}$$

Remarque A.2.5 (Reconstruction du champ électrique 3D)**.** *Si nous supposons que la densité de courant* $\mathbf{j}=0$*, alors par analogie avec les solutions du problème limite 3D obtenu par l'analyse asymptotique, nous pouvons utiliser les données initiales comme suit,*

$$\begin{cases} \mathbf{E}_0^\delta(\mathbf{x}_T,x_3) = V_0(x_3)\nabla_T\varphi(\mathbf{x}_T,x_3) + \mathbf{E}_{0,T}^r(\cdot,x_3) + O(\delta),\\ \mathbf{H}_0^\delta(\mathbf{x}_T,x_3) = I_0(x_3)\nabla_T\psi(\mathbf{x}_T,x_3) + \mathbf{H}_{0,T}^r(\cdot,x_3) + O(\delta), \end{cases} \tag{A.49}$$

les potentiels $\varphi(\cdot,x_3)$ *et* $\psi(\cdot,x_3)$ *sont définis, pour chaque* x_3 *qui joue le rôle de paramètre, comme les solutions des problèmes suivants*

$$\begin{cases} \mathrm{div}_T\Big(\varepsilon(\cdot,x_3)\,\nabla_T\varphi(\cdot,x_3)\Big)=0, & \text{dans } \Omega,\\ \varphi(\cdot,x_3)=1, & \text{sur } \Gamma_i,\\ \varphi(\cdot,x_3)=0, & \text{sur } \Gamma_e, \end{cases} \qquad \begin{cases} \mathrm{div}_T\Big(\mu(\cdot,x_3)\,\nabla_T\psi(\cdot,x_3)\Big)=0, & \text{dans } \Omega\setminus\Sigma,\\ \partial_n\psi(\cdot,x_3)=0, & \text{sur } \partial S(x_3),\\ \Big[\psi(\cdot,x_3)\Big]_\Sigma=1,\ \Big[\partial_n\psi(\cdot,x_3)\Big]_\Sigma=0, & \text{sur } \Sigma, \end{cases} \tag{A.50}$$

et, $\mathbf{E}_{0,T}^r$ *et* $\mathbf{H}_{0,T}^r$ *sont donnés par les deux problèmes suivants :*

$$\begin{cases} \mathrm{rot}_T\Big(\mathbf{E}_{0,T}^r(\mathbf{x}_T,x_3)\Big)=0s & \text{dans } \Omega,\\ \mathbf{E}_{0,T}^r\times n_T=0, & \text{sur } \partial\Omega, \end{cases} \qquad \begin{cases} \mathrm{rot}_T\Big(\mathbf{H}_{0,T}^r(\mathbf{x}_T,x_3)\Big)=0 & \text{dans } \Omega,\\ \mathbf{H}_{0,T}^r\cdot n_T=0, & \text{sur } \partial\Omega. \end{cases} \tag{A.51}$$

Enfin, nous pouvons montrer que si les données initiales sont bien préparées alors

$$\begin{aligned}\widetilde{\mathbf{E}}^\delta(\mathbf{x},t) \underset{\delta\to 0}{\sim} \widetilde{\mathbf{E}}^0(\mathbf{x},t) &:= V(x_3,t)\,\nabla_T\varphi(\mathbf{x}_T,x_3) + \int_0^t V(x_3,t-s)\,\nabla_T\varphi_r(\mathbf{x}_T,x_3,s) + \xi_e^0(\mathbf{x}_T,x_3,t)\,ds,\\ \widetilde{\mathbf{H}}^\delta(\mathbf{x},t) \underset{\delta\to 0}{\sim} \widetilde{\mathbf{H}}^0(\mathbf{x},t) &:= I(x_3,t)\,\nabla_T\psi(\mathbf{x}_T,x_3) + \xi_m^0(\mathbf{x}_T,x_3).\end{aligned} \tag{A.52}$$

Les potentiels électrostatiques ξ_e^0 *et* ξ_m^0 *sont les solutions des problèmes suivants :*

$$\begin{cases} \mathrm{div}_T\Big((\varepsilon\,\partial_t+\sigma_e)\,\xi_e^0(\cdot,x_3,t)\Big)=0, & \text{sur } S(x_3), t>0,\\ \xi_e^0=0, & \text{sur } \partial S(x_3),\\ \xi_e^0=\mathbf{E}_{0,T}^r, & \text{pour } t=0. \end{cases} \tag{A.53}$$

$$\begin{cases} \mathrm{div}_T\Big(\mu\,\xi_m^0(\cdot,x_3,t)\Big)=0, & \text{sur } S(x_3),\\ \xi_m^0=0, & \text{sur } \partial S(x_3). \end{cases} \tag{A.54}$$

A.3 Le modèle 1D dans un câble cylindrique et à section circulaire

A.3.1 Les coefficients du modèle 1D

Nous supposons que le câble de référence Ω est cylindrique et avec une section S circulaire de rayon $\mathrm{r}_2 > 0$ et constituée de deux matériaux différents.

Nous choisissons les coefficients des milieux comme suit :

$$(\varepsilon, \sigma_e, \mu, \sigma_m) = \begin{cases} (\varepsilon_1, \sigma_{e,1}, \mu_1, \sigma_{m,1}), & \mathbf{x}_T \in C(1, \mathrm{r}_1), \\ (\varepsilon_2, \sigma_{e,2}, \mu_2, \sigma_{m,2}), & \mathbf{x}_T \in C(\mathrm{r}_1, \mathrm{r}_2), \end{cases}$$

où $C(a, b)$ est la couronne de rayon interne a et de rayon extérieure b.

Les expressions de $\widehat{\varphi}_e$ et des coefficients homogénéisés C et G

On commence par introduire deux fonctions $\widehat{\varphi}_1$ et $\widehat{\varphi}_2$ qui sont les restrictions de $\widehat{\varphi}_e$ sur les deux couronnes, respectivement, $C(1, \mathrm{r}_1)$ et $C(\mathrm{r}_1, \mathrm{r}_2)$.

Selon la construction du domaine de travail, nous avons $\widehat{\varphi}_1$ et $\widehat{\varphi}_2$ solutions de

$$\begin{cases} \Delta\widehat{\varphi}_1 = 0, & \mathbf{x}_T \in C(1, \mathrm{r}_1), \\ \widehat{\varphi}_1 = 1, & \mathbf{x}_T \in \partial D(1), \end{cases} \qquad \begin{cases} \Delta\widehat{\varphi}_2 = 0, & \mathbf{x}_T \in C(\mathrm{r}_1, \mathrm{r}_2), \\ \widehat{\varphi}_2 = 0, & \mathbf{x}_T \in \partial D(\mathrm{r}_2), \end{cases}$$

avec $D(a)$ le disque de rayon a centré en 0, et Δ l'opérateur Laplacien $2D$.

Les conditions de couplage au niveau des deux couronnes sont définies par

$$\widehat{\varphi}_1 = \widehat{\varphi}_2, \qquad \nabla_T\widehat{\varphi}_1 \cdot \mathbf{n}_T = c(\omega)\nabla_T\widehat{\varphi}_2 \cdot \mathbf{n}_T, \qquad x_1^2 + x_1^2 = \mathrm{r}_1^2, \quad \text{avec} \quad c(\omega) = \frac{i\omega\varepsilon_2 + \sigma_{e,2}}{i\omega\varepsilon_1 + \sigma_{e,1}}.$$

Si nous utilisons les coordonnées polaires (r, θ), alors selon la configuration géométrique nous constatons que les $\widehat{\varphi}_i$ ne dépendent pas de θ.

Par suite, les équations précédentes se réécrivent comme suit :

$$\begin{cases} \dfrac{\partial}{\partial r} r \dfrac{\partial}{\partial r}\widehat{\varphi}_1 = 0, & r \in (1, \mathrm{r}_1), \\ \dfrac{\partial}{\partial r} r \dfrac{\partial}{\partial r}\widehat{\varphi}_2 = 0, & r \in (\mathrm{r}_1, \mathrm{r}_2), \end{cases}$$

et les conditions de couplage sont données par

$$\begin{cases} \widehat{\varphi}_1 = 1, & r = 1, \\ \widehat{\varphi}_2 = 0, & r = \mathrm{r}_2, \\ \widehat{\varphi}_1 = \widehat{\varphi}_2, & r = \mathrm{r}_1, \\ \dfrac{\partial}{\partial r}\widehat{\varphi}_1 = c(\omega)\dfrac{\partial}{\partial r}\widehat{\varphi}_2, & r = \mathrm{r}_1. \end{cases}$$

Les solutions de ce problème sont de la forme

$$\widehat{\varphi}_i = A_i(\omega)\ \ln(r) + B_i(\omega), \qquad i = 1 \text{ ou } 2.$$

- Pour $r = 1$: $\widehat{\varphi}_1 = 1 \Rightarrow B_1(\omega) = 1$,
- Pour $r = \mathrm{r}_2$: $\widehat{\varphi}_2 = 0 \Rightarrow A_2(\omega)\ \ln(\mathrm{r}_2) = -B_2(\omega)$,
- Pour $r = \mathrm{r}_1$:

$$\frac{\partial}{\partial r}\widehat{\varphi}_1 = c(\omega)\frac{\partial}{\partial r}\widehat{\varphi}_2 \Rightarrow A_1(\omega) = c(\omega)\ A_2(\omega),$$

$$\begin{aligned} \widehat{\varphi}_1 = \widehat{\varphi}_2 \ &\Rightarrow A_1(\omega)\ \ln(\mathrm{r}_1) + 1 = A_2(\omega)\ \ln(\mathrm{r}_1) + B_2(\omega), \\ &\Rightarrow c(\omega)\ A_2(\omega)\ \ln(\mathrm{r}_1) + 1 = A_2(\omega)\ \ln(\mathrm{r}_1) - A_2(\omega)\ \ln(\mathrm{r}_2), \\ &\Rightarrow A_2(\omega) = \frac{1}{c(\omega)\ \ln(\frac{1}{\mathrm{r}_1}) + \ln(\frac{\mathrm{r}_1}{\mathrm{r}_2})}. \end{aligned}$$

Par conséquent, nous avons :

- $A_2(\omega) = \dfrac{1}{c(\omega)\ \ln(\frac{1}{\mathrm{r}_1}) + \ln(\frac{\mathrm{r}_1}{\mathrm{r}_2})}$, $\quad$ - $B_2(\omega) = \dfrac{-\ln(\mathrm{r}_2)}{c(\omega)\ \ln(\frac{1}{\mathrm{r}_1}) + \ln(\frac{\mathrm{r}_1}{\mathrm{r}_2})}$,
- $A_1(\omega) = \dfrac{c(\omega)}{c(\omega)\ \ln(\frac{1}{\mathrm{r}_1}) + \ln(\frac{\mathrm{r}_1}{\mathrm{r}_2})}$, $\quad$ - $B_1(\omega) = 1$.

Il est clair maintenant que

$$\nabla_T\widehat{\varphi}_1 = \frac{1}{r}A_1(\omega)\ e_r, \ \text{ et } \nabla_T\widehat{\varphi}_2 = \frac{1}{r}A_2(\omega)\ e_r,$$

ainsi, nous avons

$$\begin{aligned} C(\omega) &= 2\pi\varepsilon_1\int_1^{\mathrm{r}_1}\frac{1}{r}|A_1(\omega)|^2\ dr\ + 2\pi\varepsilon_2\int_{\mathrm{r}_1}^{\mathrm{r}_2}\frac{1}{r}|A_2(\omega)|^2\ dr, \\ &= 2\pi\varepsilon_1|A_1(\omega)|^2\ \ln(\mathrm{r}_1) + 2\pi\varepsilon_2|A_2(\omega)|^2\ \ln(\frac{\mathrm{r}_2}{\mathrm{r}_1}), \end{aligned}$$

de même

$$G(\omega) = 2\pi\sigma_{e,1}|A_1(\omega)|^2\ \ln(\mathrm{r}_1) + 2\pi\sigma_{e,2}|A_2(\omega)|^2\ \ln(\frac{\mathrm{r}_2}{\mathrm{r}_1}).$$

Nous avons

$$A_1(\omega) \xrightarrow[|\omega|\to+\infty]{} \frac{\varepsilon_2}{\langle\varepsilon\rangle}, \quad A_2(\omega) \xrightarrow[|\omega|\to+\infty]{} \frac{\varepsilon_1}{\langle\varepsilon\rangle},$$

$$B_1(\omega) \xrightarrow[|\omega|\to+\infty]{} 1, \quad B_2(\omega) \xrightarrow[|\omega|\to+\infty]{} -\ln(\mathrm{r}_2)\,\frac{\varepsilon_1}{\langle\varepsilon\rangle},$$

avec la notation $\langle\cdot\rangle$ définie par :

$$\langle f\rangle = f_1\,\ln(\frac{\mathrm{r}_1}{\mathrm{r}_2}) + f_2\,\ln(\frac{1}{\mathrm{r}_1}), \tag{A.55}$$

où $f(r) = \begin{cases} f_1 & \text{pour } 1 < r < \mathrm{r}_1, \\ f_2 & \text{pour } \mathrm{r}_1 < r < \mathrm{r}_2. \end{cases}$

Si nous faisons tendre $|\omega|$ vers $+\infty$ dans les deux expressions $C(\omega)$ et $G(\omega)$, nous obtenons

$$C = -2\pi\frac{\varepsilon_1\varepsilon_2}{\langle\varepsilon\rangle}, \tag{A.56}$$

$$G = 2\pi\frac{\sigma_{e,1}(\varepsilon_2)^2\,\ln(\mathrm{r}_1) + \sigma_{e,2}(\varepsilon_1)^2\,\ln(\frac{\mathrm{r}_2}{\mathrm{r}_1})}{\langle\varepsilon\rangle^2}. \tag{A.57}$$

Il est possible de calculer φ_e en prenant la limite formelle de $\widehat{\varphi}_e$ lorsque $|\omega|$ tend vers l'infini,

$$\varphi_e = \begin{cases} 1 + \ln(r)\,\dfrac{\varepsilon_2}{\langle\varepsilon\rangle}, & r \le \mathrm{r}_1, \\ \dfrac{\varepsilon_1}{\langle\varepsilon\rangle}\ln(\dfrac{r}{\mathrm{r}_2}), & r > \mathrm{r}_1. \end{cases}$$

Les expressions de $\widehat{\psi}_m$ et des coefficients homogénéisés L et R

Nous choisissons la coupure Σ de cette façon :

$$\Sigma = [1, \mathrm{r}_2],$$

et nous supposons que la restriction de $\widehat{\psi}_m$ sur $C(1,\mathrm{r}_1)$ (respectivement sur $C(\mathrm{r}_1,\mathrm{r}_2)$) est égale à $\widehat{\psi}_1$ (respectivement $\widehat{\psi}_2$). Donc $\widehat{\psi}_1$ et $\widehat{\psi}_2$ sont les solutions des deux problèmes suivants :

$$\begin{cases} \Delta\widehat{\psi}_1 = 0, & \mathbf{x}_T \in C(1,\mathrm{r}_1)\setminus\Sigma, \\ \nabla_T\widehat{\psi}_1\cdot\mathbf{n}_T = 0, & \mathbf{x}_T \in \partial D(1), \\ [\widehat{\psi}_1] = 1, & \mathbf{x}_T \in C(1,\mathrm{r}_1)\cap\Sigma, \\ [\nabla_T\widehat{\psi}_1\cdot\mathbf{n}_T] = 0, & \mathbf{x}_T \in C(1,\mathrm{r}_1)\cap\Sigma, \end{cases} \qquad \begin{cases} \Delta\widehat{\psi}_2 = 0, & \mathbf{x}_T \in C(\mathrm{r}_1,\mathrm{r}_2)\setminus\Sigma, \\ \nabla_T\widehat{\psi}_2\cdot\mathbf{n}_T = 0, & \mathbf{x}_T \in \partial D(\mathrm{r}_2), \\ [\widehat{\psi}_2] = 1, & \mathbf{x}_T \in C(\mathrm{r}_1,\mathrm{r}_2)\cap\Sigma, \\ [\nabla_T\widehat{\psi}_2\cdot\mathbf{n}_T] = 0, & C(\mathrm{r}_1,\mathrm{r}_2)\cap\Sigma, \end{cases}$$

où les conditions de raccordement au niveau des couronnes $C(1,\mathrm{r}_1)$ et $C(\mathrm{r}_1,\mathrm{r}_2)$ sont :

$$\widehat{\psi}_1 = \widehat{\psi}_2, \qquad \nabla_T \widehat{\psi}_1 \cdot \mathbf{n}_T = \frac{i\omega\mu_2 + \sigma_{m,2}}{i\omega\mu_1 + \sigma_{m,1}} \nabla_T \widehat{\psi}_2 \cdot \mathbf{n}_T, \qquad x_1^2 + x_1^2 = \mathrm{r}_1^2.$$

On se place maintenant en coordonnées polaires (r, θ). Il apparaît que $\nabla_T \widehat{\psi}_i$, $i = 1$ ou 2, est indépendant de θ.

Le fait que

$$\nabla_T \widehat{\psi}_i(r) = (\frac{\partial}{\partial r} \widehat{\psi}_i \; e_r + \frac{1}{r} \frac{\partial}{\partial \theta} \widehat{\psi}_i)(r), \qquad i = 1 \;\text{ ou }\; 2,$$

implique

$$\Delta \widehat{\psi}_i(r) = 0 \Rightarrow \mathrm{div}_T \nabla_T \widehat{\psi}_i(r) = \frac{1}{r} \frac{\partial}{\partial r} r \frac{\partial}{\partial r} \widehat{\psi}_i(r) = 0,$$

$$\Rightarrow \frac{\partial}{\partial r} \widehat{\psi}_i(r) = \frac{c_i}{r}, \quad i = 1 \,\text{ou}\, 2,$$

avec $c_i \in \mathbb{C}$, or $\nabla_T \widehat{\psi}_i \cdot n = 0$ sur les frontières. Par suite $c_i = 0$, ce qui montre que $\widehat{\psi}_i$ ne dépend pas de r. Donc la forme générale de $\widehat{\psi}_i$ est :

$$\widehat{\psi}_i(r, \theta) = A_i \, \theta + B_i.$$

D'après la condition sur le cercle de rayon r_1 nous avons

$$\widehat{\psi}_1 = \widehat{\psi}_2 \Rightarrow A_1 = A_2 \text{ et } B_1 = B_2.$$

Maintenant, nous utilisons la condition de saut :

$$[\widehat{\psi}_i]_{|\Sigma} = 1 \Rightarrow \widehat{\psi}_i(r, 0) = 1 \text{ et } \widehat{\psi}_i(r, 2\pi) = 0,$$

$$\Rightarrow B = 1 \text{ et } A = -\frac{1}{2\pi}.$$

Nous obtenons alors

$$\widehat{\psi}_m(r, \theta) = \widehat{\psi}_i(r, \theta) = 1 - \frac{\theta}{2\pi}, \quad i = 1 \,\text{ou}\, 2. \tag{A.58}$$

Nous avons $\widehat{\psi}_m \equiv \psi_m$ et $\widehat{\psi}_m^r(\omega) = 0$, car $\widehat{\psi}_m$ ne dépend pas de ω. Par conséquent le noyau de convolution $k_m(t)$ est nul.

Il est clair que $\nabla_T \widehat{\psi}_m$ ne dépend pas de ω et

$$\nabla_T \widehat{\psi}_m(r, \theta) = -\frac{1}{2\pi r} \, e_\theta, \quad i = 1 \,\text{ou}\, 2.$$

Donc, nous obtenons

$$L(\omega) = L = \frac{1}{2\pi} \left(\mu_1 \, \ln(\mathrm{r}_1) + \mu_2 \, \ln(\frac{\mathrm{r}_2}{\mathrm{r}_1}) \right), \tag{A.59}$$

$$R(\omega) = R = \frac{1}{2\pi} \left(\sigma_{m,1} \, \ln(\mathrm{r}_1) + \sigma_{m,2} \, \ln(\frac{\mathrm{r}_2}{\mathrm{r}_1}) \right). \tag{A.60}$$

Les expressions de φ_e^r et du noyau de convolution $k_e(t)$

Suivant la géométrie de la section S, nous choisissons φ_e^r sous cette forme :

$$\varphi_e^r(r,t) = \begin{cases} \varphi_1^r(r,t), & r \leq \mathrm{r}_1, \\ \\ \varphi_2^r(r,t), & r > \mathrm{r}_1. \end{cases}$$

Où $\varphi_1^r(r,t)$ et $\varphi_2^r(r,t)$ sont les solutions de deux problèmes suivants :

$$\begin{cases} \dfrac{\partial}{\partial r} r \dfrac{\partial}{\partial r} \left(\varepsilon_1 \partial_t \varphi_1^r + \sigma_{e,1} \varphi_1^r\right) = 0, & r \in (1, \mathrm{r}_1),\ t > 0, \\ \varphi_1^r = 0, & r = 1,\ t > 0, \end{cases}$$

et

$$\begin{cases} \dfrac{\partial}{\partial r} r \dfrac{\partial}{\partial r} \left(\varepsilon_2 \partial_t \varphi_2^r + \sigma_{e,2} \varphi_2^r\right) = 0, & r \in (\mathrm{r}_1, \mathrm{r}_2),\ t > 0, \\ \varphi_2^r = 0, & r = \mathrm{r}_2,\ t > 0, \end{cases}$$

avec les conditions de raccordements :

$$\varphi_1^r + \varphi_2^r, \qquad \varepsilon_1 \partial_t \frac{\partial}{\partial r} \varphi_1^r + \sigma_{e,1} \frac{\partial}{\partial r} \varphi_1^r = \varepsilon_2 \partial_t \frac{\partial}{\partial r} \varphi_2^r + \sigma_{e,2} \frac{\partial}{\partial r} \varphi_2^r, \qquad x_1^2 = x_2^2 = \mathrm{r}_1^2,$$

et la condition initiale est donnée par l'égalité suivante :

$$\frac{\partial}{\partial r} r\varepsilon \frac{\partial}{\partial r} \varphi_e^r(r,0) = -\frac{\partial}{\partial r} r\sigma_e \frac{\partial}{\partial r} \varphi_e, \qquad r \in (1, \mathrm{r}_2).$$

Nous allons chercher des solutions sous la forme :

$$\varphi_i^r(r,t) = A_i(t)\ \ln(r) + B_i(t).$$

• Pour $r = 1$: $\quad \varphi_1^r = 0 \Rightarrow B_1(t) = 0,$

• Pour $r = \mathrm{r}_2$: $\quad \varphi_2^r = 0 \Rightarrow B_2(t) = -A_2(t)\ \ln(\mathrm{r}_2),$

• Pour $r = \mathrm{r}_1$: $\quad \varphi_1^r = \varphi_2^r \Rightarrow A_1(t) = -\ln\left(\dfrac{1}{\mathrm{r}_1}\right)^{-1}\ \ln\left(\dfrac{\mathrm{r}_1}{\mathrm{r}_2}\right)\ A_2(t)$, et

$$\varepsilon_1 \partial_t \frac{\partial}{\partial r} \varphi_1^r + \sigma_{e,1} \frac{\partial}{\partial r} \varphi_1^r = \varepsilon_2 \partial_t \frac{\partial}{\partial r} \varphi_2^r + \sigma_{e,2} \frac{\partial}{\partial r} \varphi_2^r$$

$$\Rightarrow \left(\varepsilon_2 + \varepsilon_1\ \ln\left(\frac{1}{\mathrm{r}_1}\right)^{-1}\ \ln\left(\frac{\mathrm{r}_1}{\mathrm{r}_2}\right)\right) \partial_t A_1(t) = -\left(\sigma_{e,2} + \sigma_{e,1}\ \ln\left(\frac{1}{\mathrm{r}_1}\right)^{-1}\ \ln\left(\frac{\mathrm{r}_1}{\mathrm{r}_2}\right)\right) A_1(t),$$

$$\Rightarrow \langle\varepsilon\rangle\ \partial_t A_1(t) = -\langle\sigma\rangle\ A_1(t),$$

$$\Rightarrow \boxed{A_1(t) = A_1(0)\, e^{-\frac{\langle\sigma\rangle}{\langle\varepsilon\rangle} t}.}$$

La condition initiale nous donne :

$$r\varepsilon \frac{\partial}{\partial r} \varphi_e^r(r,0) = -r\sigma_e \frac{\partial}{\partial r} \varphi_e + c, \quad r \in (1, \mathrm{r}_2),$$

avec c est une constante.

Par suite, il est facile de montrer que

$$\begin{cases} \varepsilon_1\, A_1(0) = \dfrac{\sigma_{e,1}\,\varepsilon_2}{\langle\varepsilon\rangle} + c, \\ \varepsilon_2\, A_2(0) = \dfrac{\sigma_{e,2}\,\varepsilon_1}{\langle\varepsilon\rangle} + c. \end{cases}$$

Alors, nous avons

$$\begin{cases} \varepsilon_2\, A_2(0) = \dfrac{\sigma_{e,2}\,\varepsilon_1}{\langle\varepsilon\rangle} + c, \\ -\varepsilon_1 \ln\left(\dfrac{1}{\mathrm{r}_1}\right)^{-1} \ln\left(\dfrac{\mathrm{r}_1}{\mathrm{r}_2}\right)\; A_2(t) = \dfrac{\sigma_{e,1}\,\varepsilon_2}{\langle\varepsilon\rangle} + c. \end{cases}$$

Par suite, nous trouvons

$$A_2(0) = \ln\left(\frac{1}{\mathrm{r}_1}\right) \frac{\sigma_{e,2}\,\varepsilon_1 - \sigma_{e,1}\,\varepsilon_2}{\langle\varepsilon\rangle^2}.$$

Ainsi, nous obtenons les expressions explicites de $A_1(t)$ et $A_2(t)$:

$$A_1(t) = \ln\left(\frac{\mathrm{r}_1}{\mathrm{r}_2}\right) \frac{\sigma_{e,1}\,\varepsilon_2 - \sigma_{e,2}\,\varepsilon_1}{\langle\varepsilon\rangle^2}\, e^{-\frac{\langle\sigma\rangle}{\langle\varepsilon\rangle}t}, \quad A_2(t) = \ln\left(\frac{1}{\mathrm{r}_1}\right) \frac{\sigma_{e,2}\,\varepsilon_1 - \sigma_{e,1}\,\varepsilon_2}{\langle\varepsilon\rangle^2}\, e^{-\frac{\langle\sigma\rangle}{\langle\varepsilon\rangle}t}.$$

Finalement, l'expression explicite de φ_e^r est donnée par :

$$\varphi_e^r = \begin{cases} \ln\left(\dfrac{\mathrm{r}_1}{\mathrm{r}_2}\right) \dfrac{\sigma_{e,1}\,\varepsilon_2 - \sigma_{e,2}\,\varepsilon_1}{\langle\varepsilon\rangle^2}\, e^{-\frac{\langle\sigma\rangle}{\langle\varepsilon\rangle}t} \ln(r), & r \le \mathrm{r}_1, \\ \ln\left(\dfrac{1}{\mathrm{r}_1}\right) \dfrac{\sigma_{e,2}\,\varepsilon_1 - \sigma_{e,1}\,\varepsilon_2}{\langle\varepsilon\rangle^2}\, e^{-\frac{\langle\sigma\rangle}{\langle\varepsilon\rangle}t} \ln\left(\dfrac{r}{\mathrm{r}_2}\right), & r > \mathrm{r}_1. \end{cases}$$

Maintenant, à l'aide des expressions explicites de φ_e^r et φ_e, nous déduisons l'expression de $k_e(t)$.

$$k_e(t) = (\sigma_e \nabla_T \varphi_e^r, \nabla_T \varphi_e)_{L^2(S)} = k_e(0)\, e^{-\frac{\langle\sigma\rangle}{\langle\varepsilon\rangle}t},$$

avec

$$k_e(0) = 2\pi \frac{\ln(\frac{1}{\mathrm{r}_1})\ln(\frac{\mathrm{r}_2}{\mathrm{r}_1})(\sigma_{e,1}\,\varepsilon_2 - \sigma_{e,2}\,\varepsilon_1)^2}{\langle\varepsilon\rangle^3}. \tag{A.61}$$

A.3.2 Discrétisation espace/temps

Après avoir calculé les coefficients homogénéisés et les noyaux de convolutions, nous nous intéressons à résoudre numériquement le modèle suivant :

$$\begin{cases} C\,\partial_t V + G\,V + \partial_{x_3} I + k_e(0) \displaystyle\int_0^t e^{-\frac{\langle\sigma\rangle}{\langle\varepsilon\rangle}s}\, V(t-s)\, ds = f(x_3,t), & x_3 \in \mathbb{R}^+, \quad t > 0, \\ L\,\partial_t I + R\,I - \partial_{x_3} V = 0, & x_3 \in \mathbb{R}^+, \quad t > 0, \end{cases} \tag{A.62}$$

avec C, G, L, R, $k_e(0)$, $\langle\varepsilon\rangle$, et $\langle\sigma\rangle$ sont des scalaires donnés par (A.56), (A.57), (A.60), (A.61), et (A.55).

Il s'agit des équations différentielles contenant un terme non local en temps ce qui pose un problème au niveau de la simulation numérique. Pour surmonter cette difficulté on propose deux approches d'approximation stables.

Première Approche

Nous pouvons utiliser cette approche juste pour le cas où la section S est circulaire, et elle consiste à simplifier la première équation de (A.62) en remplaçant le terme non local par une inconnue auxiliaire $X(x_3,t)$ telle que :

$$X(x_3,t)=\int_0^t e^{-\frac{\langle\sigma\rangle}{\langle\varepsilon\rangle}s}\,V(t-s)\,ds.$$

Puis, nous montrons facilement que X est la solution de l'équation suivante :

$$\partial_t X+c\,X=V,\quad \text{avec}\quad c=\frac{\langle\varepsilon\rangle}{\langle\sigma\rangle}.$$

Par conséquent, le problème (A.62) peut se réécrire sous la forme suivante :

$$\begin{cases} C\,\partial_t V+G\,V+\partial_{x_3} I+k_e(0)\,X=f(x_3,t), & x_3\in\mathbb{R}^+,\quad t>0,\\ \partial_t X+c\,X=V, & x_3\in\mathbb{R}^+,\quad t>0,\\ L\,\partial_t I+R\,I-\partial_{x_3} V=0, & x_3\in\mathbb{R}^+,\quad t>0. \end{cases}\tag{A.63}$$

La résolution numérique de ce problème nécessite l'utilisation de conditions de périodicité pour borner le domaine de calcul. Alors, nous cherchons à résoudre le problème suivant :

$$\begin{cases} C\,\partial_t V+G\,V+\partial_{x_3} I+k_e(0)\,X=f(x_3,t), & x_3\in[0,L],\quad t\in[0,T],\\ \partial_t X+c\,X=V, & x_3\in[0,L],\quad t\in[0,T],\\ L\,\partial_t I+R\,I-\partial_{x_3} V=0, & x_3\in[0,L],\quad t\in[0,T]. \end{cases}\tag{A.64}$$

$*$ Conditions initiales :

$$V(x_3,0)=I(x_3,0)=X(x_3,0)=0,\qquad x_3\in[0,L].$$

$*$ Conditions aux bords :

$$V(0,t)=0,\ I(0,t)=0,\qquad t\in[0,T],$$

où T est le temps final et L est la longueur du câble.
Pour résoudre numériquement ce problème, nous allons utiliser la méthode des éléments finis en espace puis la méthode des différences finies.

Discrétisation spatiale :

Nous cherchons à trouver les solutions V et I du problème, (A.64) de telle sorte que

$$V\in H_0^1(0,L),\quad I\in L^2(0,L),$$

où $H_0^1(0,L)=\{u\in H^1(0,L)\quad|\quad u(0)=u(L)=0\}$.
On commence par discrétiser l'intervalle $[0,L]$ en m points, et nous définissons les deux sous-espaces de dimensions finies

$$\mathbb{V}_h = \{u \in H_0^1(0,L) \quad | \quad u_{|[nh,(n+1)h]} \in \mathbb{P}_2,\ n \in \{0 \cdots m-1\}\},$$

$$\mathbb{I}_h = \{u \in L^2(0,L) \quad | \quad u_{|[nh,(n+1)h]} \in \mathbb{P}_1,\ n \in \{0 \cdots m-1\}\}.$$

Il est clair que $V_h \subset H_0^1(0,L)$ et $I_h \subset L^2(0,L)$.

∗ **Formulation variationnelle :**

La formulation variationnelle du problème (A.64) s'écrit comme suit :

Trouver $(V(\cdot,t), I(\cdot,t)) \in H_0^1(0,L) \times L^2(0,L)$ telles que

$\forall\, (\widetilde{V}, \widetilde{I}) \in H_0^1(0,L) \times L^2(0,L)$ et $\forall\, t > 0$ nous avons

$$\begin{cases} (C\partial_t + G\,)\,(V(\cdot,t), \widetilde{V})_{L^2(0,L)} + (I(\cdot,t), \partial_{x_3}\widetilde{V})_{L^2(0,L)} + k_e(0)(X(\cdot,t), \widetilde{V})_{L^2(0,L)} = (f(\cdot,t), \widetilde{V})_{L^2(0,L)}, \\ \partial_t\,(X(\cdot,t), \widetilde{V})_{L^2(0,L)} + \dfrac{\langle\sigma\rangle}{\langle\varepsilon\rangle}\,(X(\cdot,t), \widetilde{V})_{L^2(0,L)} = (V(\cdot,t), \widetilde{V})_{L^2(0,L)}, \\ L\partial_t\,(I(\cdot,t), \widetilde{V})_{L^2(0,L)} + R\,(I(\cdot,t), \widetilde{I})_{L^2(0,L)} - (\partial_{x_3} V(\cdot,t), \widetilde{I})_{L^2(0,L)} = 0. \end{cases}$$

∗ **Formulation variationnelle approchée :**

La formulation variationnelle approchée du problème (A.64) s'écrit comme suit :

Trouver $V_h(t)$ et $I_h(t)$ telles que $\forall\, t > 0$ nous avons

$$\begin{cases} C\mathbb{M}_h\,\partial_t\,V_h + G\mathbb{M}_h\,V_h + \mathbb{R}_h\,I_h + k_e(0)\mathbb{M}_h\,X_h = \mathbb{M}_h\,F_h(t), \\ \mathbb{M}_h\,\partial_t\,X_h + \dfrac{\langle\sigma\rangle}{\langle\varepsilon\rangle}\,\mathbb{M}_h\,X_h = \mathbb{M}_h\,V_h, \\ L\mathbb{B}_h\,\partial_t\,I_h + R\mathbb{B}_h\,I_h - \mathbb{R}_h^T\,V_h = 0, \end{cases} \tag{A.65}$$

avec :

- $\mathbb{M}_h$ est une matrice carré symétrique définie positive, $(\mathbb{M}_h)_{i,k} = \displaystyle\int_0^L \varphi_i\varphi_k\,dx.$
- $\mathbb{B}_h$ est une matrice carré symétrique définie positive, $(\mathbb{B}_h)_{i,k} = \displaystyle\int_0^L \psi_i\psi_k\,dx.$
- $\mathbb{R}_h$ est une matrice rectangulaire, $(\mathbb{R}_h)_{i,k} = \displaystyle\int_0^L \partial_x\varphi_i\ \psi_k\,dx.$

où les φ_i et les ψ_i sont respectivement les fonctions de base de l'espace $\mathbb{V}_h$ et $\mathbb{I}_h$.

- $F_h(t) = (f(x_i,t))_{i=1\cdots 2m-1}$.
- $X_h = (X_i(t))_{i=1\cdots 2m-1}$.

Discrétisation temporelle

Dans ce qui suit, nous allons chercher les solutions $(V_h(t), I_h(t))$ du problème (A.65) qui sont déjà discrétisés en espace. Les solutions $(V_h(t), I_h(t))$ seront approchées à différents

instants t^n, avec $t^n = n\,\Delta t$, où $\Delta t > 0$ est le pas de temps fixe. Nous discrétisons les solutions en notant (V_h^n, I_h^n) telles que $(V_h^n, I_h^n) \backsimeq (V_h(n\,\Delta t), I_h(n\,\Delta t))$.

Donc le problème (A.65) se réécrit comme suit

$$\begin{cases} \mathbb{M}_h \left(C\dfrac{V_h^{n+1} - V_h^n}{\Delta t} + G\dfrac{V_h^{n+1} + V_h^n}{2} + k_e(0)\dfrac{X_h^{n+1} + X_h^n}{2} \right) + \mathbb{R}_h\, I_h^{n+\frac{1}{2}} = \mathbb{M}_h\, F_h^{n+\frac{1}{2}}, \\ \dfrac{X_h^{n+1} - X_h^n}{\Delta t} + \dfrac{\langle \sigma \rangle}{\langle \varepsilon \rangle}\dfrac{X_h^{n+1} + X_h^n}{2} = \dfrac{V_h^{n+1} + V_h^n}{2}, \\ \mathbb{B}_h \left(L\dfrac{I_h^{n+\frac{3}{2}} - I_h^{n+\frac{1}{2}}}{\Delta t} + R\dfrac{I_h^{n+\frac{3}{2}} + I_h^{n+\frac{1}{2}}}{2} \right) - \mathbb{R}_h^T\, V_h^{n+1} = 0, \end{cases} \tag{A.66}$$

avec des données initiales $V_h^0 = I_h^{\frac{1}{2}} = 0$.

Deuxième Approche

Cette approche est une approche générale, nous pouvons l'utiliser même dans le cas où la section S n'est pas circulaire, et elle repose sur le même principe que la première (différences finies et éléments finis), en approchant le terme non local en temps par une somme qui est la discrétisation de l'opérateur de convolution.

$$\begin{cases} C\mathbb{M}_h\, \partial_t\, V_h + G\mathbb{M}_h\, V_h + \mathbb{R}_h\, I_h + \mathbb{M}_h \displaystyle\int_0^t k_e(t-s)\, V_h(s)\, ds = \mathbb{M}_h\, F_h(t), \\ L\mathbb{B}_h\, \partial_t\, I_h + R\mathbb{B}_h\, I_h - \mathbb{R}_h^T\, V_h = 0. \end{cases} \tag{A.67}$$

$$\Downarrow$$

$$\begin{cases} C\,\mathbb{M}_h\, \dfrac{V_h^{n+1} - V_h^n}{\Delta t} + G\,\mathbb{M}_h\, \dfrac{V_h^{n+1} + V_h^n}{2} + \mathbb{R}_h\, I_h^{n+\frac{1}{2}} + \mathbb{M}_h \displaystyle\sum_{i=0}^{n} K_e^{ni}\dfrac{V_h^{i+1} + V_h^i}{2} = \mathbb{M}_h\, F_h^{n+\frac{1}{2}}, \\ L\,\mathbb{B}_h\, \dfrac{I_h^{n+\frac{3}{2}} - I_h^{n+\frac{1}{2}}}{\Delta t} + R\,\mathbb{B}_h\, \dfrac{I_h^{n+\frac{3}{2}} + I_h^{n+\frac{1}{2}}}{2} - \mathbb{R}_h^T\, V_h^{n+1} = 0. \end{cases} \tag{A.68}$$

Où V_h^0 et $I_h^{\frac{1}{2}}$ étaient donnés et nous notons

$$K_e^{ni} = \frac{1}{\Delta t}\int_{n\Delta t}^{(n+1)\Delta t} \int_{i\Delta t}^{(i+1)\Delta t} k_e(r-s)\, ds\, dr.$$

Étude de stabilité

Nous multiplions à gauche la première et la deuxième équation du schéma (A.68) respectivement par $\dfrac{V_h^{n+1} + V_h^n}{2}$ et $\dfrac{I_h^{n+\frac{3}{2}} + I_h^{n+\frac{1}{2}}}{2}$.

Nous obtenons :

$$\begin{aligned}\frac{1}{\Delta t}\big(E_h^{n+1}-E_h^n\big) = \; & -G\Big(\frac{V_h^{n+1}+V_h^n}{2},\mathbb{M}_h\frac{V_h^{n+1}+V_h^n}{2}\Big)+\Big(\frac{V_h^{n+1}+V_h^n}{2},\mathbb{M}_h F_h^{n+\frac{1}{2}}\Big)\\ & -R\Big(\frac{I_h^{n+\frac{3}{2}}+I_h^{n+\frac{1}{2}}}{2},\mathbb{B}_h\,\frac{I_h^{n+\frac{3}{2}}+I_h^{n+\frac{1}{2}}}{2}\Big)\\ & -\Big(\frac{V_h^{n+1}+V_h^n}{2},\mathbb{M}_h\sum_{i=0}^{n}K_e^{ni}\frac{V_h^{i+1}+V_h^i}{2}\Big),\end{aligned} \tag{A.69}$$

où E_h^n est l'énergie discrète définie par :

$$E_h^n=\frac{1}{2}\Big(C\,\|V_h^n\|^2_{\mathbb{M}_h}+L\,\|I_h^{n+\frac{1}{2}}\|^2_{\mathbb{B}_h}-\Delta t(V_h^n,\mathbb{R}_h\,I_h^{n+\frac{1}{2}})_2\Big). \tag{A.70}$$

On somme maintenant la relation (A.69) pour $m=0$ jusqu'à $m=n$, nous obtenons :

$$\begin{aligned}E_h^{n+1}=E_h^0 \; & -\Delta t\,G\sum_{m=0}^{n}\Big(\frac{V_h^{m+1}+V_h^m}{2},\mathbb{M}_h\frac{V_h^{m+1}+V_h^m}{2}\Big)+\Delta t\sum_{m=0}^{n}\Big(\frac{V_h^{m+1}+V_h^m}{2},\mathbb{M}_h F_h^{m+\frac{1}{2}}\Big)\\ & -\Delta t\,R\sum_{m=0}^{n}\Big(\frac{I_h^{m+\frac{3}{2}}+I_h^{m+\frac{1}{2}}}{2},\mathbb{B}_h\,\frac{I_h^{m+\frac{3}{2}}+I_h^{m+\frac{1}{2}}}{2}\Big)\\ & -\Delta t\sum_{m=0}^{n}\sum_{i=0}^{m}K_e^{mi}\Big(\frac{V_h^{m+1}+V_h^m}{2},\mathbb{M}_h\frac{V_h^{i+1}+V_h^i}{2}\Big),\end{aligned} \tag{A.71}$$

La stabilité du schéma (A.68) sera obtenue sous les deux conditions suivantes :

• La première est la condition CFL classique déduite par la condition de positivité de l'énergie discrète (A.70).

En effet,

$$\begin{aligned}E_h^n&=\frac{1}{2}\Big(C\,\|V_h^n\|^2_{\mathbb{M}_h}+L\,\|I_h^{n+\frac{1}{2}}\|^2_{\mathbb{B}_h}-\Delta t(V_h^n,\mathbb{R}_h\,I_h^{n+\frac{1}{2}})_2\Big)\\ &\geq\frac{1}{2}\Big(C\,\|V_h^n\|^2_{\mathbb{M}_h}+L\,\|I_h^{n+\frac{1}{2}}\|^2_{\mathbb{B}_h}\Big)-\frac{\Delta t}{2}\,\|\mathbb{M}_h^{-\frac{1}{2}}\mathbb{R}_h\mathbb{B}_h^{-\frac{1}{2}}\|_2\,\|V_h^n\|_{\mathbb{M}_h}\,\|I_h^n\|_{\mathbb{B}_h}\\ &\geq\frac{C-\beta}{2}\,\|V_h^n\|^2_{\mathbb{M}_h}+\frac{L-\beta}{2}\,\|I_h^{n+\frac{1}{2}}\|^2_{\mathbb{B}_h}\end{aligned}$$

avec $\beta=\Delta t\,\dfrac{\|\mathbb{M}_h^{-\frac{1}{2}}\mathbb{R}_h\mathbb{B}_h^{-\frac{1}{2}}\|_2}{2}$.

Donc la condition CFL est donnée par :

$$\boxed{\beta^2<C\,L.}$$

• La deuxième condition pour laquelle l'énergie est bornée.

L'égalité (A.71) se réécrit comme suit :

$$E_h^{n+1}=E_h^0-K_{h,V}-K_{h,I}+\Delta t\sum_{m=0}^{n}\Big(\frac{V_h^{m+1}+V_h^m}{2},\mathbb{M}_h F_h^{m+\frac{1}{2}}\Big),$$

avec

$$K_{h,V} = \Delta t\, G \sum_{m=0}^{n} \Big(\frac{V_h^{m+1} + V_h^m}{2}, \mathbb{M}_h \frac{V_h^{m+1} + V_h^m}{2} \Big) + \Delta t \sum_{m=0}^{n} \sum_{i=0}^{m} K_e^{mi} \Big(\frac{V_h^{m+1} + V_h^m}{2}, \mathbb{M}_h \frac{V_h^{i+1} + V_h^i}{2} \Big),$$

$$K_{h,I} = \Delta t\, R \sum_{m=0}^{n} \Big(\frac{I_h^{m+\frac{3}{2}} + I_h^{m+\frac{1}{2}}}{2}, \mathbb{B}_h \frac{I_h^{m+\frac{3}{2}} + I_h^{m+\frac{1}{2}}}{2} \Big).$$

Il est clair que $K_{h,I} \geq 0$ car $\mathbb{B}_h$ est définie positive. Maintenant, nous allons montrer que $K_{h,V} \geq 0$.

Nous définissons la fonction constante par morceaux $V_h^{n\Delta t}(t)$ par

$$V_h^{n\Delta t}(t) = \begin{cases} \dfrac{V_h^{m+1} + V_h^m}{2}, & m\Delta t < t < (m+1)\Delta t, \qquad 0 \leq m \leq n \\ 0 & t < 0, \\ 0 & t > (n+1)\Delta t, \end{cases}$$

alors $K_{h,V}$ se réécrit comme une intégrale :

$$\begin{aligned} K_{h,V} \quad &= \Delta t\, G \int_0^{(n+1)\Delta t} \Big(V_h^{n\Delta t}(r), \mathbb{M}_h V_h^{n\Delta t}(r) \Big)\, dr \\ &+ \Delta t \int_0^{(n+1)\Delta t} \int_0^r k_e(r-s) \Big(V_h^{n\Delta t}(s), \mathbb{M}_h V_h^{n\Delta t}(r) \Big)\, ds\, dr. \end{aligned}$$

Lemme A.3.1.

Soit u une fonction de $L^2(\mathbb{R}^+)$, alors pour tout $t > 0$, nous avons

$$G \int_0^t u^2(s)\, ds + \int_0^T \int_0^s k_e(r-s) u(s) u(r)\, ds\, dr \geq 0,$$

$$R \int_0^t u^2(s)\, ds + \int_0^t \int_0^s k_m(r-s) u(s) u(r)\, ds\, dr \geq 0.$$

Démonstration. Voir la thèse [35] Page 107. ■

D'après le théorème (A.3.1), il est facile de montrer que

$$G \int_0^{(n+1)\Delta t} \Big(V_h^{n\Delta t}(r), \mathbb{M}_h V_h^{n\Delta t}(r) \Big)\, dr + \int_0^{(n+1)\Delta t} \int_0^r k_e(r-s) \Big(V_h^{n\Delta t}(s), \mathbb{M}_h V_h^{n\Delta t}(r) \Big)\, ds\, dr \geq 0,$$

donc, $K_{h,V} \geq 0$.

Finalement, nous obtenons la majoration suivante

$$E_h^{n+1} \leq E_h^0 + \Delta t \sum_{m=0}^{n} \Big(\frac{V_h^{m+1} + V_h^m}{2}, \mathbb{M}_h F_h^{m+\frac{1}{2}} \Big),$$

de plus, nous trouvons que l'énergie satisfait l'estimation

$$\sqrt{E_h^{n+1}} \leq \sqrt{E_h^0} + \frac{\Delta t \sqrt{2}}{2\sqrt{1-\beta}} \sum_{m=0}^{n} \| F_h^{m+\frac{1}{2}} \|_{\mathbb{M}_h}.$$

A.3.3 Tests numériques

Dans cette section, nous nous intéressons à présenter quelques résultats numériques pour la propagation du potentiel électrique V et du courant électrique I au cours du temps dans un câble. Nous utilisons des conditions de périodicité pour borner le domaine de calcul, par suite nous travaillons dans un câble borné de longueur $L = 10$. La source du problème est une source volumique de la forme :

$$f(x,t) = F(x)\, J(t),$$

où

$$F(x) = e^{-a(x-5)^2} \qquad J(t) = -\pi^2(t-1-b)\, e^{-\pi^2(t-1-b)^2},$$

avec les choix de $a = -4\ln(10^{-20})$ et $b = \dfrac{1}{10}$.

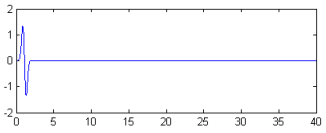

- Source temporelle J -

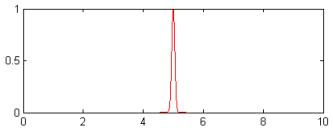

- source spatiale F -

• **Comparaison des résultats des deux approches**

On pose :

$$\mathrm{r}_1 = 1.6,\ \mathrm{r}_2 = 2, \quad \varepsilon_1 = \varepsilon_2 = \mu_1 = \mu_2 = 1, \quad \sigma_{e,1} = \sigma_{m,1} = \sigma_{m,2} = 0, \text{ et } \sigma_{e,2} = 0.5.$$

L'implémentation des deux approches a été faite via un code Matlab. Nous constatons que les résultats numériques obtenus par les deux approches sont identiques comme le montrent les figures suivantes, dans lesquelles nous présentons la propagation de la tension et du courant électrique au cours du temps.

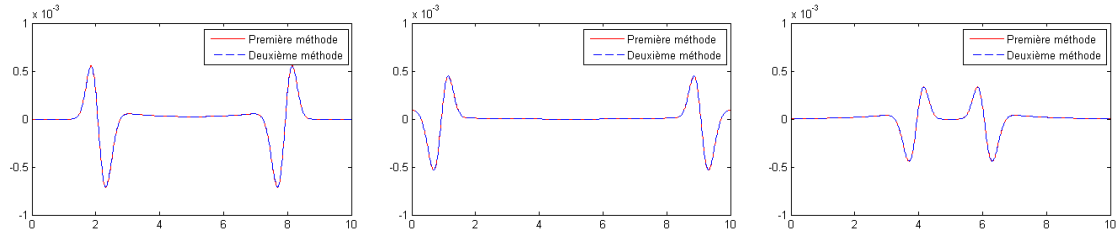

- Propagation de la tension électrique -

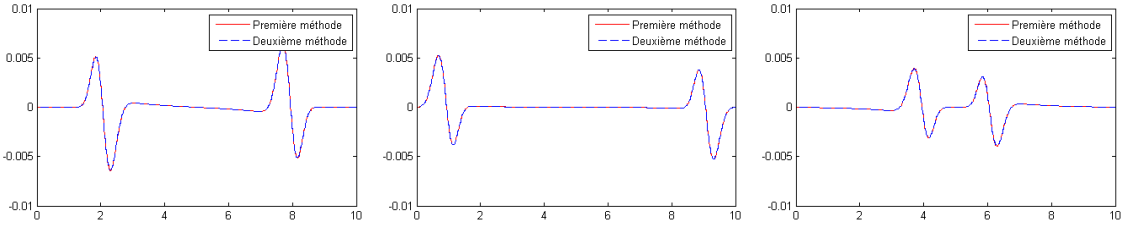

- Propagation du courant électrique -

FIGURE A.2 – Comparaison des résultats numériques du modèle télégraphique obtenu par les deux approches à $t_1 = 34$, $t_2 = 37$, $t_3 = 40$.

Bibliographie

[1] M. Admane, M. Sorine, and Q. Zhang. Inverse scattering for soft fault diagnosis in electric transmission lines. IEEE Trans. on Antennas and Propagation, Vol. 59, No. 1, 141–148, (2011).

[2] A. Beni Hamad, G. Beck, S. Imperiale, and P. Joly. An efficient numerical method for time domain electromagnetic wave propagation in co-axial cables. Computational Methods in Applied Mathematics, (2022).

[3] J. Albella Martinez, S. Imperiale, P. Joly and J. Rodriguez. Numerical analysis of a method for solving 2D linear isotropic elastodynamics with traction free boundary condition using potentials and finite elements. Mathematics of computations, Vol. 90, 1589–1636, 2021.

[4] C Alboin, J Jaffré, P Joly, JE Roberts, and C Serres. A comparison of methods for calculating the matrix block source term in a double porosity model for contaminant transport. Computational Geosciences, 6(3/4) :523-543, 2002.

[5] D. N. Arnold, F. Brezzi, B. Cockburn, and L. D. Marini, Unified analysis of discontinuous Galerkin methods for elliptic problems. SIAM J. Numer. Anal., 39, pp. 1749-1779, (2002).

[6] F. Auzanneau. Wire troubleshooting and diagnosis : Review and perspectives. Progress In Electromagnetics Research B, Vol. 49, 253279, (2013).

[7] D. H. Baffet, M. J. Grote, S. Imperiale, and M. Kachanovska. Energy decay and stability of a perfectly matched layer for the wave equation. Journal of Scientific Computing, 81(3), 2237-2270, (2019).

[8] C. E. Baum, and J. Scott Tyo, Transient Skin Effect in Cables. Phillips Laboratory, MN 47, (1996).

[9] E. Bécache, S. Fliss, M. Kachanovska, and M. Kazakova. On a surprising instability result of Perfectly Matched Layers for Maxwell's equations in 3D media with diagonal anisotropy. Comptes Rendus. Mathématique, 359(3), 249-256, (2021).

[10] G. Beck. Modélisation et étude mathématique de réseaux de câbles électriques. Thèse de doctorat. Université Paris-Saclay. (2016).

[11] G. Beck. Computer-implemented method for reconstructing the topology of a network of cables, US patent n° : US20200363462A . 16/638,451, 2020. 2017, https ://patents.google.com/patent/US20200363462A1/en.

[12] G. Beck, S. Imperiale and P. Joly. Mathematical modelling of multi conductor cables, Vol. 8, No. 3, (2014).

[13] G. Beck, S. Imperiale, P. Joly. Asymptotic modeling of Skin-effects in coaxial cables. Springer Nature : Part. Diff. Equ. and Applications, American Institute of Mathematical Science 1–42, (2020).

[14] J.P. Bérenger. "A perfectly matched layer for the absorption of electromagnetic waves." Journal of computational physics 114.2 (1994) : 185-200.

[15] M. Bergot, M. Duruflé. High-order optimal edge elements for pyramids, prisms and

hexahedra, Journal of Computational Physics, Vol. 232, 189–213, (2013).

[16] A. S. Bonnet-Bendhia, K. Berriri, and P. Joly. Régularisation de l'équation de Galbrun pour l'aéroacoustique en régime transitoire. Revue Africaine de la Recherche en Informatique et Mathématiques Appliquées, 5, 65-79. (2006).

[17] J.A. Buck and W.H. Hayt, Engineering Electromagnetics, 6th Ed., McGraw-Hill Education, (2011).

[18] A. Burel, S. Imperiale and P. Joly. Solving the homogeneous isotropic linear elastodynamics equations using potentials and finite elements. The case of the rigid boundary condition. Numerical Analysis and Applications, Vol. 5, No. 2, 136–143, (2012).

[19] J. Chabassier and S. Imperiale. Fourth-order energy-preserving locally implicit time discretization for linear wave equations. International journal for numerical methods in engineering, Vol. 106, No. 8, 593–622, (2015).

[20] J.-L. Coulomb, F.-X. Zgainski and Y. Marechal. A pyramidal element to link hexahedral, prismatic and tetrahedral edge finite elements. Institute of Electrical and Electronics Engineers, Vol. 33, No. 2, 1362–1365, (1997).

[21] R. Dautray, J. L. Lions, Mathematical analysis and numerical methods for science and technology. Vol. 1, Springer-Verlag, 1990

[22] R. Dusseaux, C. Faure, Telegraphist's equations for rectangular waveguides and analysis in nonorthogonal coordinates, Progress In Electromagnetics Research 88 (2008) 53–71.

[23] S. Descombes, S. Lanteri and L. Moya. Locally Implicit Time Integration Strategies in a Discontinuous Galerkin Method for Maxwell's Equations. Journal of Scientific Computing, vol. 56, no 1, p. 190-218. (2013).

[24] M. Grote, and I. Sim. Efficient PML for the wave equation. preprint, arXiv :1001.0319 [math :NA] (2010)

[25] M. Grote, A. Schneebeli, and D. Schötzau. Discontinuous Galerkin finite element method for the wave equation. SIAM Journal on Numerical Analysis, vol. 44, no 6, p. 2408-2431. (2006).

[26] M. Grote, A. Schneebeli, and D. Schötzau. Interior penalty discontinuous Galerkin method for Maxwell's equations : energy norm error estimates. J. Comput. Appl. Math., 204, 375-386, (2007).

[27] M. Grote, A. Schneebeli, and D. Schötzau. "Interior penalty discontinuous Galerkin method for Maxwell's equations : optimal L 2-norm error estimates." IMA journal of numerical analysis 28.3 (2008) : 440-468.

[28] M. Hochbruck, T. Jahnke and R. Schnaubelt. Convergence of an ADI splitting for Maxwell's equations, Numerische Mathematik, Vol. 129., No. 3, 535–561, (2014).

[29] M. Hochbruck and J. Leibold. An implicit-explicit time discretization scheme for second-order semilinear wave equations with application to dynamic boundary conditions. Numerische Mathematik, vol. 147, no 4, p. 869-899. (2021).

[30] M. Hochbruck and A. Sturm. Error Analysis of a Second-Order Locally Implicit Method for Linear Maxwell's Equations. SIAM Journal on Numerical Analysis, Vol. 54, No. 5, 3167–3191, (2016).

[31] P. Houston, I. Perugia, A. Schneebeli, D. Schötzau, Interior penalty method for the indefinite time-harmonic Maxwell equations, Numer. Math. 100 485-518. (2005).

[32] S. Imperiale. Asymptotic analysis of abstract two-scale wave propagation problems, Working paper, hal-03306856, (2021).

[33] S. Imperiale and P. Joly. Error estimates for 1D asymptotic models in coaxial cables with non-homogeneous cross-section. Advances in Applied Mathematics and Mechanics, Vol. 4, 647–664, (2012).

[34] S. Imperiale and P. Joly. Mathematical modeling of electromagnetic wave propagation in heterogeneous lossy coaxial cables with variable cross section, Applied Numerical Mathematics, Vol. 79, 42–61, (2014).
[35] S. Imperiale. Modélisation mathématique et numérique de capteurs piézoélectriques. Thèse de doctorat. Paris 9. (2012).
[36] A. Kameni, F.Loete, S.Ziani, K. Kahalerras, and L. Pichon. Time domain modeling of soft faults in wiring system by a nodal Discontinuous Galerkin Method with high-order hexahedral meshes, proceeding of the IEEE International Conference on the Computation of Electromagnetic Fields, (2015).
[37] J. Lee and B. Fornberg. A split step approach for the 3-D Maxwell's equations. Journal of Computational and Applied Mathematics, Vol. 158, No. 2, 485–505, (2003).
[38] J. Lee and B. Fornberg. Some unconditionally stable time stepping methods for the 3D Maxwell's equations. Journal of Computational and Applied Mathematics, Vol. 166, No. 2, 497–523, (2004).
[39] J. Li, E. Machorro, S. Shields. Numerical study of signal propagation in corrugated coaxial cables, Journal of Computational and Applied Mathematics, Vol. 309, 230–243, (2017).
[40] H. Methenni. Modélisation mathématique et méthode numérique pour la simulation du contrôle santé intégré par ultrasons de plaques composites stratifiées. PhD thesis, Institut Polytechnique de Paris. (2021).
[41] P. Monk, Finite element methods for Maxwell's equations, Oxford science publications, (2003).
[42] P. Monk and G. R. Richter, A discontinuous Galerkin method for linear symmetric hyper- bolic systems in inhomogeneous media, J. Sci. Comput., 22-23, pp. 443-477. (2005).
[43] J. C. Nédélec, Mixed finite elements in R3. Numer. Math. 35, 315-341. (1980).
[44] C. R. Paul. Analysis of Multiconductor Transmission Lines, Wiley-IEEE Press, (2008).
[45] T. Rylander, A. Bondeson. Stability of explicit-implicit hybrid time-stepping schemes for Maxwell's equations, Journal of Computational Physics, Vol. 179, No. 2, 426–438, (2002).
[46] J. Stratton, Electromagnetic Theory, second printing ed., Mcgraw Hill, (1941).
[47] W. T. Weeks, Calculation of Coefficients of Capacitance of Multiconductor Transmission Lines in the Presence of a Dielectric Interface, IEEE Trans. MTT-18,35 (1970).
[48] W. T. Weeks, Multiconductor transmission line theory in the TEM approximation, IBM Journal of Research and Development, 604D611, (1972).

ECOLE
DOCTORALE
DE MATHEMATIQUES
HADAMARD

Titre : Modélisation et simulation numérique de la propagation d'ondes électromagnétiques dans les câbles coaxiaux.

Mots clés : Câbles coaxiaux, équations de Maxwell, Éléments finis d'arête, méthode Galerkine discontinue, modèles de télégraphistes, simulations numériques.

Résumé : Dans cette thèse, nous nous intéressons à la propagation des ondes électromagnétiques dans un réseau de câbles coaxiaux minces (constitués d'un matériau diélectrique qui entoure un fil intérieur métallique) avec sections transverses hétérogènes. Le premier objectif, atteint dans la thèse de G. Beck, était de réduire les équations de Maxwell 3D à un graphe quantique dans lequel on se ramène au calcul du potentiel et du courant électriques en résolvant des modèles 1D simplifiés. Ainsi, l'objectif principal de cette thèse est la validation numérique de ces modèles 1D.
Dans un premier temps, nous avons proposé, analysé et mis en œuvre des méthodes numériques efficaces pour résoudre les modèles simplifiés 1D. Afin de réaliser la comparaison 1D/3D, un défi majeur est de concevoir des méthodes numériques pour résoudre les équations de Maxwell 3D qui sont adaptées à la spécificité des câbles électriques fins. Une procédure de discrétisation naïve basée sur un schéma explicite saute-mouton peut être vraiment coûteuse en raison de la finesse du câble. Nous avons alors proposé une approche originale consistant à adapter les éléments d'arête "Nedelec" à des mailles prismatiques allongées et à proposer une procédure de discrétisation temporelle hybride, explicite dans les directions longitudinales et implicite dans les directions transversales. En particulier, la condition de stabilité de la CFL qui en résulte n'est pas affectée par l'épaisseur du câble.
Cependant, la méthode ci-dessus n'est efficace que pour des câbles parfaitement cylindriques : son extension naïve aux câbles déformés génère un recouplage longitudinal-transversal qui détruit l'efficacité de la méthode. En présence de déformations, la méthode doit donc être modifiée. En conséquence, afin de préserver le découplage longitudinal-transversal, nous proposons une méthode hybride combinant une discrétisation conforme dans les variables longitudinales et une méthode Galerkin discontinue dans les variables transversales. Cette méthode coïncide avec la précédente dans les parties cylindriques du câble.

Title : Modeling and numerical simulation of electromagnetic wave propagation in coaxial cables.

Keywords : Coaxial cables, Maxwell's equations, Edge elements, Discontinuous Galerkin method, Telegrapher's models, Numerical simulations.

Abstract : In this thesis we are interested in the electromagnetic wave propagation in a network of thin coaxial cables (made of a dielectric material which surrounds a metallic inner wire) with heterogeneous cross sections. The first goal, achieved in the PhD thesis of G. Beck few years ago, was to reduce 3D Maxwell's equations to a quantum graph in which we reduce ourselves to the calculation of the electric potential and current by solving simplified 1D models. Thus, the main objective of this thesis is the numerical validation of these 1D models.
In a first step we have proposed, analysed and implemented efficient numerical methods for solving the 1D approximate problems. In order to achieve the 1D/3D comparison, a major challenge is to design numerical methods for solving 3D Maxwell's equations dedicated to taking into account the specificity of thin electric cables. A naive discretization procedure based on a leap-frog explicit scheme can be really costly because of the thinness of the cable. In the case have then proposed an original approach consisting in adapting Nedelec's edge elements to elongated prismatic meshes and proposing a hybrid time discretization procedure which is explicit in the longitudinal directions and implicit in the transverse ones. In particular, the resulting CFL stability condition is not affected by the small thickness of the cable.
However the above is only effective for perfectly cylindrical cables : its naive extension do deformed cables generates longitudinal-transverse recoupling that destroys the efficiency of the method. In the presence of deformations, the method needs to be modified. In order to preserve the longitudinal/transverse decoupling, we propose a hybrid method combining a conforming discretization in the longitudinal variable and a Discontinuous Galerkin method in the transverse ones. This method coincides with the previous one in the cylindrical parts of the cable.

Institut Polytechnique de Paris
91120 Palaiseau, France